Increasing our Knowledge of Structure-Activity Relationships in Transition Metal Containing Nonlinear Optical Chromophores

2005

Josephine Louise Harries

School of Chemistry

A thesis submitted to the University of Manchester for the degree of Doctor of Philosophy in the Faculty of Engineering and Physical Sciences

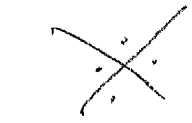

Th 26+00

Contents

List of Tables

List of Figures

List of Abbreviations

α	linear molecular polarizability
A	electron acceptor group
AcPh	4-acetylphenyl
$AcPhQ^+$	*N*-(4-acetylphenyl)-4,4′-bipyridinium
β	first molecular hyperpolarizability
β_0	static first molecular hyperpolarizability
bpa	bis(4-pyridyl)acetylene
bpbd	1,4-bis(4-pyridyl)buta-1,3-diyne
bpbt	1,4-bis(4-pyridyl)hexa-1,3,5-triyne
bpe	*E*-1,2-bis(4-pyridyl)ethylene
bpeb	1,4-bis[*E*-2-(4-pyridyl)ethynyl]benzene
bph	(*E,E,E)*-1,6-bis(4-pyridyl)hexa-1,3,5-triene
bpvb	1,4-bis[*E*-2-(4-pyridyl)ethenyl]benzene
bpy	2,2′-bipyridyl
BLA	bond length alternation
$\chi^{(1)}$	bulk linear optical susceptibility
$\chi^{(2)}$	bulk second-order nonlinear optical susceptibility
$\chi^{(3)}$	bulk third-order nonlinear optical susceptibility
$\Delta\mu_{12}$	dipole moment change
D	electron donor group
DANS	4-dimethylamino-4′-nitrostilbene
DMF	*N,N*-dimethylformamide
$DNPhbpvb^+$	*N*-(2,4-dinitrophenyl)-1,4-bis(*E*-2-(4-pyridyl)ethenyl)benzene
$DNPhQ^+$	*N*-(2,4-dinitrophenyl)-4,4′-bipyridinium
EFISHG	electric field-induced second harmonic generation
E_{max}	energy of maximal absorption
FEP	2-[2-(4-formylphenyl)ethenyl]pyridine
f_{os}	oscillator strength
γ	second molecular hyperpolarizability
H-bond	hydrogen bond

HOMO	highest occupied molecular orbital
HRS	hyper-Rayleigh scattering
ICT	intramolecular charge-transfer
ILCT	intraligand charge-transfer
IR	infrared
ITO	indium tin oxide
K_b	Boltzmann constant
KDP	potassium dihydrogen phosphate
λ_{max}	wavelength of maximal absorption
L	pyridinium-substituted ligand
L_A	electron acceptor-substituted pyridyl ligand
L_D	electron-rich ligand
LMCT	ligand-to-metal charge-transfer
Ln	lanthanide
LUMO	lowest unoccupied molecular orbital
μ	dipole moment
μ_{12}	transition dipole moment
M	metal
Me	methyl
$Mebpa^+$	*N*-methyl-4-[2-(4-pyridyl)ethynyl]pyridinium
$Mebpb^+$	*N*-methyl-4-{*E,E*-4-(4-pyridyl)buta-1,3-dienyl}pyridinium
$Mebpbd^+$	*N*-methyl-4-[4-(4-pyridyl)buta-1,3-diynyl]pyridinium
$Mebpe^+$	*N*-methyl-4-[*E*-2-(4-pyridyl)ethenyl]pyridinium
$Mebpvb^+$	*N*-methyl-1,4-bis-[*E*-2-(4-pyridyl)ethenyl]benzene
$Mepyz^+$	*N*-methylpyrazinium
MeQ^+	*N*-methyl-4,4′-bipyridinium
mim	*N*-methylimidazole
MLCT	metal-to-ligand charge-transfer
M--M	metal-to-metal bond
MMCT	metal-to-metal charge-transfer
NLO	nonlinear optical
NMR	nuclear magnetic resonance
pdma	1,2-phenylenebis(dimethylarsine)

PEPBDTM	((*E*-2-(4-pyridyl)ethenyl)phenyl)bis(1,3-diethyl-2-thiobarbitur-5-yl)methane
Ph	phenyl
$Phbpe^+$	*N*-phenyl-4-[*E*-2-(4-pyridyl)ethenyl]pyridinium
$Phbpvb^+$	*N*-phenyl-1,4-bis(*E*-2-(4-pyridyl)ethenyl)benzene
phen	1,10-phenanthroline
$Phpic^+$	*N*-phenyl-4-picolinium
PhQ^+	*N*-phenyl-4,4′-bipyridinium
py	pyridine
Pym	2-pyrimidyl
$Pymbpvb^+$	*N*-(2-pyrimidyl)-1,4-bis(*E*-2-(4-pyridyl)ethenyl)benzene
$Pympic^+$	*N*-(2-pyrimidyl)-4-picolinium
$PymQ^+$	*N*-(2-pyrimidyl)-4,4′-bipyridinium
pyr	pyridinium
pyz	pyrazine
salen	*N,N′*-ethylenebis(salicylaldiminate)
SH	second harmonic
SHG	second harmonic generation
TBACl	tetra(*n*-butyl)ammonium chloride
TD-DFT	time-dependent density functional theory
TGA	thermogravimetric analysis
THACl	tetra(*n*-hexyl)ammonium chloride
THF	tetrahydrofuran
TOACl	tetra(*n*-octyl)ammonium chloride
TODACl	tetra(*n*-octadecyl)ammonium chloride
TTF	tetrathiafulvalenyl
UV	ultraviolet
UV/Vis	ultraviolet/visible

Abstract

The work presented in this thesis concerns the design and synthesis of a variety of transition metal-containing chromophores that exhibit moderate-to-large quadratic nonlinear optical (NLO) responses. All of the complexes synthesized display intense, visible metal-to-ligand charge-transfer (MLCT) bands. Hyper-Rayleigh scattering (HRS) and Stark spectroscopy have been used to calculate values of β_0 (the static first hyperpolarizability) according to the two-state model. Ten single crystal X-ray structures have been solved, although only *trans*-$[Ru^{II}Cl(pdma)_2(pyz)]PF_6$ (pdma = 1,2-phenylenebis(dimethylarsine), pyz = pyrazine) packs noncentrosymmetrically.

A series of complexes has been prepared in which the $\{Fe^{II}(CN)_5\}^{3-}$ electron donor group is co-ordinated to pyridinium-substituted pyridyl ligands. Both the MLCT absorption energy and β_0 are highly sensitive to the nature of the solvent. HRS and Stark spectroscopic experiments have been used to demonstrate that the NLO responses of these complexes are significantly decreased upon protonation of the CN^- ligands. The linear and NLO behaviour of these novel compounds are compared and contrasted with those of previously studied $\{Ru^{II}(NH_3)_5\}^{2+}$ complexes.

The effects of extending the polyenyl conjugation within a series of pyridinium-substituted pyridyl ligands connected to *trans*-$\{Ru^{II}Cl(pdma)_2\}^+$ electron donors have been investigated. The linear and NLO properties of this series have been studied, although β_0 has only been determined using Stark spectroscopy. Extending the conjugation causes unusual optical behaviour, with the MLCT band blue-shifting after *n*

= 1 (n is the number of E-ethenyl units) and β_0 peaking at $n = 2$. Similar trends are observed in analogous Ru^{II} ammine chromophores.

A series of complexes has been prepared in which either *trans*-$\{Ru^{II}(NH_3)_4L_D\}^{2+}$ (L_D = NH_3, *N*-methylimidazole or pyridine) or *trans*-$\{Ru^{II}Cl(pdma)_2\}^{+}$ centres are connected to ethynyl-containing pyridinium-substituted pyridyl ligands. The effects of extending the ethynyl conjugation have been investigated, and comparisons are drawn with related ethenyl-containing complexes. The new ethynyl-containing complexes generally show lower NLO responses than their ethenyl counterparts due to decreased electron mobility and electronic communication.

Two new *N*-aryl derivatives of 1,4-bis-(*E*-2-(4-pyridyl)ethenyl)benzene) have been prepared and, together with their known *N*-methyl analogue, coordinated to *trans*$\{Ru^{II}Cl(pdma)_2\}^{+}$. The NLO responses of these complexes have been determined by Stark spectroscopy and it is found that intra-ligand charge-transfer, as well as MLCT transitions, contribute significantly to β_0. These complexes show large NLO responses, comparable to those seen in related polyenyl species.

Declaration

No portion of the work referred to in this thesis has been submitted in support of an application for another degree or qualification of this or any other university or other institute of learning.

Copyright Statement

Acknowledgements

Many thank yous are due to all the people that have helped me during the three years of my PhD.

In particular:

Ben Coe, for being an excellent supervisor, always there to sort out problems, listen to whingeing about organic chemistry, read through any work sent his way and for just generally being great!

All of the Coe group (past and present): James, for his help, which got me through my first year and his subsequent Stark spectroscopic measurements. Naomi, for being a great friend and aide, proof reading this monster, fixing my trousers before my viva and also for being able to dance without moving her lab coat. Simon, Emma and Cat, for providing endless entertainment both in and out of the lab!

All the technical support staff at the University of Manchester for providing the means to perform NMR, microanalytical and mass spectrometry measurements.

Simon Coles, Mark Light and Peter Horton at the University of Southampton and Madeleine Helliwell at the University of Manchester, for solving various crystal structures in this work.

Bruce Brunschwig at Caltech for employing James Harris and allowing him to perform Stark measurements on my samples.

Inge Asselberghs and Koen Clays at the University of Leuven, both for performing HRS measurements on my samples, and enabling me to spend two weeks using their HRS set up.

Gill Reid (and her students) at the University of Southampton for synthesizing the nasty diarsine ligand.

All of my friends (both chemistry and non chemistry related) that have made my long stay in Manchester pass quickly and with many laughs. Special mention to Saskia and Vicki for always being available for moaning and advice (though I feel that too many bottles of wine have been drunk in the process!).

Mum and Dad, without your constant love and support (and fighting my case with Mr Beale!) I would never have been able to achieve as much as I have, **BIG** thank you!

Dan, thanks for putting up with me (especially first thing in the morning!), introducing me to some excellent music and for your patience and love, especially during my Belgium trip.

Hooray for my Cats!

who think EVERYTHING I DO is fantastic.

Chapter 1

Introduction

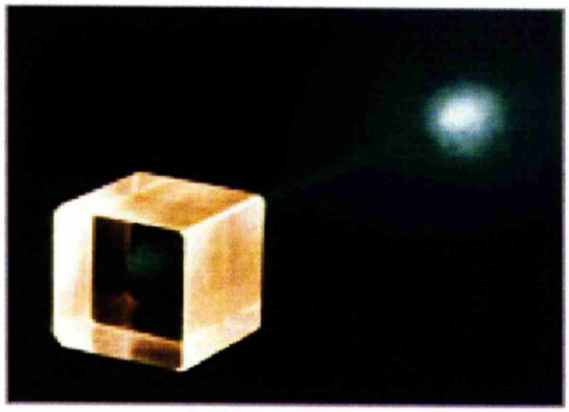

Linear optical effects have been observed and studied for centuries and give rise to phenomena such as refraction and reflection. Although nonlinear effects in magnetism and electricity have been known for some time, such effects in the optical region have only become of interest since the invention of the laser in 1960.[1] Materials that exhibit nonlinear optical (NLO) behaviour are of current interest for their potential applications in photonic and optoelectronic devices such as telecommunications and optical data processing and storage.[2] Such technologies rely on the fact that photons process information at the speed of light. Electronic technologies use electrons to process the information and this occurs at a much slower speed.[2,3] NLO materials allow the manipulation of the fundamental properties of a laser light beam, for example frequency doubling or second harmonic generation (SHG, see section 1.1).

NLO effects were first observed in 1961 when Franken *et al.* detected SHG when a ruby laser was shone onto a crystal of quartz.[4] At first, research mainly concentrated on simple inorganic crystalline solids such as quartz, potassium dihydrogen phosphate (KDP) and lithium niobate ($LiNbO_3$),[3] and many commercially available devices incorporate these materials.[5] The NLO properties of molecular materials became of interest owing to their potential advantages over conventional inorganic materials, especially the fact that their NLO responses often greatly exceed those of simple inorganics.[3] Organic compounds have other advantages emerging from their architectural flexibility and structural diversity, which allow for molecular design and flexibility through synthetic chemistry.[6] Purely organic molecules have been the most widely investigated molecular materials, but when Green *et al.* observed strong SHG from a ferrocenyl derivative in 1987,[7] the NLO properties of transition metal

complexes became of interest. Complexes of this type are attractive as they allow NLO behaviour to be combined with properties commonly associated with transition metals such as redox and/or magnetic behaviour.[6,8]

1.1 Origins of NLO behaviour

NLO responses do not involve any exchange of energy between light and a medium, but arise from a subtle interaction between the polarizable electron density of a molecule and the strong alternating electric field of a laser light beam. This causes a perturbation of the electron density, resulting in an induced polarization response, P, which changes the fundamental properties such as frequency and amplitude of the laser beam. P (which corresponds with the dipole moment per unit volume) can be expressed in terms of the strength of the applied field, E, according to

$$P = \alpha E + \beta E^2 + \gamma E^3 + ... \qquad (1)$$

where α is the linear molecular polarizability, which is related to linear optical effects such as the refractive index. The coefficient β is the first molecular hyperpolarizability which governs second-order (quadratic) NLO effects and γ is the second molecular hyperpolarizability and governs third-order (cubic) NLO effects.

When E is of 'normal' magnitude, the βE^2 and γE^3 terms in equation (1) are negligible and only linear optical behaviour is observed. For second and third-order NLO effects to be observed, extremely high values of E are required, explaining why

such effects were only experimentally demonstrated with the advent of lasers which possess unusually high intensities.[9]

On a macroscopic level, equation (1) can be rewritten as

$$P = \chi^{(1)}E + \chi^{(2)}E^2 + \chi^{(3)}E^3 + \ldots\ldots \qquad (2)$$

where the coefficients $\chi^{(2)}$ and $\chi^{(3)}$ are the bulk second and third-order NLO susceptibilities, respectively. These are analogous to the molecular coefficients in equation (1), except that the χ terms take into account local field effects. For bulk quadratic NLO effects to be observed, a material must have a non-zero value of $\chi^{(2)}$, which requires the individual molecules to pack in a non-centrosymmetric fashion. Since this study is concerned only with second-order NLO properties, third-order effects will not be discussed any further.

The most widely studied, and currently the most widely commercially exploited second-order NLO effect is SHG. The electric field of a beam of light can be expressed as

$$E = E_0 \cos(\omega t) \qquad (3)$$

where E_0 is the amplitude, ω is the angular frequency and t is time. Equation (3) can be rewritten in terms of equation (1) as

$$P = P_0 + \alpha E_0 \cos(\omega t) + \beta {E_0}^2 \cos^2(\omega t) + \gamma {E_0}^3 \cos^3(\omega t) + \ldots\ldots \qquad (4)$$

As $\cos^2(\omega t) = 1/2 + 1/2(\cos(2\omega t))$ and considering only up to the second-order term, equation (4) becomes

$$P = \left[P_0 + \frac{1}{2}\beta^2 {E_0}^2 \cos(\omega t)\right] + \alpha E_0 \cos(\omega t) + \frac{1}{2}\beta {E_0}^2 \cos(2\omega t) \quad (5)$$

The third term in equation (5) contains a new frequency-doubled component ($2\omega t$), so when an intense light beam passes through a NLO material, light with twice the frequency of the original beam is produced. SHG is a form of three-wave mixing as two photons with frequency ω combine to generate one photon with frequency 2ω, allowing the generation of new and otherwise unavailable laser sources.[5] There has historically been much interest in developing materials capable of frequency doubling low-power diode lasers from the near-IR to the blue region of the visible spectrum. Such lasers will have uses in optical data storage, because decreasing the wavelength leads to an increase in the capacity of data stored.[10] However, such work has been superseded by the recent development and commercialisation of blue lasers based on group III nitride materials.[11-13]

The Pockels (or linear electro-optic) effect involves using an external electric field to change the amplitude, phase or path of a laser beam. An applied field changes the linear polarizability α, and therefore the refractive index, allowing modulation of the light travelling thorough an electro-optic material.[14] The Pockels effect is utilized in optical switches, modulators and wavelength filters.[15]

Frequency mixing is a process which involves the mixing of a laser beam carrying information and a pump beam of fixed intensity. This process can be used to convert the frequency of the laser beam into the visible (or any other) region of the electromagnetic spectrum where detection and processing may be much simpler than at the original wavelength. Frequency mixing also allows for the production of tunable sources of laser radiation.[5]

1.2 Molecular requirements for NLO behaviour

In 1970, Davydov and co-workers screened the SHG efficiencies of a wide variety of substituted benzenes. From the results obtained it was clear that for a molecule to exhibit a large quadratic NLO response it must possess an electron donor group (D) linked to an electron acceptor group (A) through a π-conjugated bridge, as shown in Figure 1[16]

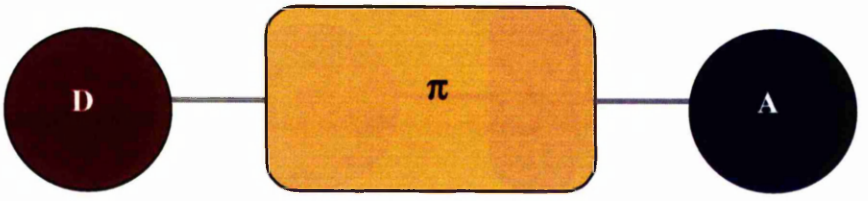

Figure 1: Graphical representation of a typical structure for a NLO chromophore

A prototypical molecule that satisfies these criteria is 4-dimethylamino-4′-nitrostilbene (DANS), which exhibits a β_0 value of 73×10^{-30} esu (where β_0 is the static first molecular hyperpolarizability).[17] The benzene rings and the trans ethylene

unit provide the π-conjugated bridge, while the dimethylamino group is the electron donor and the nitro group is the electron acceptor as depicted in Figure 2.

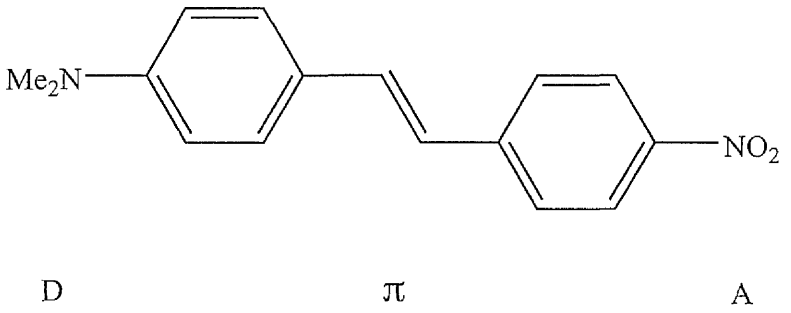

Figure 2: DANS – an organic chromophore that exhibits a relatively large second-order NLO response

The linear optical properties of such dipolar, polarizable D-π-A molecules are characterized by low energy D $\rightarrow$ A intramolecular charge-transfer (ICT) transitions. The energies of these transitions can be tailored by manipulation of the strength of the donor and/or the acceptor, or by varying the conjugation within the bridge.

1.3 The two-state model

In the 1970s, Oudar and Chemla developed a theoretical two-state model (TSM),[18,19] providing a simple representation of the relationship between the β response and an associated ICT transition. The TSM, as expressed by equations (6) and (7), can be used to guide the design of dipolar chromophores that will possess large values for β_0, the static (off-resonance) first molecular hyperpolarizability.

$$\beta = \beta_0 \frac{E_{max}}{\left[1-(2E_f)^2(E^2_{max})^{-1}\right]\left[(E_{max})^2 - E_f^2\right]} \qquad (6)$$

$$\beta_0 = \frac{3\Delta\mu_{12}(\mu_{12})^2}{2(E_{max})^2} \qquad (7)$$

E_f is the fundamental laser energy, E_{max} is the energy of the ICT, μ_{12} is the transition dipole moment and $\Delta\mu_{12}$ is the dipole moment change between the ground and excited state. β_0 corresponds to the intrinsic hyperpolarizability of the molecule in the absence of any field, and is of particular importance with respect to potential applications, as well as for drawing meaningful comparisons between chromophores.

The TSM has its limitations and breaks down when E_{max} is close to either the laser fundamental or the second harmonic (SH) wavelength, with the limiting cases being $E_{max} = E_f$ or $2E_f$ where $\beta = \infty$ and therefore $\beta_0 = 0$. As β_0 is proportional to $\Delta\mu_{12}$, the square of μ_{12} and the inverse square of E_{max}, the NLO response can be increased by manipulation of these parameters. Oudar and Chemla demonstrated the validity of the TSM for a series of stilbene derivatives,[18] and the model appears to hold well for conjugated dipolar molecules which possess a single strong ICT transition.[3]

1.4 Bond length alternation

The majority of NLO chromophores studied possess predominantly aromatic ground states and largely quinoidal structures in their ICT excited states as shown in Figure 3.[20]

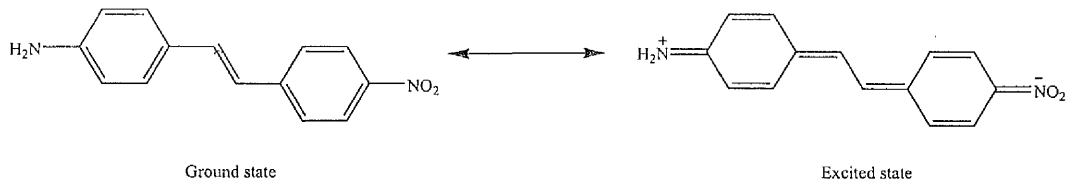

Figure 3: Limiting resonance structures for DANS with an aromatic ground state and quinoidal excited state

Consideration of these resonance forms has lead to the development of the bond length alternation (BLA) model, which correlates β with the degree of ground state polarization.[21-24] In substituted polyenes with weak donor and acceptor groups, the ground state resonance form dominates and the molecular structure possesses a high degree of BLA. As the donor and acceptor strength increase, the BLA decreases. Solvation effects can also lead to preferential stabilization of the different resonance forms, with more polar solvents stabilizing the charge-separated form.[25] If there are equal contributions from the ground and excited states, then the molecule will exhibit zero BLA, a situation called the cyanine limit. A graphical representation of these resonance forms is given in Figure 4.

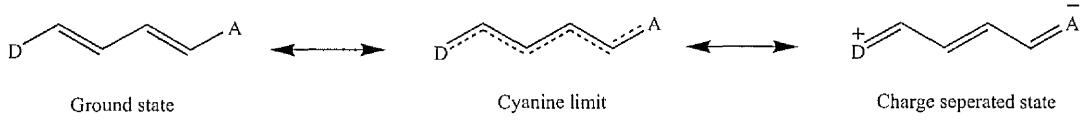

Figure 4: Resonance forms of a D–A polyene

1.5 Factors affecting the quadratic hyperpolarizability

One of the major advantages of organic chromophores over conventional inorganic crystals, such as $LiNbO_3$, is the potential for molecular engineering through synthetic chemistry. The manipulation of the individual components within the chromophore can allow structure-activity relationships to be determined. As discussed previously in section 1.3, β_0 for a simple dipolar chromophore can be related to $\Delta\mu_{12}$, μ_{12} and E_{max} through the TSM (equation (7)). Whereby, increasing $\Delta\mu_{12}$ and μ_{12} and decreasing E_{max} leads to an increase in β_0. These changes can be achieved by:

- Increasing the donor and/or the acceptor strength. This will decrease E_{max} by either destabilization of the donor-based HOMO or stabilization of the acceptor-based LUMO, therefore reducing the energy gap between the two orbitals.[1]

- Increasing the conjugation length. For example, as a polyene chain extends a bathochromic effect is expected, *i.e.* a decrease in E_{max}. Such elongation will also cause an increase in $\Delta\mu_{12}$ and therefore an increase in β_0.[1]

There is a trade-off between the optical transparency and the NLO response of a molecule and this is an important consideration when designing a chromophore. The TSM shows that large values of β_0 obtained with highly dipolar, polarizable molecules are generally accompanied by low energy ICT absorptions in the visible region of the electromagnetic spectrum.

1.6 Measurement of NLO properties

When a potential NLO chromophore has been designed, the next step is the measurement of β and $\chi^{(2)}$. Various methods have been developed for obtaining this information and in most of these methods resonance effects have to be considered. Both β and $\chi^{(2)}$ are wavelength dependent and are subject to such resonance effects when the fundamental or SH frequencies are close to the electronic excitation energy. Although for practical device considerations factors such as thermal and optical stability will also be of importance, at an academic level a large NLO response is the primary goal. Comparisons between the NLO responses measured using different techniques should be made with caution. Factors such as dispersion effects, measurements of different tensor components and the errors associated with the technique will affect the β values obtained. Therefore, when the NLO responses of molecules or materials are quoted the fundamental wavelength, the solvent used and the wavelength of the ICT absorption must also be noted.

1.6.1 The Kurtz powder test[26]

This is a rather crude method for determining $\chi^{(2)}$ and involves the collection of the SHG light after a laser has been directed onto a microcrystalline powdered sample. The SHG efficiency is then quoted with respect to a standard such as quartz or $LiNbO_3$.[26] Generally, a 1064 nm Nd^{3+}:YAG laser is used (with a SH at 532 nm), but different laser fundamentals can be used if a molecule absorbs close to 532 nm. This technique is only semi-quantitative as factors such as particle size and layer thickness of the sample will affect the results obtained and a lack of SHG does not necessarily

prove that a molecule has no NLO activity, but may just be indicative of a centrosymmetric crystal packing. This technique is therefore not useful for establishing structure-activity relationships, but is useful as a quick screening method to identify materials that possess bulk NLO behaviour.

1.6.2 Electric field-induced second harmonic generation (EFISHG)[27-29]

Until recently, EFISHG was the only reliable method for the determination of quadratic NLO responses in solution. SHG cannot be observed in an isotropic solution due to symmetry requirements,[30] but when the centrosymmetry is broken by the application of a d.c. pulse to the liquid, a SHG signal can be produced. The electric field is synchronized to a laser pulse and causes the dipolar sample molecules within the solution to align. EFISHG is a third-order NLO process and the measurements taken allow for the determination of γ_0, the effective second hyperpolarizability. The second-order NLO response is related to γ_0 by

$$\gamma_0 = \gamma + \frac{\mu\beta_{\text{EFISHG}}}{(5\text{K}_\text{b}T)} \qquad (8)$$

Where γ is the intrinsic second hyperpolarizability, μ is the dipole moment, β_{EFISHG} is the first hyperpolarizability (not corrected for resonance effects), K_b is Boltzmanns constant and T is the temperature in K.

This indirect technique is limited only to neutral compounds as the presence of ionic species makes it impractical to apply high electric fields to a solution. The

derivation of β values also requires knowledge of μ, and the results obtained from EFISHG measurements have to be corrected for resonance enhancement using the TSM.

1.6.3 Hyper-Rayleigh scattering (HRS)[31-34]

In 1991, the HRS technique was further developed to provide a versatile method for the determination of β in solution for any type of molecule, irrespective of symmetry or charge. In addition, for dipolar molecules β can be determined without prior knowledge of μ. Another advantage of this method is that β can be determined directly. This method relies on the microscopic anisotropy within a solution of active molecules producing a SH signal. A laser beam is directed into a dilute solution of the sample and the incoherently scattered SH light is measured. A typical HRS experiment involves measuring the quadratic dependence of $I_{(2\omega)}$ on $I_{(\omega)}$ (where $I_{(2\omega)}$ is the intensity of SH light and $I_{(\omega)}$ is the intensity of the laser fundamental) for a dilution series of an unknown sample against a reference chromophore in the same solvent. A typical reference compound is *para*-nitroaniline. HRS measurements are subject to resonance enhancement and therefore unreliable results may be obtained if the molecule absorbs or luminesces in the SH region. Like the data obtained via EFISHG, HRS results can often be satisfactorily corrected for resonance enhancement using the TSM.

1.6.4 Stark (electroabsorption) spectroscopy[35-39]

The effect of an external applied electric field on an electronic absorption or emission spectrum is known as the Stark or electroabsorption effect. The ICT spectrum of a frozen glass is measured in the presence of an applied field and the difference relative to the zero-field spectrum is plotted to obtain the Stark spectrum. Analysis of this spectrum in terms of the Liptay treatment (equation (9))[40] and subsequent data manipulation affords information on the change in polarizability, $\Delta\alpha$, and the value of $\Delta\mu_{12}$ associated with the optical transition.

$$\Delta\varepsilon(\nu)/\nu = \left[A_x\varepsilon(\nu)/\nu + \frac{B_x}{15h}\frac{\partial(\varepsilon(\nu)/\nu)}{\partial\nu} + \frac{C_x}{30h^2}\frac{\partial^2(\varepsilon(\nu)/\nu)}{\partial\nu^2}\right]F_{int}^2 \qquad (9)$$

The value of μ_{12} can be determined from the oscillator strength f_{os} of the transition by

$$|\mu_{12}| = \left[f_{os}/(1.08\times10^{-5}E_{max})\right]^{1/2} \qquad (10)$$

The quadratic NLO response can then be determined by application of the TSM. It should be noted that alternative forms of equation 7 are available and these will change the calculated β_0 values by factors of either 0.5 or 2.[41]

1.7 Transition metal complexes for second-order nonlinear optics

The interest in transition metal complexes for their potential uses in NLO devices started in the late 1980s when the first reports of metal complexes with large SHG efficiencies were published.[7,42-44] Since then there has been a considerable amount of research interest in this area. Metal-containing chromophores are of interest for a number of reasons, including: (i) variation in the number of d electrons, which can lead to the introduction of paramagnetism.[14] (ii) depending on the oxidation state, the metal centre can act as a powerful D or A group. (iii) metal complexes often exhibit metal-to-ligand or ligand-to-metal charge-transfer (MLCT or LMCT) transitions in the UV-visible region, which may be associated with large molecular NLO responses. (iv) redox-activity of the metal centre may provide means of switching the NLO behaviour.[8,45,46]

Many transition metal complexes have been studied for their potential uses as NLO chromophores and an overview of some of these is presented here. This review is by no means comprehensive and further details can be found in a number of published reviews.[47-50]

1.7.1 Metallocenes

Since the observation of a SHG efficiency 62 times that of urea from *cis*-[1-ferrocenyl-2-(4-nitrophenyl)ethylene] (**1**),[7] metallocene complexes have become one of the most widely studied types of organometallic compound with NLO activity.

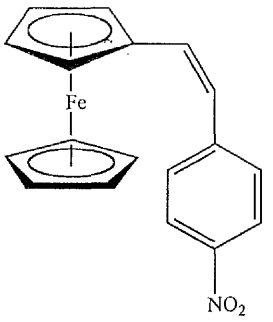

1

SHG_{1064}: 62 x urea

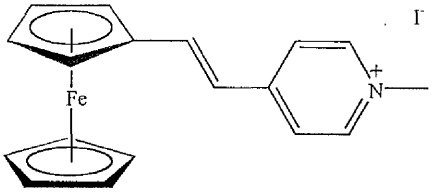

2

SHG_{1064}: 220 x urea

The highest SHG efficiency reported for a transition metal complex is that of compound **2**.[44,51] In attempts to encourage noncentrosymmetric crystal packing structures, resolved chiral metallocene chromophores have been prepared.[52] Although the individual molecules must crystallize in a noncentrosymmetric space group, they may pack with their neighbours in such a way that their dipoles cancel. Systematic NLO studies on metallocene compounds involving EFISHG and HRS measurements have allowed for structure-activity relationships to be derived.[43,53]

Metallocenes, unlike most purely organic chromophores, display two low energy ICT bands. These bands generally show positive solvatochromism, consistent with their corresponding transitions being associated with an increase in dipole moment.[54] Conformation of this has also been shown by Stark spectroscopic studies.[55] It has been suggested that the lowest energy transition corresponds with ICT from a metal-based HOMO to a ligand-based LUMO, whilst the higher energy transition can be assigned to a $\pi \rightarrow$ A process. Although this model contradicts previous assignments, where the low energy transition was assigned as being from the metal (HOMO) to the π^* orbital in the bridge,[43,56] it fits with the results obtained in the most recent studies. In any case, it is clear that the electronic structures of such chromophores

are relatively complicated and therefore application of the TSM to derive β_0 values should be approached with caution, if at all.

Calabrese *et al.* showed that replacement of the ferrocene unit with a ruthenocene moiety causes a decrease in β and this can be attributed to the Ru^{II} unit being a less efficient D.[43] Ruthenocene complexes seem more likely to crystallize in centrosymmetric space groups when compared to their ferrocene analogues,[44] and although the former possess smaller NLO responses these are compensated for in part by increased optical transparency.[57]

Recent work in this area has involved the synthesis of fullerene-ferrocene dyads by Tsuboya *et al.*[58] The quadratic NLO responses of three fullerene-containing dyads were measured using HRS at 1064 nm. Comparison of complex **3** with the purely organic phenylacetylene derivative **4**[57,59] confirms that the ferrocenyl group acts as an efficient electron donor group.

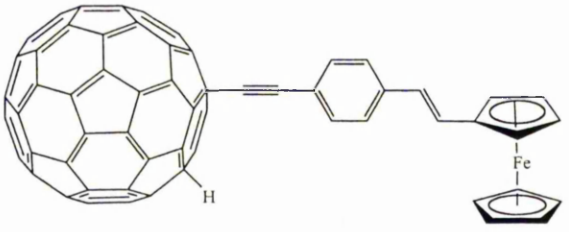

3

$\beta_0 = 317 \times 10^{-30}$ esu

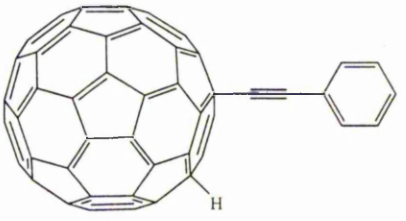

4

$\beta_0 = 83 \times 10^{-30}$ esu

Meyer-Friedrichsen *et al.* studied a series of ruthenium-containing vinylogue mono- and bimetallic sesquifulvalene complexes (*e.g.* **5**) using HRS at 1064 nm. These molecules appear to exhibit moderate NLO responses ($\beta_0 = 17–105 \times 10^{-30}$ esu), but

the derived β_0 values are likely to be underestimated because only the lowest energy ICT band was taken into consideration.[60]

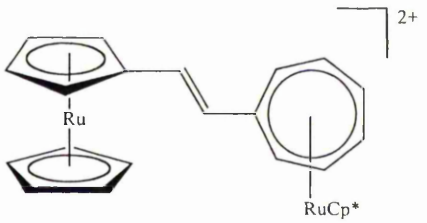

5

λ_{max} = 594, 438 nm
$\beta_0 = 17 \times 10^{-30}$ esu

1064 nm HRS studies could not be carried out on related ferrocenyl complexes as they exhibit fluorescence due to two-photon absorption.[61,62]

A highly efficient ferrocenyl NLO material has been reported by Chiffre *et al.* X-ray crystallographic studies of compound **6** revealed the adoption of the *P*1 space group with the molecular dipoles being perfectly aligned.[63]

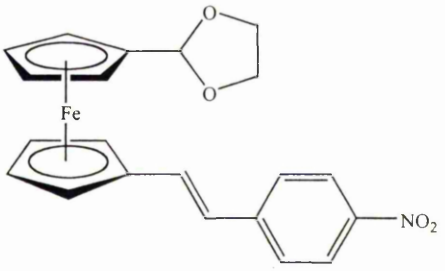

6

SHG_{1907} = 140 x urea

Balavoine *et al.* introduced chirality into a series of (*E*)-(2-(4-nitrophenyl)ethenyl)ferrocenes where the cyclopentadienyl (Cp) ring is substituted in the 2-position.[42] The trans isomer of compound **1** possesses a larger molecular NLO response ($\beta_0 = 31 \times 10^{-30}$ esu) than the cis isomer, but gives no SHG, probably due to the adoption of a centrosymmetric space group.[7,43] It was found that 2-substitution of the Cp ring with a -$SiMe_3$ group (compound **7**) gives an efficient SHG material.

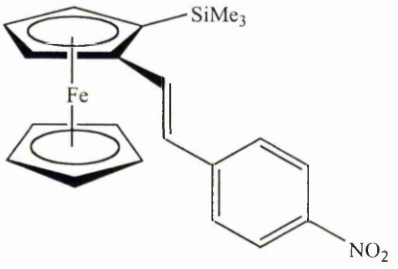

7

SHG_{1907} = 100 x urea

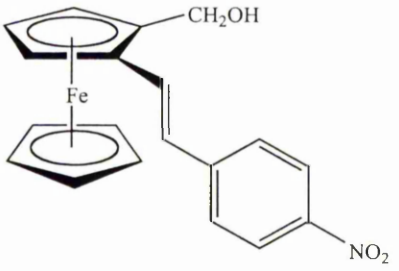

8

SHG_{1907} = 20 x urea

1.7.2 Carbonyl complexes

In 1986, Frazier and co-workers screened the SHG efficiency of a variety of group 6 metal carbonyl arene pyridyl or chiral phosphine complexes.[64] These complexes, such as Cr(η^6-styrene)$(CO)_3$ (**9**), showed only small SHG efficiencies.

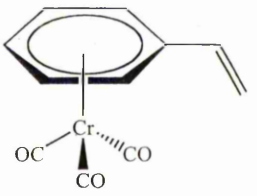

9

SHG = 1.8 x ADP

Calabrese and Tam screened the SHG efficiencies of a range of metal carbonyl complexes with pyridine or 2,2′-bipyridine ligands. The SHG efficiencies are in the region of 0.1–3 times that of urea,[65] and these low values were attributed to centrosymmetric packing of the molecules in the solid state.

EFISHG using a 1064 nm laser fundamental was used to probe the molecular NLO responses of a range of pentacarbonyl(pyridine/styrylpyridine)tungsten complexes, such as **10**. Although the NLO responses of these complexes are larger than those of the uncoordinated ligands, the β values obtained are still quite modest.[66-68]

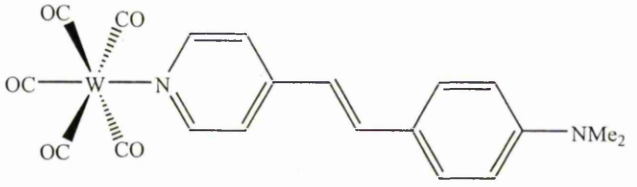

10

λ_{max} = 421 nm
$\beta_{1064} = 61 \times 10^{-30}$ esu

It has been suggested that these low β values arise from poor coupling between the metal carbonyl fragment and the π-network of the pyridyl ligands.[68]

Martín *et al.* have recently reported the first examples of tetrathiafulvalenyl (TTF) and π-extended TTF D-π-A systems bearing a tricarbonyl(η^6-arene)chromium moiety as the acceptor group, such as **11** and **12**.[69]

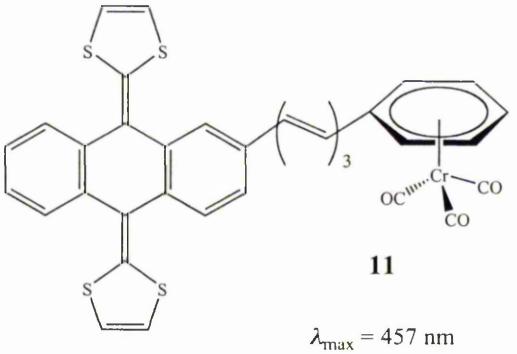

11

λ_{max} = 457 nm
$\mu\beta = 70 \times 10^{-30}$ esu

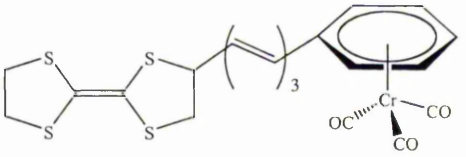

12

λ_{max} = 456 nm
$\mu\beta = 90 \times 10^{-30}$ esu

The NLO responses were determined by EFISHG at 1907 nm, and TD-DFT calculations revealed that both the ILCT and MLCT transitions are responsible for the NLO properties.

Pizzotti *et al.* observed the unexpected formation of a weak M–M bond when they attempted to bridge $[W(CO)_3(phen)(pyz)]$ (phen = 1,10-phenanthroline, pyz = pyrazine) to a range of metal carbonyl centres.[70] During the reaction the pyrazine ligand is lost and the $\{W(CO_3)(phen)\}$ unit acts as a σ-base, forming heteronuclear bimetallic compounds with weak M–M bonds, such as **13** and **14**. The visible absorption spectra reveal the presence of two bands in the region 385–517 nm, which are of equal intensity and exhibit solvatochromic behaviour. The lowest energy band has been attributed to the MLCT transition W → π* (phen). The origin of the higher energy band is unclear, but it is thought to originate from either a W → π* (phen) MLCT or a metal-to-metal charge-transfer (MMCT) process.

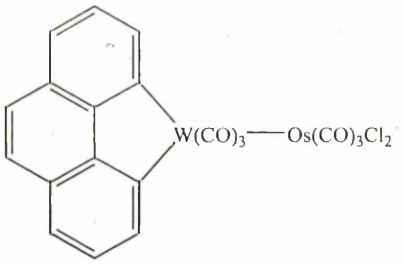

13

λ_{max} = 508, 415 nm
β_{1097} = 76 x 10^{-30} esu

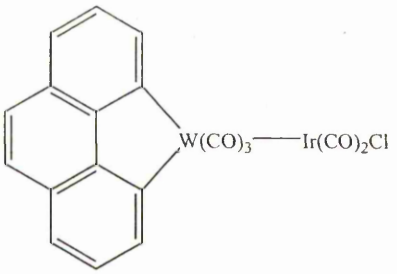

14

λ_{max} = 503, 384 nm
β_{1097} = 26 x 10^{-30} esu

The NLO responses of these complexes were measured using EFISHG at 1907 nm, affording β values in the range 13–76 × 10^{-30} esu. It was found that the M–M bond, even though only weak and slightly polar, significantly influences the NLO responses.

Carbonylrhenium bromide complexes with conjugated pyridines, such as **15**, have been synthesized and studied by Beck *et al.*[71]

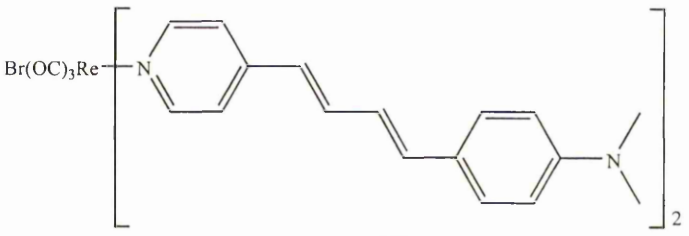

15

λ_{max} = 438 nm
β_{1500} = 208 x 10^{-30} esu
$\beta_{xxz} = \beta_{zzz}$ = 104 x 10^{-30} esu

The NLO responses were determined via HRS at the fundamental wavelengths of 1300 nm and 1500 nm in order to avoid multiphoton fluorescence. The separate tensor components could not be directly measured using this method, but were calculated using tensor addition, making the assumption that the pyridyl ligands act as separate molecules and lie at 90° to each other.

1.7.3 Schiff base complexes

Schiff base complexes incorporate the metal into the centre of the charge-transfer system, where it can act as either an D group or, if the ligand is substituted with strongly electron-donating or accepting substituents, as part of the conjugated system.[72] Metal(salen) derivatives are known to possess high thermal stability, and it has been suggested that the introduction of such compounds into polymers with high glass transition temperatures may lead to materials with NLO applications.[73]

The first report of the NLO properties of a non-polymeric Schiff base complex appeared in 1992 when Thami *et al.* used EFISHG at 1907 nm to study tetrahedral Co^{II} complexes of D/A-substituted hydrazone imine glyoxal derivatives with approximate C_{2V} symmetry, such as **16**.[74] The NLO responses of these complexes are increased when compared to that of the free ligand, although the origins of this effect are unclear.

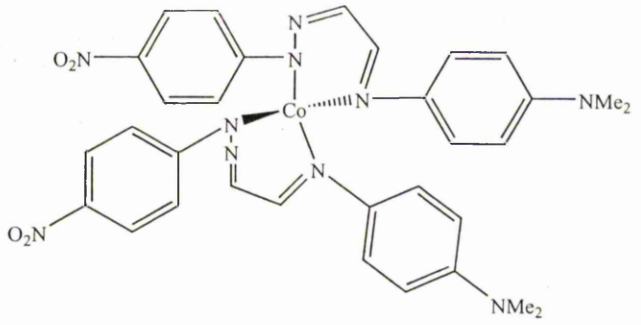

16

$\beta_{1907} = 70 \times 10^{-30}$ (dioxane)
100×10^{-30} ($CHCl_3$)

Di Bella and co-workers have investigated the NLO responses of various Ni^{II}(salen) derivatives such as **17** and **18** using EFISHG at 1907 nm in chloroform.[75]

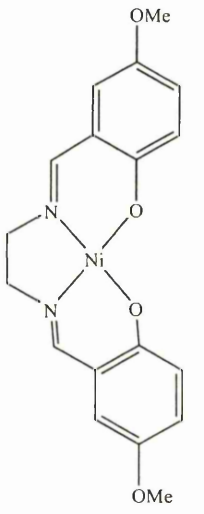

17

$\lambda_{max} = 398$ nm
$\beta_0 = 9.6 \times 10^{-30}$ esu

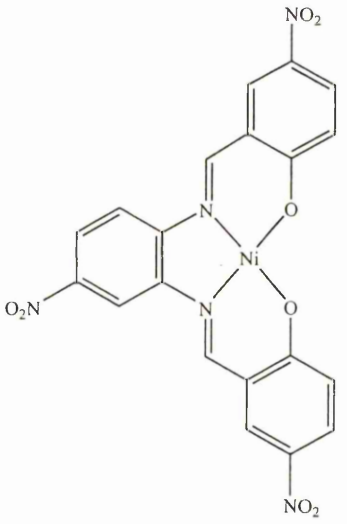

18

$\lambda_{max} = 570$ nm
$\beta_0 = 55 \times 10^{-30}$ esu

ZINDO calculations show that the NLO responses of these complexes are dominated by a HOMO → LUMO transition, with the Ni^{II} centre acting as the D. These studies

also show that moving from a closed-shell Ni^{II}(salen) to its open-shell Cu^{II} or Co^{II} analogues causes an increase in the NLO response.[76]

Recent work in this area has included an investigation of Cu^{II}–Gd^{III} Schiff base complexes by Lacroix *et al.*[77]

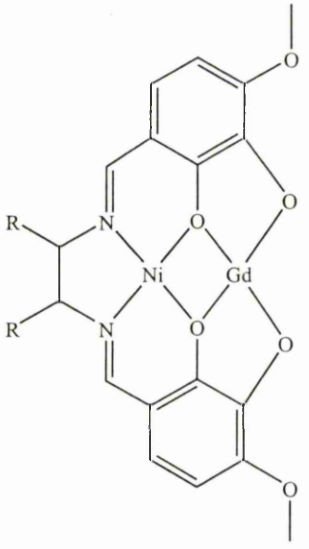

19
R = H

λ_{max} = 310nm

20
R = Ph

λ_{max} = 310nm
SHG = 0.3 x urea

Compound **20** crystallises in the noncentrosymmetric space group $P2_12_12_1$ and shows a moderate SHG efficiency. Unfortunately, the molecular NLO responses of **19** and **20** could not be determined experimentally due to dissociation of the complexes in water. Compound **20** also exhibits ferromagnetic coupling and it has been proposed that this molecule could be the basis of multiproperty materials.

Lacroix and co-workers have also synthesized some Schiff base complexes of Co, Ni or Cu with the novel ligand **21**.[78]

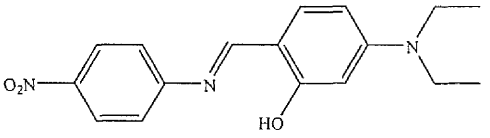

21

$\lambda_{max} = 434$ nm
$\beta_{1907} = 66 \times 10^{-30}$ esu

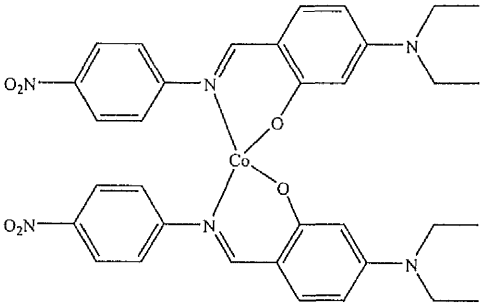

22

$\lambda_{max} = 446$ nm
$\beta_{1907} = 110 \times 10^{-30}$ esu

The complexes containing Ni^{II} or Cu^{II} both crystallize centrosymmetrically, with a planar arrangement of the ligand around the metal centre. The Co^{II} complex (**22**) however adopts the noncentrosymmetric space group *C*2/*c* with a pseudo-tetrahedral coordination sphere. EFISHG studies were carried out on the free ligand **21** and the Co^{II} complex and it was found that introduction of the Co^{II} centre causes an increase in the NLO response which is also accompanied by an increase in the thermal stability.

Panuzi *et al.* have synthesized OH-functionalized ortho-palladated complexes with Schiff base ligands. Related complexes, *e.g.* **23**, where the OH group is protected, were also synthesized to help generate detailed characterization and NLO data using EFISHG.[79]

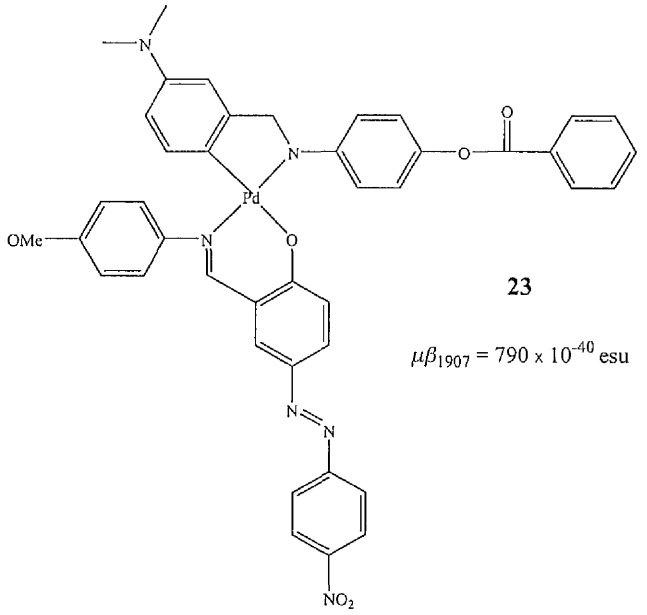

23

$\mu\beta_{1907} = 790 \times 10^{-40}$ esu

These OH-functionalized monomers were incorporated into main-chain polymers, which are amorphous, have good thermal and chemical stability and are fairly soluble in standard solvents. On the basis of the NLO measurements performed on the model complexes, large NLO activities can be expected for the polymers.[80]

1.7.4 Ruthenium ammine complexes

Ruthenium ammine complexes have been studied relatively extensively for their NLO properties, largely by Coe and co-workers. These studies have generally involved complexes of the type *trans*-$[Ru^{II}(NH_3)_4(L_D)(L_A)]^{2+}$, where L_D is an electron-rich ligand and L_A is an electron acceptor-substituted ligand. Initial work focused on the development of structure-activity relationships using HRS at a laser fundamental of 1064 nm.[81-84] Ruthenium ammine complexes such as **24–26** exhibit large β_0 values, which can be attributed to the presence of low energy MLCT

transitions between the electron rich d^6 Ru^{II} centre and the electron deficient acceptor group.

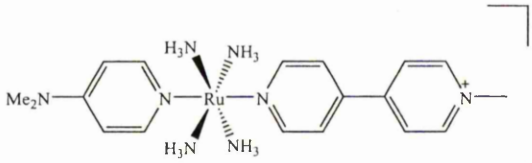

24

λ_{max} = 614 nm

$\beta_0 = 130 \times 10^{-30}$ esu

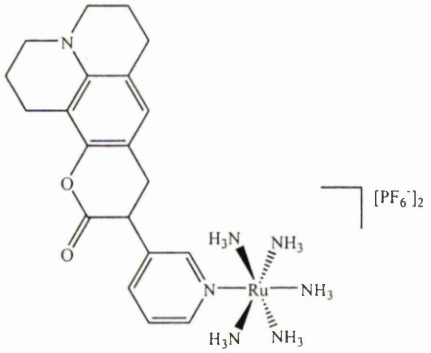

25

λ_{max} = 460 nm

$\beta_0 = 49 \times 10^{-30}$ esu

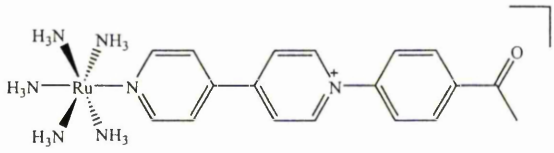

26

λ_{max} = 654 nm

$\beta_0 = 354 \times 10^{-30}$ esu

More recent work within this group has also employed Stark spectroscopy to evaluate the NLO responses.[85]

Recent published highlights have involved the comparison of the linear and NLO properties (measured using Stark spectroscopy) of dipolar pyridinium chromophores with Ru^{II} ammine or 4-(dimethylamino)phenyl D groups, such as **27** and **28**.[86-88]

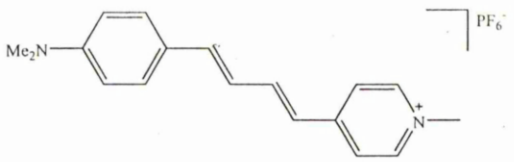

27

λ_{max} = 487 nm
$\beta_0 = 328 \times 10^{-30}$ esu

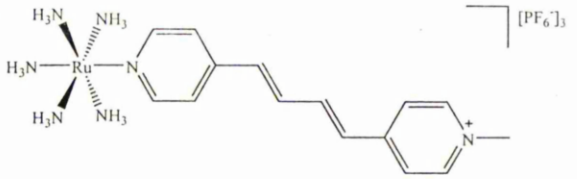

28

λ_{max} = 584 nm
$\beta_0 = 482 \times 10^{-30}$ esu

The effects on the linear and NLO properties of increasing the number of bridging ethylene units (n) was investigated within both systems. It is seen that as n increases within the purely organic system, normal optical behaviour is observed. However, in the Ru^{II} complexes unusual optical behaviour is seen, and the MLCT band begins to blue shift after $n = 1$. The NLO responses of these compounds, determined using Stark spectroscopy, show β_0 maximising at $n = 2$ for the metal complexes, but increasing as n increases within the purely organic systems. This behaviour was attributed to differences in the degree of D–A π-orbital overlap. Electrochemical, ^{1}H NMR and Stark spectroscopic studies show that such overlap is more effective in the purely organic chromophores.[87]

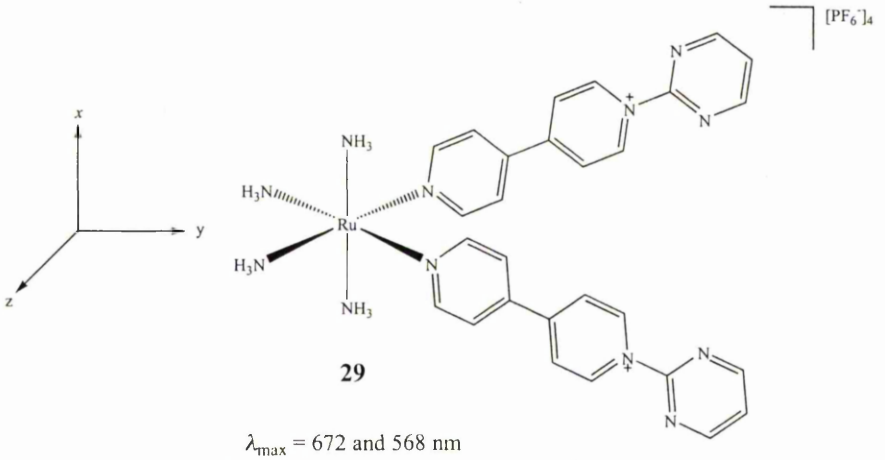

29

λ_{max} = 672 and 568 nm
$\beta_{zyy[Stark]} = 298 \times 10^{-30}$ esu, $\beta_{zzz[Stark]} = 110 \times 10^{-30}$ esu
$\beta_{800[HRS]} = 143 \times 10^{-30}$ esu

Two-dimensional chromophores incorporating a Ru^{II} ammine D group, such as **29**, have also been investigated within the Coe group, using both Stark spectroscopy and HRS.[89,90] These V-shaped dipolar chromophores contain monodentate 4,4′-bipyridyl-derived ligands and display multiple MLCT bands. They possess two non-zero components of the β tensor, β_{zzz} and β_{zyy}, which can both be estimated using Stark spectroscopy. TD-DFT studies indicate that the off-diagonal β_{zyy} response is the largest component and is associated with the lowest energy MLCT transition.

1.7.5 σ-Acetylide complexes

Complexes of functionalised σ-bonded acetylide ligands represent another important class of materials for NLO studies, largely developed by Humphrey and co-workers.[91] The metal centre in these chromophores acts as the D group and the complexes exhibit low energy MLCT transitions. These compounds are also of interest because of their ease of synthesis, linear structures, high thermal stabilities and their potential as building blocks for oligomeric and polymeric materials.[92] Group 8, 10 and 11 metals have been incorporated into the acetylide systems and various constituents of the D-π-A system have been modified to elucidate structure-activity relationships.[93]

Complexes of the group 8 metals are the most widely studied amongst σ-acetylide complexes, such as **30**–**32**.

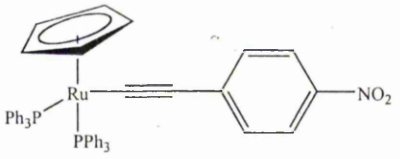

30

λ_{max} = 460 nm
$\beta_0 = 96 \times 10^{-30}$ esu

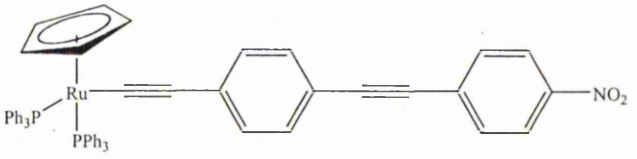

31

λ_{max} = 448 nm
$\beta_0 = 134 \times 10^{-30}$ esu

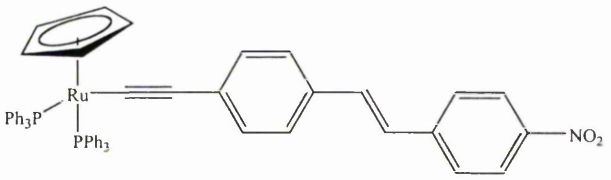

32

λ_{max} = 476 nm
$\beta_0 = 232 \times 10^{-30}$ esu

An increase in the NLO response can be achieved by increasing either the acetylide chain length,[94] or the A strength.[95,96] Bimetallics have been formed by metallation of the CN group in [Ru-C≡C-(*E*)-C=C-4-C_6H_4CN)$(PPh_3)_2(\eta$-indenyl)] with $Cr(CO)_5$, $W(CO)_5$ or $\{Ru(NH_3)_5\}^{3+}$,[95-97] with **33** having the largest value of β_0.

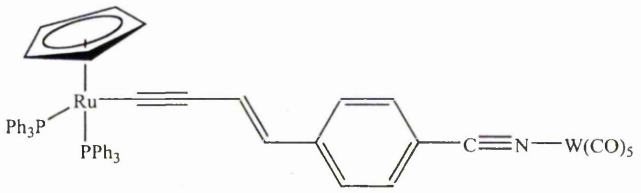

33

λ_{max} = 456 nm
$\beta_0 = 150 \times 10^{-30}$ esu

There is limited information available to date on the effect of varying the group 8 metal, but existing studies suggest that β increases in the order Fe ≤ Ru ≤ Os.[95-97]

Acetylide complexes containing Ni^{II} or Au^{I} have also been studied and electrochemical data indicate that the relative ease of oxidation (and by inference electron donor strength) follows the order $Au^{I} \leq Ni^{II} \leq Ru^{II}$. This trend is reflected in the MLCT absorption and HRS data, such as for **34–36**.[6] Although the 18 valence-electron complexes (of Ru^{II} and Ni^{II}) have larger nonlinearities than the 14-electron Au^{I} complex, the latter is considerably more transparent in the visible region.

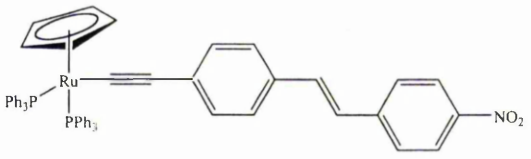

34

λ_{max} = 476 nm
$\beta_0 = 232 \times 10^{-30}$ esu

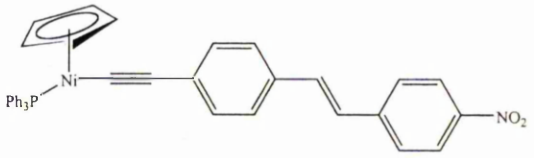

35

λ_{max} = 437 nm
$\beta_0 = 120 \times 10^{-30}$ esu

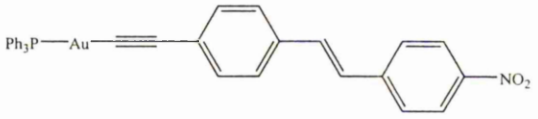

36

λ_{max} = 386 nm
$\beta_0 = 49 \times 10^{-30}$ esu

1.7.6 Complexes containing polypyridyl chelating ligands

Calabrese and Tam screened the SHG efficiencies of a variety of metal carbonyl complexes with the chelating ligand 2,2′-bipyridyl (2,2′-bpy),[65] but found only weak bulk NLO activities. The first EFISHG studies of complexes of 2,2′-bpy and phen ligands were described by Cheng *et al.* who determined β_0 for complexes of the type $M(CO)_4(phen)$ (M = Cr, Mo, W), such as **37**.[66,67]

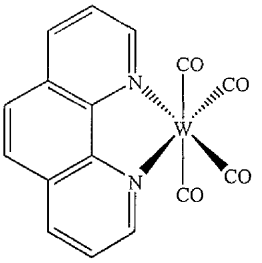

37

$\lambda_{max} = 492$ nm
$\beta_0 = 13 \times 10^{-30}$ esu

Bourgault and co-workers prepared a series of π-donor-substituted vinyl 2,2′-bpy derivatives coordinated to Re^{I}, Zn^{II} or Hg^{II}, such as **38–40,** and measured their NLO properties using EFISHG at 1340 nm.[99,100]

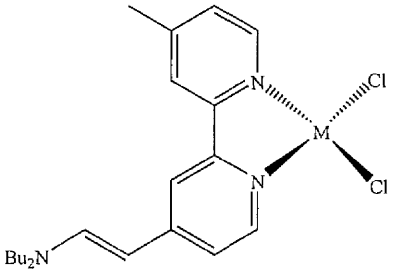

M = Zn	M = Hg	M = Re
38	**39**	**40**
$\lambda_{max} = 460$ nm	$\lambda_{max} = 442$ nm	$\lambda_{max} = 474$ nm
$\beta_0 = 71 \times 10^{-30}$ esu	$\beta_0 = 57 \times 10^{-30}$ esu	$\beta_0 = 31 \times 10^{-30}$ esu

It was observed that metal coordination causes significant increases in β_0 when compared with the free bpy ligand. The complexes containing the square planar Zn^{II} or Hg^{II} centres have increased NLO responses when compared with the octahedral complexes, which can be attributed to the MLCT and ILCT transitions occurring in

opposing directions in the latter. The Zn complexes have consistently larger β_0 values than their Hg analogues, correlating with Zn^{II} being the stronger Lewis acid.

Recent work by Sénéchal *et al.* employing chelating ligands has involved the synthesis of the first dipolar lanthanide complexes for second-order NLO studies.[101] A series of complexes (Ln = La^{III}, Gd^{III}, Dy^{III}, Yb^{III}) with an annelated dibutylaminophenyl-functionalised 2,2′:6′,2″-terpyridyl ligand, *e.g.* **41**, were subjected to HRS experiments at 1907 nm.

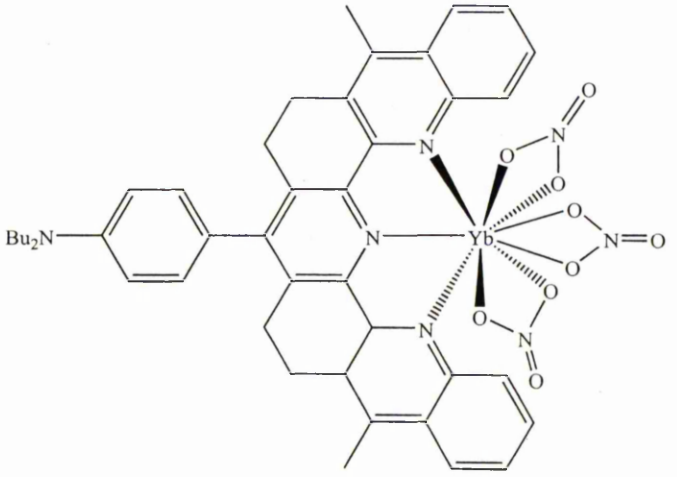

41

λ_{max} = 452 nm
$\beta_0 = 211 \times 10^{-30}$ esu

Addition of the lanthanide ion causes a blue shift in the ILCT band when compared to that of the free ligand (λ_{max} = 376 nm). There is an apparent increase in β_0 moving along the lanthanide series, although the sequential differences between the values are within experimental error. The β_0 for the Yb complex is 1.5 times that of the La complex, indicating that f electrons may contribute to the NLO responses.

Coe *et al.* have reported a series of complexes of the type **42**–**45** in which the electron-rich $\{Ru^{II}(NH_3)_4\}^{2+}$ centre is coordinated to 2,2′:4,4″:4′,4‴-quaterpyridyl ligands with either *N*-methyl or *N*-arylpyridinium groups.[90]

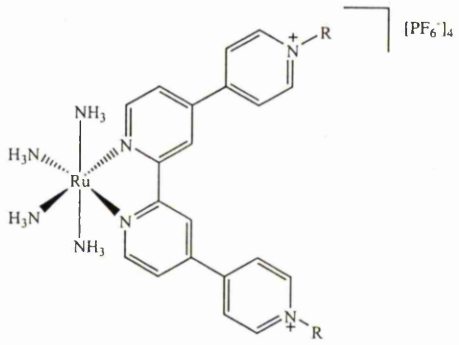

R = Me **42**	R = Ph **43**	R = AcPh **44**	R = Pym **45**
λ_{max} = 514 nm	λ_{max} = 544 nm	λ_{max} = 552 nm	λ_{max} = 574 nm
$\beta_{800[HRS]} = 32 \times 10^{-30}$ esu	$\beta_{800[HRS]} = 48 \times 10^{-30}$ esu	$\beta_{800[HRS]} = 40 \times 10^{-30}$ esu	$\beta_{800[HRS]} = 42 \times 10^{-30}$ esu
$\beta_{zyy[Stark]} = 72 \times 10^{-30}$ esu	$\beta_{0[Stark]} = 86 \times 10^{-30}$ esu	$\beta_{0[Stark]} = 97 \times 10^{-30}$ esu	$\beta_{0[Stark]} = 120 \times 10^{-30}$ esu
$\beta_{zzz[Stark]} = 62 \times 10^{-30}$ esu			

The NLO responses of these complexes were measured using both Stark spectroscopy and HRS at 800 nm. The complexes possess pseudo-C_{2v} symmetry, with two non-zero components of the β tensor, although these could only be resolved for the complex containing the *N*-methyl ligand (**42**).

Roberto and co-workers investigated the effects of coordination of a M^{II} centre (M = Cd or Zn) on the NLO properties of various substituted phen ligands, such as **46**, using EFISHG with a laser fundamental of 1340 nm.[102]

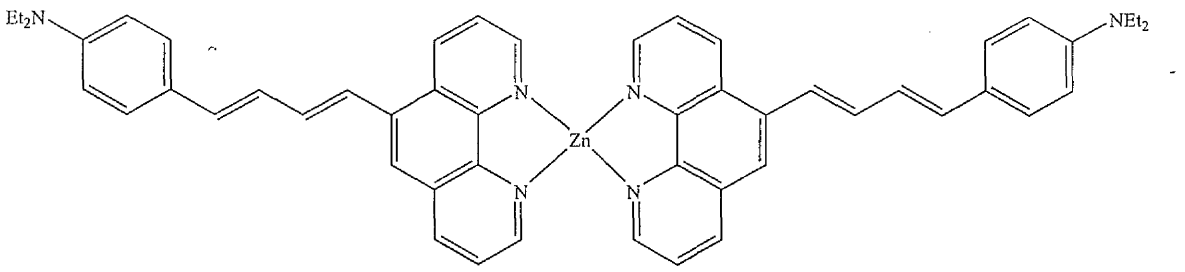

46

$\lambda_{max} = 432$ nm
$\beta_0 = 112 \times 10^{-30}$ esu

Coordination to the zinc centre causes enhancement of the NLO response, but similar behaviour is not seen in the cadmium complexes. This difference has been attributed to the stronger Lewis acidity of the Zn^{II} ion.

1.7.7 Octupolar complexes

Octupolar systems have the potential advantages over conventional dipolar species of combining noncentrosymmetric molecular structures with improved nonlinearity-transparency trade-offs.[103] Most octupolar chromophores studied to date are purely organic,[104] and are generally designed by the functionality of a central aromatic core. The first report of a metal-containing octupolar complex was by Zyss *et al.*,[105] who studied the NLO properties of the tris(bpy) and tris(phen) cations **47** and **48** using HRS at 1064 nm. These complexes possess D_3 symmetry and exhibit intense MLCT absorptions at about 460 nm.[106]

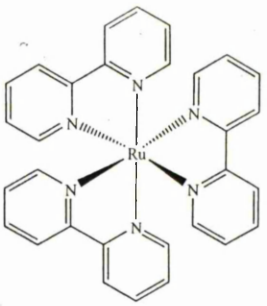

47

λ_{max} = 422 nm
β_{1064} = 210 x 10^{-30} esu

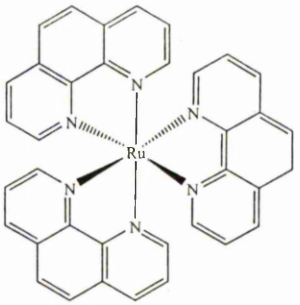

48

λ_{max} = 450 nm
β_{1064} = 170 x 10^{-30} esu

More recently, Maury and co-workers have reported a series of D_3 (Fe^{II}, Ru^{II}, Zn^{II}, Hg^{II}) and D_{2d} (Cu^{I}, Ag^{I}, Zn^{I}) octupolar complexes with a variety of functionalized 2,2′-bpy ligands.[106] For example, the octahedral Ru^{II} complex **49** possesses a very large hyperpolarizability (measured using HRS).

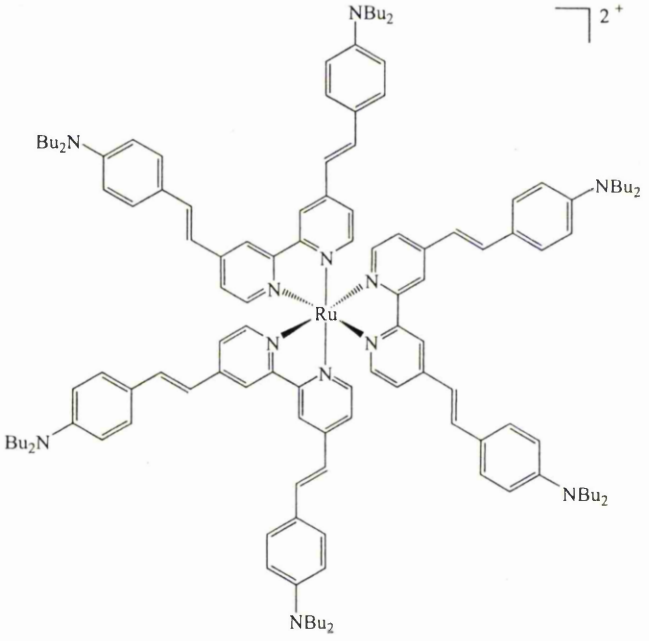

49

λ_{max} = 510 nm
β_0 = 675 x 10^{-30} esu

Le Bouder *et al.* have recently reported the NLO properties of multioctupolar Ru^{II} tris(2,2′-bpy) complexes. Controlled coordination chemistry was employed to build bimetallic (N = 2), trimetallic (N = 3), heptametallic (N = 7) and polymetallic (N = 14) (where N is the number of metal centres) assemblies, such as **50**, which were studied using HRS at 1907 nm.[107]

Trimer (N = 3)

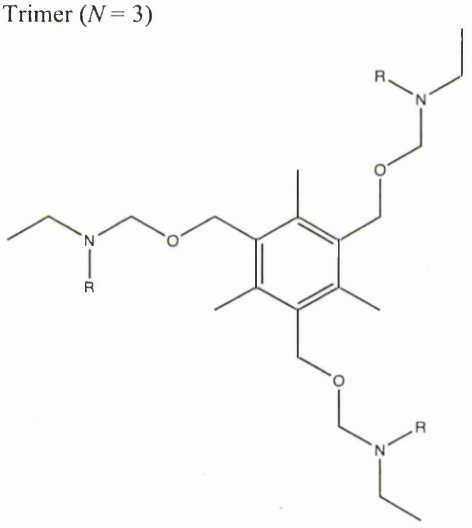

50

λ_{max} = 511 nm
$\beta_0 = 700 \times 10^{-30}$ esu

R =

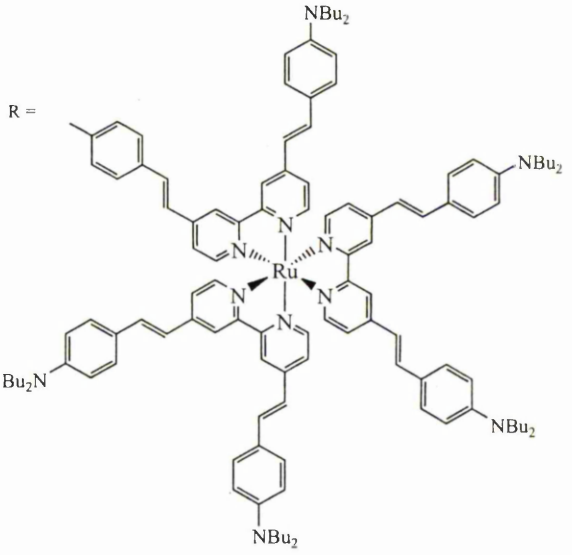

These complexes exhibit very intense visible MLCT absorptions and large quadratic hyperpolarizabilities. Their NLO responses increase on moving from the monomer to the dimer, trimer and heptamer, but then decrease for the polymer (N = 14). The heptamer has an extremely large β value (λ_{max} = 506 nm, $\beta_0 = 1271 \times 10^{-30}$ esu), which is comparable to that of the most efficient polyenic chromophore (λ_{max} = 826 nm, $\beta_0 = 1470 \times 10^{-30}$ esu),[108] but is significantly smaller than a recently reported multichromophoric dipolar dendron containing fifteen azobenzene units (λ_{max} = 475

nm, $\beta_0 = 3857 \times 10^{-30}$ esu).[109] There is also evidence for quasi-optimized octupolar ordering in this heptameric metallodendrimer.

1.7.8 Porphyrin complexes

The general structure of a porphyrin macrocycle consists of four pyrrolic subunits linked by four methine bridges. Such an extensive delocalized π-electron system leads to the presence of marked NLO effects.[110] Structural modifications at the edges can produce asymmetry within the molecule, and the incorporation of a metal centre enhances the overall conjugation and therefore the NLO response. Le Cours *et al.* reported the first example of an electronically asymmetric porphyrin.[111] In this report they described the synthesis and NLO properties (using EFISHG at 1907 nm) of some push-pull arylethynyl porphyrins containing Zn^{II} or Cu^{II}, such as **51**.

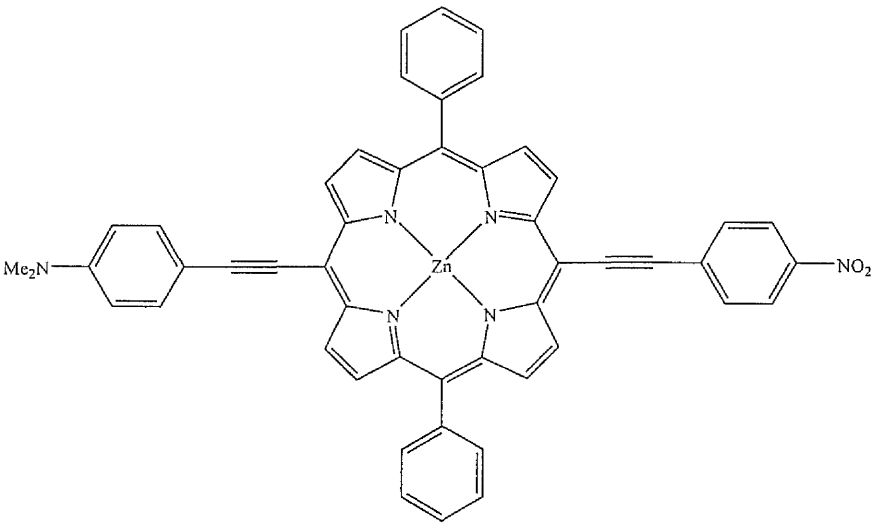

51

λ_{max} = 675 nm (Soret band)
450 nm (Q band)
$\beta_0 = 80 \times 10^{-30}$ esu

The NLO response was calculated using the Soret band with the TSM and it was found that compound **51** exhibits a reasonably large first hyperpolarizability.

Zhang *et al.* have recently studied the NLO properties of conjugated (porphinato)Zn(II)-based D–A chromophores with nitro-oligothiophenyl electron acceptors, such as **52**.[112]

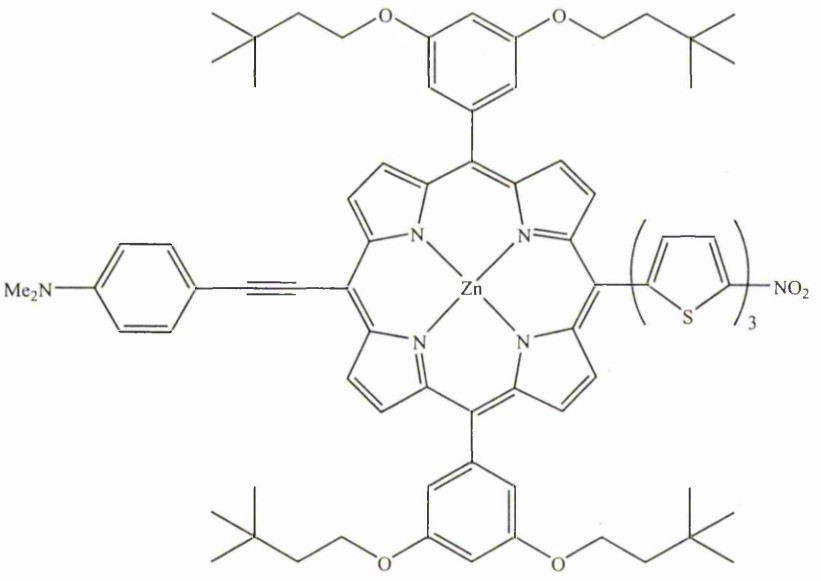

52

λ_{max} = 641 nm
579 nm
$\beta_{(800)}$ = 510 x 10^{-30} esu
$\beta_{(1300)}$ = 4350 x 10^{-30} esu

In such chromophores, increasing the number of oligothiophene units increases the NLO response, and the complex containing three thiophene units exhibits a large NLO response that is strongly frequency dependent.

1.7.9 Switching NLO responses

For a classical dipolar D–π–A system, modification of the electronic properties of any of the functional units will cause a change in the NLO response. Coe proposed three types of alterations,[8] which are represented in Figure 5.

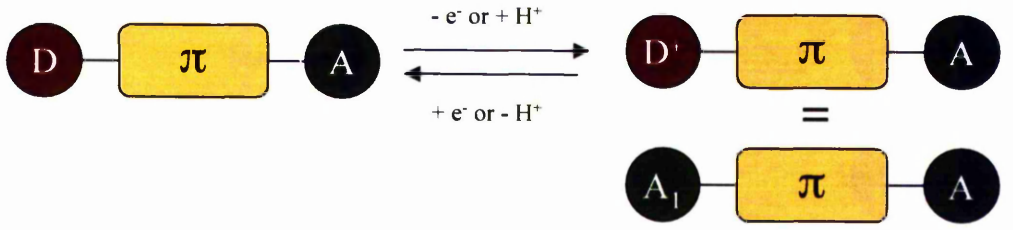

Type 1. Reduction of the donor capacity (by either proton or electron-transfer), making it more acceptor-like

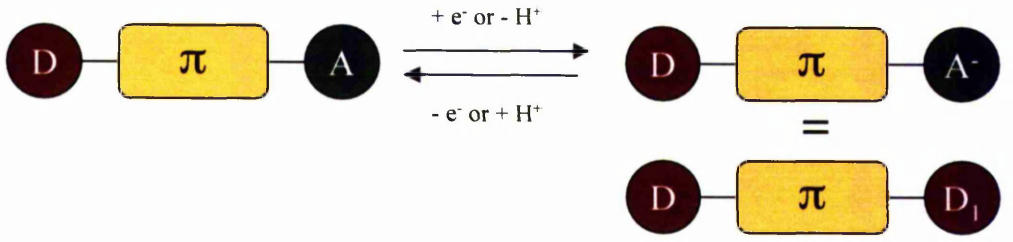

Type 2. Reduction of the acceptor capacity (by either proton or electron-transfer), making it more donor-like

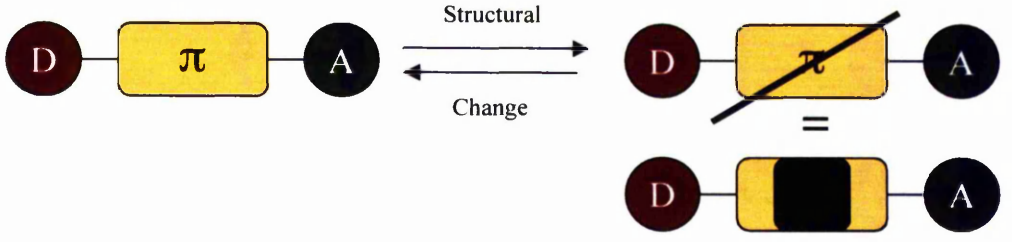

Type 3. Modification of the π-conjugated bridge, *i.e.* inserting a break

Figure 5: Approaches to switching the NLO response in a dipolar molecule

For such a switch to be of any practical use, the molecule must be stable in at least two states and reversibility of the switching effect is also essential. Approaches to switching have included photoisomerization, protonation/deprotonation and oxidation/reduction. Switching of the NLO response has been demonstrated in both organic and metal-containing chromophores,[45,46] but this section will only discuss switching effects in transition metal complexes.

The first report of a switchable molecular NLO system involving a transition metal chromophore was by Sakaguchi *et al.* in 1992, [113-115] who observed SHG photoswitching with a $[Ru(2,2'\text{-bpy})_3]^{2+/3+}$ derivative in Langmuir-Blodgett films (**53** and **53***).

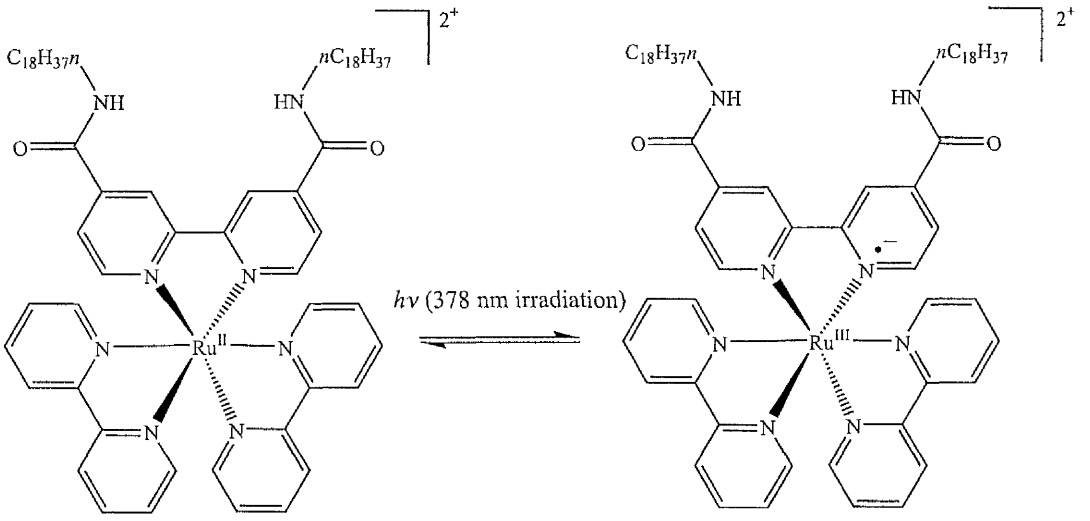

53 **53***

When the films are irradiated with a 378 nm laser, the SHG generated from a 590 nm dye laser decreases by about 30% in less than 2 ps. Restoration of the original signal

occurs within several hundred ps.[115] Irradiation with a 355 nm laser and a 1064 nm probe beam also causes similar effects.[116]

Coe *et al.* have investigated the effect of metal oxidation state on the quadratic hyperpolarizability using HRS at 1064 nm.[8] They demonstrated the effect of oxidising Ru^{II} to Ru^{III} in ammine complexes containing 4,4′-bipyridinium ligands (such as compound **26**). Oxidation with 1:1 30% aqueous H_2O_2/2M HCl causes a decrease in the intensity of the HRS signal and subsequent reduction with 62% $N_2H_4 \bullet H_2O$ completely restores the original signal.[8] The difference in the NLO responses between the oxidised and reduced forms is approximately 10–20 fold.

Weyland *et al.* have investigated the switching of NLO responses in Fe^{II}-Fe^{III} mixed-valence complexes such as **54**,[116] using HRS at 1064 nm.

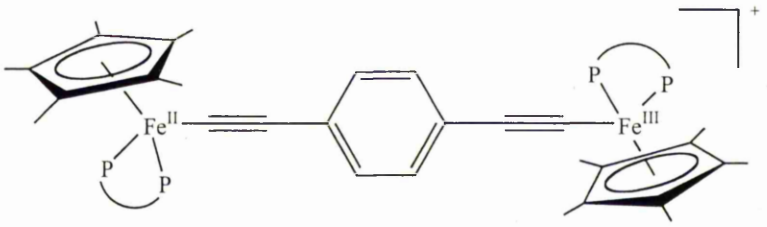

54

$\lambda_{max} = 413$ nm

These redox systems are fully reversible, with the mixed-valence complex **54** having a NLO response twice as large as that of the compounds (**55** and **56**).

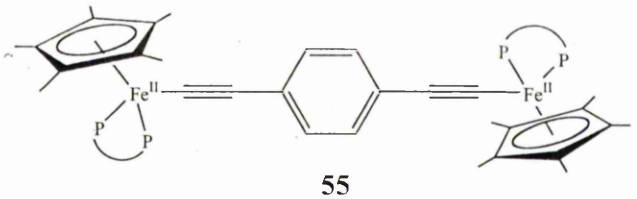

55

$\beta_0 = 180 \times 10^{-30}$ esu

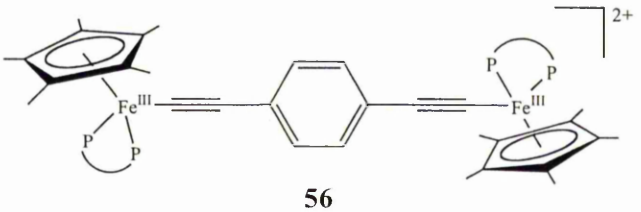

56

$\beta_0 = 200 \times 10^{-30}$ esu

Ward and co-workers have demonstrated a redox switch based on an octamethylferrocenyl donor unit (**57**), also using HRS at 1064 nm.[117]

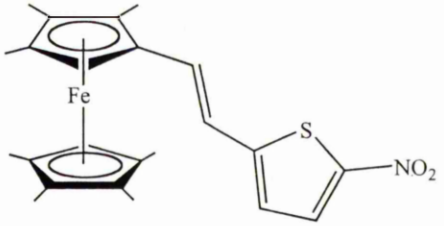

57

$\lambda_{max} = 586$ nm
$\beta_0 = 95 \times 10^{-30}$ esu

Oxidation of Fe^{II} to Fe^{III} by $[Bu_4N]Br_2$ caused a reduction of the NLO response to 10 $\times 10^{-30}$ esu. Upon re-reduction with hydrazine the original signal was restored. More recently, the reversible electrochemical switching of molecule **57** has also been demonstrated by using *in situ* HRS measurements.[118]

1.8 Aims and objectives

A major advantage of using organic molecules over simple inorganic crystalline salts is that their NLO responses can be tailored using synthetic chemistry, with any part of the chromophore being amenable to modification. As has been shown in the previous section, many different and diverse types of transition metal complex exhibit NLO effects which may be combined with properties such as redox and/or magnetic behaviour. Research in this field is still at a largely fundamental level, but new and perhaps unforeseen applications of multifunctional molecular NLO materials may be anticipated.

This project involves the syntheses and characterization of various new transition metal complexes, in which systematic changes to the D/A groups and the π-conjugated bridge are made. As the donor group *trans*-$\{Ru^{II}Cl(pdma)_2\}^+$ [pdma = 1,2-phenylenebis(dimethylarsine)], $\{Ru^{II}(NH_3)_5\}^{2+}$, *trans*-$\{Ru^{II}(NH_3)_4L\}^{2+}$ (L = pyridine or *N*-methylimidazole) or $\{Fe^{II}(CN)_5\}^{3-}$ have been employed, the last of which has never previously been used in NLO studies and introduces a new approach to protic switching of optical effects. All of the complexes feature pyridinium A units. The electronic and optical properties of these compounds have been studied using a range of techniques, allowing detailed comparisons to be drawn with previously reported related systems. The consequent elucidation of molecular structure-activity relationships serves to improve our understanding of the factors governing the NLO responses of transition metal-based chromophores. The identification of crystalline materials with favourable noncentrosymmetric structures is an additional but relatively minor objective of this work.

1.9 References

1. *The Principle of Nonlinear Optics*, Y. R. Shen, Wiley, New York, 1984
2. *Principles and Applications of Nonlinear Optical Materials*, Eds. R. W. Munn and C. N. Ironside, Blackie Academic and Professional, London, 1993
3. *Nonlinear Optics of Organic Molecules and Polymers*, Eds. H. S. Nalwa and S. Miyata, CRC Press, Boca Raton, 1997
4. P. A. Franken, A. E. Hill, C. W. Peters and G. Weinreich. *Phys. Rev. Lett.*, 1961, **7**, 118 – 120
5. S. Allen in *Molecular Electronics*, Ed G. J. Ashwell, Research Studies Press, Taunton, 1992
6. I. R. Whittall, A. M. McDonagh and M. G. Humphrey, *Adv. Organomet. Chem.*, 1998, **42**, 291 – 368
7. M. L. H. Green, S. R. Marder, M. E. Thompson, J. A. Brandy, D. Bloor, P. V. Kolinsky and R. J. Jones, *Nature*, 1987, **330**, 360 – 362
8. B. J. Coe, S. Houbrechts, I. Asselberghs and A. Persoons, *Angew. Chem. Int. Ed.*. 1999 **38**, 366 – 369
9. *Organic Nonlinear Optical Materials, Advances in Nonlinear Optics Vol 1*, Ch. Bosshard, K. Sutter, Ph. Prêtre, J. Hulliger, M. Flörsheimer, P. Kaatz and P. Günter, Gordon and Breach, Amsterdam, 1995
10. G. H. Cross in *Introduction to Molecular electronics*, Eds. M. C. Petty, M. R. Bryce and D. Bloor, Edward Arnold Press, London, 1995
11. S. Nagahama, T. Yanamoto, M. Sano and T. Mukai, *Phys. Stat. Sol. A, Appl. Res.*, 2002, **190(1)**, 235 – 246
12. I. Akasaki, *Mater. Sci. and Eng. B*, 2000, **B74**, 101 – 106

13. R. Martin, *Chemistry and Industry*, 1999, **5**, 173 – 180

14. S. R. Marder in *Inorganic Materials*, Eds. D. W. Bruce and D. O'Hare, Wiley, Chichester, 1992

15. *Molecular NLO materials, Physics and Devices*, Ed. J. Zyss, Academic Press, San Diego, 1994

16. B. L. Davydov, L. D. Derkacheva, V. V. Dunina, M. E. Zhabotinskii, V. K. Zolin. L. G. Kreneva and M. Samokhina, *JEPT letters,* 1970, **12**, 16 – 18

17. L. T. Cheng, W. Tam. S. R. Marder, A. E. Stiegman, G. Rikken and C. W. Spangler, *J. Phys. Chem.,* 1991, **95**, 10643 – 10652

18. J. L. Oudar and D. S. Chemla, *J. Chem. Phys.,* 1977, **66**, 2664 – 2668

19. J. L. Oudar, *J. Chem. Phys.,* 1977, **67**, 446 – 457

20. C. B. Gorman and S. R. Marder, *Proc. Nat. Acad. Sci. USA,* 1993, **90**, 11297 – 11301

21. S. R. Marder, B. Kippslsen, A. K.-Y. Jen and N. Peyghambarian, *Nature*, 1997, **388**, 845 – 851

22. S. R. Marder, D. N. Beratan and L.-T. Cheng, *Science,* 1991, **252**, 103 – 106

23. S. R. Marder, L.-T. Cheng, B. G. Tiemann, A. C. Friedli, M. Blanchard-Desce, J. W. Perry and J. Skindhoj, *Science*, 1994, **263**, 511 – 514

24. F. Meyers, S. R. Marder, B. M. Pierce and J. L. Bredas, *J. Am. Chem. Soc.,* 1994, **116**, 10703 - 10714

25. S. R. Marder, J. W. Perry, B. G. Tiemann, C. B. Gorman, S. Gilmour, S. L. Biddle and G. Bourhill, *J. Am. Chem. Soc.,* 1993, **115**, 2524 – 2526

26. S. R. Kurtz and T. T. Perry, *J. Appl. Phys.,* 1968, **39**, 3798 – 3813

27. B. F. Levine, C. G. Bethea, *Appl. Phys. Lett.,* 1974, **24**, 445 – 447

28. J. L. Oudar and H. Le Person, *Opt. Commun.,* 1975, **15**, 258 – 262

29. K. D. Singer and A. F. Garito, *J. Chem. Phys.*, 1981, **75**, 3572 – 3580

30. J. A. Giordmaine, *Phys. Rev. A,* 1965, **138A**, 1599 – 1606

31. K. Clays and A. Persoons, *Phys. Rev. Lett.*, 1991, **66**, 2980 – 2983

32. K. Clays and A. Persoons, *Rev. Sci. Instrum.*, 1992, **63**, 3285 – 3289

33. E. Hendrickx, K. Clays and A. Persoons, *Acc. Chem. Res.*, 1998, **31**, 675 – 683

34. S. N. Yaliraki and R. J. Silbey, *J. Chem. Phys.*, 1999, **111**, 1561 – 1568

35. Y. K. Shin, B. S. Brunschwig, C. Creutz and N. Sutin, *J. Phys. Chem. A.*, **1996**, 100, 8157 – 8169

36. G. U. Bublitz and S. G. Boxer, *Annu. Rev. Phys. Chem.*, 1997, **48**, 213 – 242

37. G. U. Bublitz, R. Ortiz, S. R. Marder and S. G. Boxer, *J. Am. Chem. Soc.*, 1997, **119**, 3365 – 3376

38. B. S. Brunschwig, C. Creutz and N. Sutin, *Coord. Chem. Rev.*, 1998, **117**, 61 – 79

39. W. D. Joseph, N. R. Pradhan, S. Singh and D. N. Rao, *Current Science*, 2004, **86**, 1283 – 1287

40. W. Liptay in *Excited States Vol. 1.*, Ed. E. C. Lum, Academic Press, New York, 1974

41. A. Willetts, J. E. Rice, D. M. Burland and D. P. Shelton, *J. Chem. Phys.* 1992, **97**, 7590 – 7599.

42. G. G. A. Balavoine, J.-C. Daran, G. Iftime, P. G. Lacroix, E. Manoury, J. A. Delaire, I. Maltey-Fanton, K. Nakatani and S. Di Bella, *Organometallics*, 1999, **18**, 21 – 29

43. J. C. Calabrese, L.-T. Cheng, J. C. Green, S. R. Marder and W. Tam, *J. Am. Chem. Soc.*, 1991, **113**, 7227 – 7232

44. S. R. Marder, J. W. Perry, B. G. Tiemann and W. P. Schaefer, *Organometallics,* 1991, **19**, 1896 – 1901

45. B. J. Coe, *Chem. Eur. J.,* 1999, **5**, 2464 – 2471

46. I. Asselberghs, K. Clays, A. Persoons, M. D. Ward and J. McCleverty, *J. Mater. Chem.,* 2004, **14,** 2831 – 2839

47. S. Di Bella, *Chem. Soc. Rev.,* 2001, **30**, 355 – 366

48. B. J. Coe, in *Nonlinear optical properties of metal complexes* in *Comprehensive Coordination Chemistry II.,* Eds. J. A. McCleverty and T. J. Meyer, Elsevier, Oxford, 2004 Vol 9, pp. 621 – 687

49. H. Le Bozec and T. Renouard, *Eur. J. Inorg. Chem.*, 2000, **2**, 229 – 239

50. N. J. Long, *Angew. Chem. Int. Ed. Eng.,* 1995, **34**, 21 – 38

51. S. R. Marder, J. W. Perry, B. G. Tiemann, W. P. Schaefer, P. C. Groves and K. J. Perry, *Proc. SPIE Int. Soc. Opt. Eng.,* 1989, **1147**, 108 – 115

52. H. E. Bunting, M. L. H. Green, S. R. Marder, M. E. Thompson, D. Bloor, P. V. Kolinsky and R. J. Jones, *Polyhedron,* 1992, **11**, 1489 – 1499

53. M. Blanchard-Desce, C. Runser, A. Fort, M. Barzoukas, J. –M. Lehn, V. Bloy and V. Alain, *Chem. Phys. Lett.,* 1995, **199**, 253 – 261

54. P. D. Beer and H. Sikanyika, *Polyhedron*, 1990, **9**, 1091 – 1094

55. J. W. Perry and S. R. Marder, *J. Am. Chem. Soc.,* 1999, **121**, 3715 – 3723

56. D. R. Kanis, M. A. Ratner and T. J. Marks, *J. Am. Chem. Soc.,* 1992, **114**, 10338 – 10357

57. S. Barlow and S. R. Marder, *Chem. Commun.,* 2000, 1555 – 1562

58. N. Tsuboya, R. Hamasaki, M. Ito, M. Mitsuishi, T. Miyashita and Y. Yumansoto, *J. Mater. Chem.,* 2003, **13**, 511 – 513

59. R. Hamasaki, M. Ito, M. Lamrani, M. Mitsuishi, T. Miyashita and Y. Yamamoto, *J. Mater. Chem.,* 2003, **13**, 21 – 26

60. T. Meyer-Friedrichsen, H. Wong, M. H. Prosenc and J. Heck, *Eur. J. Inorg. Chem.*, 2003, **5**,936 – 946

61. H. Wong, T. Meyer-Friedrichsen, T. Farrell, C. Mecker and J. Heck, *Eur. J. Inorg. Chem.,* 2000, **4**, 631 – 646

62. T. Meyer-Friedrichsen, C. Mecker, M. H. Prosenc and J. Heck, *Eur. J. Inorg. Chem.*, 2002, **1**, 239 – 248

63. J. Chiffre, F. Averseng, G. G. A. Balavoine, J. –C. Daran, G. Iftime, P. G. Lacroix, E. Manoury and K. Nakatani, *Eur. J. Inorg. Chem.,* 2001, **9**, 2221 – 2226

64. C. C. Frazier, M. A. Harvey, M. P. Cockerham, H. M. Hand, E. A. Chauchard and C. H. Lee, *J. Phys. Chem.,* 1986, **90**, 5703 – 5706

65. J. C. Calabrese and W. Tam, *Chem. Phys. Lett.,* 1987, **133**, 244 – 245

66. L. –T. Cheng, W. Tam and G. R. Meredith, *Mol. Cryst. Liq. Cryst.,* 1990, **189**, 137 – 153

67. L.-T. Cheng, W. Tam and D. F. Eaton, *Organometallics*, 1990, **9**, 2856 – 2857

68. D. R. Kanis, P. G. Lacroix, M. A. Ratner and T. J. Marks, *J. Am. Chem. Soc.,* 1994, **116,** 10089 – 10102

69. B. Insuatsty, C. Atienza, C. Seoane, N. Martin, J. Garin, J. Orduna, R. Alcalá and B. Villacampa, *J. Org. Chem.,* 2004, **69**, 6986 – 6995

70. M. Pizzotti, R. Ugo, C. Dragonetti, E. Annoni, F. Demartin and P. Mussini, *Organometallics,* 2003, **22**, 4001 – 4011

71. O. Briel, K. Sünkel, I. Krossing, H. Nöth, E. Schmälzlin, K. Meerholz, C. Bräuchle and W. Beck, *Eur. J. Inorg. Chem.* 1999, **3**, 483 – 490

72. S. Di Bella and I. Fragala, *Synth. Met.,* 2000, **115**, 191 – 196

73. R. Dagani, *Chem. Eng. News,* 1999, **March 4**, 22 – 27

74. T. Thami, P. Bassoul, M. A. Petit, J. Simon, A. Fort, M. Barzoukas and A. Villaeys, *J. Am. Chem. Soc.,* 1992, **114**, 915 – 921

75. S. Di Bella, I. Fragala, I. Ledoux, M. A. Diaz-Garcia, P. G. Lacroix and T. J. Marks, *Chem. Mater.,* 1994, **6**, 881 – 883

76. S. Di Bella, I. Fragala, I. Ledoux and T. J. Marks, *J. Am. Chem. Soc.,* 1995, **117,** 9481 – 9485

77. O. Margeat, P. Lacroix, J. P. Costes, B. Donnadieu, C. Lepetit and K. Nakatani, *Inorg. Chem.,* 2004, **43**, 4743 – 4750

78. P. G. Lacroix, F. Averseng, I. Malfant and K. Nakatani, *Inorg. Chim. Acta.,* 2004, **357**, 3825 – 3835

79. F. Cariati, U. Caruso, R. Centore, A. DeMaria, M. Fusco, B. Panuzi, A. Roviello and A. Tuzi, *Inorg. Chim. Acta.,* 2004, **357**, 548 – 556

80. C. Heldmann, D. Neher, H. –J. Winkelhahn and G. Wegner, *Macromol.* 1996, **29**, 4697 – 4705

81. B. J. Coe, S. Hayat, R. L. Beddoes, M. Helliwell, J. C. Jeffery, S. R. Batten and P. S. White, *J. Chem. Soc. Dalton Trans.,* 1997, **37**, 1705 – 1711

82. B. J. Coe, M. C. Chamberlain, J. P. Essex-Lopresti, S. Gaines, J. C. Jeffery, S. Houbrechts and A. Persoons, *Inorg. Chem.,* 1997, **36**, 3284 – 3292

83. B. J. Coe, J. P. Essex-Lopresti, J. A. Harris, S. Houbrechts and A. Persoons, *Chem. Comm.* 1997, 1645 – 1646

84. B. J. Coe, J. A. Harris, L. J. Harrington, J. C. Jeffery, L. H. Rees, S. Houbrechts and A. Persoons, *Inorg. Chem.,* 1998, **37**, 3391 – 3399

85. B. J. Coe, J. A. Harris and B. S. Brunschwig, *J. Phys. Chem. A,* 2002, **106**, 897 – 905

86. B. J. Coe, L. A. Jones, J. A. Harris, B. S. Brunschwig, I. Asselberghs, K. Clays and A. Persoons, *J. Am. Chem. Soc.,* 2003, **125**, 862 – 863

87. B. J. Coe, L. A. Jones, J. A. Harris, B. S. Brunschwig, I. Asselberghs, K. Clays, A. Persoons, J. Garin and J. Orduna, *J. Am. Chem. Soc.,* 2004, **126**, 3880 – 3891

88. B. J. Coe, L. A. Jones, J. A. Harris, I. Asselberghs, K. Wostyn, K. Clays, A. Persoons, B. S. Brunschwig, J. Garin and J. Orduna, *Proc. SPIE Int. Soc. Opt. Eng.,* 2003, **5212**, 122 – 136

89. B. J. Coe, J. A. Harris and B. S. Brunschwig, *Dalton Trans.,* 2003, **12**, 2384 – 2386

90. B. J. Coe, J. A. Harris, L. A. Jones, B. S. Brunschwig, K. Song, K. Clays, J. Garin, J. Orduna, S. J. Coles and M. B. Hursthouse, *J. Am. Chem. Soc.,* 2005, **127**, 4845 – 4859

91. M. P. Cifuentes and M. G. Humphrey, *J. Organomet. Chem.,* 2004, **689**, 3968 – 3981

92. N. J. Long and C. K. Williams, *Angew. Chem. Int. Ed.,* 2003, **42**, 2586 – 2617

93. C. E. Powell and M. G. Humphrey, *Coord. Chem. Rev.,* 2004, **248**, 725 – 756

94. S. K. Hurst, M. P. Cifuentes, J. P. L. Morrall, N. T. Lucas, I. R. Whittall, M. G. Humphrey, I. Asselberghs, A. Persoons, M. Samoc, B. Luther-Davies and A. C. Willis, *Organometallics*, 2001, **20**, 4664 – 4675

95. V. Cadierno, S. Conejero, M. Pilar Gamasa, J. Gimeno, I. Asselberghs, S. Houbrechts, K. Clays, A. Persoons, J. Borge and S. García-Granda, *Organometallics*, 1999, **18**, 582 – 597

96. S. Houbrechts, K. Clays, A. Persoons, V. Cadierno, M. Pilar Gamasa and J. Gimeno, *Organometallics*, 1996, **15**, 5266 – 5268

97. S. Houbrechts, K. Clays, A. Persoons, V. Cadierno, M. P. Gamasa, J. Gimeno, I. R. Whittall and M. G. Humphrey, *Proc. SPIE Int. Soc. Opt.* 1996, **2852**, 98 – 108

98. C. E. Powell, M. P. Cifuentes, A. M. McDonagh, S. K. Hurst, N. T. Lucas, C. D. Delfs, R. Stranger, M. G. Humphrey, S. Houbrechts, I. Asselberghs, A. Persoons and D. C. R. Hockless, *Inorg. Chim. Acta.,* 2003, **352**, 9 – 18

99. M. Bourgault, C. Mountassir, H. Le Bouzec, I. Ledoux, G. Pucetti and J. Zyss, *J. Chem. Soc. Chem. Commun.,* 1993, **21**, 1623 –1624

100. M. Bourgault, K. Baum, H. Le Bozec, G. Pucetti, I. Ledoux and J. Zyss, *New. J. Chem.,* 1998, **22**, 517 – 523

101. K. Sénéchal, L. Toupet, I. Ledoux, J. Zyss, H. Le Bozec and O. Maury, *Chem. Commun.,* 2004, 2180 – 2181

102. D. Roberto, R. Ugo, F. Tessore, E. Lucenti, S. Quici, S. Vezza, P. Fantucci, I. Invernizzi, S. Bruni, I. Ledoux-Rak and J. Zyss, *Organometallics,* 2002, **21**, 161 – 170

103. O. Maury and H. Le Bozec, *Acc. Chem. Res.,* 2005, **38**, 691 – 704

104. O. Riant, G. Bluet, S. Brasselet, N. Druze, I. Ledoux, F. Lefloch, A. Skibniewski and J. Zyss, *Mol. Cryst. Liq. Cryst. Sci. and Tech. Sec. A.,*1998, **322**, 35 – 42

105. J. Zyss, C. Dhenaut, T. Chauvan and I. Ledoux, *Chem. Phys. Lett.,* 1993, **206**, 409 – 414

106. O. Maury, L. Viau, K. Sénéchal, B. Corre, J.-P. Guégan, T. Renouard, I. Ledoux, J. Zyss and H. Le Bouzec, *Chem. Eur. J.*, 2004, **10**, 4454 – 4466

107. T. Le Bouder, O. Maury, A. Bondon, K. Costuas, E. Amouyal, I. Ledoux, J. Zyss and H. Le Bozec, *J. Am. Chem. Soc.,* 2003, **125**, 12284 – 12299

108. M. Blanchard-Desce, V. Alain, P. V. Bedworth, S. R. Marder, A. Fort, C. Runser, M. Barzoukas, S. Lebus and R. Wortmann, *Chem. Eur. J.,* 1997, **3**, 1091 – 1104

109. S. Yokoyama, T. Nakahama, A. Otomo and S. Mashiko, *J. Am. Chem. Soc.,* 2000, **122**, 3174 – 3181

110. M. Calvete, G. Y. Yand and M. Hanack, *Synth Met.,* 2004, **141**, 231 – 243

111. S. M. LeCours, H. –W. Guan, S. G. DiMagno, C. H. Wang and M. J. Therien *J. Am. Chem. Soc.,* 1996, **118**, 1497 – 1503

112. T. -G. Zhang, Y. Zhao, I. Asselberghs, A. Persoons, K. Clays and M. J. Therien, *J. Am. Chem. Soc.,* 2005, **127**, 9710 – 9720.

113. T. Nagamura, H. Sakaguchi and T. Matsu, *Thin Solid Films*, 1992, **210**, 160 – 162

114. H. Sakaguchi, L. A. Comez-Jahn, M. Prichard, T. L. Penner, D. G. Whitten and T. Nagamura, *J. Phys. Chem.* 1993, **97**, 1474 – 1476

115. H. Sakaguchi, T. Nagamura, T. L. Penner and D. G. Whitten, *Thin Solid Films,* 1994, **244**, 947 – 950

116. T. Weyland, I. Ledoux, S. Brasselet, J. Zyss and C. Lapinte, *Organometallics*, 2000, **19**, 5235 – 5237

117. M. Malaun, Z. R. Reeves, R. L. Paul, J. C. Jeffery, J. A. McCleverty, M. D. Ward, I. Asselberghs, K. Clays and A. Persoons, *Chem. Commun.*, 2001, 49 – 50.

118. I. Asselberghs, K. Clays, A. Persoons, A. M. McDonagh, M. D. Ward and J. A. McCleverty, *Chem. Phys. Lett.*, 2003, **368**, 408 – 411.

Chapter 2

Iron(II) Pentacyanide Complexes: A Novel Electron Donor Group

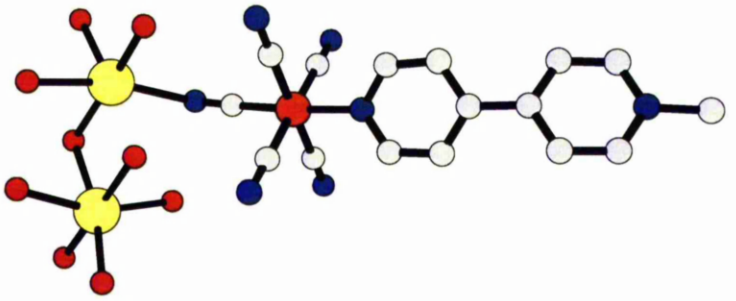

2.1 Introduction

The low-spin d^6 iron pentacyanide unit, $\{Fe^{II}(CN)_5\}^{3-}$, is a strong electron donor group, but until now has not been incorporated into any NLO chromophores. The cyanide ion forms complexes with the majority of transition metals, and due to the high position of CN^- in the spectrochemical series most complexes adopt a low-spin configuration.[1] Prussian blue, $Fe^{III}_4[Fe^{II}(CN)_6]_3$, is one of the best known iron cyanide complexes and one of the first reported co-ordination compounds,[2] and since its discovery many iron cyanide complexes have been reported in the literature.[3] The CN^- ion usually binds through the carbon atom, although it can also act as a bridging ligand forming dinuclear complexes.[4-6] Toma and Malin initiated interest in iron pentacyanide complexes with N-heterocycles in 1973.[7,8] Since then a wide variety of such ligands have been complexed to the iron pentacyanide centre and the spectroscopic and kinetic properties of these compounds have been extensively studied.[3,9-13] The electronic absorption spectra of $\{Fe^{II}(CN)_5\}^{3-}$ complexes characteristically feature strong bands that are attributable to MLCT transitions,[14] with their energies being sensitive to the nature of the sixth ligand and its ability to act as a π-acceptor.[15] More electron-withdrawing ligands cause red-shifts of the MLCT maxima.[6]

The work presented in this chapter concentrates on the preparation of a series of complexes $Na_2[Fe^{II}(CN)_5L_A]$, where L_A is a pyridyl pyridinium ligand, and the investigation of their electronic and optical properties using a range of spectroscopic techniques. The complexes $[Fe^{II}(CN)_5(MeQ^+)]^{2-}$ (MeQ^+ = *N*-methyl-4,4′-pyridinium) (**58**) and $[Fe^{II}(CN)_5(Mebpe^+)]^{2-}$ ($Mebpe^+$ = *N*-methyl-4-[*E*-2-(4-

pyridyl)ethenyl]pyridinium) (**62**) have been reported previously,[6,12,16-21] but no NLO studies have been performed.

2.2 Experimental

2.2.1 Materials and procedures

$Na_3[Fe^{II}(CN)_5(NH_3)]$ was obtained from Aldrich and purified by recrystallisation before use. The pro-ligand salts *N*-methyl-4,4′-bipyridinium chloride ($[MeQ^+]Cl{\bullet}0.7H_2O$),[22] *N*-phenyl-4,4′-bipyridinium chloride ($[PhQ^+]Cl{\bullet}2H_2O$),[23] *N*-(4-acetylphenyl)-4,4′-bipyridinium chloride ($[4\text{-}AcPhQ^+]Cl{\bullet}2H_2O$),[23] *N*-(2-pyrimidyl)-4,4′-bipyridinium chloride ($[2\text{-}PymQ^+]Cl$[24], *N*-methyl-4-[*trans*-2-(4-pyridyl)-ethenyl]pyridinium iodide ($[Mebpe^+]I$)[25] and *N*-phenyl-4-picolinium chloride $[Phpic^+]Cl{\bullet}1.25H_2O$[24] were synthesized according to published methods. We have previously reported preparations of the intermediate *N*-(2,4-dinitrophenyl)-4,4′-bipyridinium chloride ($[2,4\text{-}DNPhQ^+]Cl$),[23] and *N*-phenyl-4-[*trans*-2-(4-pyridyl)ethenyl]pyridinium chloride ($[Phbpe^+]Cl{\bullet}2.25H_2O$),[24] but considerably improved methods are included here. All other reagents were obtained commercially and used as supplied. All solvents were degassed by argon purging for 10 minutes prior to use and all reactions were conducted under an argon atmosphere in the dark. Products were dried at room temperature in a vacuum desiccator ($CaSO_4$) for *ca.* 24 h prior to characterization.

Purification of $Na_3[Fe^{II}(CN)_5(NH_3)]$

Commercial $Na_3[Fe^{II}(CN)_5(NH_3)]$ (5.0 g) was heated to reflux in aqueous ammonia solution (100 cm^3, 70%). After 10 min under reflux, the solution was filtered whilst hot to remove a dark impurity. After cooling to room temperature, ethanol (100 cm^3) was added slowly with stirring. The precipitate was filtered off, washed with ethanol then diethyl ether, and dried to afford a light yellow solid (4.7 g).

2.2.2 Syntheses

[2,4-DNPhQ$^+$]Cl. A solution of 2,4-dinitrochlorobenzene (6.49 g, 32 mmol) and 4,4′-bipyridine (5.00 g, 32 mmol) in ethanol (50 cm^3) was heated under reflux for 23 h. The solution was cooled to room temperature and added to diethyl ether (500 cm^3), with stirring. The golden brown precipitate was collected by filtration, washed with diethyl ether and stored under vacuum: yield 9.46 g (82%). $\delta_H(D_2O)$ 9.38 (1 H, d, $J_{3,5}$ 2.4, H^3), 9.23 (2 H, d, J 6.9, C_5H_4N–Ph), 8.92 (1 H, dd, $J_{5,6}$ 8.7, $J_{3,5}$ 2.5, H^5), 8.82 (2 H, d, J 6.3, C_5H_4N), 8.68 (2 H, d, J 6.8, C_5H_4N–Ph), 8.25 (1 H, d, $J_{5,6}$ 8.6, H^6), 8.01 (2 H, d, J 6.3, C_5H_4N). *Note: The product is hygroscopic and prolonged contact with air causes formation of a sticky brown solid.*

[Phbpe$^+$]Cl. To a solution of [Phpic$^+$]Cl•1.25H_2O (100 mg, 0.44 mmol) and pyridine-4-carboxaldehyde (0.05 cm^3, 0.45mmol) in ethanol (*ca.* 0.5 cm^3) was added one drop of pyridine. The solution was heated at 95 °C for 3.5 h. The resulting dark brown solution was cooled to room temperature and the product precipitated by the dropwise addition of diethyl ether. A dark brown solid was collected by filtration

and washed with diethyl ether: yield 119 mg (84%). $\delta_H(D_2O)$ 8.94 (2 H, d, *J* 6.7, C_5H_4N), 8.51 (2 H, d, *J* 6.0, C_5H_4N), 8.21 (2 H, d, *J* 6.9, C_5H_4N), 7.75 (1 H, d, *J* 16.2, CH), 7.69 (5 H, s, Ph), 7.63 (2 H, d, *J* 6.1, C_5H_4N), 7.56 (1 H, d, *J* 16.4, CH). (Found: C, 63.17; H, 5.74; N, 7.95 Calc for $C_{18}H_{15}N_2Cl•2.75H_2O$: C, 62.79; H, 6.00; N, 8.14%).

$Na_2[Fe^{II}(CN)_5(MeQ^+)]$ 58. A solution of $Na_3[Fe^{II}(CN)_5(NH_3)]$ (136 mg, 0.500 mmol) and $[MeQ^+]Cl•0.7H_2O$ (103 mg, 0.470 mmol) in water (5 cm^3) was stirred at room temperature for 6 h in the dark. Ethanol (30 cm^3) was added and the mixture stored in a refrigerator at 4 °C overnight. The purple/blue solid was collected by filtration and washed with ethanol. The product was purified by three reprecipitations from water/ethanol to afford a dark purple/blue solid: yield 164 mg (72%). $\delta_H(D_2O)$ 9.15 (2 H, d, *J* 6.7, C_5H_4N), 8.80 (2 H, d, *J* 6.7, C_5H_4N), 8.17 (2 H, d, *J* 6.7, C_5H_4N), 7.48 (2 H, d, *J* 6.9, C_5H_4N), 4.41 (3H, s, Me). ν(C≡N) 2080 w, 2048 m, 2042 s cm^{-1}, (Found: C, 39.87; H, 3.70; N, 20.14. Calc for $C_{16}H_{11}N_7FeNa_2•4.5H_2O$: C, 39.69; H, 4.16; N, 20.25%). Thermogravimetric (TGA) analysis indicates the loss of 4.1 molecules of water upon heating.

$Na_2[Fe^{II}(CN)_5(PhQ^+)]$ 59. This was prepared and purified in manner similar to **58**, using $[PhQ^+]Cl•2H_2O$ (134 mg, 0.440 mmol) in place of $[MeQ^+]Cl•0.7H_2O$ to afford a dark blue solid: yield 170 mg (65%). $\delta_H(D_2O)$ 9.18 (2 H, d, *J* = 6.6 Hz, C_5H_4N), 9.14 (2 H, d, *J* = 6.9 Hz, C_5H_4N), 8.48 (2 H, d, *J* = 6.6 Hz, C_5H_4N), 7.73 (5 H, m, Ph), 7.62 (2 H, d, *J* = 6.3 Hz, C_5H_4N). ν(C≡N) 2100 w, 2080 m, 2048 s cm^{-1} (Found: C, 42.28; H, 4.18; N, 16.92. Calc for $C_{21}H_{13}N_7FeNa_2•7H_2O$: C, 42.66; H,

4.60; N, 16.58%). TGA analysis indicates the loss of 6.2 molecules of water upon heating.

$Na_2[Fe^{II}(CN)_5(4\text{-}AcPhQ^+)]$ 60. This was prepared and purified in manner similar to **58**, using $[4\text{-}AcPhQ^+]Cl{\bullet}2H_2O$ (155 mg, 0.447 mmol) in place of $[MeQ^+]Cl$ to afford a dark blue solid: yield 200 mg (69%). $\delta_H(D_2O)$ 9.25 (2 H, d *J* 6.3, C_5H_4N), 9.16 (2 H, d, *J* 5.9, C_5H_4N), 8.5 (2 H, d, *J* 5.7, C_5H_4N), 8.23 (2 H, d, *J* 8.3, C_6H_4), 7.95 (2 H, d, *J* 8.2, C_6H_4), 7.61 (2 H, d, *J* 6.4, C_5H_4N), 2.72 (3 H, s, Me). ν(C≡N) 2110 w, 2084 m, 2048 s cm^{-1} (Found: C, 42.16; H, 4.15; N, 15.56. Calc for $C_{23}H_{15}N_7FeNa_2O{\bullet}8H_2O$: C, 42.41; H, 4.80; N, 15.05%). TGA analysis indicates the loss of 7.3 molecules of water upon heating.

$Na_2[Fe^{II}(CN)_5(2\text{-}PymQ^+)]$ 61. This was prepared and purified in manner similar to **58**, using $[2\text{-}PymQ^+]Cl$ (135 mg, 0.499 mmol) in place of $[MeQ^+]Cl$ to afford a dark blue/green solid: yield 120 mg (39%). $\delta_H(D_2O)$ 10.01 (2 H, d, *J* 6.6, C_5H_4N), 9.24 (2 H, d, *J* 6.0, C_5H_4N), 9.06 (2 H, d, *J* 4.8, $C_4H_3N_2$), 8.57 (2 H, d, *J* 6.9, C_5H_4N), 7.90 (1 H, t, *J* 11.2, $C_4H_3N_2$), 7.66 (2 H, d, *J* = 6.4 Hz, C_5H_4N). ν(C≡N) 2119 w, 2086 m, 2050 s cm^{-1} (Found: C, 36.38; H, 3.73; N, 20.95: Calc for $C_{19}H_{11}N_9FeNa_2{\bullet}8.5H_2O$: C, 36.79; H, 4.55; N, 20.32%). TGA analysis indicates the loss of 7.0 molecules of water upon heating.

$Na_2[Fe^{II}(CN)_5(Mebpe^+)]$ 62. This was prepared and purified in manner similar to **58**, using $[Mebpe^+]I$ (162 mg, 0.500 mmol) in place of $[MeQ^+]Cl$ to afford a dark purple/blue solid: yield 82 mg (29%). $\delta_H(D_2O)$ 8.86 (2 H, d *J* 6.6, C_5H_4N), 8.48 (2 H, d, *J* 6.6, C_5H_4N), 7.73 (2 H, d, *J* 6.9, C_5H_4N), 7.36–7.17 (2 H, m, CH=CH), 7.01

(2 H, d, *J* 6.9, C_5H_4N), 4.24 (3 H, s, Me). ν(C≡N) 2086 w, 2044 s cm^{-1} (Found: C, 37.82; H, 4.37; N, 17.03. Calc for $C_{18}H_{13}N_7FeNa_2 \cdot 7.5H_2O$: C, 38.31; H, 5.00; N, 17.38%). TGA analysis indicates the loss of 7.6 molecules of water upon heating.

$Na_2[Fe^{II}(CN)_5(Phbpe^+)]$ 63. This was prepared and purified in manner similar to **58**, using $[Phbpe^+]Cl \cdot 2.25H_2O$ (146 mg, 0.435 mmol) in place of $[MeQ^+]Cl$ to afford a dark blue solid: yield 161 mg (66%). $\delta_H(D_2O)$ 8.93 (4 H, m, C_5H_4N), 8.10 (2 H, d, *J* 6.6, C_5H_4N), 7.71–7.57 (6 H, m, Ph and CH), 7.36 (1 H, d, *J* 16.5, CH) 7.18 (2 H, d, *J* 6.6, C_5H_4N). ν(C≡N) 2092 w, 2058 s cm^{-1} (Found: C, 41.96; H, 4.44; N, 15.88. Calc for $C_{23}H_{15}N_7FeNa_2 \cdot 9H_2O$: C, 42.28; H, 5.09; N, 15.01%). TGA analysis indicates the loss of 8.1 molecules of water upon heating.

2.3 Results and Discussion

2.3.1 Molecular design and synthesis

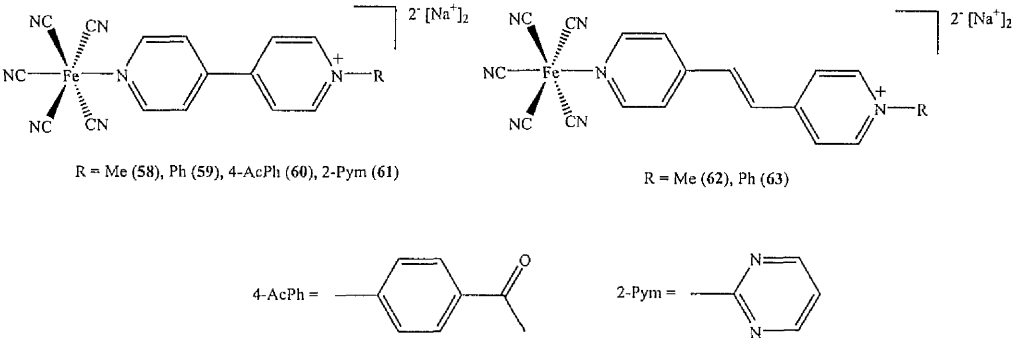

Figure 6: Structures of the new complex salts **58–63**

Ligands are referred to in the text as MeQ^+ when R = Me, PhQ^+ when R = Ph, $AcPhQ^+$ when R = 4-AcPh, $PymQ^+$ when 2-Pym for salts **58–61** and $Mebpe^+$ when R = Me and $Phbpe^+$ when R = Ph for salts **62** and **63**.

Complex salts **58–63**, shown in Figure 6, were synthesized from $Na_3[Fe^{II}(CN)_5(NH_3)]$. The labile ammonia ligand readily undergoes aquation to produce the aquopentacyanoferrate(II) ion, the N-heterocyclic ligand then displaces the aquo ligand to produce the desired compound as outlined in Figure 7. All of the new novel compounds show diagnostic proton NMR spectra, IR spectra confirm the presence of the cyanide groups and elemental analyses provide further confirmation of identity and purity. Both TGA and elemental analysis showed that all the complexes contained associated water molecules. This is consistent with previous complexes of this type[1,3] and is expected due to the strong H-bonding ability of the CN^- ligand.

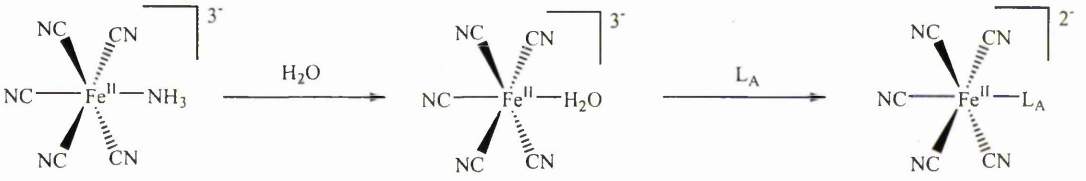

Figure 7: Reaction scheme for the formation of $Na_2[Fe(CN)_5L_A]$

2.3.2 Electronic absorption spectroscopy studies

The UV/Visible absorption spectra of salts **58–63** have been measured in water and methanol at 293 K and the results presented in Table 1. A representative spectrum of

salt **61** is shown in Figure 8. These compounds show intense, sharp absorptions in the UV region caused by $\pi \rightarrow \pi^*$ intraligand charge-transfer (ILCT) transitions along with intense, broad $d\pi[Fe^{II}] \rightarrow \pi^*[L_A]$ (L_A = pyridinium-substituted ligand) visible MLCT bands with maxima in the region 530–620 nm in water and 680–860 nm in methanol, giving rise to their purple/blue colours.

Table 1: UV/Vis data for complex salts **58–63** in water and methanol

Salt	Water [a]		Methanol [a]		Assignment
	λ_{max} [nm] (ε_{max} [M^{-1} cm^{-1}])	E_{max} [eV]	λ_{max} [nm] (ε_{max} [M^{-1} cm^{-1}])	E_{max} [eV]	
58	534 (3700)	2.32	686 (5800)	1.81	$d\pi \rightarrow \pi^*$
	266 (16 300)	4.66	270 (17 900)	4.59	$\pi \rightarrow \pi^*$
59	566 (3900)	2.18	738 (6600)	1.68	$d\pi \rightarrow \pi^*$
	282 (18 700)	4.37	290 (21 800)	4.28	$\pi \rightarrow \pi^*$
60	584 (4900)	2.12	771 (6300)	1.61	$d\pi \rightarrow \pi^*$
	284 (32300)	4.37	291 (26 000)	4.26	$\pi \rightarrow \pi^*$
61	618 (6400)	1.99	854 (7300)	1.45	$d\pi \rightarrow \pi^*$
	290 (32 800)	4.28	293 (24 900)	4.23	$\pi \rightarrow \pi^*$
62	538 (5000)	2.30	685 (5800)	1.81	$d\pi \rightarrow \pi^*$
	318 (26 800)	3.90	319 (27 500)	3.89	$\pi \rightarrow \pi^*$
	232 (16 300)	5.34	228 (18 700)	5.44	$\pi \rightarrow \pi^*$
63	562(6600)	2.18	742 (6500)	1.67	$d\pi \rightarrow \pi^*$
	334 (37 600)	3.69	336 (35 400)	3.69	$\pi \rightarrow \pi^*$
	232 (21 100)	5.34	231 (18 900)	5.37	$\pi \rightarrow \pi^*$

[a] Solutions *ca.* 3–8 × 10^{-5} M.

Within the series **58–61**, irrespective of the solvent, the energy of the $d\pi \rightarrow \pi^*$ MLCT transition decreases as the acceptor strength of L_A increases. The energies of these absorptions depend on the relative energies of the metal-based HOMO and L_A-based LUMO,[14,15,26] and the red-shifting of the MLCT band can be attributed to the LUMO energy decreasing as the acceptor strength of L_A increases in the order $MeQ^+ < PhQ^+ < AcPhQ^+ < PymQ^+$. From the electrochemical data obtained (see section 2.3.3) it can be seen that the energy of the Fe-based HOMO is independent of the nature of L_A and does not change within the series. These results parallel the trends observed in both the ruthenium pentaammine and ruthenium diarsine series studied by Coe *et al.*[22,23,27] The addition of a *trans*-ethylene unit to the ligand has no significant effect on the MLCT energy, with the values for the $Mebpe^+$ and $Phbpe^+$ complexes (in **62** and **63**) being very similar to those of their 4,4′-bipyridinium counterparts (in **58** and **59**).

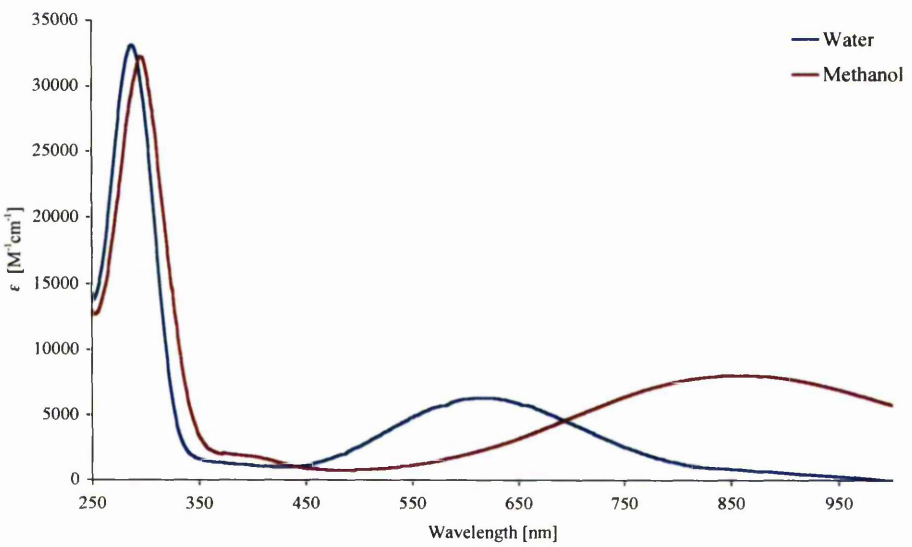

Figure 8: UV/Vis absorption spectra of **61** in water and methanol

Large negative solvatochromic shifts of the MLCT absorption are observed on moving from water to methanol (ΔE = 0.49–0.54 eV) and these red-shifts are also accompanied by decreases in intensity. The lone pairs on the cyanide nitrogens are able to form H-bonds with the O-H groups of the solvent. Because methanol is a weaker hydrogen bond donor than water, there is more electron density at the metal centre therefore making it a better electron donor group and shifting the MLCT to a lower energy in this solvent.[28-30] The sodium salts of complexes **58–63** are appreciably soluble only in water and methanol, so a full solvatochromic study in a range of solvents could not be carried out. To try to increase the solubility of these compounds in other less polar solvents, attempts were made to metathesize the sodium cations with more lipophilic species. However, the addition of saturated aqueous solutions of *tetra*-(*n*-butyl)ammonium chloride (TBACl), tetraphenylphosphonium chloride (TPPCl), tetra-(*n*-hexyl)ammonium chloride (THACl), tetra-(*n*-octyl)ammonium bromide (TOABr) or tetra-(*n*-octadecyl)ammonium bromide (TODABr) to a solution of any of the compounds **58–63** in a minimum of water gave no precipitation in any case.

2.3.3 Electrochemical studies

The complex salts **58–63** were studied by cyclic voltammetry in both water and methanol. The results are presented in Table 2, with representative voltammograms of salt **61** shown in Figure 9. All salts show reversible or not fully electrochemically reversible $Fe^{III/II}$ oxidation waves and generally irreversible L_A-based reduction processes, although complexes **58** and **59** in water and **58–61** in methanol do show reversible first L_A reductions.

Increasing the π-acceptor strength of L_A has no significant effect on the $Fe^{III/II}$ $E_{1/2}$ values, indicating that the nature of this ligand has little effect on the iron-based HOMO. The L_A-based E_{pc} values show large anodic shifts as the π-acceptor strength increases, caused by the L_A-based LUMOs becoming more stabilized; this trend correlates with the red-shifting of the MLCT bands seen in section 2.3.2.

Table 2: Electrochemical data for complex salts **58–63**

Salt	Water [a]		Methanol [b]	
	$E_{1/2}$ [V vs. Ag-AgCl] (ΔE_p [mV])		$E_{1/2}$ [V vs. Ag-AgCl] (ΔE_p [mV])	
	$E_{1/2}$ [$Fe^{III/II}$]	$E_{1/2}$[$L_A^{+/0}$] or E_{pc} [c]	$E_{1/2}$ [$Fe^{III/II}$]	$E_{1/2}$[$L_A^{+/0}$] or E_{pc} [c]
58	0.48 (190)	–0.90 (325) –1.42	0.28 (125)	–0.72 (140)
59	0.48 (135)	–0.74 (245) –0.86	0.29 (140)	–0.53 (160)
60	0.46 (135)	–0.78	0.31 (105)	–0.43 (145)
61	0.46 (160)	–0.61	0.30 (105)	–0.23 (140)
62	0.45 (135)	–0.94	0.24 (145)	–0.60
63	0.45 (140)	–0.82	0.25 (120)	–0.52

[a] Solutions *ca.* 10^{-3} M in 1 M potassium nitrate in water at a glassy carbon working electrode with a scan rate of 200 mV s^{-1}. [b] Solutions *ca.* 10^{-3} M in 0.1 M tetra-*n*-butylammonium hexafluorophosphate in methanol at a platinum disc working electrode with a scan rate of 200 mV s^{-1}. Ferrocene internal reference $E_{1/2}$ = 0.67 V (ΔE_p = 130 mV). [c] For an irreversible reduction process.

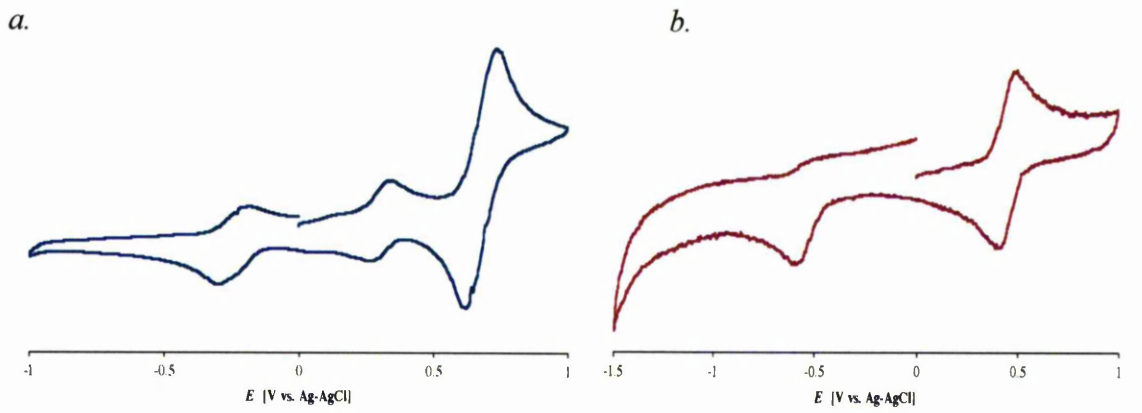

Figure 9: Cyclic voltammograms for **61** in methanol (with ferrocene internal reference $E_{1/2}$ = 0.67 V) (*a*) and in water (*b*)

An ethylene unit is slightly electron donating and causes an increase in the basicity of the Mebpe$^+$ and Phbpe$^+$ ligands compared to MeQ$^+$ and PhQ$^+$. The Fe^{II} centre therefore becomes easier to oxidise, with the $E_{1/2}$ values for **62** and **63** shifted by –30 mV in water and –40 mV in methanol compared with those of **58** and **59**. Comparison of the Fe$^{III/II}$ $E_{1/2}$ values for **62** and **63** shows that replacing the methyl group with a phenyl group has a negligible effect on the reduction potential. However, the E_{pc} values show a shift to a more positive potential as the L_A-based LUMO becomes more stabilized as the π-acceptor strength of the ligand increases.

There are large negative solvent induced shifts of the Fe$^{III/II}$ $E_{1/2}$ values on moving from water to methanol ($\Delta E_{1/2}$ = 0.15–0.25 eV). In methanol, the $E_{1/2}$ values are lower in every instance when compared to those measured in water. This correlates with methanol being a weaker H-bond donor than water: the iron centre is more electron rich in methanol and this makes it easier to oxidise. This data supports the

solvatochromic trends that are observed in the MLCT absorption studies (section 2.3.2).

2.3.4 X-ray crystallographic studies

A single crystal X-ray structure of salt **58**•$9H_2O$ was obtained and a representation of the molecular structures is shown in Figure 10. Selected crystallographic and refinement details are shown in Table 3, and selected bond angles and lengths in Table 4.

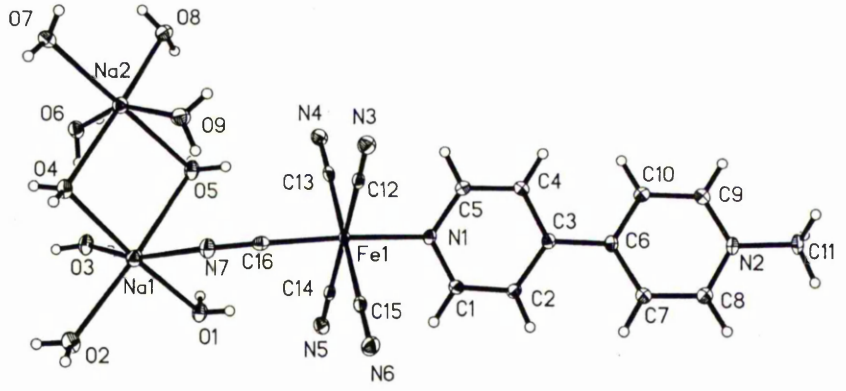

Figure 10: Structural representation of the complex salt **58**•$9H_2O$ (50% probability ellipsoids)

The Fe–C bond located *trans* to the MeQ^+ ligand is shorter by about 0.03 Å than the four other Fe–C bonds. This observation can be attributed to the differing structural trans effects of the MeQ^+ and cyanide ligands.[31] Because the MeQ^+ ligand is a weaker π-acceptor than CN^-, more π-back-bonding can occur to the *trans* cyanide when compared to the *cis* ones. The MeQ^+ ligand shows no significant evidence for

ground-state charge-transfer, with a dihedral angle of 24.26(4)° between the two pyridyl rings.

Unfortunately, salt **58** crystallizes in a centrosymmetric space group and is therefore not expected to show bulk NLO effects.

Table 3: Crystallographic data and refinement details for salt **58**•$9H_2O$

Crystal system	Triclinic
Space group	$P\bar{1}$
Unit cell dimensions [Å, °]	
a	8.5761(12)
b	8.9830(12)
c	17.030(2)
α	100.830(2)
β	95.083(2)
γ	99.411(2)
Volume [Å^3]	1261.6(3)
Z	2
Absorption coefficient [mm^{-1}]	0.690
Reflections collected	10089
Independent reflections	5084
	(R_{int} = 0.0248)
Final R indices [$F^2 > 2\sigma(F^2)$]	1.059
$R1$	0.0292
$wR2$	0.0761
R indices (all data)	
$R1$	0.0320
$wR2$	0.0812

Table 4: Selected interatomic distances (Å) and angles (°) for complex salt **58**•$9H_2O$

Fe(1)–C(16)	1.8927(16)	N(5)–C(14)	1.165(2)
Fe(1)–C(15)	1.9179(16)	N(6)–C(15)	1.160(2)
Fe(1)–C(14)	1.9209(16)	N(7)–C(16)	1.166(2)
Fe(1)–C(12)	1.9211(16)	C(1)–C(2)	1.380(2)
Fe(1)–C(13)	1.9216(16)	C(2)–C(3)	1.397(2)
Fe(1)–N(1)	2.0257(13)	C(3)–C(4)	1.401(2)
N(1)–C(5)	1.348(2)	C(3)–C(6)	1.480(2)
N(1)–C(1)	1.350(2)	C(4)–C(5)	1.384(2)
N(2)–C(9)	1.347(2)	C(6)–C(10)	1.397(2)
N(2)–C(8)	1.348(2)	C(6)–C(7)	1.402(2)
N(2)–C(11)	1.4829(19)	C(7)–C(8)	1.377(2)
N(3)–C(12)	1.169(2)	C(9)–C(10)	1.372(2)
N(4)–C(13)	1.162(2)		
C(16)–Fe(1)–C(15)	89.58(7)	C(14)–Fe(1)–C(13)	91.64(6)
C(16)–Fe(1)–C(14)	86.74(6)	C(12)–Fe(1)–C(13)	89.63(6)
C(15)–Fe(1)–C(14)	90.01(7)	C(16)–Fe(1)–N(1)	175.86(6)
C(16)–Fe(1)–C(12)	92.04(7)	C(15)–Fe(1)–N(1)	89.38(6)
C(15)–Fe(1)–C(12)	88.72(7)	C(14)–Fe(1)–N(1)	89.25(6)
C(14)–Fe(1)–C(12)	178.24(6)	C(12)–Fe(1)–N(1)	91.94(6)
C(16)–Fe(1)–C(13)	89.99(6)	C(13)–Fe(1)–N(1)	91.18(6)
C(15)–Fe(1)–C(13)	178.27(6)		

2.3.5 Hyper-Rayleigh scattering studies

The β values of salts **58–63** were measured in water and methanol using the HRS technique with a 1064 nm Nd:YAG laser fundamental. The β_0 values were estimated using the TSM and the results are presented in Table 5. It should be noted that a relatively large experimental error (±15%) applies to these measurements.

Table 5: Visible MLCT and HRS data for salts **58–63** in water and methanol

Salt	Water				Methanol			
	λ_{max} [nm]	E_{max} [eV]	β_{1064}[a] [10^{-30} esu]	β_0[a] [10^{-30} esu]	λ_{max} [nm]	E_{max} [eV]	β_{1064}[a] [10^{-30} esu]	β_0[a] [10^{-30} esu]
58	534	2.32	311	2	686	1.81	330	127
59	566	2.18	228	22	738	1.68	339	162
60	584	2.12	218	31	771	1.61	728	376
61	618	1.99	214	50	854	1.45	485	272
62	538	2.30	239	4	685	1.881	369	139
63	562	2.18	259	22	742	1.67	396	192

[a] The value β_{1064} is the uncorrected first hyperpolarizablity measured using a 1064 nm Nd:YAG laser (±15% error); the static first hyperpolarizability β_0 is estimated using the TSM.[32,33] The esu units can be converted into SI units (C^3 m^3 J^{-2}) by dividing by a factor of 2.693×10^{-20}.

The β_0 values obtained for these complexes in water are moderately large, but the β and β_0 values obtained in methanol are very large, with salt **60** having a value amongst the largest found for metal-containing chromophores.

Within the series **58–61** in water, β_0 increases as the π-acceptor strength of L_A increases, with salt **61** having the largest value. This corresponds with the $PymQ^+$ ligand being the strongest electron acceptor. These results correlate with both the MLCT data (see section 2.3.2) and the electrochemical data (see section 2.3.3).

In water, the complexes of $Mebpe^+$ and $Phbpe^+$ (**62** and **63**) have values of β_0 similar to those of their 4,4′-bipyridinium counterparts, **58** and **59**. It is generally found in organic chromophores that as the length of the π-conjugation increases so does β_0,[34] though the results obtained here show no such trend. However, similar unusual behaviour has been seen in related ruthenium ammine complexes studied within our group.[24] Changing the methyl group in **62** for the phenyl group in **63** causes an increase in β_0, correlating with the red-shifting seen in the MLCT absorption data. Due to the proximity of λ_{max} to 532 nm, the β values determined in water are subject to considerable resonance enhancement, causing overestimation of β_{1064} and therefore underestimation of β_0. This effect is most pronounced in the complexes containing MeQ^+ and $Mebpe^+$, since their MLCT absorptions lie closest to 532 nm.

In methanol, as the π-acceptor strength of L_A increases, generally so do β_{1064} and β_0, although salt **60** (L_A = $AcPhQ^+$) has a higher value for β_0 than might be expected. From the MLCT data it would be predicted that salt **61** (L_A = $PymQ^+$) should have the largest value of β_0, as it has the lowest value for E_{max}. Previous HRS studies performed on related $[Ru^{II}(NH_3)_5L_A][PF_6]_3$ complex salts have shown similar behaviour which was rationalized by the $AcPhQ^+$ ligand having an increased π-conjugation length when compared to $PymQ^+$.[24]

The quadratic NLO responses of salts **58–61** increase substantially when the measurements are taken in methanol, a phenomenon which can be attributed primarily to the marked red-shifting of the MLCT transitions.

2.3.6 Stark spectroscopic studies

Stark spectroscopic studies were carried out on complex salts **58–63** in water-glycerol (50:50 vol %) glasses at 77 K and the results are presented in Table 6.

In all cases there is a red-shifting of the MLCT band upon glassing at 77 K. A similar effect has been observed previously with Ru^{II} ammine or arsine complex salts on moving from acetonitrile solutions to butyronitrile glasses.[35,36] The observed changes in E_{max} within the pairs **58/62** and **59/63** are more pronounced at 77 K than when measured at room temperature.

Within the series **58–61**, as the π-acceptor strength of L_A increases, so do f_{os}, μ_{12}, $\Delta\mu_{12}$ and $\Delta\mu_{ab}$, although a decrease in E_{max} is seen. The same trends are also observed on moving from salt **62** to **63**. The quadratic NLO responses of salts **58–63** are directly related to $\Delta\mu_{12}$ and μ_{12} and it can be assumed that both of these lie along the Fe–L bond. The values obtained for μ_{12} have a small range (3.5–4.8 D) and increase within the series **58–61** in the order $MeQ^+ < PhQ^+ < AcPhQ^+ < PymQ^+$ and on moving from **62** to **63**. Addition of a *trans*-ethylene unit in pairs **58/62** and **59/63** causes increases in μ_{12} of 0.9 and 0.8 D, respectively. As the size of L_A increases, so too does $\Delta\mu_{12}$: addition of the *trans*-CH=CH moiety causes an increase of 3.4 D in **58/62** and 5.8 D in **59/63**. Such increases in $\Delta\mu_{12}$ upon conjugation extension have

been observed previously in both transition metal-containing and purely organic systems.[34-36] The values obtained for c_b^2 and H_{ab} are not affected by the nature of the N-heterocyclic ligand and are more or less constant within the series **58–63**. These values are indicative of a limited degree of orbital overlap and electronic coupling within the complexes.

Table 6: MLCT absorption and Stark spectroscopic data for complex salts **58–63**[a]

Salt	λ_{max} [nm] 298 K	λ_{max} [nm] 77 K	E_{max} [eV]	f_{os}	μ_{12} [D][b]	$\Delta\mu_{12}$ [D][c]	$\Delta\mu_{ab}$ [D][d]	c_b^{2e}	H_{ab} [cm^{-1}][f]	β_0 [10^{-30} esu][g]
58	560	533	2.33	0.11	3.5	22.5	23.6	0.02	2800	61
59	602	559	2.22	0.13	4.0	23.5	24.8	0.03	2900	88
60	618	581	2.13	0.14	4.1	26.3	27.5	0.03	2600	114
61	660	617	2.01	0.17	4.7	26.5	28.1	0.03	2700	166
62	564	557	2.23	0.16	4.4	25.9	27.4	0.03	2900	119
63	598	582	2.13	0.19	4.8	29.3	30.9	0.02	2700	174

[a] Measured in glycerol-water (50:50 vol %) glasses at 77 K. [b] Calculated from eqn. 13. [c] Calculated from $f_{int}\Delta\mu_{12}$ using $f_{int} = 1.33$. [d] Calculated from eqn. 12. [e] Calculated from eqn. 14. [f] Calculated from eqn. 15. [g] Calculated from eqn. 7.

The MLCT transitions will dominate the NLO response of these complexes and β_0 has been derived using the TSM. The β_0 values within the 4,4′-bipyridinium series **58–63** increase as the π-acceptor strength of L_A increases in the order $MeQ^+ < PhQ^+ < AcPhQ^+ < PymQ^+$. β_0 also increases on moving from **62** to **63**. Extension of the conjugation within the pairs **58/62** and **59/63** causes increases in β_0 of about two-fold.

2.4 Protic Switching

The ability to switch the NLO response of a molecule could significantly enhance the potential utility at a device level and recently there has been interest in turning NLO responses reversibly 'on and off'.[37] A simple dipolar NLO chromophore has D and A groups linked through a π-conjugated bridge, and varying the electronic properties of any of these functional units will cause alteration of the NLO response,[38] although for a pronounced switching effect to be seen the 'on' and 'off' states must be stable. Protic switching has been demonstrated in both organic and metal-containing chromophores,[39-42] but only one example has demonstrated a well-understood switching of β_0.[49]

It has previously been observed that the lone pairs of electrons on the nitrogen atoms of the CN^- ligands in $\{Fe^{II}(CN)_5\}^{3-}$ complexes can be reversibly protonated, causing the energy of the MLCT absorption to increase.[7,43,44] It can therefore be expected that protonation may also alter the NLO responses of such complexes.

When a dilute solution of any of the complex salts **58–63** is acidified to below pH 1 using concentrated hydrochloric acid, the MLCT absorption shifts to a much higher energy (corresponding to a colour change of blue to orange). Restoration of the original MLCT band is achieved by neutralization with triethylamine. A pH titration was performed on salt **60** in aqueous solution, measuring the position of the MLCT band. Upon acidification, no isosbestic points are observed, indicating that protonation does not occur at specific CN^- sites. A representative spectrum is shown in Figure 11. It should be noted that there is a small overall shift of the MLCT band

upon treatment with acid followed by neutralization with base in methanol, due to both of the added reagents containing water and therefore changing the solvent medium slightly.

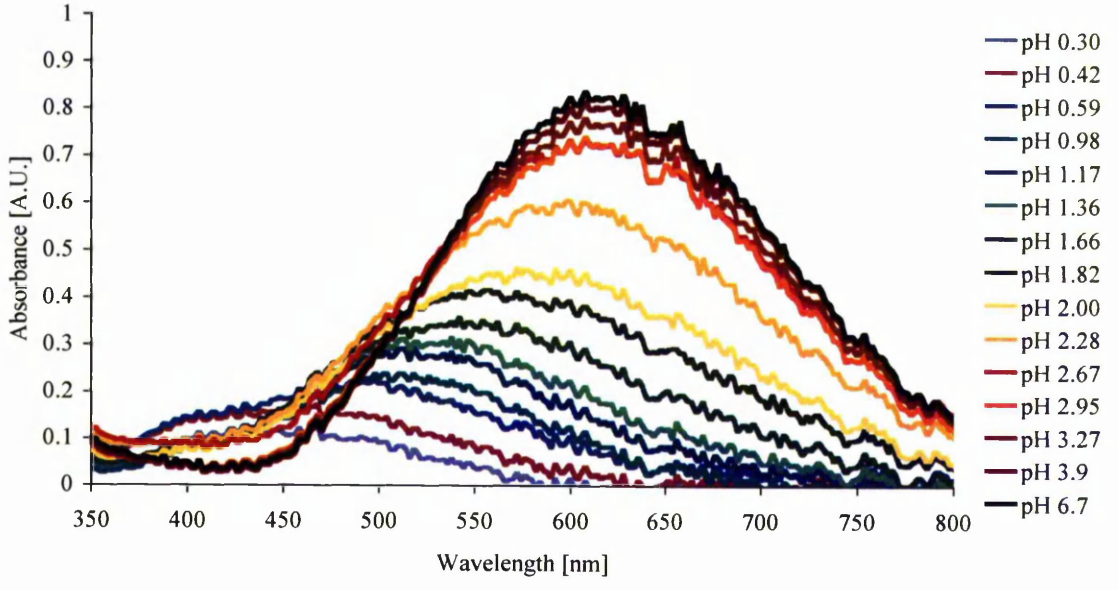

Figure 11: pH titration of salt **61** (aqueous solution *ca.* 10^{-5} M).

According to the TSM, it can be predicted that as the energy of the MLCT absorption increases, then β_0 should decrease.[32,33] Both Stark spectroscopy and HRS have been employed to demonstrate that the NLO responses of these Fe^{II} pentacyanide complexes can be switched by protonation of the CN^- groups.

2.4.1 Protic switching demonstrated *via* HRS studies

Due to negligible HRS signals from the protonated samples when using a fundamental wavelength of 1064 nm, measurements were carried out using a 800 nm Ti^{3+}:sapphire laser. Samples of **58**–**61** (5 mg) were dissolved in water (20 cm^3) and

portions (8 cm^3) of these solutions were acidified by the addition of hydrochloric acid (38%, 2 cm^3) to generate the fully protonated forms. The β_0 values for both the neutral and acidified solutions were estimated from the β_{800} data using the TSM, and the results are presented in Table 7. Reversibility of the switching effect was demonstrated with salt **61** using the following method. Four samples (numbered 1–4) of the stock solution (each 3 cm^3) were placed in 10 cm^3 capacity volumetric flasks. Hydrochloric acid (38%, 1 drop) was added to three of these samples (2–4), and then samples 3 and 4 were neutralized by the addition of triethylamine until their blue colours were completely restored. Hydrochloric acid (38%, 1 drop) was then added to sample 4, and all four samples were diluted up to 10 cm^3 so that each contained the same concentration of the complex species. The quadratic curves for samples 1–4 are shown in Figure 12, and the quadratic coefficients derived from these curves (with the value for the solvent subtracted) are shown in Figure 13.

Upon acidification, there are large increases in E_{max} (ΔE = 0.45–0.65 eV) correlating with colour changes from blue to orange. Both β_{800} and β_0 are largest in the neutral solutions and increasing the proton concentration causes decrease in the NLO responses of *ca.* 70%. It should be noted that this effect in salt **58** is overestimated due to the MLCT absorption for **58A** (where A = the acidified sample) being very close to the SH frequency of 400 nm.

Table 7: HRS data for the acidified solutions of **58A–61A** alongside data for the untreated compounds

Salt	λ_{max} [nm]	E_{max} [eV]	$\beta_{800}{}^{a}$ [10^{-30} esu]	$\beta_0{}^{a}$ [10^{-30} esu]
58	534	2.28	87	38
58A	410	3.02	35	2
59	566	2.19	123	62
59A	465	2.67	66	15
60	584	2.12	135	71
60A	455	2.73	92	18
61	618	2.00	211	117
61A	500	2.48	82	28

[a] The value β_{800} is the uncorrected first hyperpolarizablity measured using a 800 nm Ti^{3+}:Saphire laser (±15% error); β_0 is estimated using the TSM.[32,33] The esu units can be converted into SI units (C^3 m^3 J^{-2}) by dividing by a factor of 2.693×10^{-20}.

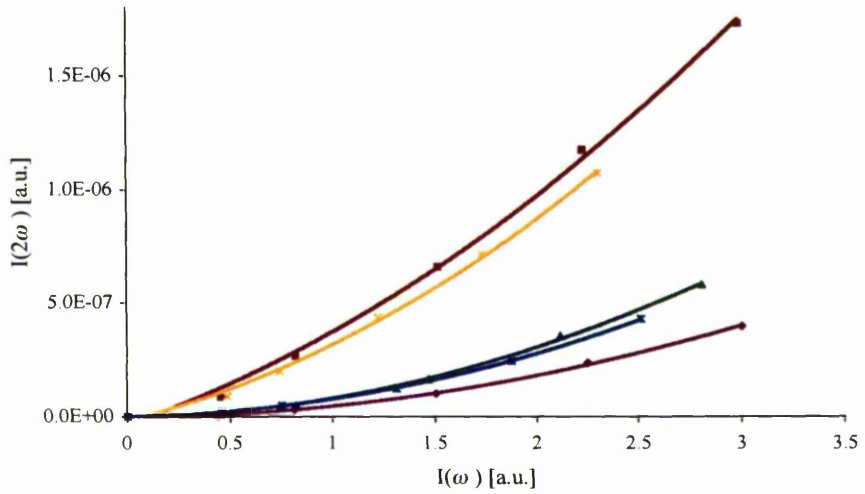

Figure 12: Quadratic curves recorded at 800 nm for Salt **61** and **61A**

Where solvent (water) = purple line; untreated = red line (sample 1); once-acidified = green line (sample 2); neutralized = yellow line (sample 3); twice-acidified = blue line (sample 4)

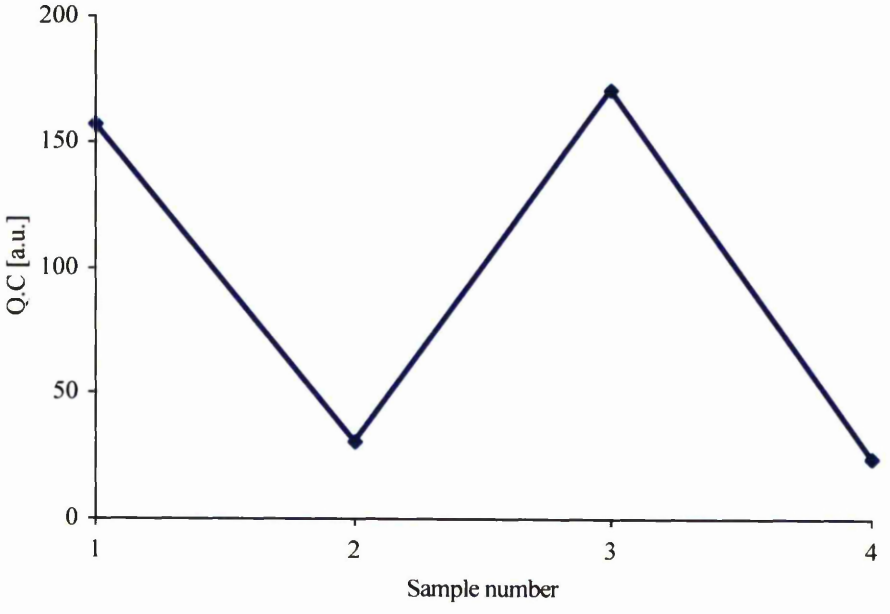

Figure 13: Plot showing the quadratic coefficient for each of the curves in Figure 12 for salt **61** with the solvent (water) value subtracted

2.4.2 Protic switching demonstrated *via* Stark spectroscopic studies

Measurements were carried out in water-glycerol glasses at 77 K, with the solutions being acidified with hydrochloric acid. Initially α-cyanoacrylate spin-coated slides were used as it was thought that the acid would damage the ITO coating on the slides (acid will etch the ITO coating off in about 30 minutes), but it was found that if the samples are frozen quickly this precaution is not necessary. Some of the samples precipitated out after addition of 50 μL of acid, and all of the samples precipitated out of solution over the course of a few hours. The results obtained for frozen acidified solutions of salts **58B, 60B** and **61B** are shown alongside the results for the pH neutral solutions **58, 60** and **61** in Table 8.

Table 8: Stark spectroscopic data for acidified solutions of complex salts **58B**, **60B** and **61B** alongside the data obtained for the untreated compounds [a]

Salt	λ_{max} [nm] 77K	E_{max} [eV]	f_{os}	μ_{12} [D][b]	$\Delta\mu_{12}$ [D][c]	$\Delta\mu_{ab}$ [D][d]	c_b^{2}[e]	H_{ab} [cm^{-1}][f]	β_0 [10^{-30} esu][g]
58	533	2.33	0.11	3.5	22.5	23.6	0.02	2800	61
58B[h]	432	2.87	0.08	2.8	24.4	25.0	0.01	2500	26
58B[i]	432	2.87	0.09	2.9	24.3	25.0	0.01	2700	29
60	581	2.13	0.14	4.1	26.3	27.5	0.03	2600	114
60B[h]	457	2.71	0.10	3.1	28.6	29.3	0.01	2300	42
60B[i]	469	2.64	0.09	3.0	28.4	29.0	0.01	2200	42
61	617	2.01	0.17	4.7	26.5	28.1	0.03	2700	166
61B[j]	444	2.79	0.11	3.2	29.7	30.4	0.01	2400	47
61B[j,k]	439	2.82	0.13	3.4	28.5	29.3	0.01	2700	49

[a] Measured in glycerol–water (50:50 vol %) glasses at 77 K. [b] Calculated from eqn. 13. [c] Calculated from $f_{int}\Delta\mu_{12}$ by using $f_{int} = 1.33$. [d] Calculated from eqn. 12. [e] Calculated from eqn. 14. [f] Calculated from eqn. 15. [g] Calculated from eqn. 7. [h] 100 μL of concentrated HCl added to 0.5 μL of water–glycerol sample solution (2 M HCl concentration). [i] 50 μL of concentrated HCl added to 0.5 μL water–glycerol sample solution (1.1 M HCl concentration). [j] 200 μL of concentrated HCl added to 0.5 μL water–glycerol sample solution (3.5 M HCl concentration). [k] Using α-cyanoacrylate coated slides.

Upon acidification there is a large increase in E_{max} (ΔE = 0.51–0.81 eV), with the largest change being for salt **61** (ΔE = 0.78–0.81 eV), consistent with a decrease in the electron-donating properties of the Fe^{II} centre. The values obtained for μ_{12} are consistently higher for the neutral solutions, although the differences are not very large. $\Delta\mu_{12}$ and $\Delta\mu_{ab}$ increase only slightly in the acidified solution and there are no significant changes in c_b^2 and H_{ab} between the acidified and neutral media.

Increasing the proton concentration causes large decreases in β_0, which can be attributed largely to the significant increase in E_{max}. The consistently smaller values obtained for μ_{12} in the acidified media also contribute towards the smaller β_0 values observed.

We have successfully demonstrated, using both the HRS technique and Stark spectroscopy, that the NLO responses of salts **58**–**61** are considerably decreased upon protonation of the CN^- ligands. This phenomenon is directly related to the blue-shifting of the MLCT bands, and reversibility of the switching effect has been proven using HRS with salt **61**.

2.5 Spectroscopic and quadratic NLO behaviour of ruthenium(II) pentaammine complexes

The electronic and quadratic NLO properties of complexes $[Ru^{II}(NH_3)_5L_A]^{3+}$ (where L_A is a 4,4′-bipyridinium ligand) have been previously studied within our group and it is of interest to draw comparisons between these and the related iron pentacyanide complexes.[22-24] $[Ru^{II}(NH_3)_5]^{2+}$ is a powerful electron donor group and its complexes exhibit large first molecular hyperpolarizabilities; in fact $[Ru^{II}(NH_3)_5(AcPhQ^+)][PF_6]_3$ shows one of the largest β_0 values found in transition metal-containing complexes.[24] All previous NLO studies of ruthenium pentaammine complexes have involved measurements in aprotic solvents. For the quadratic NLO properties of the two systems to be directly compared with one another, measurements must be taken in the same solvent system using the same technique.

We have therefore now also studied these ruthenium ammine complexes in protic solvents, with a view to drawing comparisons with the iron pentacyanide species.

2.5.1 Materials

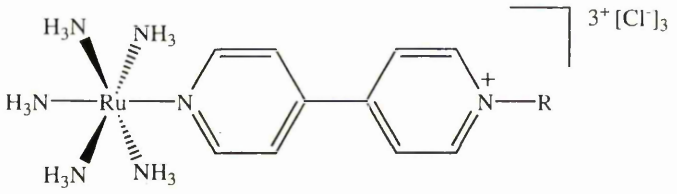

R = Me (**64**), Ph (**65**), 4-AcPh (**66**), 2-Pym (**67**)

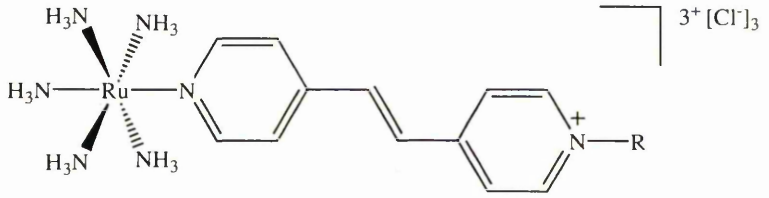

R = Me (**68**), Ph(**69**)

Figure 14: Structures of the complex salts **64–69**

The complexes in **64–69**, depicted in Figure 14, were synthesized as their PF_6^- salts according to published procedures.[23,24] These PF_6^- salts are not appreciably soluble in water and only partially soluble in methanol, so to allow for direct comparisons between the $[Fe^{II}(CN)_5L]^{2-}$ and $[Ru^{II}(NH_3)_5L]^{3+}$ systems, the PF_6^- salts were metathesized to the water-soluble Cl^- salts. This was achieved by dissolution of the complex salt in a minimum of acetone and adding, dropwise, a solution of lithium chloride in acetone until precipitation of the chloride salt occurred. This precipitate was collected by filtration and washed with copious amounts of acetone. There is

some uncertainty regarding the precise formulations of the $[Ru^{II}(NH_3)_5L_A]Cl_3$ materials, due to their hygroscopic nature, coupled with the well established difficulties in obtaining satisfactory CHN elemental analyses for such Ru^{II} ammine salts. Previous studies of the chloride salts **64–66** indicated that these compounds retain 2.5–3.5 molecules of water of crystallization after drying at room temperature.[45] Unfortunately, satisfactory CHN analyses for salts **67–69** could not be obtained, even after prolonged drying under vacuum. As the salts **64–69** were prepared by simple anion metathesis from their PF_6^- counterparts, confirmed pure by ^1H NMR and CHN analyses, there is no doubt of the chromophoric purity of **64–69**. However, for the purposes of calculating the solution concentrations for physical studies the assumption has been made that all of these samples contain 3 molar equivalents of water of crystallization.

2.5.2 Electronic absorption spectroscopy studies

The UV/Visible spectra of salts **64–69** have been measured in water and methanol at 293 K. The results are presented in Table 9, with representative spectra of complex salt **66** shown in Figure 15. These complexes exhibit intense, broad $d\pi[Ru^{II}] \rightarrow \pi^*[L_A]$ visible MLCT bands in the region of 600–720 nm, which account for their blue/purple colours.

The MLCT absorption data show the same trends as when measured in acetonitrile,[24] with the E_{max} values decreasing as the acceptor strength of L_A increases in the order $MeQ^+ < PhQ^+ < AcPhQ^+ < PymQ^+$. Addition of the *trans*-CH=CH unit has no significant effect on the energy of the MLCT. Both methanol and water can form H-

bonds with the NH_3 protons, destabilizing the Ru^{II} forms by increasing the electron density at the metal centre. Previous studies on the solvatochromism of $\{Ru^{II}(NH_3)_5\}^{2+}$ complexes have shown that the energy of the MLCT can be related to the Gutmann donor number of the solvent,[46] although correlations can only be accurately made with data for aprotic solvents.[47,48]

Table 9: UV/Vis data for complex salts **64–69** in water and methanol[a]

Salt	Water		Methanol		
	λ_{max} [nm] (ε_{max} [M^{-1} cm^{-1}])	E_{max} [eV]	λ_{max} [nm] (ε_{max} [M^{-1} cm^{-1}])	E_{max} [eV]	Assignment
64	606 (9300)	2.05	622 (10 300)	1.99	$d\pi \rightarrow \pi^*$
	262 (22 300)	4.73	265 (16 100)	4.68	$\pi \rightarrow \pi^*$
65	622 (11 900)	1.99	655 (17 200)	1.89	$d\pi \rightarrow \pi^*$
	283 (14 500)	4.38	287 (14 300)	4.32	$\pi \rightarrow \pi^*$
66	638 (13 200)	1.94	672 (17 200)	1.85	$d\pi \rightarrow \pi^*$
	287 (18 300)	4.32	291 (14 300)	4.26	$\pi \rightarrow \pi^*$
67	677 (13 400)	1.83	715 (13 000)	1.73	$d\pi \rightarrow \pi^*$
	287 (18 200)	4.32	286 (15 600)	4.34	$\pi \rightarrow \pi^*$
68	596 (7700)	2.07	625 (11 900)	1.98	$d\pi \rightarrow \pi^*$
	316 (19 800)	3.92	318 (18 400)	3.90	$\pi \rightarrow \pi^*$
	227 (9500)	5.46	228 (8100)	5.44	$\pi \rightarrow \pi^*$
69	620 (13 600)	2.00	657 (15 300)	1.89	$d\pi \rightarrow \pi^*$
	334 (27 300)	3.71	337 (25 100)	3.67	$\pi \rightarrow \pi^*$
	230 (9800)	5.39	231 (9500)	5.37	$\pi \rightarrow \pi^*$

[a] Solutions *ca.* 3–8 × 10^{-5} M. All concentrations calculated by assuming that each sample contains 3 molar equivalents of water of crystallization.

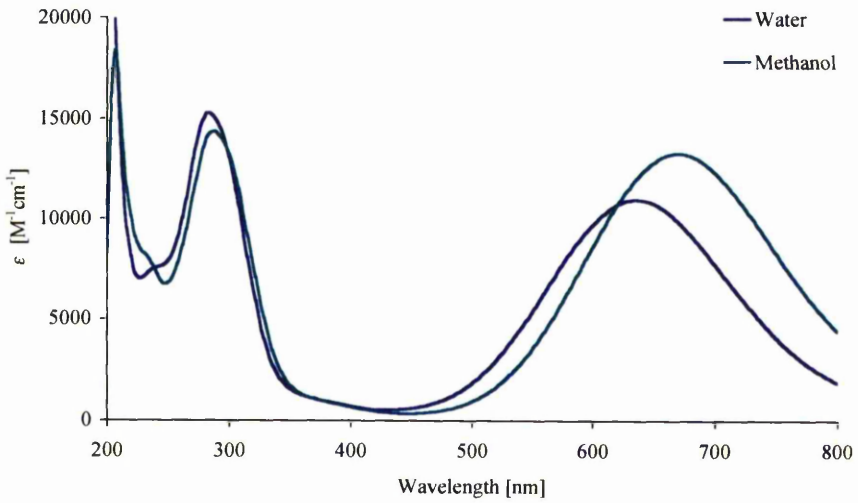

Figure 15: UV/Vis absorption spectra for salt **66** in water and methanol

2.5.3 Electrochemical studies

Cyclic voltammograms of complex salts **64–69** have been measured in aqueous solutions at 293 K and the results are presented in Table 10, with a representative voltammogram shown in Figure 16. The solubility of **64–69** in methanolic electrolyte solution was too low for data to be obtained. All of the salts studied show reversible or not fully electrochemically reversible $Ru^{III/II}$ oxidations and generally irreversible L_A-based reduction processes, although salts **64** and **65** do show reversible first L_A-based reductions.

The $E_{1/2}$ values for the $Ru^{III/II}$ waves are unaffected by the strength of the π-acceptor ligand L_A, but the E_{pc} values for the L_A-based reductions shift anodically as its acceptor strength increases. This is attributed to the L_A-based LUMOs becoming more stabilized in the order $MeQ^+ < PhQ^+ < AcPhQ^+ < PymQ^+$. The energy of the Ru-based HOMO is unaffected by the acceptor strength of L_A. Addition of a *trans*-

ethylene unit in **64** and **65** to form **68** and **69**, respectively, causes the $E_{1/2}$ of the $Ru^{III/II}$ wave to shift cathodically, as the basicity of L_A increases because the ethylene unit is slightly electron donating. The trends seen within the series **64–69** mirror those observed previously in the corresponding PF_6^- salts.[24]

Table 10: Electrochemical data for complex salts **64–69** in aqueous solution[a]

Salt	$E_{1/2}$ [V vs. Ag-AgCl] (ΔE_p [mV]) $Ru^{III/II}$	$E_{1/2}$ or E_{pc}[b] [V vs. Ag-AgCl] (ΔE_p [mV]) L_A-based
64	0.26 (130)	–0.88 (205)
		–1.33[b]
65	0.27 (125)	–0.76 (155)
66	0.29 (115)	–0.71[b]
67	0.28 (115)	–0.62[b]
68	0.21 (105)	–0.95[b]
69	0.22 (110)	–0.78[b]

a. Solutions *ca.* 10^{-3} M in 1 M aqueous potassium nitrate at a glassy carbon working electrode with a scan rate of 200 mV s^{-1}. [b.] For an irreversible process.

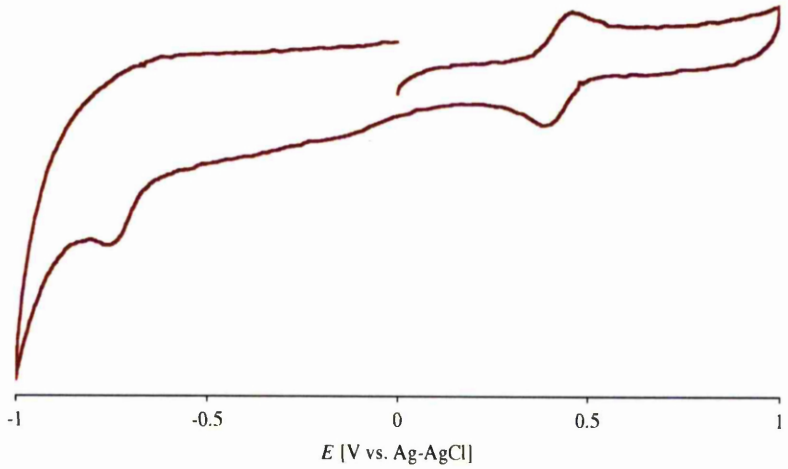

Figure 16: Cyclic voltammogram for salt **68** measured in water

2.5.4 Hyper-Rayleigh scattering studies

The β values of salts **64–69** were measured in water and methanol by HRS under the same conditions used for salts **58–63** (see section 2.3.5). β_0 values were estimated using the TSM and the results are presented in Table 11.

The β and β_0 values obtained for complex salts **64–69** in water and methanol are moderately large, but are consistently smaller than when measured in acetonitrile.

The new HRS data for salts **64–69** exhibit the same trends in β_0 as previously seen when studied in acetonitrile.[24] Moving from water to methanol causes the MLCT energy to shift to a lower energy and, as expected, the β_0 values in methanol are much larger than those measured in water. The addition of the *trans*-ethylene unit causes different behaviour in the two solvents; in water there appears to be a slight

decrease in β_0 as the conjugation length increases, but in methanol an increase in β_0 is seen, although the apparent changes are not very large.

Table 11: Visible MLCT and HRS data for salts **64–69** in water and methanol

Salt	Water				Methanol			
	λ_{max} [nm]	E_{max} [eV]	β_{1064}[a] [10^{-30}esu]	β_0[a] [10^{-30}esu]	λ_{max} [nm]	E_{max} [eV]	β_{1064}[a] [10^{-30}esu]	β_0[a] [10^{-30}esu]
64	606	2.05	169	34	622	1.99	455	110
65	622	1.99	255	62	655	1.89	493	158
66	638	1.94	333	93	672	1.85	522	178
67	677	1.83	402	148	715	1.73	497	220
68	596	2.07	150	26	625	1.98	589	147
69	620	2.00	212	50	657	1.89	522	170

[a] β_{1064} is the uncorrected first hyperpolarizablity measured using a 1064 nm Nd:YAG laser (±15% error); the static first hyperpolarizability β_0 is estimated using the TSM.[32,33] The esu units can be converted into SI units (C^3 m^3 J^{-2}) by dividing by a factor of 2.693×10^{-20}.

2.5.5 Stark spectroscopic studies

Stark spectroscopic studies have been carried out on complex salts **64–69** in water-glycerol (50:50 vol %) glasses at 77 K and the results are presented in Table 12.

In all cases glassing at 77 K causes a red shift in the MLCT band, as also observed in the iron pentacyanide complexes (see section 2.3.6). Generally, the trends observed mirror those seen in butyronitrile glasses at 77 K, with β_0 increasing as the π-acceptor strength and/or the conjugation length of L_A increases. However, because a

satisfactory data fit could not be obtained previously for salt **67**, these are the first Stark data available for this compound.[22]

Table 12: MLCT absorption and Stark spectroscopic data for complex salts **64–69**[a]

Salt	λ_{max} [nm] 298 K	λ_{max} [nm] 77 K	E_{max} [eV]	f_{os}	μ_{12} [D][b]	$\Delta\mu_{12}$ [D][c]	$\Delta\mu_{ab}$ [D][d]	c_b^{2e}	H_{ab} [cm^{-1}][f]	β_0 [10^{-30} esu][g]
64	614	633	1.96	0.14	4.3	13.2	15.8	0.08	4300	74
65	632	678	1.83	0.17	4.9	15.2	18.1	0.08	4000	129
66	658	705	1.76	0.35	7.2	14.1	20.1	0.15	5000	275
67	696	751	1.65	0.25	6.4	15.3	19.9	0.12	4300	267
68	592	653	1.90	0.10	3.8	16.9	18.6	0.04	3200	80
69	640	690	1.80	0.29	6.6	18.2	22.4	0.09	4200	282

[a] Measured in glycerol-water (50:50 vol %) glasses at 77 K. All concentrations calculated by assuming that each sample contains 3 molar equivalents of water of crystallization. [b] Calculated from eqn. 13. [c] Calculated from $f_{int}\Delta\mu_{12}$ using $f_{int} = 1.33$. [d] Calculated from eqn. 12. [e] Calculated from eqn. 14. [f] Calculated from eqn. 15. [g] Calculated from eqn. 7.

2.6 Comparisons between the $\{Fe^{II}(CN)_5\}^{3-}$ and $\{Ru^{II}(NH_3)_5\}^{2+}$ centres as electron donors

Complexes of the form $[Fe^{II}(CN)_5L_A]^{2-}$ and $[Ru^{II}(NH_3)_5L_A]^{3+}$ both possess low-spin d^6 electronic configurations and have filled d orbitals which are of the correct symmetry to interact with the low-lying, unoccupied, π^* orbitals on L_A. The two types of complex differ not only in the radial extension of the 3d iron and 4d ruthenium orbitals, but also in the spectator ligands present (CN^- vs. NH_3). In the

iron pentacyanide complexes, metal-to-ligand back-bonding can occur because the cyanide ligands are both σ-donors and π-acceptors. This back-bonding interaction stabilizes the metal-based HOMO, which greatly reduces the ability of the metal to back-bond with a sixth π-acceptor ligand as shown in Figure 17.[15] Ammine ligands are σ-donors only and therefore have no capacity to participate in any back-bonding interactions. In both systems, L_A is both a σ-donor and π-acceptor, and in the iron(II) pentacyanide complexes there are competing back-bonding interactions involving the spectator CN^- groups and L_A.

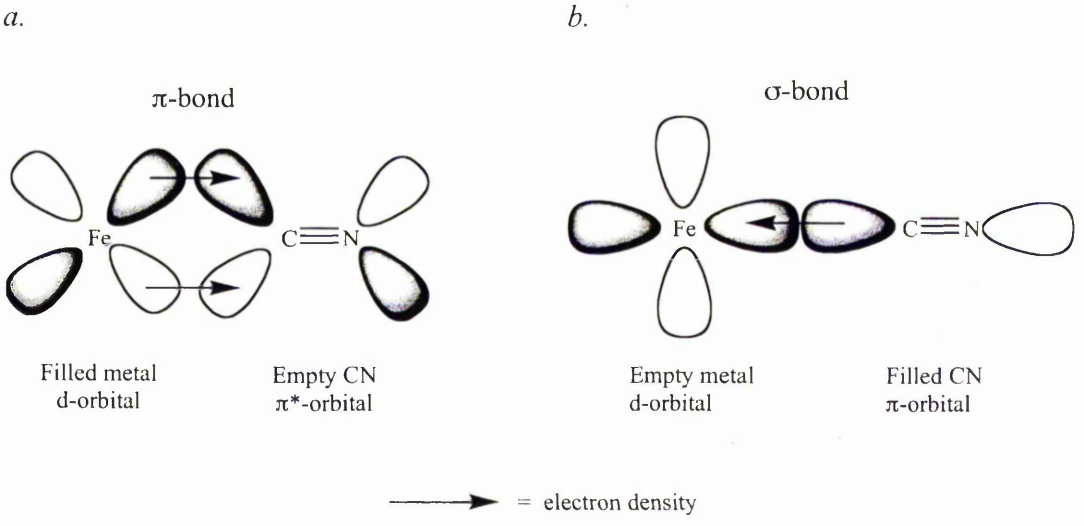

Figure 17: The CN^- ligand participating in π-back-bonding (*a*). The CN^- ligand acting as a σ-donor (*b*).

The $[Fe^{II}(CN)_5L_A]^{2-}$ and $[Ru^{II}(NH_3)_5L_A]^{3+}$ complexes will interact very differently with the protic solvents used in the various measurements. As mentioned earlier the nitrogens of the cyanide ligands can act as H-bond acceptors with the O-H groups of the solvents. In contrast, the ammine ligands are H-bond donors and have no H-bond accepting ability.

Several previous studies have involved comparisons between these two metal centres[3,7,12,15] but none feature either Stark spectroscopy or HRS. The data presented herein allow detailed comparisons between the two systems to be made.

2.6.1 MLCT absorption and electrochemical data

The MLCT absorption data for the iron pentacyanide complexes **58–63** and their ruthenium pentaammine counterparts **64–69** measured in both water and methanol are shown in Table 12. The $E_{1/2}$ values for the $Fe^{III/II}$ and $Ru^{III/II}$ oxidation couples for **58–69** measured in water are also presented in Table 12. Representative UV-visible spectra for salts **59** and **65** measured in both water and methanol are shown in Figure 18.

In water, the MLCT absorption energies of complex salts **58-63** are higher than those of **64–69**. The $Fe^{III/II}$ $E_{1/2}$ values are also higher than the $Ru^{III/II}$ $E_{1/2}$ values, suggesting that the $\{Fe^{II}(CN)_5\}^{3-}$ group is less electron rich than the $\{Ru^{II}(NH_3)_5\}^{2+}$ centre. In methanol, the opposite behaviour is observed, the MLCT absorptions of the ruthenium pentaammine complexes are blue-shifted by between 0.17–0.28 eV when compared to those of their iron pentacyanide counterparts. However, the molar extinction coefficients for **64–69** are consistently larger (by *ca.* 50%) when compared with those measured for **58–63** in both solvents.

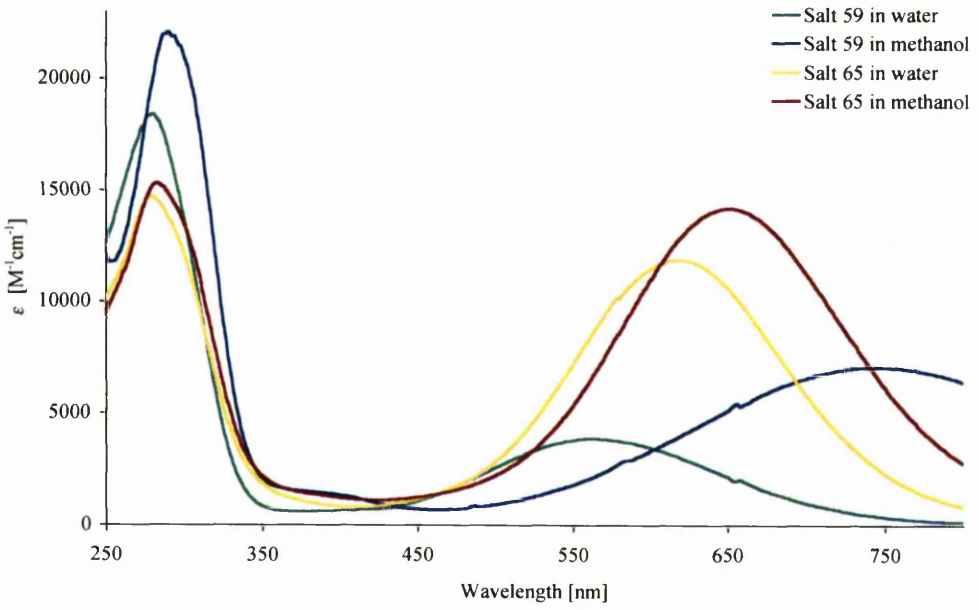

Figure 18: UV/Vis absorption spectra for salts **59** and **65** (L_A = PhQ^+) in water and methanol

Given their lower MLCT energies and reduction potentials, it could be expected that in water the ruthenium pentaammine complexes will exhibit larger NLO responses than their iron pentacyanide analogues, due to $\{Ru^{II}(NH_3)_5\}^{2+}$ being the more electron-rich centre. However, in methanol the $\{Fe^{II}(CN)_5\}^{3-}$ complexes may have the larger β_0 values due to their markedly red-shifted MLCT transitions.

Table 13: Comparison of the MLCT absorption and electrochemical data for complex salts **58–63** and **64–69** in water and methanol

	$Na_2[Fe^{II}(CN)_5L_A]$						$[Ru^{II}(NH_3)_5L_A]Cl_3$					
	Water			Methanol			Water			Methanol		
Salt	λ_{max} [nm] (ε_{max} [M^{-1} cm^{-1}])	E_{max} [eV]	$E_{1/2}[Fe^{III/II}]$ [V vs. Ag-AgCl]	λ_{max} [nm] (ε_{max} [M^{-1} cm^{-1}])	E_{max} [eV]	Salt	λ_{max} [nm] (ε_{max} [M^{-1} cm^{-1}])	E_{max} [eV]	$E_{1/2}[Ru^{III/II}]$ [V vs. Ag-AgCl]	λ_{max} [nm] (ε_{max} [M^{-1} cm^{-1}])	E_{max} [eV]
58	534 (3700)	2.32	0.48	686 (5800)	1.81	**64**	606 (9300)	2.05	0.26	622 (10 300)	1.99
59	566 (3900)	2.18	0.48	738 (6600)	1.68	**65**	622 (11 900)	1.99	0.27	655 (14 200)	1.89
60	584 (4900)	2.12	0.46	771 (6300)	1.61	**66**	638 (13 200)	1.94	0.29	672 (17 200)	1.85
61	618 (6400)	1.99	0.46	854 (7300)	1.45	**67**	677 (13 400)	1.83	0.28	715 (13 000)	1.73
62	538 (5000)	2.30	0.45	685 (5800)	1.81	**68**	596 (7700)	2.07	0.21	625 (11 900)	1.98
63	562 (6600)	2.18	0.45	742 (6500)	1.67	**69**	620 (13 600)	2.00	0.22	657 (15 300)	1.89

2.6.2 Hyper-Rayleigh scattering data

In order to test the above hypotheses, the HRS data obtained for complex salts **58–63** and **64–69** in both water and methanol are presented in Tables 14 and 15.

Table 14: MLCT and HRS data for salts **58–63** and **64–69** in water

$Na_2[Fe^{II}(CN)_5L_A]$				$[Ru^{II}(NH_3)_5L_A]Cl_3$			
Salt	λ_{max} [nm]	β_{1064} [10^{-30} esu]	β_0 [10^{-30} esu]	Salt	λ_{max} [nm]	β_{1064} [10^{-30} esu]	β_0 [10^{-30} esu]
58	534	311	2	**64**	606	169	34
59	566	228	22	**65**	622	255	62
60	584	218	31	**66**	638	333	93
61	618	214	50	**67**	677	402	148
62	538	239	4	**68**	596	150	26
63	562	259	22	**69**	620	212	50

As predicted from the MLCT and electrochemical data, the β_0 values measured in water for the iron pentacyanide complexes (**58–63**) are consistently smaller than those of their ruthenium pentaammine analogues (**64–69**). It should however be noted that the β_{1064} values obtained for **58–63** are subject to greater resonance enhancement (especially for complexes **58** and **62**) due to the proximity of their MLCT maxima to the SH at 532 nm, causing underestimation of β_0.

In methanol, the β_0 values obtained for the iron pentacyanide complexes are generally larger than those of their ruthenium pentaammine counterparts, with the values for the $AcPhQ^+$ complexes (**60** and **66**) having the largest difference. These

observations are consistent with the considerably lower E_{max} values obtained for the iron species.

Table 15: MLCT and HRS data for salts **58–63** and **64–69** in methanol

$Na_2[Fe^{II}(CN)_5L_A]$				$[Ru^{II}(NH_3)_5L_A]Cl_3$			
Salt	λ_{max} [nm]	β_{1064} [10^{-30} esu]	β_0 [10^{-30} esu]	Salt	λ_{max} [nm]	β_{1064} [10^{-30} esu]	β_0 [10^{-30} esu]
58	686	330	127	**64**	622	455	110
59	738	339	162	**65**	655	493	158
60	771	728	376	**66**	672	522	178
61	854	485	272	**67**	715	497	220
62	685	369	139	**68**	625	589	147
63	742	396	192	**69**	657	522	170

2.6.3 Stark spectroscopic data

Stark spectroscopic data for the complex salts **58–69** are shown in Table 16. In water-glycerol glasses (50:50 % vol) at 77 K, the MLCT absorptions for complex salts **58–63** are blue-shifted when compared with those of **64–69**. In general, the values of c_b^2, H_{ab} and μ_{12} are larger in the $\{Ru^{II}(NH_3)_5\}^{2+}$ complexes than for their $\{Fe^{II}(CN)_5\}^{3-}$ analogues. These observations are indicative of better orbital overlap between the Ru^{II} donor and bipyridinium acceptor and can be related to the ruthenium 4d orbitals being larger and more diffuse than the iron 3d orbitals. The iron pentacyanide complexes have significantly smaller c_b^2 values than their ruthenium pentaammine counterparts (by *ca.* 70–80%, with the exception of the pair **62/68**). This observation indicates that in the iron pentacyanide compounds a

significant amount of electron density is located at the metal centre, whereas in the ruthenium pentaammine complexes the electron density is more delocalized over the bipyridinium ligand.

Table 16: MLCT and Stark spectroscopic data for complex salts **58–63** and **64–69**[a]

Salt	E_{max} [eV]	f_{os}	μ_{12} [D][b]	$\Delta\mu_{12}$ [D][c]	$\Delta\mu_{ab}$ [D][d]	c_b^{2e}	H_{ab} [cm^{-1}][f]	r_{12}[g] [Å]	r_{ab}[h] [Å]	β_0 [10^{-30} esu][i]
58	2.33	0.11	3.5	22.5	23.6	0.02	2800	4.7	4.9	61
59	2.22	0.13	4.0	23.5	24.8	0.03	2900	4.9	5.2	88
60	2.13	0.14	4.1	26.3	27.5	0.03	2600	5.5	5.7	114
61	2.01	0.17	4.7	26.5	28.1	0.03	2700	5.5	5.8	166
62	2.23	0.16	4.4	25.9	27.4	0.03	2900	5.4	5.7	119
63	2.13	0.19	4.8	29.3	30.9	0.02	2700	6.1	6.4	174
64	1.96	0.12	4.05	13.23	15.51	0.07	4100	2.8	3.2	66
65	1.82	0.15	4.71	15.06	17.76	0.07	3900	3.1	3.7	117
66	1.76	0.32	6.94	14.26	19.90	0.14	4900	3.0	4.1	260
67	1.65	0.25	6.37	15.20	19.83	0.12	4300	3.2	4.1	264
68	1.90	0.10	3.77	16.86	18.46	0.04	3100	3.5	3.8	78
69	1.80	0.29	6.50	18.20	22.36	0.09	4200	3.8	4.7	278

[a] Measured in glycerol-water (50:50 vol %) glasses at 77 K. [b] Calculated from eqn. 13. [c] Calculated from $f_{int}\Delta\mu_{12}$ using $f_{int} = 1.33$. [d] Calculated from eqn. 12. [e] Calculated from eqn. 14. [f] Calculated from eqn. 15. [g] delocalised electron transfer distance calculated using $\Delta\mu_{12}$/e. [h] effective (localised) electron transfer distance calculated using $\Delta\mu_{ab}$/e. [i] Calculated from eqn. 7.

$\Delta\mu_{12}$ is related to $\Delta\mu_{ab}$ through the degree of delocalization, c_b^2 by equation 11:

$$\Delta\mu_{ab} = \frac{\Delta\mu_{12}}{1-2c_b^2} \tag{11}$$

$\Delta\mu_{12}$ relates to a transition from a delocalized ground state and $\Delta\mu_{ab}$ relates to a transition from a localized ground state (*i.e.* corrected for the effects of metal-to-ligand bonding). In every case, $\Delta\mu_{12}$ and $\Delta\mu_{ab}$ decrease quite considerably on moving from a $\{Fe^{II}(CN)_5\}^{3-}$ complex to its $\{Ru^{II}(NH_3)_5\}^{2+}$ analogue, so the electron-transfer distances r_{12} and r_{ab} are also smaller for the Ru^{II} complexes. In the Ru^{II} complexes the charge is transferred onto the first pyridyl ring, whereas in the Fe^{II} complexes the charge is transferred further towards the middle of the L_A ligand. The smaller values of $\Delta\mu_{12}$ in the Ru^{II} complexes can be attributed to stronger π-back-bonding to L_A . The amount of charge transferred is given by $(1 - 2c_b^2)e$, so as c_b^2 increases less charge is transferred and $\Delta\mu_{12}$ also decreases. The difference between $\Delta\mu_{12}$ and $\Delta\mu_{ab}$ is larger in the ruthenium complexes. $\Delta\mu_{ab}$ allows for the 'correction' of the dipole moment for the manner of bonding and the extent of delocalization between the metal and L_A. If the only difference between the Fe^{II} and Ru^{II} complexes was the increased π back-bonding interaction of the Ru centre, then both series of complexes should exhibit similar values of $\Delta\mu_{ab}$. Therefore, another effect must contribute to the decreased $\Delta\mu_{12}$ values seen in the Ru^{II} complexes. This other effect is likely to be the repolarization of the ligand valence electrons in the excited state. When a molecule is excited to its M^{III} state, the now positively charged metal centre causes displacement of the ligand-based valence electrons. This repolarization causes the electronic distribution to be shifted towards the metal centre. This produces a dipole moment change in the opposite direction to that of the MLCT excitation, so a decreased value for $\Delta\mu_{12}$ is observed. In the iron complexes, the π-electrons in the CN^- ligands are more easily polarized than the electrons of the NH_3 ligands and therefore stabilize the increased charge at the metal centre.

Therefore, the valence electrons of L_A are not as displaced and $\Delta\mu_{12}$ is larger than in the corresponding Ru^{II} complexes.

Except for **68**, the β_0 values derived from the Stark data are larger for the ruthenium pentaammine complexes than for their iron pentacyanide counterparts, primarily due to the decreased MLCT energies and the slightly increased μ_{12} values.

2.7 Conclusions

A novel series of iron(II) pentacyanide complex salts has been synthesized and their molecular quadratic NLO properties have been investigated using both Stark spectroscopy and HRS.

The solubility of the sodium salts of these iron(II) pentacyanide complexes is very limited and measurements can only be made in methanol and water. These complexes show very large solvatochromic shifts on moving from water to methanol. In water, the $\{Fe^{II}(CN)_5\}^{3-}$ centre is a moderately effective electron donor group and the complexes studied exhibit relatively modest β_0 values measured using HRS. In methanol, the $\{Fe^{II}(CN)_5\}^{3-}$ centre becomes a better electron donor due to weaker H-bond accepting interactions with the solvent, and therefore the β_0 values determined using HRS are very large. Stark spectroscopic measurements in glycerol:water (50:50 % vol) show that in this medium the NLO responses are moderately large. Both Stark and HRS data show that as the π-acceptor strength of L_A increases, so too does β_0. Extending the conjugation within L_A causes an increase in β_0, although a convincing increase is only seen *via* Stark spectroscopy.

Reversible switching of the NLO responses of the Fe^{II} pentacyanide complexes can be achieved by protonation of the lone pairs of electrons on the nitrogens of the CN^- ligands. The substantial decreases in β_0 derived from HRS and Stark data can be attributed primarily to large increases in E_{max}, with the original MLCT band and the β_0 response being restored by the addition of base.

Comparisons between the linear and NLO behaviour of the Fe^{II} pentacyanide and related Ru^{II} pentaammine complexes have been made. In water, the $\{Ru^{II}(NH_3)_5\}^{2+}$ unit is more electron rich than the $\{Fe^{II}(CN)_5\}^{3-}$ centre, corresponding with lower values of E_{max} and $E_{1/2}[M^{III/II}]$ (M = Ru or Fe), and larger values of β_0 (measured using HRS). In methanol, an opposite behaviour is observed, with the iron centre acting as the stronger electron donor. Stark spectroscopic measurements performed in water-glycerol glasses at 77 K allow for insights into the MLCT transitions. Under such conditions, the $\{Ru^{II}(NH_3)_5\}^{2+}$ complexes have the larger β_0 values. This observation can be rationalized by these complexes having increased π-orbital overlap when compared to their iron counterparts, and also more effective back-bonding to the pyridinium ligand because there are no competing back-bonding interactions with the spectator ligands.

2.8 Future Work

Investigating the electronic and quadratic NLO behaviour of complexes containing the $\{Ru^{II}(CN)_5\}^{3-}$ D group with 4,4′-bipyridinium ligands would provide further

insights into the effects of back-bonding between the metal and CN^- groups. Although it might be predicted that the NLO responses of such complexes will be smaller than those of their iron counterparts, due to increased values of E_{max},[15] however, this is not a forgone conclusion since other factors also influence β_0. In addition, further direct comparisons could be made with the $\{Fe^{II}(CN)_5\}^{3-}$ complexes and insights gained concerning the effects of the radial extension of the metal orbitals. Comparisons could also be made with the Ru^{II} pentaammines, providing information on the effects of back-bonding to the spectator ligands on the MLCT transitions.[15]

The cyanide groups in the $\{Fe^{II}(CN)_5\}^{3-}$ complexes are amenable to functionalisation.[4,49] For example, coordination of the free N atoms to other metal centres may strongly affect the central iron centre and therefore afford polymetallic and multifunctional (*e.g.* paramagnetic) chromophores with substantial NLO responses.

2.9 References

1. The Chemistry of cyano complexes of the transition metals, A. G. Sharpe, Academic Press, London, 1976
2. J. Brown, *Philos. Trans.*1724, **33**, 17 – 24
3. D. H. Macartney, *Rev. Inorg. Chem.,* 1988, **9** (2-3), 101 – 151
4. P. Alborés, L. D. Slep, T. Weyhermuller and L. M. Baraldo, *Inorg. Chem.,* 2004, **43**, 6762 – 6773
5. R. Lescouëzec, J. Vaissermann, C. Ruiz-Pérez, F. Lloret, R. Carrasco, M. Julue, M. Verdaguer, Y. Dromzee, D. Gatteschi and W. Wernsdorfer, *Angew. Chem. Int. Ed.,* 2003, **42**, 1483 – 1486
6. L. M. Bararldo, P. Forlano, A. R. Parise, L. D. Slep and J. A. Olabe, *Coord. Chem. Rev.*, 2001 **213 – 221**, 881 – 921
7. H. E. Toma and J. M. Malin, *Inorg. Chem.,* 1973, **46**, 1039 – 1045
8. H. E. Toma and J. M. Malin, *Inorg. Chem.,* 1973, **12**, 2080 – 2083
9. J. L. Brisset and M. Biquard, *Inorg. Chim. Acta.,* 1981, **53**, L125 – L128
10. J. E. Figuard and J. D. Peterson, *Inorg. Chem.,* 1978, **17** (4), 1059 – 1063
11. C. H. Hung, J. Y. Liao, A. Yeh, *Inorg. Chem.,* 1990, **29**, 2941 – 2944
12. K. J. Moore, L.-S. Lee, G. A. Mabbott, J. D. Petersen, *Inorg. Chem.,* 1983, **22**, 1108 – 1112.
13. P. Alborés, Slep, L. D. Slep, T. Weyhermüller, L. M. Baraldo, *Inorg. Chem.* 2004, **43**, 6762 – 6773.
14. P. Ford, De F. P. Rudd, R. Gaunder and H. Taube, *J. Am. Chem. Soc.,* 1968, **90**, 1187 – 1194
15. C. R. Johnson and R. E. Shepherd, *Inorg. Chem.,* 1983, **22**, 2439 – 2444

16. J. E. Figard and J. D. Petersen, *Inorg. Chem.* 1978, **17**, 1059 – 1063.

17. J. E. Figard, J. V. Paukstelis, E. F. Byrne and J. D. Petersen, *J. Am. Chem. Soc.* 1977, **99**, 8417 – 8425.

18. H. E. Toma, *Can. J. Chem.* 1979, **57**, 2079 – 2084.

19. L. D. Slep, L. M. Baraldo and J. A. Olabe, *Inorg. Chem.* 1996, **35**, 6327 – 6333.

20. D. H. Macartney and L. J. Warrack, *Can. J. Chem.* 1989, **67**, 1774 – 1779.

21. I. Ando, K. Ujimoto and H. Kurihara, *Bull. Chem. Soc. Japan* 2001, **74**, 717 – 721.

22. B. J. Coe, L. A. Jones, J. A. Harris, B. S. Brunschwig, I. Asselberghs, K. Clays, A. Persoons, J. Garin and J. Orduna, *J. Am. Chem. Soc.,* 2004, **126**, 3880 – 3891

23. B. J. Coe, J. A. Harris, L. J. Harrington, J. C. Jeffery, L. H. Rees, T. Gelbrich and M. B. Hursthouse, *Inorg. Chem.,* 1998, **37**, 3391 – 3399

24. B. J. Coe, J. A. Harris, I. Asselberghs, A. Persoons, J. C. Jeffery, L. H. Rees, T. Gelbrich and M. Hursthouse, *J. Chem. Soc. Dalton Trans.,* 1999, 3617 – 3625

25. E. D. Bergman, F. E. Crane, Jr. and R. M. Fuoss, *J. Am. Chem. Soc.,* 1952, **74**, 5979 – 5983

26. A. L. Coelho, H. E. Toma and J. M. Malin, *Inorg. Chem.,* 1983, **22**, 2703 – 2707

27. B. J. Coe, T. Beyer, J. C. Jeffery, S. J. Coles, T. Gelbrich, M. B. Hursthouse and M. E. Light, *J. Chem. Soc. Dalton Trans.,* 2000, 797 – 803

28. R. E. Shepherd, M. F. Hoq, N. Hoblack and C. R. Johnson, *Inorg. Chem.,* 1984, **23**, 3249 – 3252

29. E. Waldhör, W. Kaim, J. A. Olabe, L. D. Slep and J. Fielder, *Inorg. Chem.*, 1997, **36**, 2969 – 2974

30. C. J. Timpson, C. A. Bignozzi, B. P. Sullivan, E. M. Kober and T. J. Meyer, *J. Phys. Chem.*, 1996 2915 – 2925

31. B. J. Coe, S. J. Glenwright, *Coord. Chem. Rev.*, 2000, **203**, 5 – 80.

32. J. L. Oudar and D. S. Chemla, *J. Chem. Phys.*, 1977, **66**, 2664 – 2668

33. J. L. Oudar, *J. Chem. Phys.*, 1977, **67**, 446 – 457

34. S. R. Marder, B. Kipplen, A. K.-Y. Jen and N. Peyghambarian, *Nature (London)*, 1997, **388**, 845 – 851

35. Y. K. Shin, B. S. Brunschwig, C. Creutz and N. J. Sutin, *J. Phys. Chem.*, 1996, **100**, 8157 – 8169

36. B. J. Coe, J. A. Harris and B. S. Brunschwig, *J. Phys. Chem. A*, 2002, **106**, 897 – 905

37. I. Asselberghs, K. Clays, A. Persoons, M. D. Ward and J. A. McCleverty, *J. Mater. Chem.*, 2004, **14**, 2831 – 2839

38. B. J. Coe, *Chem. Eur. J.*, 1999, **5**, 2464 – 2471

39. P. G. Lacroix, C. Lepetit and J. C. Daran, *New. J. Chem.*, 2001, **25**, 451 – 457

40. S. K. Hurst, M. P. Cifuentes, J. P. L. Morrall, N. T. Lucas, I. R. Whitall, M. G. Humphrey, I. Asselberghs, A. Persoons, M. Samec, B. Luther-Davies and A. C. Willis, *Organometallics*, 2001, **20**, 4664 – 4675

41. I. Asselberghs, Y. Zhao, K. Clays, A. Persoons, A. Comito and Y. Rubin, *Chem. Phys. Lett.*, 2002, **364**, 279 – 283

42. S. K. Hurst, M. G. Humphrey, J. P. Morrall, M. P. Cifuentes, M. Samoc, B. Luther-Davies, G. A. Heath and A. C. Willis, *J. Organomet. Chem.*, 2003, **670**, 56 – 65

43. A. A. Schilt, *J. Am. Chem. Soc.,* 1960, **82**, 5779 – 5783

44. N. K. Hamer and L. E. Orgel, *Nature (London)*, 1961, **190**, 439 – 440

45. B. J. Coe, S. Houbrechts, I. Asselberghs, A. Persoons, *Angew. Chem., Int. Ed.,* 1999, **38**, 366 – 369

46. *The Donor-Acceptor Approach to Molecular Interactions*, V. Gutmann, Plenum Press, New York, 1978

47. B. J. Coe, M. C. Chamberlain, J. P. Essex-Lopresti, S. Gaines, J. C. Jeffery, S. Houbrechts and A. Persoons, *Inorg. Chem.*, 1997, **36**, 3284 – 3292

48. J. C. Curtis, P. Sullivan and T. J. Meyer, *Inorg. Chem.,* 1983, **22**, 224 – 236

49. C. A. Bignozzi, R. Argazzi, O. Bortolini, F. Scandola and A. Harriman, *New J. Chem.,* 1996, **20**, 731 - 738

Chapter 3

Effects of Extending the π-Conjugation in Polyene Containing Ruthenium(II) Diarsine Complexes

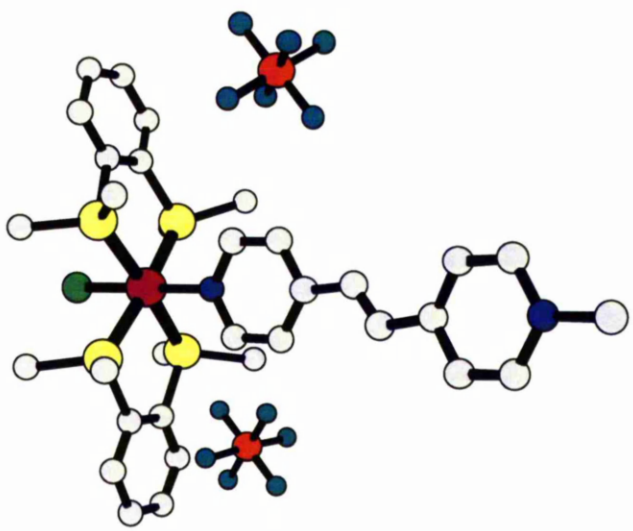

3.1 Introduction

The work presented in this chapter concentrates on comparing the linear and NLO properties of a novel series of Ru^{II} diarsine complexes with those of their previously studied ammine counterparts.[1] The primary aim of this study is to establish whether the unusual effects of extending the polyene bridging unit observed in the ammine system are also seen in this set of analogous compounds.

The syntheses and optical properties of Ru^{II} complexes of the chelating ligand 1,2-phenylenebis(dimethylarsine) (pdma) have been previously studied within our group,[2] but until now, no NLO studies on such complexes have been performed. This is because MLCT and electrochemical data indicate that the *trans*-$\{Ru^{II}Cl(pdma)_2\}^+$ centre is a less effective electron donor group when compared with a $\{Ru^{II}(NH_3)_5\}^{2+}$ centre, and therefore the NLO responses of the pdma complexes are likely to be smaller than those of related ammine complexes. The MLCT absorptions of these pdma complexes are near 532 nm, the SH frequency of a 1064 Nd:YAG laser. Therefore measurements using this laser fundamental would be of limited usefulness as they would be resonance enhanced, causing underestimation of β_0. Stark spectroscopy has recently been found by our group to be a useful approach to determining the β_0 values of dipolar transition metal complexes.[3,4] Although this approach is indirect, the resonance effects which may limit the utility of HRS measurements can be discounted and meaningful data relating to the NLO responses of these complexes can be collected.

Crystallographic data for the related Ru^{II} ammine complexes is very limited as growing single crystals suitable for X-ray diffraction studies has proved difficult.[5-7] Previous work with pdma complex salts[2,8] has shown that these often crystallize readily. This means that crystallographic data can be obtained along with NLO and other electronic data, and there is also a greater likelihood of obtaining materials which may exhibit bulk NLO behaviour.

3.2 Experimental

3.2.1 Materials and procedures

$RuCl_3 \cdot 2H_2O$ was supplied by Apollo and pdma obtained from Dr G. Reid, University of Southampton. The salts *trans*-$[Ru^{II}Cl(pdma)_2(NO)][PF_6]_2$,[9] *trans*-$[Ru^{II}Cl(pdma)_2(pyz)]PF_6$[8] (pyz = pyrazine) **70**, *trans*-$[Ru^{II}Cl(pdma)_2(Mepyz^+)][PF_6]_2$[8] ($Mepyz^+$ = *N*-methylpyrazinium) **71**, *trans*-$[Ru^{II}Cl(pdma)_2(4,4'\text{-bpy})]PF_6$[10] (4,4'-bpy = 4,4'-bipyridyl) **72**, *trans*-$[Ru^{II}Cl(pdma)_2(MeQ^+)][PF_6]_2$ **73**, *trans*-$[Ru^{II}Cl(pdma)_2(bpe)]PF_6$[10] (bpe = *E*-1,2-bis(4-pyridyl)ethylene) **74**, the pro-ligand (*E,E,E*)-1,6-Bis(4-pyridyl)hexa-1,3,5-triene (bph)[11] and the pro-ligand salts *N*-methyl-4-[(*E*)-2-(4-pyridyl)ethynyl]pyridinium hexafluorophosphate ($[Mebpe^+]PF_6$)[7] *N*-methyl-4-{*E,E*-4-(4-pyridyl)buta-1,3-dienyl}pyridinium hexfluorophosphate ($[Mebpb^+]PF_6$)[4] were prepared according to published procedures. All other reagents were obtained commercially and used as supplied. All reactions were conducted under an argon atmosphere. Products were dried at room temperature in a vacuum desiccator ($CaSO_4$) for *ca.* 24 h prior to characterization.

3.2.2 Syntheses

***trans*-[$Ru^{II}Cl(pdma)_2(Mebpe^+)][PF_6]_2$ 75.** A solution of *trans*-[$Ru^{II}Cl(pdma)_2(NO)][PF_6]_2$ (75 mg, 0. 073 mmol) and NaN_3 (4.9 mg, 0.075 mmol) in acetone (5 cm^3) was stirred at room temperature for 2 h. Butan-2-one (10 cm^3) and [$Mebpb^+$]PF_6 (125 mg, 0.365 mmol) were added and the acetone removed *in vacuo*. The solution was heated under reflux for 2 h, cooled to room temperature, and diethyl ether added to afford a dark red/orange precipitate. The excess [$Mebpe^+$]PF_6 was removed by two precipitations from acetone-diethyl ether. The product was further purified by precipitation from acetone-aqueous NH_4PF_6, then acetone-diethyl ether to afford a brick red solid. Recrystallisation from acetonitrile-diethyl ether afforded dark red needles: yield 43 mg 49%. $\delta_H(CD_3COCD_3)$ 8.91 (2 H, d, J = 6.9 Hz, C_5H_4N), 8.31 (4 H, m, $2C_6H_2$), 8.22 (2 H, d, J = 6.9 Hz, C_5H_4N), 7.84 (4 H, m, $2C_6H_2$), 7.76–7.58 (4 H, m, CH=CH, C_5H_4N), 7.32 (2 H, d, J= 6.7 Hz), 4.48 (3 H, s, C_5H_4N-*Me*) 1.91 (12 H, s, 4AsMe), 1.79 (12 H, s, 4AsMe). (Found: C, 33.71; H, 3.63; N, 2.30. Calc. for $C_{33}H_{45}N_2RuAs_4ClP_2F_6$: C, 33.14; H, 3.63; N, 2.34%).

***trans*-[$Ru^{II}Cl(pdma)_2(Mebpb^+)][PF_6]_2$ 76.** This salt was prepared in an identical fashion to **6**, using [$Mebpb^+$]PF_6 (134 mg, 0.364 mmol) in place of [$Mebpe^+$]PF_6. Recrystallisation from acetonitrile-diethyl ether afforded dark red needles: yield 53 mg, 59%. $\delta_H(CD_3COCD_3)$ 8.52 (2 H, d, J= 6.7 Hz, C_5H_4N), 8.29 (4 H, m, $2C_6H_2$), 7.98 (2 H, d, J = 6.9 Hz, C_5H_4N), 7.91 (4 H, m, $2C_6H_2$), 7.57 (1 H, m, CH), 7.43 (2 H, d, J = 6.7 Hz, C_5H_4N), 7.23 (1 H, m, CH), 6.99 (2 H, d, J = 6.6 Hz, C_5H_4N), 6.86 (2 H, m, CH=CH), 4.28 (3 H, s, C_5H_4N-*Me*), 1.91 (12 H, s, 4AsMe), 1.73 (12 H, s, 4AsMe). (Found: C, 34.33; H, 3.56; N, 2.32. Calc. for $C_{35}H_{47}N_2RuAs_4ClP_2F_6$: C, 34.40; H, 3.88; N, 2.29%).

***trans*-[Ru^{II}Cl(pdma)$_2$(bph)]PF$_6$ 77.** This salt was prepared and purified in a similar fashion to **6** using *trans*-[Ru^{II}Cl(pdma)$_2$(NO)][PF$_6$]$_2$ (125 mg, 0.123 mmol) and NaN_3 (8.1 mg, 0.125 mmol) in acetone (10 cm^3) and bph (286 mg, 1.22 mmol) in place of [Mebpe$^+$]PF$_6$. The product was obtained as a dark red solid: yield 47 mg, 35%. $\delta_H(CD_3COCD_3)$ 8.51 (2 H, d, J = 7.2 Hz, C_5H_4N), 8.32 (4 H, m, $2C_6H_2$), 7.84 (4 H, m, $2C_6H_2$), 7.53 (2 H, d, J = 6.7 Hz, C_5H_4N), 7.42 (2 H, d, J = 7.3 Hz, C_5H_4N), 7.31–7.13 (2 H, m, 2CH), 7.09 (2 H, d, J = 6.7 Hz, C_5H_4N), 6.75–6.66 (3 H, m, 3CH), 6.52 (1 H, d, J = 15.5 Hz, CH), 1.90 (12 H, s, 4AsMe), 1.78 (12 H, s, 4AsMe). (Found: C, 39.14; H, 4.06; N, 2.57. Calc for $C_{36}H_{36}N_2RuAsClPF_6$: C, 39.67; H, 4.44; N, 2.57%).

***trans*-[Ru^{II}Cl(pdma)$_2$(Mebph$^+$)][PF$_6$]$_2$ 78.** A solution of **77** (50 mg, 0.041 mmol) in DMF (1.5 cm^3) and methyl iodide (0.5 cm^3) was stirred for 24 h. The excess methyl iodide was removed *in vacuo* and addition of aqueous NH_4PF_6 to the dark red solution gave a brick red precipitate, which was collected by filtration, washed with water and dried. Purification was effected by precipitation from acetone-diethyl ether: yield 48 mg, 94%. $\delta_H(CD_3COCD_3)$ 8.84 (2 H, d, J = 6.9 Hz C_5H_4N), 8.32 (4 H, m, $2C_6H_2$), 8.14 (2 H, d, J = 6.7 Hz, C_5H_4N), 7.88 (4 H, m, $2C_6H_2$), 7.74–7.66 (1 H, m, CH), 7.53 (2 H, d, J = 6.9 Hz, C_5H_4N), 7.27–7.18 (1 H, m, CH), 7.12 (2 H, d, J = 6.9 Hz, C_5H_4N), 6.96 (1 H, d, J = 15.5 Hz, CH), 6.89–6.74 (2 H, m, 2CH), 6.66 (1 H, d, J = 15.7 Hz, CH), 4.48 (3 H, s, C_5H_4N-*Me*), 1.90 (12 H, s, 4AsMe), 1.78 (12 H, s, 4AsMe). (Found: C, 35.59; H, 3.50; N, 2.25. Calc. for $C_{37}H_{49}N_2RuAs_4ClP_2F_6$: C, 35.61; H, 3.96; N, 2.24%).

3.3 Results and Discussion

3.3.1 Molecular Design and Synthesis

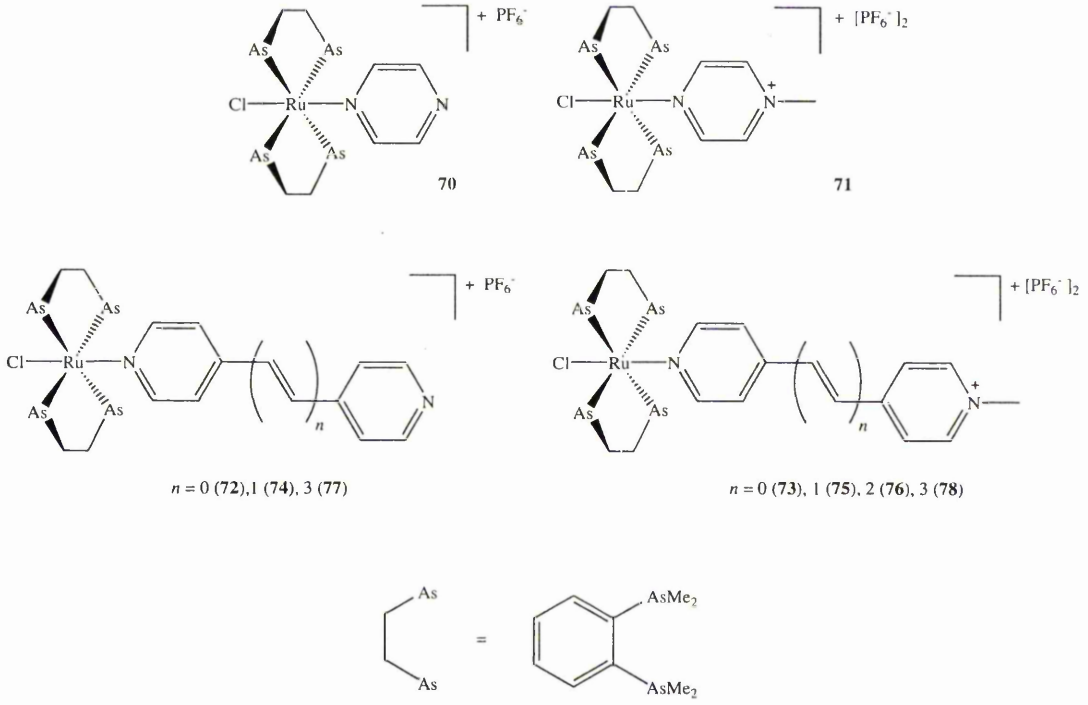

Figure 19: Structures of the complex salts **70–78**

The new complex salts **75–78**, shown in Figure 19, were designed to probe the effects of extending the π-conjugated polyene bridge on the electronic absorption and quadratic NLO properties. The salts **70–74** have been reported previously,[2,8,10] but no Stark data obtained. All of the new compounds show diagnostic proton NMR spectra, and mass spectra and elemental analyses provide further confirmation of identity and purity.

The compound bph is synthesized by a Wittig condensation between pyridine-4-carboxaldehyde and tetraethyl-(*E*)-(2-butene-1,4-diyl)diphosphonate (Figure 20).[11]

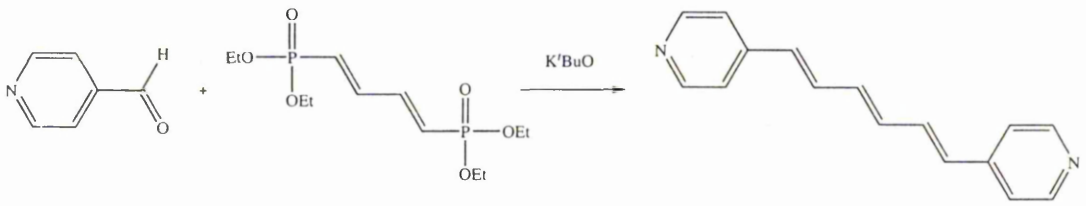

Figure 20: Reaction scheme for the formation of the ligand bph

The known pro-ligand salt [Mebpb$^+$]PF_6 was synthesized by a Wittig reaction of pyridine-4-carboxaldehyde with (1,3-dioxolan-2-yl-methyl)tributyl phosphonium bromide,[4] followed by a base-catalyzed (Knoevenagel-type) condensation reaction with *N*-methyl-4-picolinium iodide (Figure 21). See Chapter 5 for a full discussion of the Knoevenagel reaction mechanism.

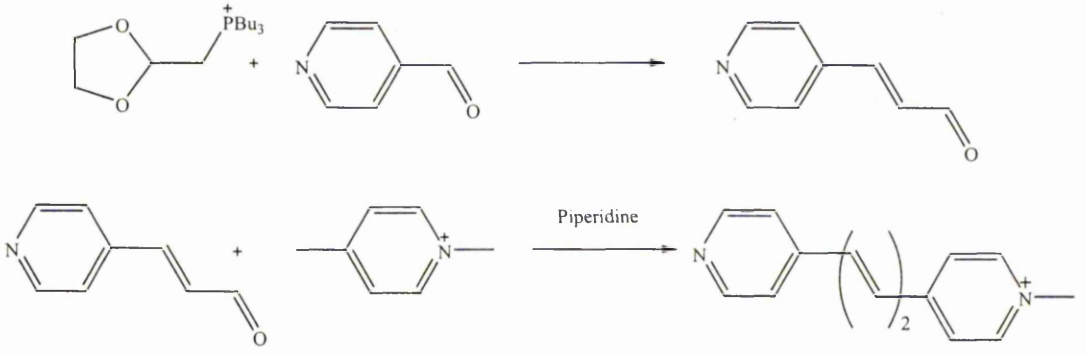

Figure 21: Reaction scheme for the formation of [Mebpb$^+$]

The mechanism of the Wittig reaction is given in Figure 22:[12] aldehydes (and ketones) react with phosphorus ylides to produce alkenes and trialkyl/arylphosphine oxides. In the first step, the ylide acts as a carbanion and attacks the carbonyl carbon of the aldehyde to form a betaine. This unstable intermediate then becomes an

unstable four-membered oxaphosphatane cyclic system, which spontaneously loses trialkyl/arylphosphine oxide to become an alkene.

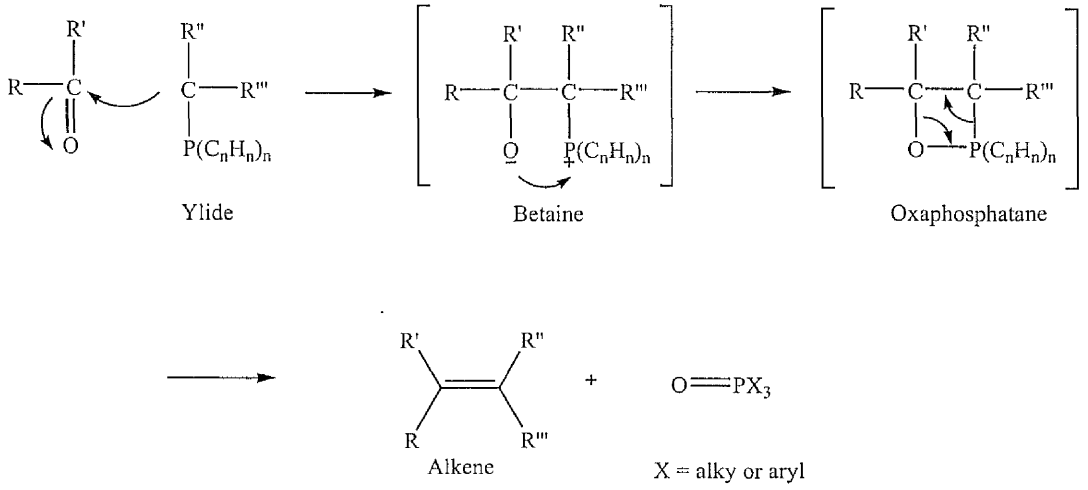

Figure 22: Mechanism of the Wittig reaction

The complex salts **70**, **72**, **74** and **77** were made *via* complexation of the neutral ligands with the sodium azide-treated complex precursor *trans*-$[Ru^{II}Cl(pdma)_2(NO)]^{2+}$, as shown in Figure 23.[9] Complex salts **73**, **75** and **76** were prepared similarly but using the pro-ligand salts of the appropriate *N*-methylated cations. The complex salts **71** and **78** were prepared via methylation of **70** and **77**, respectively, using methyl iodide in DMF.

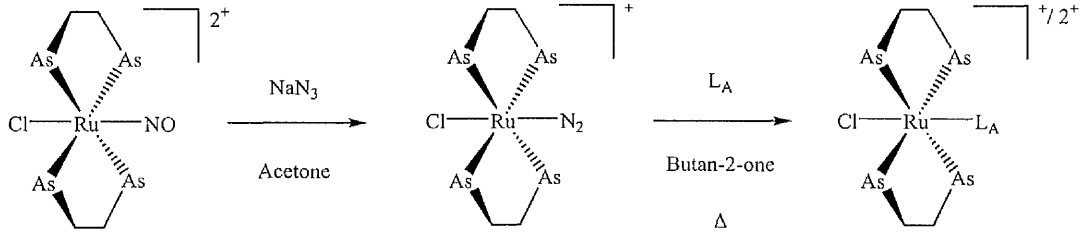

Figure 23: Reaction scheme for the formation of complexes *trans*-$[Ru^{II}Cl(pdma)_2L_A]^{2+}$

The complex *trans*-$[Ru^{II}Cl(pdma)_2(NO)]^{2+}$ is readily prepared by the reaction of $[Ru^{II}Cl_3(NO)]\bullet 5H_2O$ with two equivalents of pdma.[9] The azide-assisted labilization of electrophilic NO ligands is a useful method for generating substituted Ru^{II} complexes.[8] The reaction is thought to proceed via the dinitrogen intermediate *trans*-$[Ru^{II}Cl(pdma)_2(N_2)]^{+}$ (Figure 21).[9,13] Feltham *et al.* proposed a mechanism for this reaction using ^{15}N isotope labelling; they demonstrated that the reaction of *trans*-$[Ru^{II}Cl(pdma)_2(^{15}NO)]^{2+}$ with azide proceeds *via* the formation of a 5-membered heterocycle comprising both the NO and N_3 components, which then decomposes to form the dinitrogen ligand with the loss of N_2O (Figure 22).

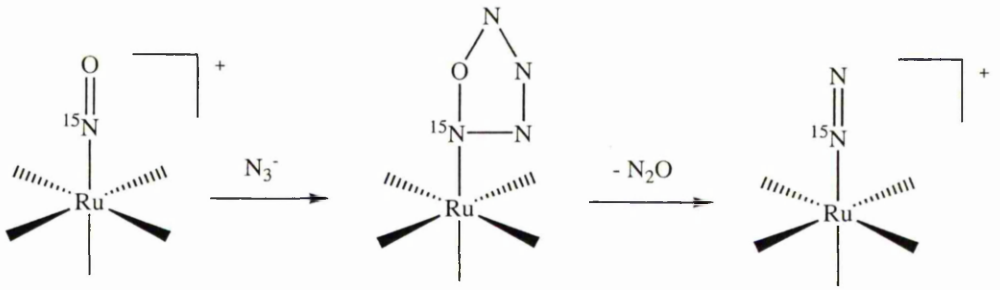

Figure 24: Feltham's proposed mechanism for the formation of *trans*-$[Ru^{II}Cl(pdma)_2(N_2)]^{+}$

3.3.2 Electronic absorption spectroscopic studies

The electronic absorption spectra of the complex salts **75**–**78** were recorded in acetonitrile at 293 K and the results are presented in Table 17, with a representative spectrum shown in Figure 25. The complexes show intense, broad $d\pi[Ru^{II}] \rightarrow \pi^*[L_A]$ MLCT bands with maxima in the region 430–490 nm, which give rise to the dark red colour of these complexes. Intense absorptions due to intraligand $\pi \rightarrow \pi^*$ transition are also observed, which show red-shifting on extension of the

conjugation. The MLCT absorption data for the novel complexes **75–78** are shown in Table 18, alongside the corresponding data for the previously studied complexes.[2,8,10]

Table 17: UV/Vis absorption data for complex salts **75–78** in acetonitrile

Salt	λ_{max} [a] [nm]	ε [a] [$M^{-1}cm^{-1}$]	E_{max} [a] [eV]	Assignment
75	492	13 000	2.52	$d\pi \rightarrow \pi^*$
	316	28 500	3.92	$\pi \rightarrow \pi^*$
76	486	15 700	2.53	$d\pi \rightarrow \pi^*$
	356	37 900	3.48	$\pi \rightarrow \pi^*$
77	446	18 800	2.78	$d\pi \rightarrow \pi^*$
	362	37 300	3.43	$\pi \rightarrow \pi^*$
78	472	15 000	2.58	$d\pi \rightarrow \pi^*$
	394	26 800	3.15	$\pi \rightarrow \pi^*$

[a] Solutions *ca.* 3–8 × 10^{-5} M

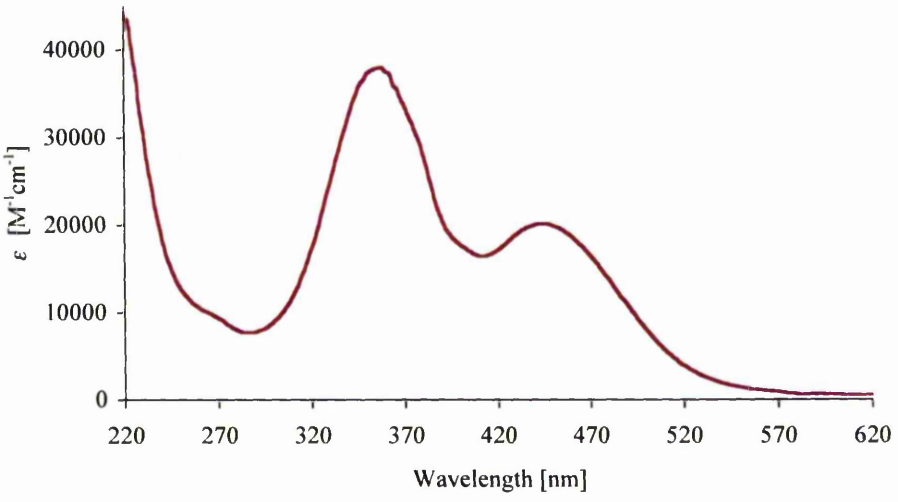

Figure 25: UV/Vis absorption spectrum of salt **77**

Table 18: MLCT absorption data for complexes **70**–**78** in acetonitrile

Salt	λ_{max} [a] [nm]	ε [a] [$M^{-1} cm^{-1}$]	E_{max} [a] [eV]
70[b]	422	6100	2.94
71[b]	558	12 000	2.22
72[c]	418	8400	2.97
73[c]	486	8300	2.55
74[d]	434	14 300	2.86
75	492	13 000	2.52
76	486	15 700	2.53
77	446	18 800	2.78
78	472	15 000	2.58

[a] Solutions *ca.* 3–8 × 10^{-5} M. [b] Ref 8. [c] Ref 10. [d] Ref 2.

As expected, when the uncoordinated pyridyl nitrogen in **70**, **72**, **74** and **77** is methylated (to give **71**, **73**, **75** and **78**, respectively) large red-shifts of the MLCT bands are observed, caused by the pyridinium group being a better π-electron acceptor than the pyridyl group. In complex **70**, this red-shift is accompanied by a substantial increase in intensity, which can be attributed to better D–A orbital overlap.

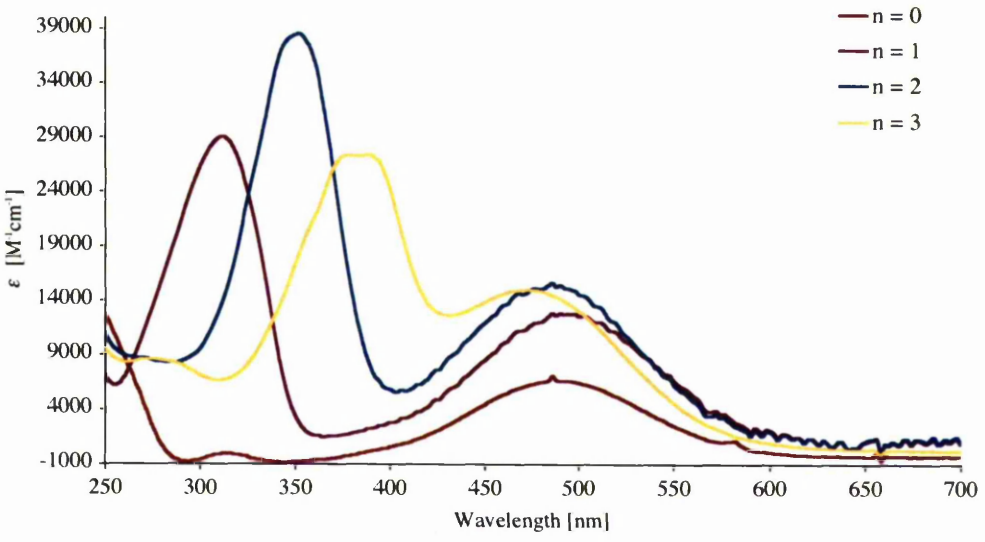

Figure 26: Spectra showing the unusual blue-shifting of the MLCT band in complex salts **73**, **75**, **76** and **78.**

As shown in Figure 26 within the methylated polyene series (**73**, **75**, **76** and **78**) there is an initial red-shift of the MLCT band on moving from $n = 0$ to 1, but a blue-shift then occurs on moving from $n = 1$ to 2. The MLCT energy increases further as the chain is extended to 3 ethylene units. It would be expected that as the conjugation is extended there should be a steady red-shift in the MLCT absorption band, and such behaviour has been seen in many D–A polyenes (including transition metal complexes).[14-18] The only previous reports of unusual blue-shifting of the ICT/MLCT bands with increasing conjugation length in D–A polyenes involve compounds containing tetrathiafulvalenyl (TTF) donor groups with various electron acceptors[19] and also complexes previously studied within our group which are related to compounds **70**–**78** but contain Ru^{II} ammine D centres.[1,4]

3.3.3 Electrochemical studies

The new complex salts **75**–**78** were studied using cyclic voltammetry in acetonitrile and the results, along with those for compounds **70**–**74**, are presented in Table 19. A representative cyclic voltammogram is shown in Figure 27. All of the complexes show reversible $Ru^{III/II}$ oxidation waves, together with generally irreversible L_A-based reductions, although **71**, **73** and **74** do show reversible L_A-based reduction processes.

Table 19: Electrochemical data for complex salts **70**–**78**

Salt	E [V vs. Ag-AgCl] (ΔE_p [mV])[a]	
	$E_{1/2}$ [$Ru^{III/II}$]	$E_{1/2}$ [$L_A^{+/0}$] or E_{pc} [b]
70[c]	1.22 (70)	-1.48 [b]
71[c]	1.48 (75)	–0.35 (65)
72[d]	1.10 (60)	–1.46 [b]
73[d]	1.14 (70)	–0.74 (80)
74[e]	1.08 (60)	–1.33 (60)
75	1.10 (95)	–0.79 [b]
76	1.09 (105)	–0.80 [b]
77	1.05 (120)	–1.31 [b]
78	1.07 (110)	–0.80 [b]

[a] Solutions *ca.* 10^{-3} M in analyte and 0.1 M in $NBu^n_4PF_6$ at a platinum bead/disc working electrode with a scan rate of 200 mVs^{-1}. Ferrocene internal reference $E_{1/2}$ = 0.43 V. [b] For an irreversible reduction process. [c] Ref 8. [d] Ref 10. [e] Ref 2.

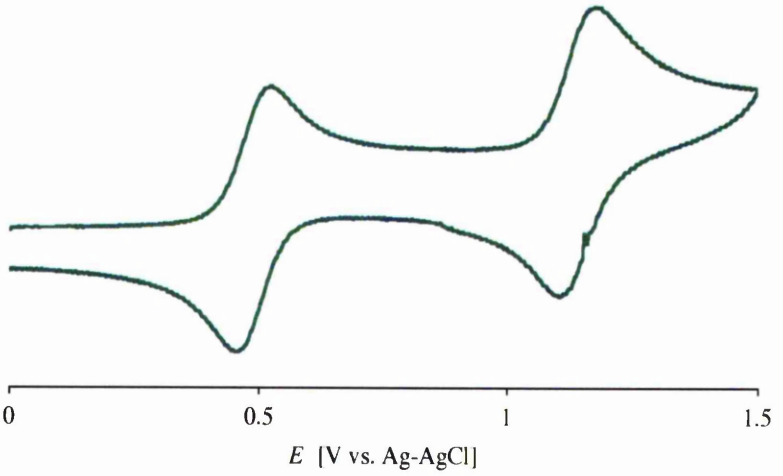

Figure 27: Cyclic voltamogramm for salt **76**

The red-shifting of the MLCT absorption bands upon methylation of **70**, **72**, **74** and **77** to form **71**, **73**, **75** and **78** can be largely attributed to stabilization of the L_A-based LUMOs. However these electrochemical results show some stabilization of the Ru-based HOMOs, especially on moving from **70** to **71**. This effect can be attributed to greater D–A electronic coupling and the extent of orbital overlap is expected to be by far the largest in the pyrazine complex in **71**.

Within the polyene series, there is only a small change in $Ru^{III/II}$ $E_{1/2}$ upon methylation and the change in this potential decreases as *n* increases. The sequential addition of *trans*-ethylene units within the series **73**, **75**, **76** and **78** causes the $Ru^{III/II}$ $E_{1/2}$ to shift slightly to a more negative potential. This can be attributed to the slight electron-donating properties of a CH=CH group, a similar trend was seen in the complexes discussed in Chapter 2. The largest cathodic shift in the $Ru^{III/II}$ $E_{1/2}$ values is seen between **73** and **75**, corresponding to the addition of one *trans*-CH=CH unit, and smaller changes occur as the conjugation is extended further because the effect of each extension becomes less significant.

3.3.4 X-ray crystallographic studies

Single crystal X-ray structures for salts **70**•2.5MeCN, **74**•2MeCN and **75** were obtained and representations of their molecular structures are shown in Figures 28–30. Selected crystallographic and refinement details are shown in Table 20 and selected bond angles and lengths in Table 21.

The dihedral angles between the pyridyl rings in salts **74** and **75** are 5.21(23)° and 12.32(62)°, respectively, apparently consistent with significant D–A π-electronic coupling. It is however worth noting that such dihedral angles in complexes of this type do not give meaningful indications of electronic properties, but are more strongly influenced by solid-state effects.[2]

Salt **71** crystallizes in a noncentrosymmetric space group and so may exhibit bulk NLO behaviour, although as it possess a relatively small β_0 value (see section 3.3.5) its value as a NLO material may be limited. Unfortunately, salts **74** and **75** crystallize centrosymmetrically and so are not expected to exhibit bulk NLO behaviour, although the crystal packing structures could potentially be altered by changing the counter anion.

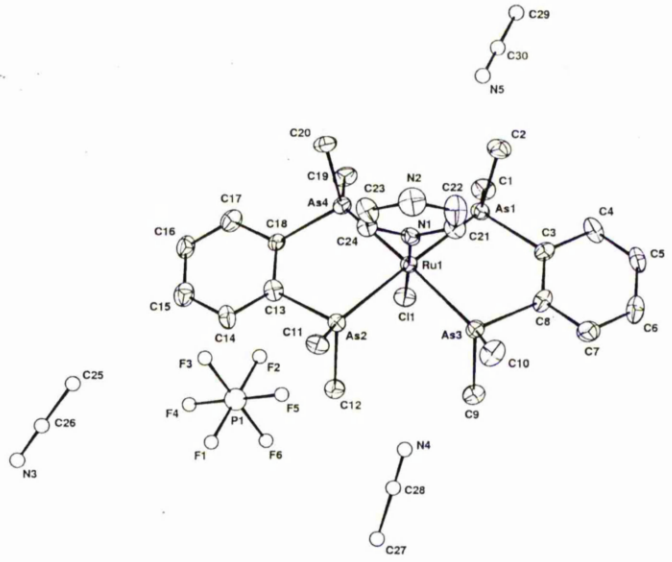

Figure 28: Structural representation of the complex salt **70**•2.5MeCN (50% probability ellipsoids)

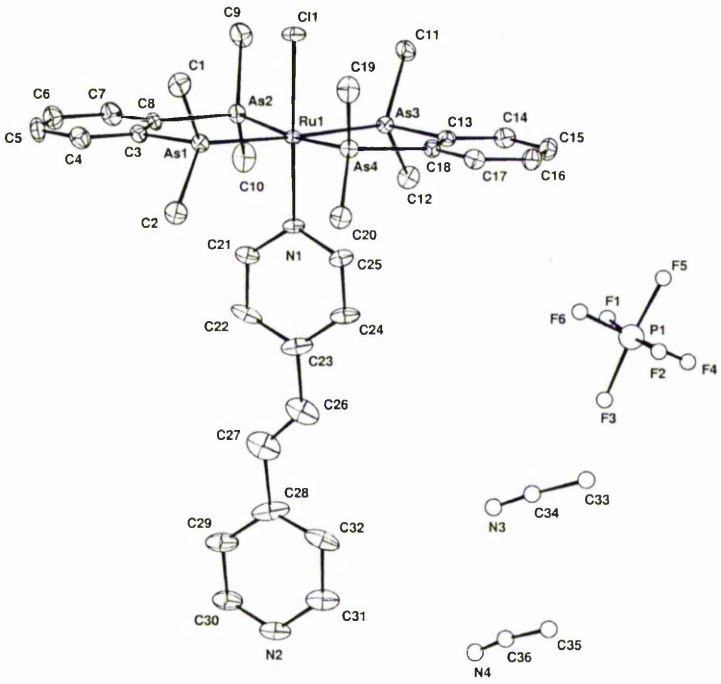

Figure 29: Structural representation of the complex salt **74**•2MeCN (50% probability ellipsoids)

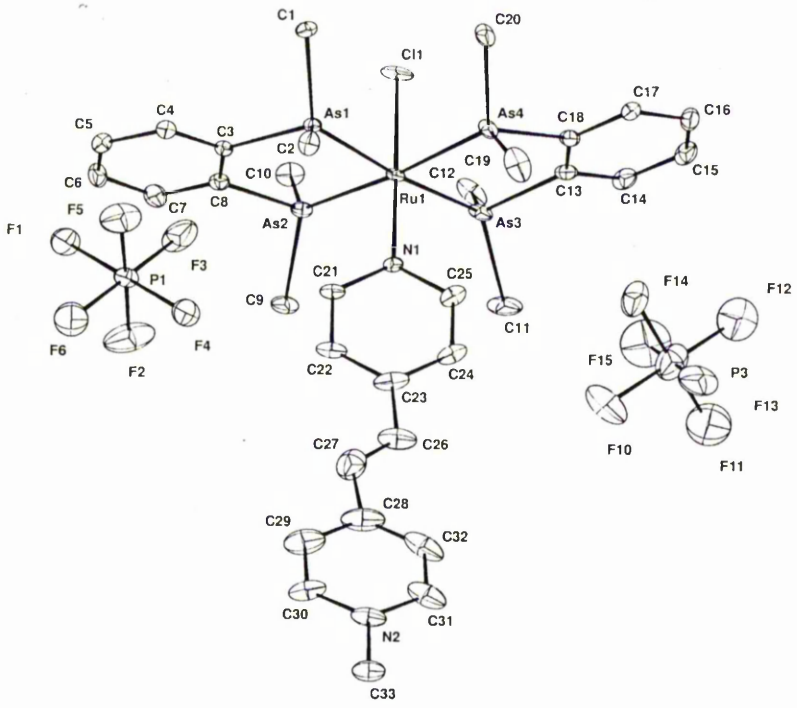

Figure 30: Structural representation of the complex salt **75** (50% probability ellipsoids)

Table 20: Crystallographic data and refinement details for complex salts **70**•2.5MeCN, **74**•2MeCN and **75**

	Salt		
	70•2.5MeCN	**74**•2MeCN	**75**
Crystal system	Orthorhombic	Monoclinic	Monoclinic
Space group	Fdd_2	$P2_1/n$	$P2_1/c$
Unit cell dimensions [Å,°]			
a	21.9898(5)	12.214(5)	20.4769(2)
b	43.4293(11)	13.109(5)	9.44240(10)
c	16.3636(4)	26.675(5)	24.6388(3)
α	90	90	90
β	90	90.7850(13)	112.9200(10)
γ	90	90	90
Volume [Å]	15627.3(7)	4271(3)	4387.82(8)
Z	16	4	4
Absorption coefficient [mm^{-1}]	3.928	3.600	3.563
Reflections collected	35833	37632	14172
Independent reflections	6876 (R_{int} = 0.0936)	7489 (R_{int} = 0.0656)	7731 (R_{int} = 0.0221)
Final R indices [$F^2 > 2\sigma(F^2)$]			
$R1$	0.0443	0.0392	0.0558
$wR2$	0.1086	0.0895	0.1564
R indices (all data)			
$R1$	0.0509	0.0699	0.0617
$wR2$	0.1131	0.1007	0.1628

Table 21: Selected interatomic distances (Å) and angles (°) for complex salts **70**•2.5MeCN, **74**•2MeCN and **75**

	Salt		
	70•2.5MeCN	**74**•2MeCN	**75**
Ru1–N1	2.118(10)	2.114(4)	2.110(4)
Ru1–As1	2.4270(15)	2.4133(7)	2.4127(11)
Ru1–As2	2.4290(15)	2.4228(7)	2.4210(12)
Ru1–As3	2.4320(15)	2.4122(7)	2.4226(12)
Ru–As4	2.4259(15)	2.4179(7)	2.4179(12)
Ru1–Cl1	2.436(3)	2.4292(14)	2.441(3)
N1–Ru1–As1	94.0(3)	92.52(13)	92.27(16)
N1–Ru1–As2	93.0(3)	93.82(12)	91.84(16)
N1–Ru1–As3	93.9(3)	90.96(13)	94.67(16)
N1–Ru1–As4	94.4(3)	92.70(12)	94.39(16)
As1–Ru1–As2	172.98(6)	84.90(2)	85.51(4)
As1–Ru1–As3	84.71(5)	176.46(3)	172.98(5)
As1–Ru1–As4	94.65(5)	95.26(2)	93.16(4)
As2–Ru1–As3	94.60(5)	94.17(2)	95.33(4)
As2–Ru1–As4	85.03(5)	173.46(3)	173.67(5)
As4–Ru1–As3	171.77(6)	85.27(2)	85.25(4)
N1–Ru1–Cl1	178.6(3)	178.47(13)	179.11(18)
As1–Ru1–Cl1	87.30(8)	88.01(4)	87.85(7)
As2–Ru1–Cl1	85.69(8)	87.66(4)	87.29(8)
As3–Ru1–Cl1	86.95(8)	88.54(4)	85.23(7)
As4–Ru1–Cl1	84.83(8)	85.81(4)	86.48(8)

3.3.5 Stark spectroscopic studies

Stark spectroscopy has been carried out on complex salts **70**–**76** and **78** in butyronitrile glasses at 77 K and the results are presented in Table 22. Representative electronic absorption and Stark spectra for salts **73**, **75**, **76** and **78** are shown in Figure 31. Satisfactory data fits could only be obtained for the MLCT bands and not the higher energy ILCT bands. The E_{max} values generally decrease on moving from acetonitrile solution to a butyronitrile glass, as has previously been seen in related Ru^{II} ammine compounds,[3,20] but the opposite behaviour is seen for compound **71**, where E_{max} increases slightly.

Table 22: MLCT absorption and Stark spectroscopic data for complex salts **70**–**76** and **78** in butyronitrile at 77 K

Salt	λ_{max} [nm]	E_{max} [eV]	f_{os}	μ_{12}[a] [D]	$\Delta\mu_{12}$[b] [D]	$\Delta\mu_{ab}$[c] [D]	c_b^2[d]	H_{ab}[e]	β_0[f] [10^{-30} esu]
70	424	2.92	0.10	3.0	8.2	10.2	0.10	7000	10
71	545	2.28	0.31	6.0	6.1	13.5	0.27	8200	50
72	422	2.94	0.21	4.3	11.1[g]	14.0	0.11	7300	28
73	491	2.53	0.41	6.6	14.3	19.4	0.13	6900	113
74	506	2.45	0.26	5.5	18.6	21.5	0.07	4900	100
75	515	2.41	0.33	6.0	16.9	20.7	0.09	5600	123
76	506	2.45	0.94	10.0	20.6	28.7	0.14	6900	401
78	501	2.48	1.04	10.5	22.2	30.6	0.14	6900	468

[a] Calculated from eqn. 13. [b] Calculated from $f_{int}\Delta\mu_{12}$ using $f_{int} = 1.33$. [c] Calculated from eqn. 12. [d] Calculated from eqn. 15. [e] Calculated from eqn. 14. [f] Calculated from eqn. 7. [g] Inferior data fit.

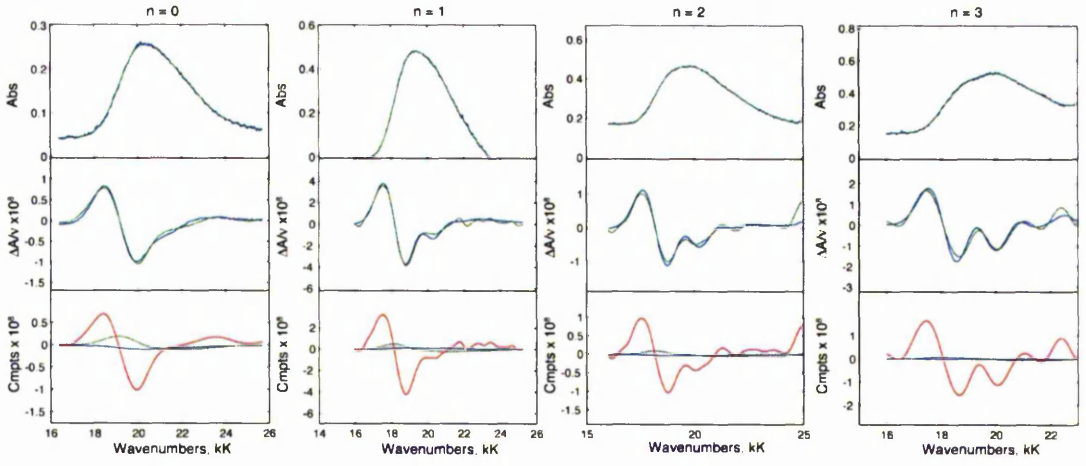

Figure 31: Electroabsorption spectra and calculated fits for **73** (n = 0), **75** (n = 1), **76** (n = 2) and **78** (n = 3) in external fields of 3.42, 3.43, 2.93 and 2.17 × 10^7 V m^{-1}, respectively. Top panel: absorption spectrum; middle panel: electroabsorption spectrum, experimental (blue) and fits (green) according to the Liptay equation; bottom panel: contribution of 0^{th} (blue), 1^{st} (green) and 2^{nd} (red) derivatives of the absorption spectrum to the calculated fits.

On moving from L_A = $Mepyz^+$ (**71**) to MeQ^+ (**73**), there is a large increase in E_{max}. However, μ_{12} and especially $\Delta\mu_{12}$ both increase upon moving from **71** to **73**, and these effects correlate with an increase in β_0 upon extension of the conjugation.

Within the *N*-methylpyridinium polyene series **73**, **75**, **76** and **78**, as n increases from 0 to 1 there is a slight decrease in μ_{12}. As n increases further, so does μ_{12}, with a large increase between n = 1 and 2. The $\Delta\mu_{12}$ values increase steadily with n, as is normal for D–A polyenes, correlating with the increase in the conjugation pathlength. The values for $\Delta\mu_{ab}$ are consistently larger than for their adiabatic counterparts, but the same trends are observed. As the conjugation length increases

from n = 0 to 1, there is a small increase in β_0, but this is within the large experimental error (±20%). As the conjugation extends further to n = 2, there is a large increase in β_0, but as the conjugation is extended further up to n = 3 there is no significant additional increase in β_0. This trend in β_0 is unexpected: it is predicted by the TSM that as the conjugation length increases so should β_0, and this type of behaviour has been observed in many metal containing D–A polyenes.[18,21-23] The behaviour exhibited by these complexes is similar to that seen in related Ru^{II} ammine complexes within our group,[1,4] and a full comparison between these two systems can be found in section 3.4.

Upon methylation of **70**, **72** and **74**, E_{max} decreases predictably, as discussed earlier for the room temperature data. Methylation also causes μ_{12} to increase, with the largest increase between the pair **70/71** (Δ = 3 D). Small decreases in $\Delta\mu_{12}$ are observed in pairs **70/71** and **74/75**, but the inferior data fit for salt **72** means that the values for the pair **72/73** cannot be accurately compared. The values of $\Delta\mu_{ab}$ for the pair **70/71** show an increase, but for pair **74/75** there is a small decrease. As expected due to the increased acceptor strength, methylation leads to increases in β_0 in every case.

Complex **71** has the largest values for both c_b^2 and H_{ab}, consistent with it having the strongest D–A electronic communication of the complexes studied. The maximum possible value that can be obtained for c_b^2 is 0.5, which corresponds to complete delocalization of the orbitals involved in the electronic transition.

3.4 Comparisons with ruthenium(II) ammine complexes

From the MLCT and electrochemical data obtained for *trans*-$\{Ru^{II}Cl(pdma)_2\}^+$ complexes, it has been assumed that these complexes will have considerably smaller β_0 responses than their ammine analogues.[2] This assumption is based upon the MLCT absorptions of the pdma species having higher energies and smaller extinction coefficients than those of their ammine counterparts. The $Ru^{III/II}$ $E_{1/2}$ values are also higher, showing that the *trans*-$\{Ru^{II}Cl(pdma)_2\}^+$ centre is less electron rich than the $\{Ru^{II}(NH_3)_5\}^{2+}$ centre, causing it to be a poorer electron donor. Previous comparative studies have shown that this difference can be largely attributed to the stabilization of the Ru-based HOMOs in the pdma species, and the molar extinction coefficients of these complexes are about 50–60% lower than their ammine counterparts at room temperature.[2] The MLCT absorption and electrochemical data recorded in acetonitrile at room temperature for salts **73**, **75**, **76** and **78** are shown in Table 23, alongside those of their ammine counterparts (**73A**, **75A**, **76A** and **78A**).[1,6,7]

The MLCT absorptions of the pdma complexes are blue-shifted by 0.4–0.45 eV when compared with those of their ammine counterparts. The molar extinction coefficients of the pdma complexes are also smaller than those of the ammines, with the largest difference between salts **73** and **73A** of 47%. As expected, the electrochemical data show that the *trans*-$\{Ru^{II}Cl(pdma)_2\}^+$ centre is harder to oxidise than the $\{Ru^{II}(NH_3)_5\}^{2+}$ centre; the $E_{1/2}$ values for the pdma complexes are higher in every instance by about 600 mV. It would therefore be expected that the pdma complexes will exhibit smaller NLO responses than their ammine counterparts

Table 23: MLCT absorption and electrochemical data for complex salts **73**, **75**, **76** and **78** and their $\{Ru^{II}(NH_3)_5\}^{2+}$ analogues

Salt	λ_{max} [nm]	E_{max} [eV]	ε [M^{-1} cm^{-1}]	E [V vs. Ag-AgCl] $E_{1/2}[Ru^{III/II}]$
73	486	2.55	8300	1.14
73A[a]	590	2.10	15 800	0.51
75	492	2.52	13 000	1.10
75A[b]	595	2.08	16 100	0.46
76	486	2.55	15 700	1.09
76A[c]	584	2.12	18 700	0.45
78	472	2.58	15 000	1.07
78A[c]	568	2.18	17 500	0.45

[a] Ref. 6. [b] Ref. 7. [c] Ref. 1.

The Stark spectroscopic data collected in this study allow us to make direct comparisons between the two systems to test this premise. Selected data for the complex salts **73**, **75**, **76** and **78** and for their $\{Ru^{II}(NH_3)_5\}^{2+}$ analogues[1,4] (**73A**, **75A**, **76A** and **78A**) are presented in Table 24. Representative UV-Visible absorption spectra of the $n = 2$ complex salt (**76**) and of its ammine analogue (**76A**) are shown in Figure 32.

Table 24: MLCT absorption and Stark spectroscopic data for salts **73**, **75**, **76** and **78** and their $\{Ru^{II}(NH_3)_5\}^{2+}$ analogues in butyronitrile at 77 K

Salt	λ_{max} [nm]	E_{max} [eV]	μ_{12} [D]	$\Delta\mu_{12}$ [D]	β_0 [10^{-30} esu]
73	491	2.53	6.6	14.3	113
73A	645	1.92	5.2	13.8	120
75	515	2.41	6.0	16.9	123
75A	681	1.82	5.5	16.2	175
76	506	2.45	10.0	20.6	401
76A	675	1.84	7.9	22.4	482
78	501	2.48	10.5	22.2	468
78A	669	1.85	7.2	27.1	475

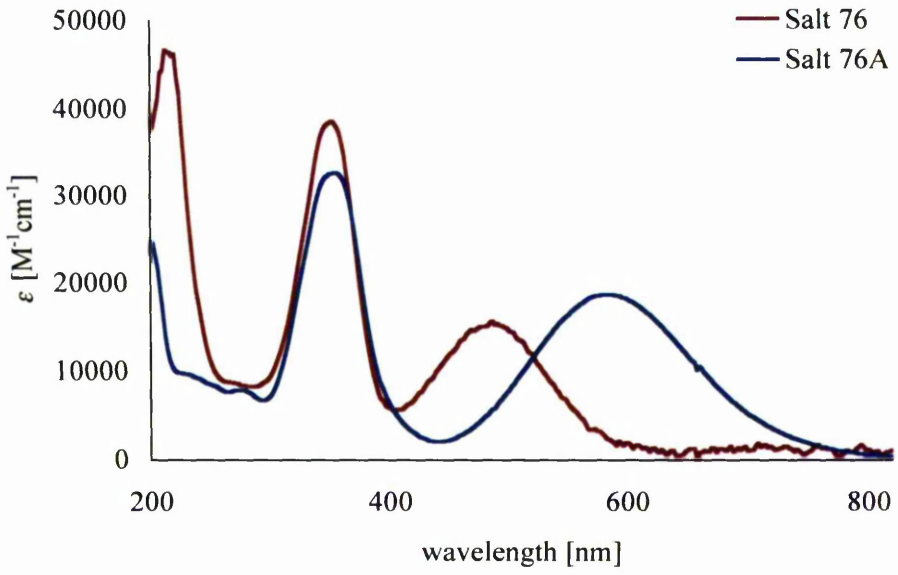

Figure 32: UV/Vis absorption spectra for salts **76** and **76A**

When measured in butyronitrile at 77 K, the MLCT bands of the pdma complexes are blue-shifted by about 0.6 eV when compared to their ammine analogues.

Although the pdma complexes have lower molar extinction coefficients at room temperature, their μ_{12} values are actually higher in every case, since the band intensities increase substantially upon freezing. The $\Delta\mu_{12}$ values show no consistent variation between the two types of complexes, but are generally of a similar magnitude (with the exception of **78** and **78A**). The values of β_0 derived using the TSM are only slightly larger for the $\{Ru^{II}(NH_3)_5\}^{2+}$ based chromophores, although the differences are within the experimental error. However, the consistency of this trend is reasonably convincing evidence that the Ru^{II} ammine chromophores have the larger NLO responses, although this difference is smaller than would have been predicted.

3.5 Conclusion

The work presented in this chapter investigates the effects of extending the conjugation within a series of complexes of pyridinium-substituted ligands with *trans*-$\{Ru^{II}Cl(pdma)_2\}^{+}$ as the D group. The results obtained allow for direct comparisons to be drawn with analogous $\{Ru^{II}(NH_3)_5\}^{2+}$ complexes.

The linear and NLO properties of these pdma complexes show trends that mirror those found previously in the ammine series. Unusual blue-shifting of the MLCT bands is observed in both types of complex, in contrast to the red-shifting that would be expected in 'normal' D–A polyenes. The data obtained *via* Stark spectroscopy show a large increase in β_0 on moving from $n = 1$ to 2, and then a small (although perhaps not significant) increase on extending the chain further to $n = 3$. The clear evidence for a decrease in β_0 on chain extension that is observed in the ammine

series is not observed within these new complexes, but there is certainly no significant increase in β_0 on moving from $n = 2$ to 3.

The MLCT absorption and electrochemical data obtained at room temperature show that a $\{Ru^{II}(NH_3)_5\}^{2+}$ centre is considerably more electron rich than a *trans*-$\{Ru^{II}Cl(pdma)_2\}^{+}$ unit. However, when the Stark spectroscopic data is analyzed according to the TSM it can be seen that the β_0 responses of the pdma complexes are only slightly smaller than those of their ammine analogues, at least when measured in frozen butyronitrile at 77 K. This unexpected behaviour can be attributed, at least in part, to an increase in the band intensities upon freezing, and it may be expected that at room temperature the NLO responses of the ammine complexes will be substantially larger than those of their pdma counterparts.

Finally, these pdma complexes show relatively large quadratic NLO responses that are accompanied by an increase in the visible transparency, thermal stability and also crystallizing ability when compared with their ammine analogues.

3.6 Future work

Further studies involving long wavelength HRS and/or theoretical calculations will be required in order to establish whether the behaviour of these dipolar ruthenium pdma complexes is actually fundamentally different from that of the ammine species. Such studies may also afford a deeper understanding of the effects of temperature changes on the optical properties.

The presence of a trans chloride ligand allows for the potential of axial ligand substitutions, which may allow manipulation of the electron density at the metal centre, potentially making the *trans*-$\{Ru^{II}(pdma)_2\}^{2+}$ centre a better D group. Previous work done by Coe *et al.* has shown that the trans chloride can be substituted by a *N*-methylimidazole ligand via stepwise reactions of the precursor *trans*-$[Ru^{II}Cl(pdma)_2(NO)][PF_6]_2$.[8] Other common anionic ligands which are stronger electron donors than chloride include azide, hydroxide and thiolates.

The ability to grow crystals and obtain structural data was one of the driving forces for the use of the *trans*-$\{Ru^{II}Cl(pdma)_2\}^{+}$ centre. Such structural investigations reveal the crystal packing of the molecules and indicate whether or not the material may exhibit bulk NLO behaviour. Unfortunately, only crystals of salt **70** possess a noncentrosymmetric space group and this is accompanied by the smallest β_0 of the complexes studied. The crystal packing of **74** and **75** may be altered by anion exchange; a bulkier anion, such as tetraphenylborate, may encourage noncentrosymmetric packing and may even allow crystallization of the other complexes synthesized. It is worth noting that previous studies have shown that the salt *trans*-$[Ru^{II}Cl(pdma)_2(4\text{-}AcPhQ^{+})][PF_6]_2 \cdot Me_2CO$ adopts the noncentrosymmetric space group $Pna2_1$,[2] proving that favourable structures of such complex chromophores can be obtained.

3.7 References

1. B. J. Coe, L. A. Jones, J. A. Harris, B. S. Brunschwig, I. Asselberghs, K. Clays and A. Persoons, *J. Am. Chem. Soc.*, 2003, **125**, 862 – 863
2. B. J. Coe, T. Beyer, J. C. Jeffery, S. J. Coles, T. Gelbrich, M. B. Hursthouse and M. E. Light, *J. Chem. Soc., Dalton Trans.*, 2000, 797 – 803
3. B. J. Coe, J. A. Harris and B. S. Brunschwig, *J. Phys. Chem. A*, 2002, **106**, 897 – 905
4. B. J. Coe, L. A. Jones, J. A. Harris, B. S. Brunschwig, I. Asselberghs, K. Clays, A. Persoons, J. Garín and J. Orduna, *J. Am. Chem. Soc.*, 2004, **126**, 3880 – 3891
5. B. J. Coe, M. C. Chamberlin, J. P. Essex-Lopresti, S. Gaines, J. C. Jeffery, S. Houbrechts and A. Persoons, *Inorg. Chem.*, 1997, **36**, 3284 – 3292
6. B. J. Coe, J. A. Harris, L. J. Harrington, J. C. Jeffery, L. H. Rees, S. Houbrechts and A. Persoons, *Inorg. Chem.*, 1998, **37**, 3391 – 3399
7. B. J. Coe, J. A. Harris, I. Asselberghs, A. Persoons, J. C. Jeffery, L. H. Rees, T. Gelbrich and M. B. Hursthouse, *J. Chem. Soc. Dalton Trans.*, 1999, 3617 – 3625
8. B. J. Coe, M. Chery, R. L. Beddoes, H. Hope and P. S. White, *J. Chem. Soc., Dalton Trans.*, 1996, 3917 – 3924
9. P. G. Douglas, R. D. Feltham and H. G. Metzger, *J. Am. Chem. Soc.*, 1971, **93**, 84 – 90
10. B. J. Coe, S. Hayat, R. L. Beddoes, M. Helliwell, J. C. Jeffery, S. R. Batten and P. S. White, *J. Chem. Soc. Dalton Trans.*, 1997, 591 – 600

11. S. Woitellier, J. P. Launay and C. W. Spangler, *Inorg. Chem.,* 1989, **28**, 758 – 762

12. T. W. Graham Solomans, *Organic Chemistry*, 5th Edition, Wiley, 1992

13. P. G. Douglas and R. D. Feltman, *J. Am. Chem. Soc.,* 1972, **94**, 5254 – 5258

14. S. R. Marder, L. T. Cheng, B. G. Tiemann, A. C. Friedli, M. Blanchard-Desce, J. W. Perry and J. Skindhoj, *Science*, 1994, **263**, 511 – 514

15. M. Blanchard-Desce, V. Alain, P. V. Bedworth, S. R. Marder, A. Fort, C. Runser, M. Barzoukas, S. Lebus and R. Wortmann, *Chem. Eur. J.,* 1997, **3**, 1091 – 1104

16. U. Lawrentz, W. Grahn, K. Lukaszuk, C. Klein, R. Wortmann, A. Feldner and D. Scherer, *Chem. Eur. J.,* 2002, **8**, 1573 – 1590

17. M. Blanchard-Desce, C. Runser, A. Fort, M. Barzoukas, J.-M. Lehn, V. Bloy and V. Alain, *Chem. Phys.,* 1995, **199**, 253 – 261

18. T. Farell, A. R Manning, T. C. Murphy, T. Meyer-Friedrichsen, J. Heck, I. Asselberghs and A. Persoons, *Eur. J. Inorg. Chem.,* 2001, 2365 – 2375

19. M. Gonzalez, J. L. Segura, C. Seroane, N. Martin, J. Garín, J. Orduna, R. Alcala, B. Villacampa, V. Hernandez and J. T. Lopez Navarrette, *J. Org. Chem.,* 2001, **66**, 8872 – 8882

20. Y. K. Shin, B. S. Brunschwig, C. Creutz and N. Sutin, *J. Phys. Chem.,* 1996, **100**, 8157 – 8169

21. I. S. Lee, H. Seo and Y. K. Chung, *Organometallics,* 1999, **18**, 1091 – 1096

22. K. N. Jayaprakash, P. C. Ray, I. Matsuoka, M. M. Bhadbhade, V. G. Puranik, P. K. Das, H. Nishihara and A. Sarkar, *Organometallics,* 1999, **18**, 3851 – 3858

23. T. Farrell, T. Meyer-Friedrichsen, M. Malessa, D. Hasse, W. Saak, I. Asselberghs, K. Worstyn, K. Clays, H. Persoons, J. Heck and A. R. Manning, *J. Chem. Soc. Dalton Trans.*, 2001, 29 – 36

Chapter 4

Nonlinear Optical Properties of Ru(II) Complexes Containing Ethynyl Linkages

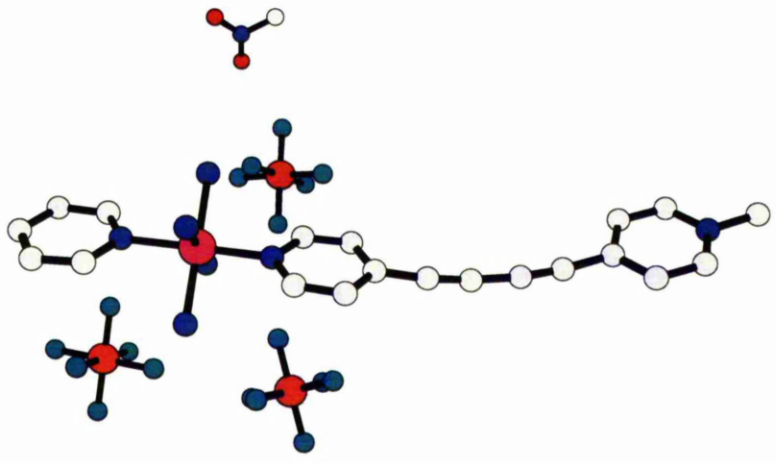

4.1 Introduction

It is well established that for a dipolar chromophore to exhibit a large quadratic NLO response, it must possess an electron donor group linked to an electron acceptor group through a π-conjugated bridge.[1] A common strategy for increasing β_0, in both organic and metal-containing chromophores, is by extending the π-conjugation within the bridge, and it has been found that increasing the number of ethylene units is an effective way to increase the NLO responses of polyene systems.[2] Previous studies within our group have involved the incorporation of *trans*-ethylene units into pyridyl ligands, and the effects of increasing the conjugation length have been investigated in both Ru^{II} ammine[3,4] and diarsine complexes (see Chapter 3). To our knowledge, no NLO studies have been carried out on transition metal pyridyl complexes with ethynyl-connected pyridinium rings, although bis(4-pyridyl)acetylene and related molecules have been used as bridging ligands due to their linear structures.[5-9] In purely organic compounds, it has been observed that the replacement of an ethenyl with an ethynyl linkage causes a decrease in the observed NLO response, with stilbene derivatives having β_0 values about 40–50% larger than those of their diphenylacetylene counterparts,[2] and both experimental and theoretical studies have been carried out in order to rationalize this behaviour.[10-15] However, related extended polyyne systems have not been extensively studied.

The work presented in this chapter involves the synthesis of Ru^{II} ammine and diarsine complexes with ethynyl-containing polypyridyl ligands. The linear and NLO properties of these complexes have been studied, with the primary aims of

investigating the effects of increasing the conjugation pathlength and comparing these systems with previously studied ethenyl-containing chromophores.

4.2 Experimental

4.2.1 Materials and procedures

The ligand pdma was obtained from Dr G. Reid, University of Southampton. The compounds $[Ru^{III}(NH_3)_5(H_2O)][PF_6]_2$,[16] *trans*-$[Ru^{II}Cl(NH_3)_4(SO_2)]Cl$,[16] *trans*-$[Ru^{III}(SO_4)(NH_3)_4(py)]Cl$,[16] *trans*-$[Ru^{II}Cl(pdma)_2(NO)][PF_6]_2$,[17] and 1,4-bis(4-pyridyl)buta-1,3-diyne (bpbd)[18] were prepared according to published procedures. The ligand bis(4-pyridyl)acetylene (bpa) was prepared via a modification of a literature procedure (see below),[19] with chromatographic purification resulting in improved yields. All other reagents were obtained commercially and used as supplied. All reactions were performed under an argon atmosphere. Products were dried at room temperature in a vacuum desiccator ($CaSO_4$) for *ca.* 24 hours prior to characterization.

4.2.2 Syntheses

Bis(4-pyridyl)acetylene. Br_2 (3.5 cm^3, 10.8 g, 68 mmol) was added dropwise to a stirred solution of *E*-1,2-bis(4-pyridyl)ethylene (3.52 g, 19.3 mmol) in HBr (48%, 46.5 cm^3) at 0°C. The mixture was stirred at 120 °C for 2 h, then cooled to room temperature. Chilling in ice caused the precipitation of an orange solid, which was recovered by filtration and washed with water, then stirred, as a suspension, in NaOH

(2 M, 120 cm^3) for 30 min. The resulting white solid, 1,2-dibromo-1,2-bis(4-pyridyl)ethane, was recovered by filtration, washed with a large amount of water and dried. Yield 4.0 g (61%) δ_H ($CDCl_3$) 8.69 (4 H, d, J = 5.9 Hz, C_5H_4N), 7.39 (4 H, d, J = 5.9 Hz, C_5H_4N), 5.27 (2 H, s, CH). Finely cut sodium (1.2 g, 52 mmol) was stirred in *t*-BuOH (120 cm^3) at 80 °C under argon until dissolution was complete (overnight). 1,2-Dibromo-1,2-bis(4-pyridyl)ethane (4.0 g, 11.7 mmol) was added in portions and the mixture was stirred at 80 °C for 4 h. The mixture was cooled to 40 °C and ethanol was added (20 cm^3), followed by water (20 cm^3 CAUTION!). The brown solution was extracted with $CHCl_3$ until the extracts become colourless (*ca.* 6 × 50 cm^3), the extracts dried ($CaCl_2$), and evaporated to dryness. The solid was dissolved in a minimum volume of $CHCl_3$, loaded onto a silica gel column and eluted with diethyl ether-THF (85:15). The major band was collected and evaporated to afford a white solid. Yield 2.0 g (95%). δ_H ($CDCl_3$) 8.60 (4 H, d, J = 6.0 Hz, C_5H_4N), 7.35 (4 H, d, J = 6.0 Hz, C_5H_4N) (Found: C 79.92; H, 4.42; N, 15.31. Calc. for $C_{12}H_8N_2$: C, 79.98; H, 4.47; N, 15.54%). *Note. bpa causes severe and painful blistering of the skin several days after contact, therefore gloves must be worn at all times when handling.*

***N*-Methyl-4-[2-(4-pyridyl)ethynyl]pyridinium iodide, [Mebpa$^+$]I.** To a stirred solution of bpa (500 mg, 2.77 mmol) in diethyl ether (200 cm^3) was added methyl iodide (60 cm^3) and the solution was stirred for 24 h in the dark. The orange precipitate was collected by filtration and washed with diethyl ether. Yield 345 mg (39%). δ_H (500 MHz, D_2O) 8.79 (2 H, d, J = 6.7 Hz, C_5H_4N), 8.60 (2 H, d, J = 6.2 Hz, C_5H_4N), 8.10 (2 H, d, J = 6.8 Hz, C_5H_4N), 7.64 (2 H, d, J = 6.2 Hz, C_5H_4N), 4.37

(3 H, s, Me). ν(C≡C) 2230 m and 2186 m cm^{-1} (Found: C, 48.30; H, 3.36; N, 8.58. Calc. for $C_{13}H_{11}N_2I$: C, 48.47; H, 3.44; H, 3.44 N, 8.70%)

***N*-Methyl-4-[4-(4-pyridyl)buta-1,3-diynyl]pyridinium iodide, [Mebpbd$^+$]I.** This compound was prepared in a manner identical to [Mebpa$^+$]I, using bpbd (500 mg, 2.45 mmol) in place of bpa. An orange solid was obtained. Yield 285 mg (34%). δ_H (500 MHz, D_2O) 8.63 (2 H, d, J = 6.9 Hz, C_5H_4N), 8.40 (2 H, d, J = 6.3 Hz, C_5H_4N), 7.92 (2 H, d, J = 6.9 Hz, C_5H_4N), 7.43 (2 H, d, J = 6.3 Hz, C_5H_4N), 4.17 (3 H, s, Me). ν(C≡C) 2220 m and 2140 m cm^{-1} (Found: C, 52.31; H, 2.81; N, 8.11. Calc. for $C_{15}H_{11}N_2I$: C, 52.05; H, 3.20; N, 8.09%).

***trans*-[Ru^{III}(SO$_4$)(NH$_3$)$_4$(Mebpa$^+$)]Cl$_2$.** A mixture of *trans*-[Ru^{II}Cl(NH$_3$)$_4$(SO$_2$)]Cl (100 mg, 0.329 mmol) and [Mebpa$^+$]I (159 mg, 0.494 mmol) was dissolved in Ar-degassed water (10 cm^3) and heated with stirring at *ca.* 45 °C under Ar for 30 mins. Acetone was added to the brown solution and a dark brown precipitate was collected by filtration, washed with acetone and dried to afford crude *trans*-[Ru^{II}(NH$_3$)$_4$(SO$_2$)(Mebpa$^+$)]X$_3$ (X = Cl and/or I). This material was dissolved in water (5 cm^3) and oxidised by the addition of a 1/1 mixture of 30% aqueous H_2O_2/2 M HCl (2 cm^3). After 10 min at room temperature, acetone was added and the golden precipitate collected by filtration, washed with acetone and dried. Crude yield 104 mg (59 %). This material was used in a subsequent reaction without further purification.

***trans*-[$Ru^{III}(SO_4)(NH_3)_4(Mebpbd^+)$]$Cl_2$.** This compound was prepared in a manner identical to *trans*-[$Ru^{III}(SO_4)(NH_3)_4(Mebpa^+)$]$Cl_2$ using [$Mebpbd^+$]I (171 mg, 0.494 mmol) in place of [$Mebpa^+$]I to afford a golden solid. Crude yield 100 mg (55%).

[$Ru^{II}(NH_3)_5(Mebpa^+)$][PF_6]$_3$ 80. A solution of [$Ru^{II}(NH_3)_5(H_2O)$][PF_6]$_2$ (100 mg, 0.202 mmol) and [$Mebpa^+$]I (65 mg, 0.202 mmol) in Ar-degassed acetone (20 cm^3) was stirred at room temperature under Ar in the dark for 6 h. The addition of diethyl ether afforded a dark precipitate, which was collected by filtration, washed with diethyl ether and dried. Purification was effected by precipitations from acetone/aqueous NH_4PF_6 and then from acetone/diethyl ether (three times) to afford a dark blue-purple solid: yield 50 mg (30%). δ_H(200 MHz, CD_3COCD_3) 9.09 (2 H, d, J = 6.5 Hz, C_5H_4N), 9.01 (2 H, d, J = 6.9 Hz, C_5H_4N), 8.31 (2 H, d, J = 6.7 Hz, C_5H_4N), 7.37 (2 H, d, J = 6.7 Hz, C_5H_4N), 4.58 (3 H, s, Me), 3.51 (3 H, s, *trans*-NH_3), 2.63 (12 H, s, 4 × *cis*-NH_3). ν(C≡C) 2229m and 2195m cm^{-1} (Found: C, 19.69; H, 3.26; N, 11.45. Calc. for $C_{13}H_{26}F_{18}N_7P_3Ru$: C, 19.13; H, 3.21; N, 12.01%).

[$Ru^{II}(NH_3)_5(Mebpbd^+)$][$PF_6$]$_3$ 81. This compound was prepared in a manner identical to **80**, using [$Mebpbd^+$]I (70 mg, 0.202 mmol) in place of [$Mebpa^+$]I. A dark blue-purple solid was obtained: yield 45 mg (27%). δ_H(200 MHz, CD_3COCD_3) 9.13 (2 H, d, J = 6.5 Hz, C_5H_4N), 8.96 (2 H, d, J = 5.8 Hz, C_5H_4N), 8.36 (2 H, d, J = 6.7 Hz, C_5H_4N), 7.40 (2 H, d, J = 6.7 Hz, C_5H_4N), 4.68 (3 H, s, Me), 3.53 (3 H, s, *trans*-NH_3), 2.63 (12 H, s, 4 × *cis*-NH_3). ν(C≡C) 2214m and 2157m cm^{-1} (Found: C, 19.41; H, 2.71; N, 10.35. Calc. for $C_{15}H_{26}F_{18}N_7P_3Ru$: C, 21.44; H, 3.12; N, 11.67%).

***trans*-[$Ru^{II}(NH_3)_4(py)(Mebpa^+)$][$PF_6$]$_3$ 83.** A solution of *trans*-[$Ru^{III}(SO_4)(NH_3)_4(py)$]Cl (100 mg, 0.263 mmol) in Ar-degassed water (6 cm^3) was reduced over zinc amalgam (3 lumps) with Ar agitation for 20 min. The resulting yellow/brown solution was filtered under Ar into a flask containing [$Mebpa^+$]I (127 mg, 0.394 mmol) in Ar-degassed water (4 cm^3) and the solution was stirred at room temperature in the dark under Ar for 6 h. The addition of solid NH_4PF_6 to the deep blue-purple solution gave a dark precipitate, which was allowed to settle overnight in a refrigerator. The solid was collected by filtration, washed with water and dried. Purification was effected by precipitation from acetone/diethyl ether, acetone/LiCl, acetone/aqueous NH_4PF_6 and finally acetone/diethyl ether (three times) to afford a dark purple solid: yield 50 mg (22%). δ_H(200 MHz, CD_3COCD_3) 9.13 (2 H, d, J = 6.7 Hz, C_5H_4N), 9.04 (2 H, d, J = 7.0 Hz, C_5H_4N), 8.90 (2 H, d, J = 5.3 Hz, $H^{2,6}$), 8.37 (2 H, d, J = 6.9 Hz, C_5H_4N), 8.00 (1 H, t, J = 7.47 Hz, H^4), 7.68–7.55 (4 H, m, C_5H_4N + $H^{3,5}$), 4.62 (3 H, s, Me), 2.80 (12 H, s, 4 × NH_3). ν(C≡C) 2233m and 2198m cm^{-1} (Found: C, 26.67; H, 2.63; N, 9.54. Calc. for $C_{18}H_{28}F_{18}N_7P_3Ru$: C, 24.61; H, 3.21; N, 11.16%).

***trans*-[$Ru^{II}(NH_3)_4(py)(Mebpbd^+)$][$PF_6$]$_3$ 84.** This compound was prepared and purified in a manner identical to **83**, using [$Mebpbd^+$]I (137 mg, 0.396 mmol) in place of [$Mebpa^+$]I. A dark purple solid was obtained: yield 51 mg (21%). δ_H(200 MHz, CD_3COCD_3) 9.14 (2 H, d, J = 6.6 Hz, C_5H_4N), 8.98 (2 H, d, J = 6.7 Hz, C_5H_4N), 8.87 (2 H, d, J = 5.1 Hz, $H^{2,6}$), 8.38 (2 H, d, J = 6.9 Hz, C_5H_4N), 7.97 (1 H, t, J = 7.6 Hz, H^4), 7.63–7.54 (4 H, m, C_5H_4N + $H^{3,5}$), 4.63 (3 H, s, Me), 2.79 (12 H, s, 4 × NH_3). ν(C≡C) 2213m and 2151m cm^{-1} (Found: C, 29.36; H, 2.66; N, 9.20. Calc. for $C_{20}H_{28}F_{18}N_7P_3Ru$: C, 26.62; H, 3.13; N, 10.86%).

***trans*-[$Ru^{II}(NH_3)_4$(mim)(Mebpa$^+$)][PF_6]$_3$ 86.** A solution of *trans*-[$Ru^{III}(SO_4)(NH_3)_4$(Mebpa$^+$)]Cl_2 (100 mg, 0.188 mmol) in Ar-degassed water (6 cm^3) was reduced over zinc amalgam (3 lumps) with Ar agitation for 20 min. The resulting purple solution was filtered under Ar into a flask containing *N*-methylimidazole (0.2 cm^3, 2.51 mmol) in Ar-degassed water (4 cm^3) and the solution was stirred at room temperature in the dark under Ar for 6 h. The crude product was precipitated by the addition of solid NH_4PF_6 to the deep blue-purple solution, and purification was effected as for **83** to afford a dark purple solid: yield 35 mg (21%). δ_H(200 MHz, CD_3COCD_3) 9.09 (2 H, d, J = 6.6 Hz, C_5H_4N), 9.01 (2 H, d, J = 6.4 Hz, C_5H_4N), 8.35(2 H, d, J = 6.9 Hz, C_5H_4N), 8.20 (1 H, s, $C_3N_2H_3$), 7.54–7.37 (4 H, m, C_5H_4N + $C_3N_2H_3$), 4.58 (3 H, s, C_5H_4N-*Me*), 3.91 (3 H, s, $C_3N_2H_3$-*Me*), 2.65 (12 H, s, 4 × NH_3). ν(C≡C) 2229m and 2195m cm^{-1} (Found: C, 23.58; H, 3.36; N, 11.79. Calc. for $C_{17}H_{29}F_{18}N_8P_3Ru$: C, 23.17; H, 3.32; N, 12.71%).

***trans*-[$Ru^{II}(NH_3)_4$(mim)(Mebpbd$^+$)][PF_6]$_3$ 87.** This compound was prepared and purified in a manner identical to **86**, using *trans*-[$Ru^{III}(SO_4)(NH_3)_4$(Mebpbd$^+$)]Cl_2 (100 mg, 0.180 mmol) in place of *trans*-[$Ru^{III}(SO_4)(NH_3)_4$(Mebpa$^+$)]Cl_2. A dark purple solid was obtained: yield 31 mg (19%). δ_H(200 MHz, CD_3COCD_3) 9.14 (2 H, d, J = 6.6 Hz, C_5H_4N), 8.99 (2 H, d, J = 6.7 Hz, C_5H_4N), 8.37 (2 H, d, J = 6.7 Hz, C_5H_4N), 8.15 (1 H, s, $C_3N_2H_3$), 7.49–7.35 (4 H, m, C_5H_4N + $C_3N_2H_3$), 4.62 (3 H, s, C_5H_4N-*Me*), 3.93 (3 H, s, $C_3N_2H_3$-*Me*), 2.69 (12 H, s, 4 × NH_3). ν(C≡C) 2212m and 2157m cm^{-1} (Found: C, 24.84; H, 3.11; N, 10.15. Calc. for $C_{19}H_{29}F_{18}N_8P_3Ru$: C, 25.20; H, 3.23; N, 12.38%).

***trans*-[RuCl(pdma)$_2$(bpa)]PF$_6$ 89.** A solution of *trans*-[RuCl(pdma)$_2$(NO)][PF$_6$]$_2$ (125 mg, 0.123 mmol) and NaN_3 (8.1 mg, 0.125 mmol) in acetone (10 cm^3) was stirred at room temperature for 2 h. Butan-2-one (15 cm^3) and bpa (221 mg, 1.22 mmol) were added and the acetone removed *in vacuo*. The solution was heated to reflux for 2 h, cooled to room temperature, and diethyl ether added to afford a dark red/brown precipitate. The excess bpa was removed by two precipitations from acetone-diethyl ether. The product was further purified by precipitation from acetone-aqueous NH_4PF_6, then from acetone-diethyl ether to afford a red/brown solid. Yield 79 mg (58%). δ_H(CD_3COCD_3, 300 MHz) 8.70 (2 H, br s, C_5H_4N), 8.30 (4 H, m, C_6H_4), 7.83 (4 H, m, C_6H_4), 7.77 (2 H, d, J = 6.7 Hz, C_5H_4N), 7.50 (2 H, d, J = 6.6 Hz, C_5H_4N), 7.19 (2 H, d, J = 6.7 Hz, C_5H_4N), 1.90 (12 H, s, 4AsMe), 1.80 (12 H, s, 4AsMe). (Found: C, 36.33; H, 3.62; N, 2.61. Calc. for $C_{32}H_{40}RuAs_4ClPF_6$: C, 37.18; H, 3.62; N 2.70). ν(C≡C) 2230 m cm^{-1}

***trans*-[RuCl(pdma)$_2$(bpbd)]PF$_6$ 90.** This compound was prepared in a manner identical to **89**, using *trans*-[RuCl(pdma)$_2$(NO)][PF$_6$]$_2$ (150 mg, 0.148 mmol) and NaN_3 (9.6, 0.148 mmol) in acetone (5 cm^3) and bpbd (149 mg, 0.73 mmol) in place of bpa. The product was obtained as an orange solid. Yield 42 mg (26%). δ_H(CD_3CN, 300 MHz) 8.61 (2 H, d, J = 6.0 Hz, C_5H_4N), 8.17 (4 H, m, C_6H_4), 7.80 (4 H, m, C_6H_4), 7.42–7.39 (4 H, m 2C_5H_4N), 6.88 (2 H, d, J = 6.9 Hz, C_5H_4N), 1.80 (12 H, s, 4AsMe), 1.61 (12 H, s, 4AsMe)(Found: C, 38.27; H, 3.70; N, 2.53. Calc. For $C_{34}H_{40}N_2RuAs_4ClPF_6$: C, 38.60; H, 3.81; N, 2.65). ν(C≡C) 2220 m cm^{-1}

trans-**[RuCl(pdma)$_2$(Mebpa$^+$)][PF$_6$]$_2$ 92**. A solution of **88** (50 mg, 0.048 mmol) in DMF (1.5 cm^3) and methyl iodide (0.5 cm^3) was stirred for 24 h. The excess methyl iodide was removed *in vacuo* and addition of aqueous NH_4PF_6 to the dark red solution gave a brick red precipitate, which was collected by filtration, washed with water and dried. Purification was effected by precipitation from acetone-diethyl ether. Yield 48 mg (94%). δ_H(CD_3COCD_3, 300 MHz) 9.06 (2 H, d, J = 6.7 Hz, C_5H_4N), 8.30 (4 H, m, C_6H_4), 8.21 (2 H, d, J = 6.9 Hz, C_5H_4N), 7.83 (6 H, m, C_6H_4 and C_5H_4N), 7.26 (2 H, d, J = 6.9 Hz, C_5H_4N), 4.57 (3 H, s, C_5H_4N-*Me*), 1.91 (12 H, s, 4AsMe), 1.85 (12 H, s, 4AsMe). (Found: C, 33.20; H, 3.63; N, 2.35. Calc. for $C_{33}H_{43}N_2RuAs_4ClP_2F_6$: C, 33.21; H, 3.26; N, 2.41). ν(C≡C) 2234 m and 2199 m cm^{-1}

trans-**[RuCl(pdma)$_2$(Mebpbd$^+$)][PF$_6$]$_2$ 93**. This compound was prepared and purified in a manner identical to **92**, using **90** (20 mg, 0.019 mmol) in place of **88**. The product was obtained as a dark red solid. Yield 19 mg (83%). δ_H(CD_3CN, 300 MHz) 8.57 (2 H, d, J = 6.9 Hz, C_5H_4N), 8.17 (4 H, m, C_6H_4), 7.98 (2 H, d, J = 6.9 Hz, C_5H_4N), 7.80 (4 H, m, C_6H_4), 7.51 (2 H, d, J = 6.7 Hz, C_5H_4N), 6.89 (2 H, d, J = 6.9 Hz, C_5H_4N), 4.24 (3 H, s, C_5H_4N–*Me*), 1.80 (12 H, s, 4AsMe), 1.61 (12 H, s, 4AsMe) (Found: C, 34.47; H, 3.57; N, 2.21. Calc for $C_{35}H_{43}N_2RuClAs_4P_2F_{12}$: C, 34.52; H, 3.56; N, 2.30). ν(C≡C) 2217 m and 2154 m cm^{-1}

4.3 Results and Discussion

4.3.1 Molecular design and synthesis

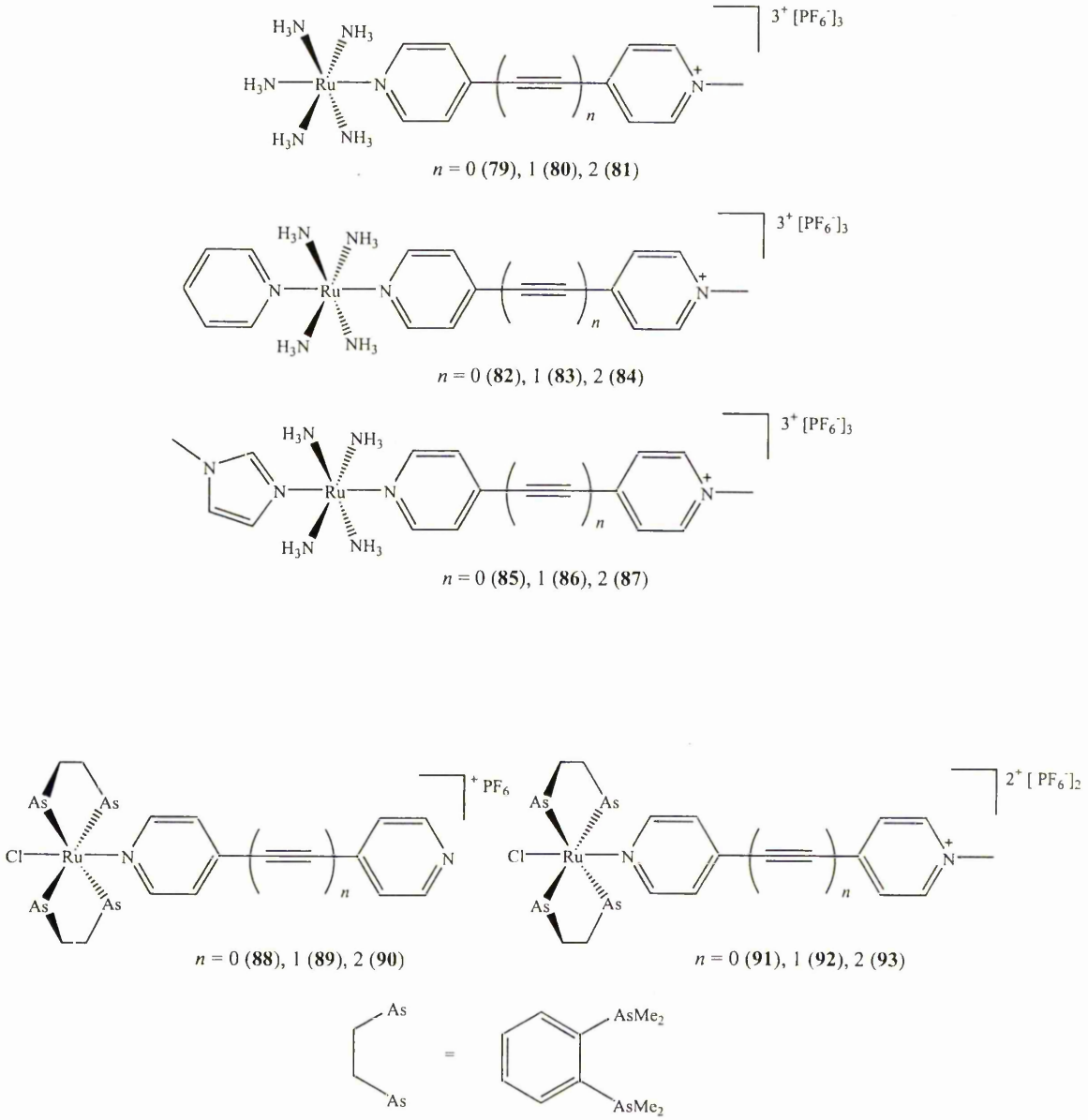

Figure 33: Structures of the complex salts **79**–**93**

The novel complex salts **80**, **81**, **83**, **84**, **86**, **87**, **89**, **90**, **92** and **93**, as shown in Figure 33, were synthesized in order to probe the effects of separating the D and A units by an ethynyl linkage, and alongside the existing compounds **79**,[20] **82**,[4] **85**,[20] **88**[21] and **91**[22] will provide insights into the electronic and NLO properties of such compounds. All of the new salts show diagnostic proton NMR spectra, and infrared spectra confirm the presence of the ethynyl units. Elemental analyses are only useful in providing further confirmation of identity and purity for the complex salts containing the pdma ligand. Although satisfactory CHN data for related compounds have previously been reported,[4,20] the new compounds **80**, **81**, **83**, **84**, **86** and **87** repeatedly gave poor results. The results obtained could not be improved by adding burn-aids such as V_2O_5 or by invoking solvents of crystallization (water and acetone have been found in related compounds). In most cases, the values obtained for carbon are high and the values for nitrogen low, but this behaviour is not always consistent or reproducible. It can therefore be concluded that there is some inherent problem with the Ru^{II} ammine complexes containing ethynyl groups. The NMR data obtained show clean products and with the standard synthetic and purification procedures used, it is reasonable to assume that the compounds isolated are at least sufficiently pure for the studies we describe herein.

The synthesis of bis(4-pyridyl)acetylene (bpa), as outlined in Figure 34, firstly involves the conversion of *E*-1,2-bis(4-pyridyl)ethylene to its perbromide by stirring in hydrobromic acid (63%) and bromine.[19] Debromination of the pyridyl nitrogens with sodium hydroxide affords 1,2-dibromo-1,2-bis(4-pyridyl)ethane. Dehydrobromination is then achieved using sodium *tert*-butoxide (this is made *in situ* by the dissolution of sodium in *tert*-butanol), producing bpa. This solid product

must be handled with care as it causes severe and painful blistering of the skin several days after contact, so gloves must be worn at all times.

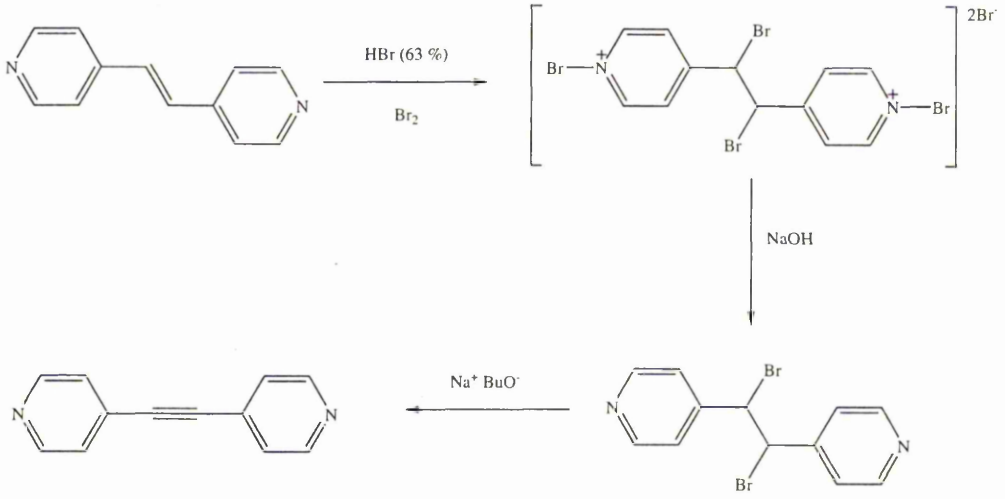

Figure 34: Reaction scheme for the formation of bpa

The compound 1,4-bis(4-pyridyl)buta-1,3-diyne (bpbd) is synthesized in a three-step reaction, shown in Figure 35. Firstly, 4-bromopyridine hydrochloride is coupled with 2-methyl-but-3-yn-2-ol, a commercially available protected terminal alkyne. This coupling reaction is catalyzed by bis(triphenylphosphine)palladium(II) dichloride and copper(I) iodide, with diethylamine acting as both the solvent and the base. Removal of acetone by heating to reflux with sodium hydroxide in toluene, produces the unprotected alkyne, which is unstable and decomposes over the course of a few hours. When a solution of 4-ethynylpyridine is stirred in oxygenated pyridine in the presence of copper(I) chloride, bpbd is formed. This type of reaction is known as an Eglington coupling.[23]

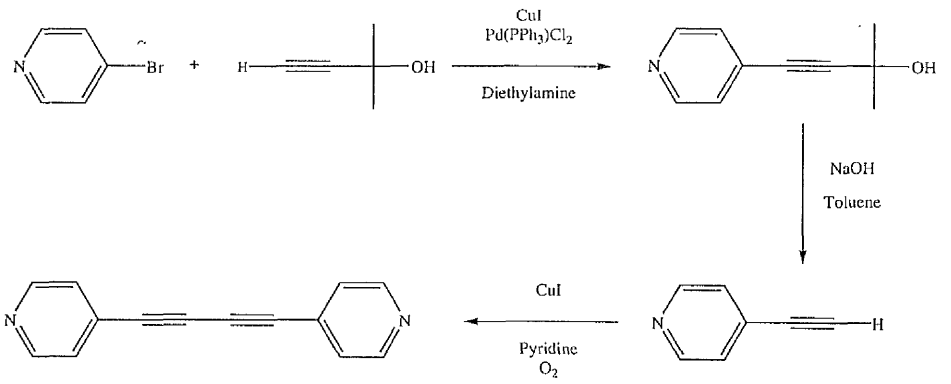

Figure 35: Reaction scheme for the formation of bpbd

The Eglington reaction (Figure 36) provides a facile route to the formation of symmetrical acetylenes.[23,24]

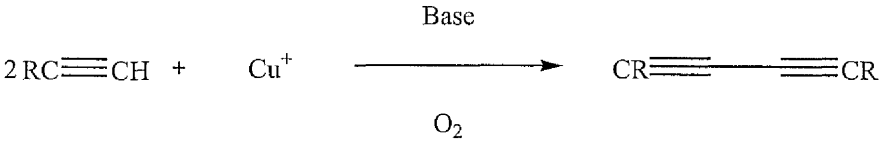

Figure 36: The Eglington reaction

Pyridine is chosen as both the base and the solvent because as well as deprotonating the terminal alkyne, it removes any HCl liberated during the reaction. The mechanism of the Eglington reaction is still not truly understood, but is thought to be ion-radical in nature.[25] The first step probably involves the deprotonation of the acidic terminal hydrogen and the final step probably involves the coupling of two radicals (Figure 37):

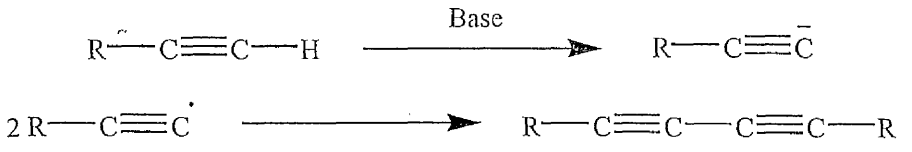

Figure 37: Possible reaction scheme for the Eglington coupling

It is unclear exactly how the carbanion is oxidised to the radical, but after much speculation this process is thought to somehow involve the cuprous ion.[23]

The synthesis of 1,4-bis(4-pyridyl)hexa-1,3-5-triyne (bpbt) (n = 3) was also attempted, with the aim of further extending the acetylenic conjugation. This compound, to our knowledge, has never been synthesized before. The initial strategy proposed was to perform a Cadiot-Chodkiewicz coupling reaction between 4-(buta-1,3-diynyl)pyridine and 4-(bromoethynyl)pyridine (Figure 38):[26]

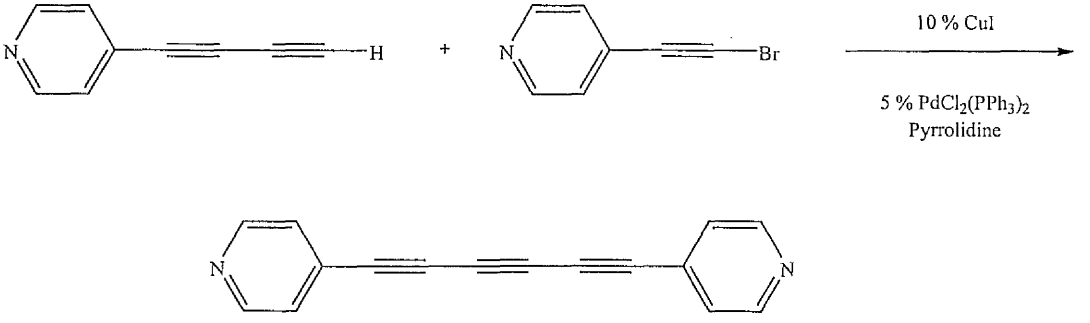

Figure 38: Proposed reaction scheme for the formation of bpbt

The Cadiot-Chodkiewicz reaction provides a synthetic route for the formation of unsymmetrical acetylenes (Figure 39):[24]

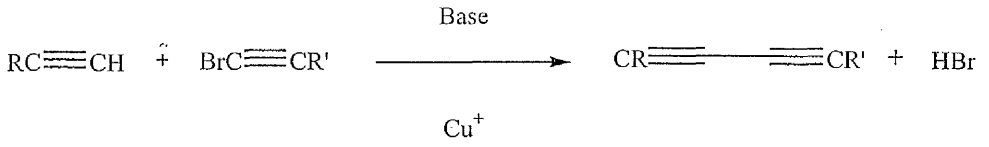

Figure 39: The Cadiot-Chodkiewicz coupling

A catalytic amount of a cuprous salt in a primary amine is added to a solution of the terminal acetylene, and the highly reactive bromoacetylene is added slowly in order to avoid homocoupling.

A proposed mechanism for this reaction is given in Figure 40:

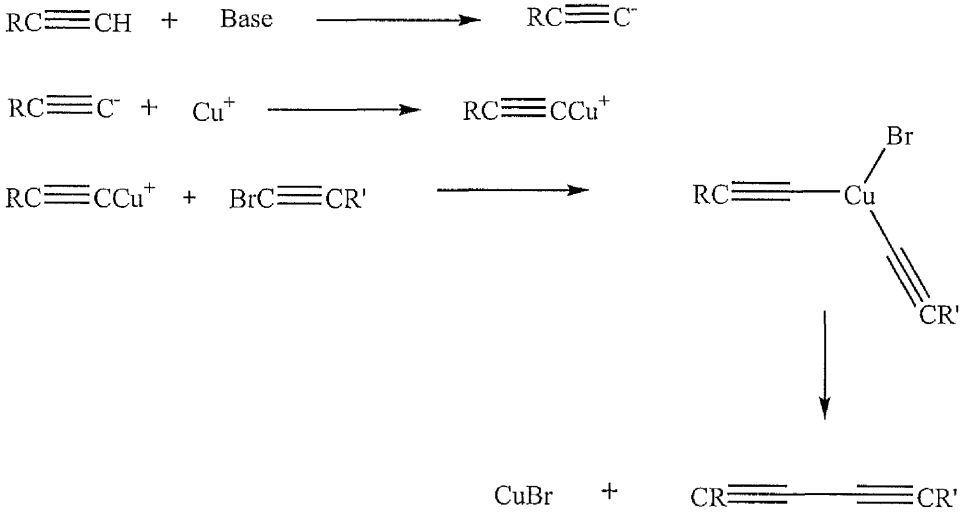

Figure 40: Proposed reaction mechanism for the Cadiot-Chodkiewicz coupling

Catalytic concentrations of the cuprous ion must be maintained to avoid homocoupling of the highly reactive bromoacetylene, and the reducing agent, hydroxylamine hydrochloride is added in order to maintain the Cu^+ concentration.

The required starting materials 4-(butadiynyl)pyridine and 4-(bromoethynyl)pyridine are known but not commercially available and therefore must be synthesized. The synthesis of 4-(bromoethynyl)pyridine was attempted by using two methods:

i. The conversion of 4-pyridinecarboxaldehyde to its β,β-dibromostyryl derivative by a dehydrohalogenation reaction with carbon tetrabromide and triphenylphosphine in the presence of zinc dust.[27] Reaction with potassium *tert*-butoxide in boiling toluene was intended to convert the bromoalkene to the bromoacetylene (Figure 38).[28]

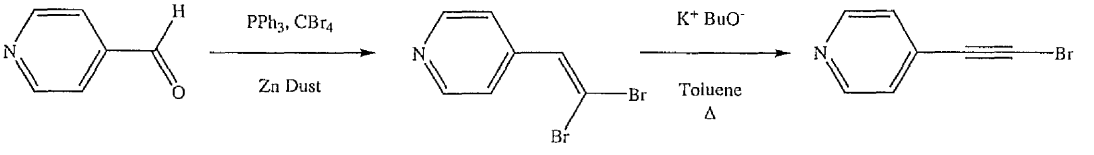

Figure 41: Initial synthetic method for the attempted formation of 4-(bromoethynyl)pyridine

After work up, a cream coloured solid was obtained, but unfortunately no ν(C≡C) band was seen in the IR spectrum (quoted literature value = 2195 cm^{-1}) and the ^1H NMR showed a complex product mixture.

ii. The second method attempted involved the reaction between 4-ethynylpyridine and sodium hypobromite (Figure 42).[29] Sodium hypobromite was formed *in situ* by the slow addition of bromine to a solution of sodium hydroxide at 0 °C, and 4-ethynylpyridine was then added. After

work up, ^{1}H NMR spectroscopy confirmed the presence of only the starting material, 4-ethynylpyridine, which slowly decomposed.

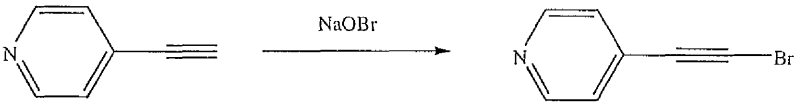

Figure 42: Second method for the attempted formation of 4-(bromoethynyl)pyridine

The synthesis of 4-(buta-1,3-diynyl)pyridine is a two-step reaction (Figure 43): firstly, 4-ethynylpyridine is coupled with 1-bromo-2-(triethylsily)acetylene, and the unprotected diyne is then formed by the removal of the triethylsilyl group.[30]

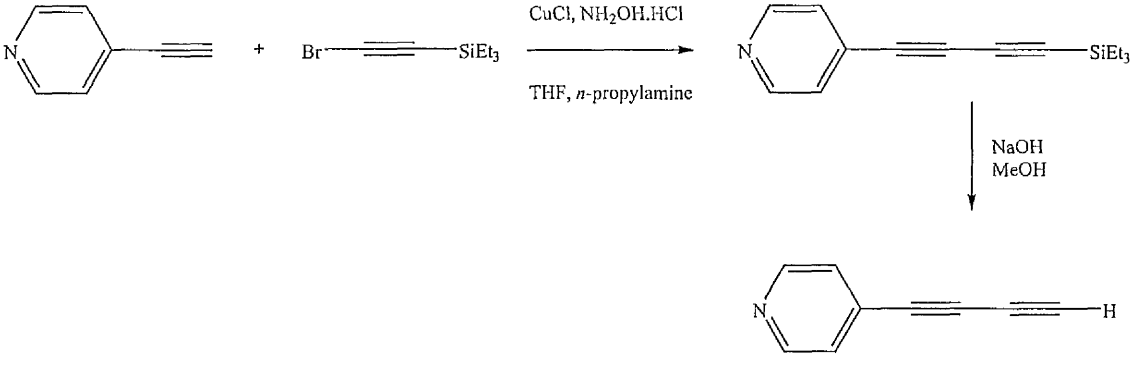

Figure 43: Reaction scheme for the attempted synthesis of 4-(butadiynyl)pyridine

1-Bromo-2-(triethylsilyl)acetylene was synthesized by reaction between triethylsilyacetylene, ethylmagnesium bromide and bromine,[31] and the resulting clear liquid was stored in the fridge because it is very reactive. IR spectroscopy showed

the presence of both 1-bromo-2-(triethylsilyl)acetylene (ν(C≡C) 2123 vs) and unreacted triethylsilyacetylene (ν(C≡C) 2034 vs) which could not be separated. Therefore, an alternative preparation was tried.[32] This involved the reaction of triethylsilyacetylene with silver nitrate and *N*-bromosuccinimide. Once again however, the IR spectrum showed the presence of both 1-bromo-2-(triethylsilyl)acetylene and triethylsilyacetylene.

A coupling reaction between 4-ethynylpyridine and the impure 1-bromo-2-(triethylsilyl)acetylene was attempted. This reaction was catalyzed by copper chloride in THF with hydroxylamine hydrochloride (this prevents the oxidation of Cu^{I} to Cu^{II}), using *n*-propylamine as the base.[30] Unfortunately, after work up, only the starting material 4-ethynylpyridine was recovered, probably a result of the 1-bromo-2-(triethylsilyl)acetylene being impure.

Given that neither 4-(buta-1,3-diynyl)pyridine nor 4-(bromoethynyl)pyridine were successfully synthesised, the coupling reaction could not be performed. Since the synthetic demands in making these starting materials are high and all the reactions time-consuming, it was decided to abandon the pursuit of bpbt, at least for the present.

The new complex salts **80**, **81**, **83**, **84**, **86** and **87** were synthesized according to established co-ordination chemistry as shown in Figure 44.[16,33] The precursor compound $[Ru^{II}(NH_3)_5(H_2O)][PF_6]_2$ was prepared by the reduction of $[Ru^{III}(NH_3)_5Cl]Cl_2$ with Zn(Hg) in acidified water with argon agitation. The very

labile aquo ligand is easily substituted for either of the L_A ligands, Mebpa$^+$ or Mebpbd$^+$ to form complex salts **80** and **81**.

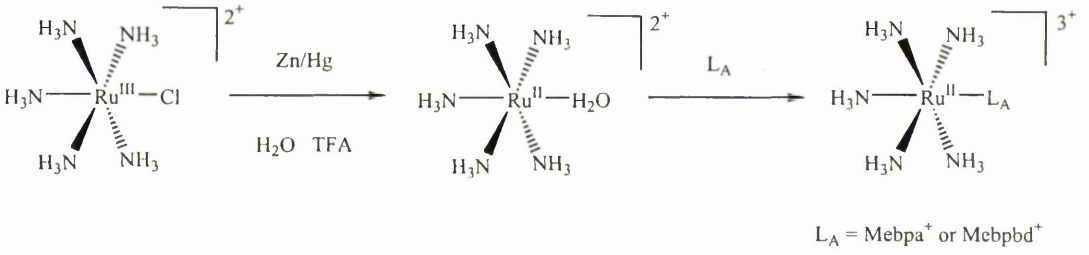

Figure 44: Reaction scheme for the formation of $[Ru^{II}(NH_3)_5L_A]^{3+}$

The synthesis of **83**, **84**, **86** and **87** occurs in a stepwise fashion from *trans*-$[Ru^{II}(NH_3)_4(SO_2)Cl]Cl$ as shown in Figure 45. The SO_2 ligand labilizes the chloride and allows for substitution by L_D = pyridine (in the preparations of **83** and **84**) or by L_A = Mebpa$^+$ or Mebpbd$^+$ (in the preparations of **86** and **87**, respectively). It has previously been reported that the substitution of SO_2 for L_D = *N*-methylimidazole (mim) can be achieved,[20] but when this synthesis was repeated, a sticky black oil was formed and the desired product could not be isolated. Oxidation by H_2O_2/HCl produces the Ru^{III} SO_4^{2-} complex and Zn(Hg) reduces Ru^{III} to Ru^{II} in aqueous solution, affording *trans*-$[Ru^{II}(NH_3)_4L_{A/D}(H_2O)]^{2+/3+}$ (L_D = pyridine, L_A = Mebpa$^+$ or Mebpbd$^+$). The latter, when added to an aqueous solution of the second ligand (Mebpa$^+$ or Mebpbd$^+$ for **83** and **84**, respectively, or mim for **86** and **87**) lose their labile aquo groups to produce the desired compounds.

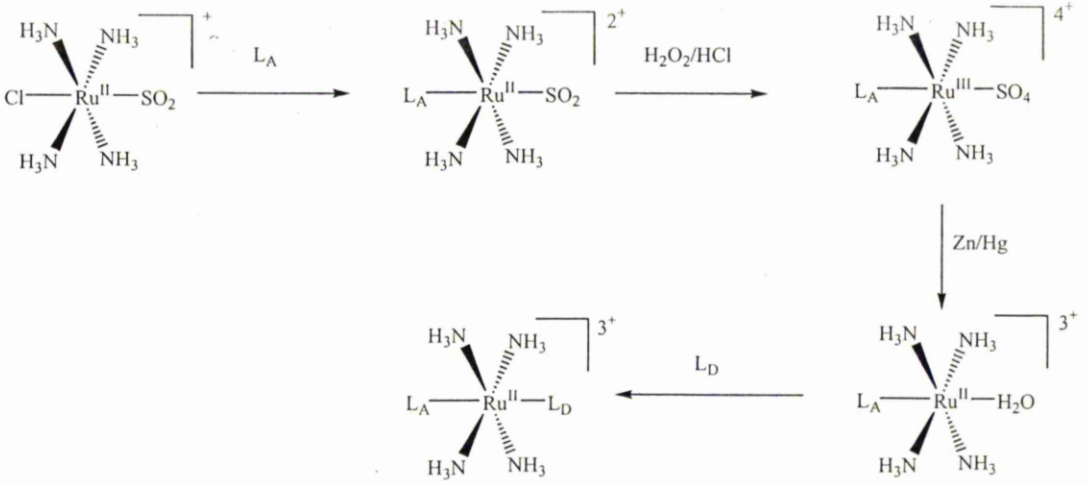

Figure 45: Reaction scheme for the formation of the complexes *trans*-$[Ru^{II}(NH_3)_5L_AL_D]^{3+}$

The complex salts **89** and **90** were made *via* complexation of the neutral ligands with the sodium azide-treated precursor *trans*-$[Ru^{II}Cl(pdma)_2(NO)]^{2+}$ (see section 3.3.1 for a full discussion of the reaction mechanism), and the *N*-methylated complexes **92** and **93** were prepared *via* methylation of **89** and **90**, respectively, using methyl iodide in DMF.

4.3.2 Electronic absorption spectroscopy studies

The electronic absorption spectra of the novel complex salts **80**, **81**, **83**, **84**, **86**, **87**, **89**, **90**, **92** and **93** were recorded in acetonitrile at 293 K and the results are presented in Table 25, with a representative spectrum shown in Figure 46. All the complexes show intense $d\pi[Ru^{II}] \rightarrow \pi^*[L_A]$ MLCT bands, with maxima in the region 450–600 nm. Intense absorptions caused by intraligand $\pi \rightarrow \pi^*$ transitions are also observed and in the extended pyridyl ligands (in **81**, **84**, **87**, **90** and **93**) vibronic fine structure

is observed. The MLCT absorption data for the novel complexes and their previously studied 4,4′-bipyridinium counterparts (**79**, **82**, **85**, **88** and **91**) are shown in Table 26.

It would be expected that as the conjugation is extended, a red-shifting in the MLCT band should occur. However, in the three ammine series (**79–87**), as n increases, the MLCT bands show slight blue-shifts. For any given L_A, the E_{max} of the MLCT absorption decreases in the order py < NH_3 < mim, correlating with mim being the most electron-donating of the three L_D ligands. Such red-shifting of the MLCT bands can be attributed to destabilization of the Ru-based HOMOs, and these trends are also reflected in the electrochemical data (see section 4.3.3).

Within the unmethylated pdma systems (**88–90**), as n increases, E_{max} decreases. Methylation of the uncoordinated pyridyl nitrogen in **88–90** (to form **91–93**, respectively) leads to red-shifting of the MLCT band, correlating with the *N*-methylpyridinium group being a better π-acceptor than pyridyl. This red-shift upon methylation of **89** to form **92** is accompanied by a large increase in intensity, which is indicative of more effective D–A orbital overlap. Within the series **91–93**, addition of one ethynyl unit has no significant effect on E_{max}, but as the conjugation is extended further to $n = 2$, a slight blue-shifting of the MLCT is seen.

Table 25: UV/Vis absorption data for complex salts **80**, **81**, **83**, **84**, **86**, **87**, **89**, **90**, **92** and **93** [a]

Salt	λ_{max} [nm]	ε [$M^{-1} cm^{-1}$]	E_{max} [eV]	Assignment
80	586	19 000	2.12	$d\pi \rightarrow \pi^*$
	296	27 500	4.19	$\pi \rightarrow \pi^*$
81	580	20 500	2.14	$d\pi \rightarrow \pi^*$
	324	23 000	3.83	$\pi \rightarrow \pi^*$
	306 (sh)	20 500	4.05	$\pi \rightarrow \pi^*$
	268	24 000	4.63	$\pi \rightarrow \pi^*$
	254 (sh)	22 500	4.88	$\pi \rightarrow \pi^*$
83	558	15 500	2.26	$d\pi \rightarrow \pi^*$
	286	40 500	4.34	$\pi \rightarrow \pi^*$
84	546	18 000	2.27	$d\pi \rightarrow \pi^*$
	345 (sh)	18 500	3.59	$\pi \rightarrow \pi^*$
	324	22 500	3.83	$\pi \rightarrow \pi^*$
	304 (sh)	20 000	4.08	$\pi \rightarrow \pi^*$
	268	26 000	4.63	$\pi \rightarrow \pi^*$
	258 (sh)	25 500	4.81	$\pi \rightarrow \pi^*$
86	596	14 000	2.08	$d\pi \rightarrow \pi^*$
	284	33 200	4.37	$\pi \rightarrow \pi^*$
87	586	16 500	2.12	$d\pi \rightarrow \pi^*$
	324	19 000	3.83	$\pi \rightarrow \pi^*$
	304 (sh)	17 500	4.08	$\pi \rightarrow \pi^*$
	270	21 000	4.59	$\pi \rightarrow \pi^*$
89	434	6000	2.86	$d\pi \rightarrow \pi^*$
	286	22 100	4.33	$\pi \rightarrow \pi^*$
90	454	8800	2.73	$d\pi \rightarrow \pi^*$
	324	17 300	3.82	$\pi \rightarrow \pi^*$
	302	23 000	4.11	$\pi \rightarrow \pi^*$
	286	23 400	4.34	$\pi \rightarrow \pi^*$
	272	28 800	4.56	$\pi \rightarrow \pi^*$
	240	36 200	5.16	$\pi \rightarrow \pi^*$
92	488	11 500	2.54	$d\pi \rightarrow \pi^*$
	300	21 900	4.13	$\pi \rightarrow \pi^*$
93	482	10 700	2.57	$d\pi \rightarrow \pi^*$
	342	13 800	3.63	$\pi \rightarrow \pi^*$
	320	16 100	3.88	$\pi \rightarrow \pi^*$
	298	15 500	4.16	$\pi \rightarrow \pi^*$
	280 (sh)	18 000	4.43	$\pi \rightarrow \pi^*$
	264	20 000	4.70	$\pi \rightarrow \pi^*$

[a] Solutions *ca.* $3–8 \times 10^{-5}$

Table 26: MLCT absorption data for salts **79–93** [a]

Salt	λ_{max} [nm]	ε [M^{-1} cm^{-1}]	E_{max} [eV]
79[b]	590	15 800	2.10
80	586	19 000	2.12
81	580	20 500	2.14
82[c]	566	17 200	2.19
83	558	15 500	2.22
84	546	18 000	2.27
85[d]	602	16 200	2.06
86	596	14 000	2.08
87	586	16 500	2.12
88[e]	418	8400	2.97
89	434	6000	2.86
90	454	8800	2.73
91[f]	486	8300	2.55
92	488	11 500	2.54
93	482	10 700	2.57

[a] Solutions *ca.* 3–8 × 10^{-5} M. [b] Ref 20. [c] Ref. 4. [d] Ref. 20. [e] Ref. 21. [f] Ref. 22.

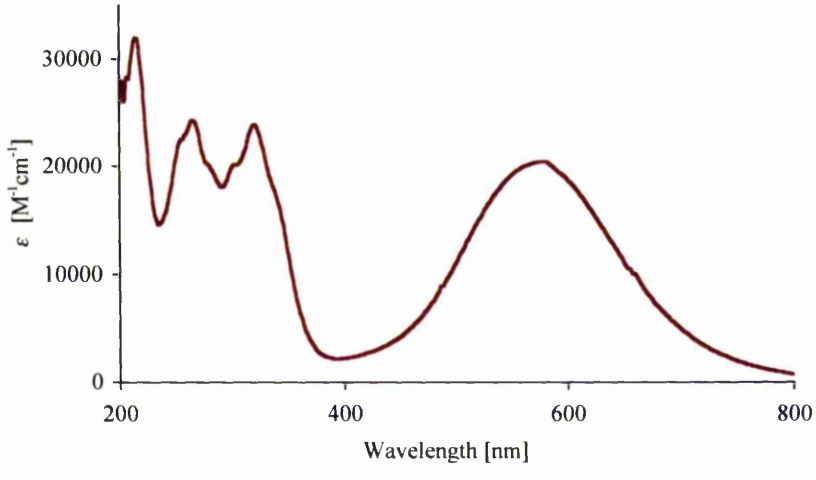

Figure 46: UV/Vis absorption spectrum for salt **84**

Comparison of the MLCT data for the ammine (**79–87**) and diarsine (**91–93**) complexes shows that the ammines have lower values of E_{max} in every instance, due to $\{Ru^{II}(NH_3)_5\}^{2+}$ being a more efficient electron donor than *trans*-$\{Ru^{II}Cl(pdma)_2\}^{+}$ (see also Section 3.4). The intensity of this transition is also consistently higher for the ammine complexes, indicative of more effective D–A orbital overlap.

4.3.3 Electrochemical studies

The new complex salts **80**, **81**, **83**, **84**, **86**, **87**, **89**, **90**, **92** and **93** were studied using cyclic voltammetry in acetonitrile and the results, alongside those for **79**, **82**, **85**, **88** and **91** are presented in Table 27, with a representative voltammogram for salt **81** shown in Figure 47. All of the complexes show reversible $Ru^{III/II}$ oxidation waves, together with generally irreversible L_A-based reductions, although **79**, **85** and **91** do show reversible L_A-based processes

Within the three ammine series (**79–87**), for any given L_D, the $E_{1/2}$ values for the $Ru^{III/II}$ couple are essentially independent of the nature of L_A, showing that the π-acceptor strength of the latter has no significant influence on the energy of the Ru-based HOMO. For any given L_A, the $Ru^{III/II}$ $E_{1/2}$ values shift cathodically in the order py > NH_3 ≅ mim, with the py complexes being the hardest to oxidise.

Table 27: Electrochemical data for complex salts **79–93**

Salt	E [V vs. Ag-AgCl] (ΔE_p [mV])[a]	
	$E_{1/2}[Ru^{III/II}]$	$E_{1/2}[L_A^{+/0}]$ or E_{pc}[b]
79[c]	0.48 (75)	–0.91 (70)
		–1.52 (70)
80	0.50 (100)	–0.83
81	0.49 (85)	–0.73
		–1.49
82[d]	0.66 (85)	–0.81
83	0.65 (80)	–0.81
84	0.65 (100)	–0.73
		–1.52
85[e]	0.49 (75)	–0.83 (70)
86	0.48 (115)	–0.82
87	0.46 (115)	–0.75
88[f]	1.10 (60)	–1.49
89	1.12 (95)	–1.10
90	1.15 (70)	–1.28
91[g]	1.14 (70)	–0.74 (80)
92	1.15 (105)	–0.98
93	1.14 (70)	–0.69

[a] Solutions *ca.* 10^{-3} M in analyte and 0.1M in $NBu^n_4PF_6$ at a platinum disc working electrode with a scan rate of 200 mVs^{-1}. Ferrocene internal reference $E_{1/2}$ = 0.43 V. [b] For an irreversible process. [c] Ref. 20. [d] Ref. 4. [e] Ref. 20. [f] Ref. 21. [g] Ref. 22.

The red-shifting of the MLCT absorption band upon methylation of **88–90** to form **91–93**, respectively, can largely be attributed to stabilization of the L_A-based LUMOs. The electrochemical studies, however, show evidence of a slight stabilization of the Ru-based HOMO for pairs **88/91** and **89/92**, while the absence of such an effect for the pair **90/93** is likely to be associated with decreased D–A electronic coupling when compared with the shorter chromophores.

Further comparison of the $Ru^{III/II}$ $E_{1/2}$ values shows that the ammine compounds consistently have more negative $E_{1/2}$ values than their diarsine counterparts. This trend reflects the fact that the $\{Ru^{II}(NH_3)_5\}^{2+}$ centre is a more efficient electron donor than *trans*-$\{Ru^{II}Cl(pdma)_2\}^{+}$, as also observed in the MLCT data (see also Section 3.4).

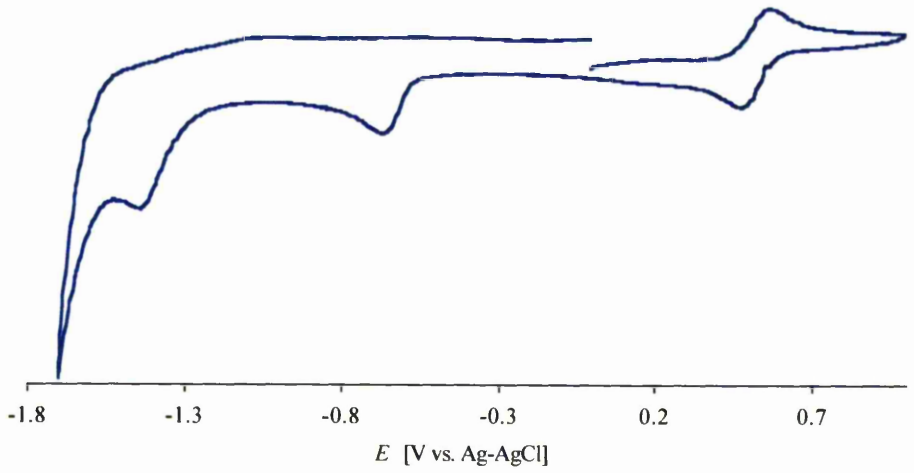

Figure 47: Cyclic voltammogram for salt **81**

4.3.4 X-ray crystallographic studies

Single crystal X-ray structure were obtained for salts **84**•$MeNO_2$ and **92** and representations of their molecular structures are shown in Figures 48 and 49. Selected crystallographic and refinement details are shown in Table 28 and selected bond angles and lengths in Table 29.

The dihedral angles between the pyridyl and pyridinium rings are 18.32(0.21)° in **84**•$MeNO_2$ and 12.66(3)° in **92**. Although these data might appear to indicate more effective D–A electronic communication in **92**, they are likely to result largely from solid-state effects.[22] In addition, there is substantial bending of the buta-1,3-diynyl unit within **84**•$MeNO_2$. The trans coordinated pyridyl rings in **84**•$MeNO_2$ are almost coplanar, with a dihedral angle of 4.79(0.22)°, and essentially bisect the (ammine)N–Ru–N(ammine) angles. Unfortunately, both of these salts crystallize in centrosymmetric space groups, so no significant bulk NLO behaviour can be expected.

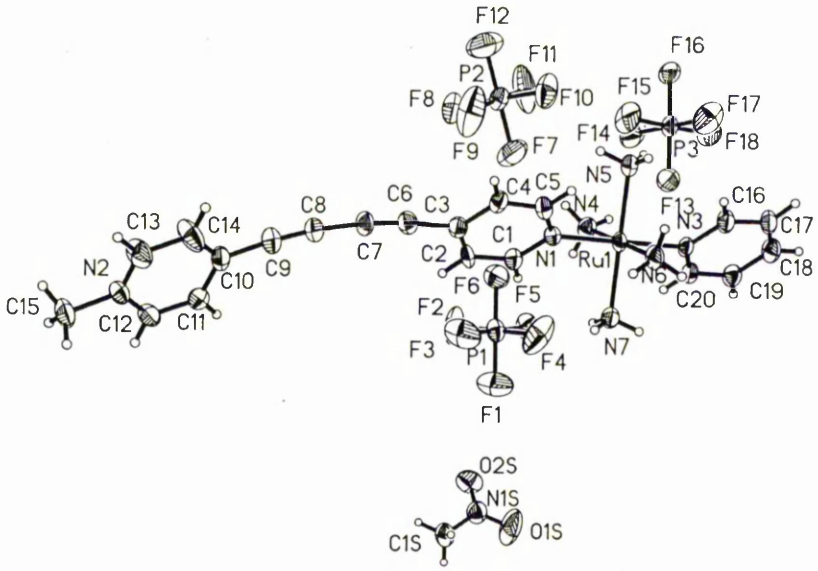

Figure 48: Structural representation of salt **84**•$MeNO_2$ (50% probability ellipsoids)

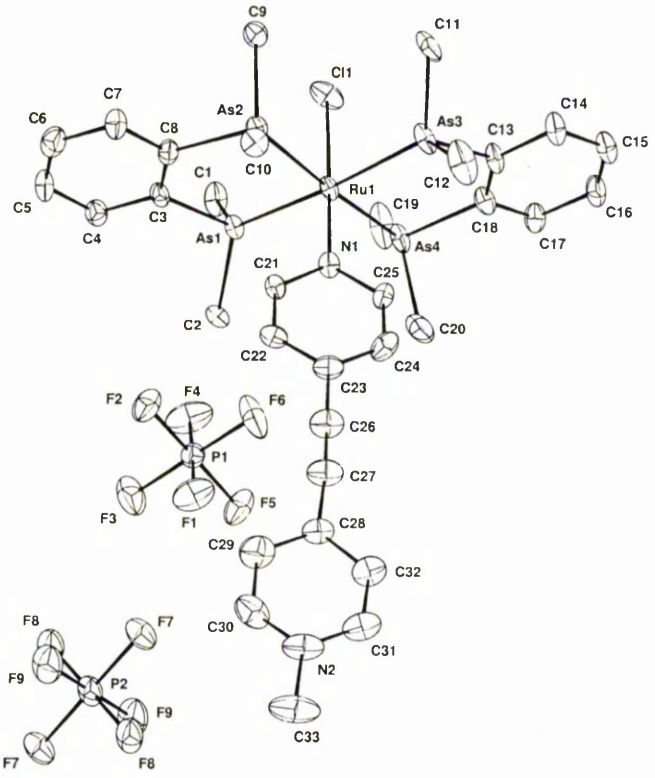

Figure 49: Structural representation of salt **92** (50% probability ellipsoid

Table 28: Crystallographic data and refinement details for salts **84**•$MeNO_2$ and **92**

	84•$MeNO_2$	**92**
Crystal system	Monoclinic	Monoclinic
Space group	$P2_1/c$	$P2_1/c$
Unit cell dimensions [Å, °]		
a	8.912(3)	20.2299(11)
b	20.527(7)	9.5405(4)
c	18.680(6)	24.5138(14)
α	90	90
β	92.498(6)	112.535(2)
γ	90	90
Volume [$Å^3$]	3413.8 (19)	4370.0 (4)
Z	4	4
Absorption coefficient [mm^{-1}]	0.736	3.544
Reflections collected	17196	28451
Independent reflections	6005 ($R_{int} = 0.0676$)	8355 ($R_{int} = 0.0774$)
Final R indices [$F^2 > 2\sigma(F^2)$]		
$R1$	0.0630	0.0527
$wR2$	0.1513	0.1243
R indices (all data)		
$R1$	0.0993	0.0923
$wR2$	0.1664	0.1372

Table 29: Selected interatomic distances (Å) and angles (°) for complex salts **84**•$MeNO_2$ and **92**

84•$MeNO_2$		**92**	
Ru1–N1	2.051(5)	Ru1–N1	2.081(5)
Ru1–N3	2.087(5)	Ru1–As1	2.4094(7)
Ru1–N4	2.129(6)	Ru1–As2	2.4163(7)
Ru1–N5	2.136(5)	Ru1–As3	2.4210(7)
Ru1–N6	2.132(6)	Ru–As4	2.4159(7)
Ru1–N7	2.135(5)	Ru1–Cl1	2.4360(16)
N1–Ru–N3	178.2(2)	N1–Ru1-As1	92.19(12)
N1–Ru–N4	89.9(2)	N1–Ru1–As2	91.63(13)
N1–Ru–N5	98.49(19)	N1–Ru1–As3	94.99(12)
N1–Ru–N6	90.32(19)	N1–Ru1–As4	94.43(13)
N1–Ru–N7	90.8(7)	As1–Ru1–As2	85.61(2)
N3–Ru–N4	89.0(2)	As1–Ru1–As3	172.72(3)
N3–Ru–N5	89.98(19)	As1–Ru1–As4	93.25(2)
N3–Ru–N6	90.8(2)	As2–Ru1–As3	95.39(3)
N3–Ru–N7	89.71(19)	As2–Ru1–As4	173.87(3)
N4–Ru–N5	87.2(2)	As4–Ru1–As3	84.99(2)
N4–Ru–N6	179.5(2)	N1–Ru1–Cl1	178.59(13)
N4–Ru–N7	93.1(2)	As1–Ru1–Cl1	87.62(4)
N5–Ru–N6	93.3(2)	As2–Ru1–Cl1	86.96(5)
N5–Ru–N7	179.6(2)	As3–Ru1–Cl1	85.23(4)
N6–Ru–N7	86.4(2)	As4–Ru1–Cl1	86.97(5)
C6–C7	1.186(9)	C26–C27	1.190(9)
C8–C9	1.200(9)		

4.3.5 Hyper-Rayleigh scattering studies

The β values of the novel complex salts **80**, **81**, **83**, **84**, **86**, **87**, **92** and **93** were measured *via* HRS using a 1064 nm Nd:YAG laser. The values of β_0 were estimated using the TSM and the results, alongside the data for the previously studied compounds **79**, **82** and **84**[4] are presented in Table 30. Previous studies within the group involving complexes containing the *trans*-$\{Ru^{II}Cl(pdma)_2\}^+$ centre have included no HRS data,[21,22] due to the close proximity of λ_{max} to the SH frequency of 532 nm. However, since the λ_{max} values of the complex salts **79–87** are as well separated from 532 nm as are those for salts **91–93**, HRS measurements on the latter are worthwhile.

For the two series **79–81** and **85–87**, as n increases from 0 to 1 there is an apparent increase in β_0, but further extension of the conjugation causes a decrease in β_0, although the difference between the values for **86** and **87** is within the experimental error. For salts **82–84**, as n increases, β_0 apparently decreases, although due to the proximity of the MLCT λ_{max} to the SH, the β_0 for **84** may be underestimated. For any given L_A, the mim complexes generally have the largest β_0 values, corresponding with this being the most electron-donating of the L_D ligands, supporting the trends observed in both the MLCT and electrochemical data (see sections 4.3.2 and 4.3.3). For the series **91–93**, there is no change in β_0 as n increases from 0 to 1, but as the conjugation is extended further to $n = 2$, β_0 increases.

Table 30: MLCT absorption and HRS data for complex salts **79–87** and **91–93**[a]

Salt	λ_{max} [nm]	β_{1064} [10^{-30} esu]	β_0 [10^{-30} esu]
79	590	750	123
80	586	1136	169
81	580	884	117
82	566	899	85
83	588	1076	78
84	546	1280	50
85	602	523	100
86	596	1143	200
87	586	1300	193
91	486	341	45
92	488	359	45
93	482	490	70

[a] The value β_{1064} is the uncorrected first hyperpolarizablity measured using a 1064 nm Nd:YAG laser (±15% error); the static first hyperpolarizability β_0 is estimated using the TSM.[34,35] The esu units can be converted into SI units ($C^3\ m^3\ J^{-2}$) by dividing by a factor of 2.693×10^{-20}.

Although these HRS data show no clear trend in the NLO responses for salts **79–87** and **91–93**, with the exception of the latter pdma complexes, the estimated β_0 values are largest when L_A is $Mebpa^+$.

4.3.6 Stark spectroscopic studies

Stark spectroscopy has been carried out on the novel complex salts **80**, **81**, **83**, **84**, **86**, **87**, **89**, **90**, **92** and **93** in butyronitrile glasses at 77 K and the results are presented, alongside data previously obtained for salts **79**, **82**, **85**, **88** and **91**, in Table

31. As observed previously in related systems, the E_{max} values decrease on moving from an acetonitrile solution to a butyronitrile glass.[36,3]

Table 31: MLCT absorption and Stark spectroscopic data for complex salts **79–93** in butyronitrile glasses at 77 K

Salt	λ_{max} [nm]	E_{max} [eV]	f_{os}	μ_{12}[a] [D]	$\Delta\mu_{12}$[b] [D]	$\Delta\mu_{ab}$[c] [D]	c_b^2[d]	H_{ab}[e]	β_0[f] [10^{-30} esu]
79[g]	645	1.92	0.20	5.2	13.8	17.3	0.10	4700	120
80	648	1.91	0.25	5.9	19.6	22.9	0.07	4000	216
81	664	1.87	0.28	6.3	23.4	26.6	0.06	3600	308
82[g]	611	2.03	0.29	6.1	16.2	20.3	0.10	4900	171
83	618	2.01	0.24	5.6	19.8	22.7	0.06	4000	178
84	627	1.98	0.32	6.6	25.7	28.9	0.05	3600	331
85[g]	658	1.88	0.22	5.5	17.1	20.3	0.08	4100	170
86	661	1.88	0.24	5.8	21.6	24.5	0.06	3600	241
87	667	1.86	0.34	7.0	27.6	31.0	0.05	3400	457
91[h]	491	2.53	0.41	6.6	14.3	19.4	0.13	6900	113
92	509	2.44	0.38	6.4	18.2	22.3	0.09	5600	146
93	506	2.45	0.22	4.9	22.8	24.8	0.04	3900	106

[a] Calculated from eqn. 13. [b] Calculated from $f_{int}\Delta\mu_{12}$ using $f_{int} = 1.33$. [c] Calculated from eqn. 12. [d] Calculated from eqn. 15. [e] Calculated from eqn. 14. [f] Calculated from eqn. 7. [g] Ref 4. [h] This work, Ch.3.

The trends in E_{max} for the three ammine series within **79–87** measured in 77 K glasses differ from those determined in solutions at 293 K. In butyronitrile glasses, as n increases, E_{max} decreases, whereas in acetonitrile solutions the opposite behaviour is observed. Generally, as the conjugation is extended, there is a slight increase in both f_{os} and μ_{12}, although salt **83** has lower than expected values for both

parameters. $\Delta\mu_{12}$ and $\Delta\mu_{ab}$ both increase as the conjugation is extended, *i.e.* as the size of L_A increases. In contrast, H_{ab} and c_b^2 both decrease as n increases, and as these parameters are related to the extent of D–A orbital overlap, it is evident that as the number of triple bonds increases, the orbital overlap becomes less effective. The derived values for β_0 increase as n increases, and for any given L_D the complexes containing the Mebpbd$^+$ ligand ($n = 2$) always have the larger value. This trend in β_0 can be attributed to a slight decrease in E_{max}, alongside increases in both $\Delta\mu_{12}$ and μ_{12}. For a given L_A, the mim complexes generally have the larger values for β_0, corresponding with mim being the strongest electron donor of the L_D ligands.

Within the pdma series **91–93**, as for the ammine series **79–87**, the E_{max} values exhibit different trends when measured in butyronitrile glasses at 77 K or in acetonitrile solutions. At 77 K, as n increases from 0 to 1, there is a decrease in E_{max}, but as the bridge length is increased to $n = 2$, there is no significant change. For this series, f_{os}, μ_{12}, c_b^2 and H_{ab} all decrease as n increases, again indicative of poorer orbital overlap in the more extended systems. $\Delta\mu_{12}$ and $\Delta\mu_{ab}$, as expected, increase as the L_A length increases and the values for $\Delta\mu_{ab}$ are larger in every instance. Most importantly, β_0 peaks at $n = 1$, meaning that this diarsine series shows a different trend when compared with the analogous ammine series.

Generally, the diarsine complexes have substantially smaller NLO responses than their ammine counterparts (although the β_0 values for the $n = 0$ complexes in **79** and **91** are of a similar magnitude). This behaviour can be attributed to the *trans*-$\{Ru^{II}Cl(pdma)_2\}^+$ centre being a less effective electron donor when compared with $\{Ru^{II}(NH_3)_5\}^{2+}$ (see above and Section 3.4).

4.4 Comparisons between ethynyl and ethenyl-containing ligands

Ru^{II} ammine complexes containing pyridyl-pyridinium polyene ligands have been previously studied within our group.[4] These ligands have also been attached to *trans*-$\{Ru^{II}Cl(pdma)_2\}^+$ D groups and the linear and NLO properties of such complexes have been studied as part of this thesis (see Chapter 3). Unusual optical behaviour is seen for both series of compounds, with E_{max} blue-shifting after $n = 1$ and β_0 peaking at $n = 2$.

Electron mobility and D–A communication are important factors in nonlinear optics. A sp-hybridized ethynyl unit possessing a short carbon–carbon triple bond (with an average bond length of 1.20 Å), cannot overlap very efficiently with a sp^2-hybridized pyridyl ring. An ethenyl unit, on the other hand, consisting of a bent sp^2-hybridized carbon–carbon double bond (with an average bond length of 1.33 Å) can overlap effectively with a pyridyl ring. The electrons in an ethynyl unit are also less mobile than those in an ethenyl group because they are held closer to the backbone. It could be expected that larger NLO responses may be observed in polyene as opposed to polyyne-based chromophores due to better D–A communication and the greater polarizability of the π-electrons within the bridge. Although quite limited, existing studies (both theoretical and experimental) on purely organic systems confirm such an expectation.[10-15,38-41] Complexes incorporating polyyne-bridging units into pyridyl-pyridinium ligands have not been studied previously for their NLO properties, and Stark spectroscopy has not been used to compare ethenyl with ethynyl chromophores of any sort.

4.4.1 Ruthenium ammine complexes

Within this section, the optical and electronic properties of only the $\{Ru^{II}(NH_3)_5\}^{2+}$ complexes (salts **80** and **81**) will be discussed, but the conclusions drawn are applicable to any of the Ru^{II} ammine complexes studied.

The MLCT absorption and electrochemical data for salts **80** and **81** measured in acetonitrile at 293 K are shown in Table 32, alongside the data for their ethenyl-containing counterparts **80D** and **81D**.[4] Representative UV-visible spectra for salts **81** and **81D** are shown in Figure 50.

The MLCT bands for the ethynyl-containing complexes are slightly blue-shifted when compared with those of their ethenyl counterparts, but both types of complex show an increase in E_{max} as n increases from 1 to 2. The ε values for salts **80** and **81** are larger than those of **80D** and **81D**, with a greater difference for $n = 1$. The ethynyl-containing chromophores have slightly higher $Ru^{III/II}$ $E_{1/2}$ values, indicating that their Ru centres are less electron-rich due to the mildly electron-donating properties of ethenyl units.

Table 32: MLCT absorption and electrochemical data for complex salts **80** and **81** and their ethenyl counterparts

Salt	λ_{max} [nm]	E_{max} [eV]	ε [M^{-1} cm^{-1}]	E [Ag vs. AgCl] $E_{1/2}[Ru^{III/II}]$
80	586	2.12	19 000	0.50
80D	595	2.08	16 100	0.46
81	580	2.14	20 500	0.49
81D	584	2.12	18 700	0.45

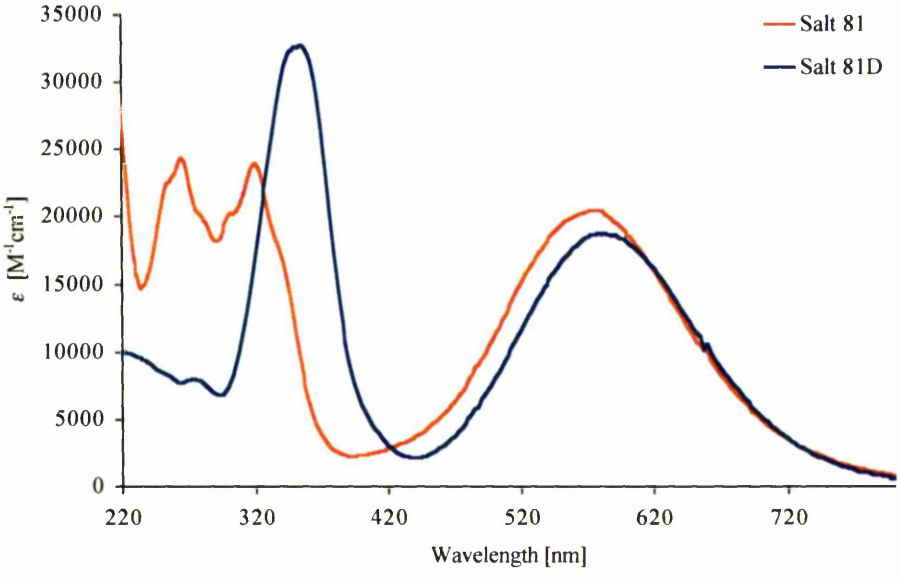

Figure 50: UV/Vis absorption spectra for salts **81** and **81D**

Selected Stark spectroscopic and HRS data for complexes **80** and **81**, along with those for their ethenyl analogues,[4] are presented in Table 33.

Table 33: MLCT and selected Stark spectroscopic data for salts **80** and **81** and their ethenyl counterparts (**80D** and **81D**)

Salt	λ_{max}[a] [nm]	E_{max}[a] [eV]	μ_{12}[a] [D]	$\Delta\mu_{12}$[a] [D]	β_0[Stark][a] [10^{-30} esu]	β_0[HRS][b] [10^{-30} esu]
80	648	1.91	5.9	19.6	216	169
80D	681	1.82	5.5	16.2	175	142
81	664	1.87	6.3	23.4	308	117
81D	675	1.84	7.9	22.4	482	372

[a.] Measured in butyronitrile at 77 K. [b.] Measured in acetonitrile at 293 K

As at 293 K in acetonitrile solutions, in butyronitrile glasses the ethynyl-containing complexes (in **80** and **81**) have slightly higher values for E_{max} than their ethenyl counterparts. In the ethynyl complexes, E_{max} red-shifts as n increases, but in the ethenyl complexes an opposite behaviour is observed. The μ_{12} values for salts **80** and **80D** (n = 1) are of similar magnitude, and as the conjugation extends further to n = 2, an increase in μ_{12} is observed for both types of complex. However, this increase is greater within the ethenyl pair, so that **81D** has a somewhat higher value of μ_{12} than does **81**. $\Delta\mu_{12}$ increases with n for both types of complex, but the ethynyl species have slightly larger values than their ethenyl analogues. The β_0[Stark] values show an increase as n increases for both the ethynyl and ethenyl compounds, and this can be attributed to increases in both μ_{12} and $\Delta\mu_{12}$ and decreases in E_{max}. However, the estimated NLO responses measured using HRS show different behaviour to those determined using Stark spectroscopy. In the ethynyl compounds, β_0[HRS] decreases on moving from n = 1 to 2, whereas in the ethenyl complexes, β_0[HRS] increases

with the same change. The origins of these differing trends are unclear, but may be related to temperature effects.

4.4.2 Ruthenium diarsine complexes

The MLCT absorption and electrochemical data for salts **92** and **93** are presented in Table 34, along with those for their ethenyl counterparts **93D** and **93D**. Representative UV-visible spectra for salts **93** and **93D** shown in Figure 51.

Table 34: MLCT and electrochemical data for salts **92** and **93** and their ethenyl counterparts

Salt	λ_{max} [nm]	E_{max} [eV]	ε [M^{-1} cm^{-1}]	E [V Ag vs. AgCl] $E_{1/2}[Ru^{III/II}]$
92	488	2.54	11 500	1.15
92D	492	2.52	13 000	1.10
93	482	2.57	10 700	1.14
93D	486	2.55	15 700	1.09

The ethynyl-containing complexes have slightly larger E_{max} values than their ethenyl counterparts, and for both types of complex E_{max} increases on moving from $n = 1$ to 2. In contrast with the ammine complexes, the extinction coefficients for the ethynyl chromophores are smaller than those of the ethenyl complexes, and the difference is largest for $n = 2$. As for the ammines, the ethynyl-containing complexes have slightly higher $Ru^{III/II}$ $E_{1/2}$ values than their ethenyl analogues.

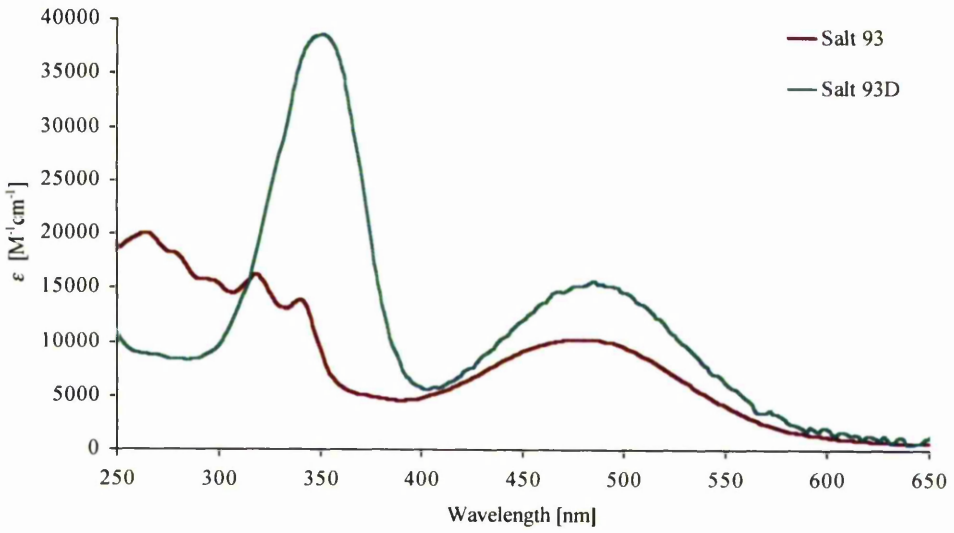

Figure 51: UV/Vis absorption spectra for salts **93** and **93D**

Table 35 shows the Stark spectroscopic data for complex salts **92**, **92D**, **93** and **93D**. HRS measurements have not been performed on salts **92D** and **93D** due to the proximity of their MLCT absorptions to 532 nm, so comparisons of the NLO responses of these complexes using this technique cannot be made.

The increase in E_{max} on moving from n = 1 to 2 at 77 K is most pronounced for the ethenyl complexes. The μ_{12} values for all four complexes are of a similar magnitude. $\Delta\mu_{12}$ increases on moving from n = 1 to 2 for both types of complex, but the ethynyl-containing chromophores have slightly higher values, as also observed in the ammine complexes. For the ethenyl chromophores, β_0[Stark] increases sharply on moving from n = 1 to 2, but the same structural change produces a decrease in the NLO response in the ethynyl species. This behaviour contrasts with that of the ammine systems in which β_0[Stark] increases with conjugation extension for both types of

complex; these observations may be attributed to differences in the behaviour of μ_{12} within the diarsine and ammine series.

Table 35: MLCT and selected Stark spectroscopic data for complex salts **92** and **93** and their ethenyl counterparts (**92D** and **93D**)

Salt	$\lambda_{max}{}^{a}$ [nm]	$E_{max}{}^{a}$ [eV]	$\mu_{12}{}^{a}$ [D]	$\Delta\mu_{12}{}^{a}$ [D]	β_0[Stark]^{a} [10^{-30} esu]
92	509	2.44	6.4	18.2	146
92D	515	2.41	6.0	16.9	123
93	506	2.45	4.9	22.8	106
93D	506	2.45	10.0	20.6	401

4.5 Conclusions

The work presented in this chapter has investigated the effects of incorporating an ethynyl linkage into pyridyl-pyridinium ligands in both Ru^{II} ammine and diarsine chromophores. The optical and electronic properties of these complexes have been studied and compared with the data obtained for ethenyl-containing compounds.

It might be expected that as the number of ethynyl units increases, the MLCT absorption band should red-shift, but in the complexes studied, the MLCT bands actually blue-shift as n increases. The NLO responses of the complex salts were measured using both Stark spectroscopy and HRS, and the trends in β_0 differ depending on the technique used. Within the ammine series, β_0[Stark] increases with

n, but β_0[HRS] generally peaks at $n = 1$. This different behaviour may be related to the measurements being carried out under different physical conditions, which may affect the electronic properties of the molecules. For the diarsine complexes, β_0[Stark] peaks at $n = 1$, although the HRS measurements indicate that the $n = 2$ complex has the largest NLO response. It should be noted that the β values obtained using HRS will be subject to resonance enhancement due to the close proximity of the MLCT λ_{max} to 532 nm, so these data for both types of complex should be treated with caution.

Comparison of the optical properties of the ethynyl and ethenyl-containing complexes shows that the MLCT absorptions of the polyyne complexes are slightly blue-shifted when compared to those of their polyene analogues. Although the trends observed using the two different measurement techniques are not consistent, the ethynyl complexes generally have slightly larger NLO responses than their ethenyl analogues, but the differences are within the experimental errors. However the buta-1,3-diynyl chromophores have lower NLO responses in every instance when compared to their buta-1,3-dienyl counterparts. This result may be related to poorer D–A communication in the ethynyl complexes, attributed to orbital mismatch between the sp-hybridized triple bonds and the sp^2-hybridized pyridyl rings.

As expected from the MLCT absorption and electrochemical data, the NLO responses of the pdma complexes are consistently lower than those of their ammine counterparts. This outcome can be attributed to the $\{Ru^{II}(NH_3)_5\}^{2+}$ centre being a more efficient electron donor than *trans*-$\{Ru^{II}Cl(pdma)_2\}^{+}$ (see also Section 3.4).

4.6 Future work

From a synthetic viewpoint, the most obvious next step is to make the $n = 3$ (and possibly the $n = 4$) ethynyl-containing pyridyl-pyridinium ligands and to complex these to both the Ru^{II} ammine and diarsine centres. The purity of the starting materials seemed to be the major factor in the synthesis of the $n = 3$ ligand, and was probably the reason why the Cadiot-Chodkiewicz coupling reaction was unsuccessful. Different synthetic routes could also be considered, using alternative terminal acetylenes and haloacetylenes. However, the results obtained indicate that pursuing such studies may not be worthwhile from a NLO perspective.

Long wavelength HRS studies could be performed on both the existing Ru^{II} ammine and diarsine complexes, in order to eliminate the problems of resonance enhancement encountered when using a 1064 nm laser.

Dinuclear complexes of the ethynyl-containing bridging ligands (possibly including the $n = 3$ and $n = 4$ species) could be synthesized, and electrochemical and spectroscopic measurements performed to probe the metal-metal communication *via* the polyyne bridge. Comparisons could then be drawn between dinuclear complexes of ethynyl-containing ligands, affording insights into the electronic properties of the two systems. Finally, molecular orbital calculations performed on the complexes synthesized within this study (and perhaps also on related dinuclear species) may allow rationalization of the optical and electronic properties of such compounds.

4.7 References

1. B. L.Davydov, L.D. Derkacheva, V. V. Dunina, M. E. Zhabotinskii, V. K. Zolin, L. G. Kreneva and M. Samokhina, *JEPT Letters,* 1970, **12**, 16 – 18
2. *Nonlinear Optics of Organic Molecules and Polymers,* Eds. H. S. Nalwa and S. Miyata, CRC Press, Boca Raton, 1997
3. B. J. Coe, L. A. Jones, J. A. Harris, B. S. Brinschwig, I. Asselberghs, K. Clays and A. Persoons, *J. Am. Chem. Soc.,* 2003, **125**, 862 – 862
4. B. J. Coe, L. A. Jones, J. A. Harris, B. S. Brunschwig, I. Asselberghs, K. Clays, A. Persoons, J. Garin and J. Orduna, *J. Am. Chem. Soc.,* 2004, **126**, 3880 – 3891
5. T. Rajendran, B. Marimaran, T. –T. Liao, R. –J. Lin, P. Thanasekaram, G. –H. Lee, S. –M. Peng, Y. –H. Liu, I. –J. Chang, S. Rajagopal and K. –L. Lu, *Inorg. Chem.,* 2003, **42**, 6388 – 6394
6. S. –S. Sun, J. A. Anspach, A. J. Lees and P. Y. Zavalij, *Organometallics,* 2002, **21**, 685 – 693
7. M. Ferrer, L. Rodriguez and O. Rossel, *J. Organomet. Chem.,* 2003, **681**, 158 – 166
8. S. –S. Sun and A. J. Lees, *J. Am. Chem. Soc.,* 2000, **122**, 8956 – 8967
9. Md. B. Zaman, K. Udachin, Md. Akhtaruzzaman, Y. Yamashita and J. A. Ripmeester, *Chem. Comm.,* 2002, 2322 – 2323
10. A. E. Stiegmann, E. Graham, K. J. Perry, L. R. Khundkar, L.-T. Cheng and J. W. Perry, *J. Am. Chem. Soc.,* 1991, **113**, 7658 – 7666
11. L.-T. Cheng, W. Tam, S. R. Marder, A. E. Stiegmann, G. Rikken and C. W. Spangler, *J. Phys. Chem.,* 1991, **95**, 10643 – 10652

12. A. E. Stiegman and J. W. Perry and L.-T. Cheng in *Organic Materials for Nonlinear Optics II*, Eds. R. A. Hann and D. Bloor, RSC, London, 1991

13. A. E. Stiegmann, V. M. Miskowski, J. W. Perry and D. R. Coulter, *J. Am. Chem. Soc.,* 1987, **109**, 5884 – 5886

14. C. Dehu, F. Meyers and J. L. Bredas, *J. Am. Chem. Soc.* 1993, **115**, 6198 – 6206

15. J. L. Bredas, C. Dehu, F. Meyers, A. Persoons and J. Zyss, *Mol. Cryst. Liq. Cryst. Sci. and Tech. Sec. B,* 1994, **6**, 263 – 287

16. J. C. Curtis, B. P. Sullivan and T. J. Meyer, *Inorg. Chem.,* 1983, **22**, 224 – 236

17. P. G. Douglas, R. D. Feltham and H. G. Metzger, *J. Am. Chem. Soc.,* 1971, **93**, 84 – 90

18. L. D. Ciana and A. Haim, *J. Heterocyclic Chem.,* 1984, **21**, 607 – 608

19. M. Tanner and A. Ludi, *Chimia,* 1980, **34**, 23 – 24

20. B. J. Coe, J. A. Harris, L. J. Harrington, J. C. Jeffery, L. H. Rees, S. Houbrechts and A. Persoons, *Inorg. Chem.,* 1998, **37**, 3391 – 3399

21. B. J. Coe, S. Hayat, R. L. Beddoes, M. Helliwell, J. C. Jeffery, S. R. Batte and P. S. White, *J. Chem. Soc. Dalton Trans.,* 1997, 591 – 599

22. B. J. Coe, T. Beyer, J. C. Jeffery, S. J. Coles, T. Gelbrich, M. B. Hursthouse and M. E. Light, *J. Chem. Soc. Dalton Trans.,* 2000, 797 – 803

23. G. Eglington and W. McCrae, in *Advances in Organic Chemistry*, Eds. R. Raphael, E. C. Taylor and H. Wynberg, Interscience, New York, 1963

24. *Chemistry of acetylenes,* Ed. H. G. Viehe, Marcel Decker, New York, 1969

25. P. Siemsen, R. C. Livingstone and F. Diederich, *Angew. Chem. Int. Ed.,* 2000, **39**, 2632 – 2657

26. Based upon M. Alami and F. Ferri, *Tet. Lett.,* 1996, **37**(16), 2763 – 2766

27. R. J. Corey and P. L. Fuche, *Tet. Lett.,* 1972, **13**, 3769 – 3772

28. Based upon B. Grant, N. J. Clecak and R. J. Cox, *Mol. Cryst. Liq. Cryst.,* 1979, **51**, 209 – 214

29. S. Hayashi, K. Itoh, N. Murayama, Y. Iwase, K. Kamada, K. Ohta and K. Kondo, *J. Macromol. Sci. Part A, Pure and Applied Chem.,* 2002, **A39**, 1393 – 1405

30. R. Zissel, J. Suffert and M. T. Youinou, *J. Org. Chem.,* 1996, **61**, 6535 – 6546

31. R. Eastmond and D. R. M. Walton, *Tetrahedron*, 1972, **28**, 4591 – 4599

32. R. Dembinski, T.Lis, S. Szafert, C. L. Mayne, T. Bartiz and J. A. Gladysz, *J. Organomet. Chem.,* 1999, **578**, 229 – 246

33. J. P. Chang, E. Y. Fung and J. C. Curtis, *Inorg. Chem.,* 1986, **25**, 4233 – 4241

34. J. L. Oudar and D. S. Chemla, *J. Chem. Phys.,*1977, **66**, 2664 – 2668

35. J. L. Oudar, *J. Chem. Phys.,* 1977, **67**, 446 – 457

36. Y. K. Shin, B. S. Brunschwig, C. Creutz and N. J. Sutin, *J. Phys. Chem.,* 1996, **100**, 8157 – 8169

37. B. J. Coe, J. A. Harris and B. S. Brunschwig, *J. Phys. Chem. A,* 2002, **106**, 897 – 905

38. J. Y. Lee, S. Bum Suh and K. S. Kim, *J. Chem. Phys.,* 2000, **112**, 344 – 438

39. J. O. Morley, *J. Phys. Chem.,* 1995, **99**, 10166 – 10174

40. M. Jain and J. Chandrasekhar, *J. Phys. Chem.,* 1993, **97**, 4044 – 4049

41. I. D. L. Albert, J. O. Morley and D. Pugh, *J. Phys. Chem. A.,* 1997, **101**, 1763 – 1766

Chapter 5

A New Family of Extended Ligands and their Complexes with Ruthenium(II) Diarsine Centres

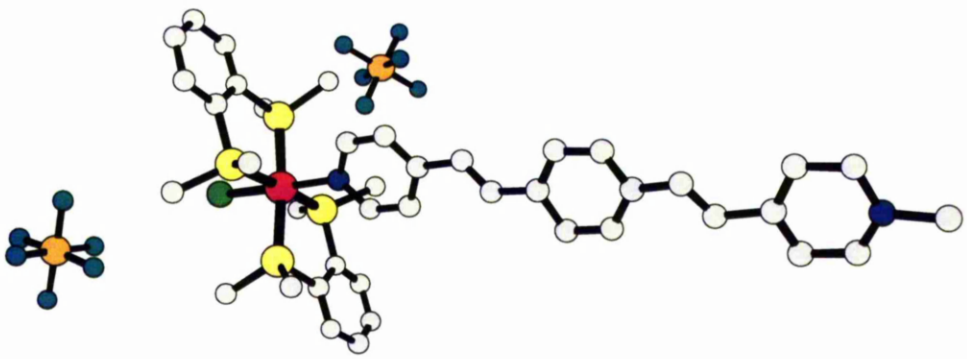

5.1 Introduction

When designing a chromophore to exhibit a large second-order NLO response an important consideration is the optical transparency. For a molecule to have any application at a device level it must be transparent at both the operating and SH frequencies.[1] For example, for the efficient frequency doubling of short wavelength diode lasers a molecule should be transparent at both 800 and 400 nm.[2] For diode laser-based modulators absorption in the region 630–980 nm will result in large optical losses[3] and transparency at the telecommunications operating wavelengths of 1300 or 1550 nm (and therefore at the respective SHs of 650 and 775 nm) is required for all-optical signal processing.[4] According to the TSM the magnitude of β is inversely proportional to the square of the ICT energy.[5-7] This relationship leads to the so-called nonlinearity-transparency trade off, whereby increases in β_0 are generally achieved at the cost of decreased optical transparency. Increasing the length of the π-conjugated pathway has proved to be an efficient method for increasing molecular NLO responses, causing $\Delta\mu_{12}$ to increase and E_{max} to decrease, which in accordance with the TSM leads to an increase in β_0.[8] However, such a red-shifting of the ICT band leads to reduced transparency in the visible region. It has been found that the introduction of a 1,4-phenylene group into a conjugated pathway causes hypsochromic shifting of ICT bands, increasing the visible transparency.[9-13] The NLO properties of Ru^{II} ammine complexes of the ligand *N*-methyl-1,4-bis-(*E*-2-(4-pyridyl)ethenyl)benzene ($Mebpvb^+$) have been previously reported by our group.[9] Such species show large NLO responses combined with increased optical transparencies, when compared with analogous polyenyl chromophores.

The work presented in this chapter concerns the synthesis of some novel *N*-aryl analogues of Mebpvb$^+$ and their complexation to the *trans*-{$Ru^{II}Cl(pdma)_2$}$^+$ centre. The optical and electronic properties of these complexes have been studied, with the aim of achieving large NLO responses accompanied by appreciable optical transparencies. A new potential ligand containing a bis(1,3-diethyl-2-thiobarbitur-5-yl)methane A group has also been synthesised, but unfortunately the coordination of this molecule to the *trans*-{$Ru^{II}Cl(pdma)_2$}$^+$ centre proved unsuccessful.

5.2 Experimental

5.2.1 Materials and Procedures

$RuCl_3 \bullet 2H_2O$ was supplied by Apollo Scientific and the pdma ligand was provided by Dr. G. Reid, University of Southampton. *trans*-[$Ru^{II}Cl(pdma)_2(NO)$][PF_6]$_2$,[14] 2-[2-(4-formylphenyl)ethenyl]pyridine (FEP),[15] *N*-phenyl-4-picolinium chloride ([Phpic$^+$]Cl),[16] *N*-(2-pyrimidyl)-4-picolinium hexafluorophosphate ([Pympic$^+$]PF_6),[2] 1,4-bis[*E*-2-(4-pyridyl)ethenyl]benzene (bpvb),[17] 1,4-bis[*E*-2-(4-pyridyl)ethynyl]benzene (bpeb)[18] and *N*-methyl-1,4-bis-(*E*-2-(4-pyridyl)ethenyl)benzene hexafluorophosphate ([Mebpvb$^+$]PF_6)[9] were synthesised according to the literature procedures. All other reagents were obtained commercially and used as supplied. All reactions were performed under an inert Argon atmosphere. Products were dried in a vacuum desiccator ($CaSO_4$) for *ca.* 24 h prior to characterization.

5.2.2 Syntheses

***N*-Phenyl-1,4-bis(*E*-2-(4-pyridyl)ethenyl)benzene Chloride, [Phbpvb$^+$]Cl.** [Phpic$^+$]Cl•1.25H_2O (100 mg, 0.438 mmol) and FEP (108 mg, 0.516 mmol) were dissolved in methanol (1 cm^3) and heated to 95 °C. Pyridine (1 drop) was added and the mixture heated for a further 3.5 h. The dark brown solution was cooled to room temperature and diethyl ether was added to afford a brown precipitate, which was collected by filtration and washed with diethyl ether. Purification was effected by precipitation from methanol-diethyl ether to afford a yellow solid. Yield 95 mg (48%). δ_H (300 MHz, CD_3OD) 9.04 (2 H, d, J = 6.7 Hz, C_5H_4N), 8.34 (2 H, d, J = 6.7 Hz, C_5H_4N), 8.11 (1 H, d, J = 15.5 Hz, CH), 7.86–7.58 (15 H, C_5H_4N + 2CH + C_6H_4 + Ph + C_5H_4N), 7.31 (1 H, d, J = 16.1 Hz, CH). (Found: C, 68.59; H, 5.58; N, 6.29. Calc. for $C_{26}H_{21}ClN_2$•3.25H_2O: C; 68.56, H; 6.09, N; 6.15%). *m/z*: 362 ([M – Cl]$^+$).

***N*-Phenyl-1,4-bis(*E*-2-(4-pyridyl)ethenyl)benzene Hexafluorophosphate, [Phbpvb$^+$]PF_6.** [Phbpvb$^+$]Cl•3.25H_2O (500 mg, 1.10 mmol) was dissolved in methanol (20 cm^3) and aqueous NH_4PF_6 was added to produce a yellow precipitate, which was collected by filtration and washed with water. Purification was effected by several reprecipitations from DMF-water to afford a yellow solid. Yield 747 mg (96%). δ_H (500 MHz, $(CD_3)_2SO$) 9.22 (2 H, d, J = 6.9 Hz, C_5H_4N), 9.14 (2 H, d, J = 5.9 Hz, C_5H_4N), 8.38 (2 H, d, J = 6.9 Hz, C_5H_4N), 8.21 (1 H, d, J = 16.3 Hz, CH), 7.89–7.70 (13 H, C_5H_4N + 2CH + C_6H_4, Ph), 7.47 (1 H, d, J = 16.4 Hz, CH). (Found: C, 43.98; H, 3.27; N, 4.63. Calc. for $C_{26}H_{21}F_6N_2P$•HPF_6•3H_2O: C; 44.21, H; 3.99, N; 3.97%). *m/z*: 362 ([M – PF_6]$^+$). Orange shards suitable for X-ray crystallography were grown via slow diffusion of diethyl ether vapour into an acetonitrile/DMF

solution. (Found: C, 53.05; H, 4.42; N, 6.35. Calc. for $C_{26}H_{21}F_6N_2P \cdot 0.5HPF_6 \cdot DMF$: C; 53.38, H; 4.40, N; 6.44%)

***N*-(2-Pyrimidyl)-1,4-bis(*E*-2-(4-pyridyl)ethenyl)benzene Hexafluorophosphate, [Pymbpvb$^+$]PF$_6$.** This compound was prepared in a fashion identical to [Phbpvb$^+$]Cl, using [Pympic$^+$]$PF_6 \cdot 0.06C_4H_{10}O$ (154 mg, 0.479 mmol) in place of [Phpic$^+$]$Cl \cdot 1.25H_2O$. Purification of the brown solid was achieved by several reprecipitations from acetone-diethyl ether. Yield 132 mg (58%). δ_H (300 MHz, $(CD_3)_2SO$), 9.84 (2 H, d, J = 6.6 Hz, C_5H_4N), 9.17 (2 H, d, J = 4.8 Hz, C_5H_4N), 8.56 (2 H, d, J = 4.8 Hz, $C_4H_3N_2$), 8.36 (2 H, d, J = 6.9 Hz, C_5H_4N), 8.35 (1 H, d, J = 16.5 Hz, CH), 7.88–7.72 (6 H, C_6H_4 + CH + $C_4H_3N_2$), 7.62–7.55 (3 H, C_5H_4N + CH), 7.52 (1 H, d, J = 16.2 Hz, CH). (Found: C, 52.35; H, 4.08; N, 9.67. Calc. for $C_{24}H_{19}F_6N_4P \cdot 2.5H_2O$: C, 52.09; H, 4.37; N, 10.12%). *m/z*: 363 ([M – PF$_6$]$^+$).

((*E*-2-(4-Pyridyl)ethenyl)phenyl)bis(1,3-diethyl-2-thiobarbitur-5-yl)methane, PEPBDTM. To a solution of FEP (135 mg, 0.645 mmol) in ethanol (50 cm^3) was added a solution of 1,3-diethyl-2-thiobarbituric acid (513 mg, 2.56 mmol) in ethanol (45 cm^3). The clear yellow solution was stirred under argon and became cloudy within 10 min. After 8 h, a fine yellow/brown solid was collected by filtration and washed with ethanol. Purification was effected by precipitation from DMF-water to afford a dark yellow solid. Yield 295 mg (75%). δ_H (300 MHz, $(CD_3)_2SO$), 8.79 (2 H, d, J = 6.3 Hz, C_5H_4N), 8.16 (2 H, d, J = 6.6 Hz, C_5H_4N), 7.94 (1 H, d, J = 16.2 Hz, C_2H_4), 7.59 (2 H, d, J = 8.1 Hz, C_6H_4), 7.40 (1 H, d, J = 16.2 Hz, C_2H_4), 7.09 (2 H, d, J = 7.8 Hz, C_6H_4), 6.32 (1 H, s, CH), 4.45 (8 H, d, J = 6.6 Hz, 4CH_2), 1.17 (12 H, br s, 4Me). ν(C=O) 1618s cm^{-1}. (Found: C, 59.22; H, 5.21; N, 11.32. Calc. for $C_{30}H_{33}N_5S_2O_4 \cdot H_2O$: C, 59.09; H, 5.45; 11.49%). *m/z*: 592 ([M]$^+$).

***trans*-[Ru^{II}Cl(pdma)$_2$(FEP)]PF$_6$ 94.** A solution of *trans*-[Ru^{II}Cl(pdma)$_2$(NO)][PF$_6$]$_2$ (250 mg, 0.243 mmol) and NaN_3 (16.2 mg, 0.249 mmol) in acetone (20 cm^3) was stirred at room temperature for 2 h. Butan-2-one (20 cm^3) and FEP (102 mg, 0.487 mmol) were added and the acetone removed *in vacuo*. The solution was heated under reflux for 4 h, then cooled to room temperature. Diethyl ether was added, affording a dark orange precipitate which was collected by filtration and washed with diethyl ether. Purification was effected by precipitation from acetone-aqueous NH_4PF_6, followed by three reprecipitations from acetone-diethyl ether to afford an orange solid. Yield 125 mg (48%). δ_H (300 MHz, $(CD_3)_2CO$) 10.00 (1 H, s, CHO), 8.33 (4 H, m, $C_6H_4(AsMe_2)_2$), 7.91–7.84 (6 H, $C_6H_4(AsMe_2)_2$ + C_5H_4N), 7.85 (2 H, d, J = 8.4 Hz, C_6H_4), 7.63 (2 H, d, J = 6.9 Hz, C_5H_4N), 7.50 (1 H, d, J = 16.5 Hz, CH), 7.28–7.22 (3 H, C_5H_4N + CH), 1.91 (12 H, s, 4AsMe), 1.80 (12 H, s, 4AsMe). (Found: C, 37.40; H, 3.81; N, 1.69. Calc. for $C_{34}H_{43}As_4ClF_6NOPRu \cdot H_2O$: C, 37.78; H, 4.20; N, 1.30%). *m/z*: 918 ([M – PF$_6$]$^+$).

***trans*-[Ru^{II}Cl(pdma)$_2$(bpvb)][PF$_6$]$_2$ 95.** This compound was prepared in a fashion identical to salt **94** using *trans*-[Ru^{II}Cl(pdma)$_2$(NO)][PF$_6$]$_2$ (125 mg, 0.122 mmol) and NaN_3 (8.1 mg, 0.125 mmol) in acetone (10 cm^3), bpvb (179 mg, 0.629 mmol) and butan-2-one (10 cm^3). A red solid was isolated. Yield 32 mg (23%). δ_H (300 MHz, $(CD_3)_2CO$) 8.63 (2 H, d, J = 5.4 Hz, C_5H_4N), 8.29 (4 H, m, $C_6H_4(AsMe_2)_2$), 7.92 (4 H, m, $C_6H_4(AsMe_2)_2$), 7.86 (2 H, d, J = 6.5 Hz, C_5H_4N), 7.76–7.64 (5 H, CH + C_6H_4), 7.41–7.34 (4 H, 2CH + C_5H_4N), 7.11–7.01 (3 H, CH + C_5H_4N), 1.90 (12 H, s, 4AsMe), 1.73 (12 H, s, 4AsMe). (Found: C, 41.50; H, 4.20; N, 2.43. Calc. for $C_{40}H_{48}As_4ClF_6N_2PRu \cdot H_2O$: C, 41.56; H, 4.36; N, 2.42%). *m/z*: 993 ([M – PF$_6$]$^+$).

***trans*-[Ru^{II}Cl(pdma)$_2$(Mebpvb$^+$)][PF_6]$_2$ 96.** A solution of **95**•H_2O (32 mg, 0.028 mmol) in DMF (1.5 cm^3) and methyl iodide (0.4 cm^3) was stirred at room temperature for 24 h. The excess methyl iodide was removed *in vacuo* and addition of aqueous NH_4PF_6 to the dark red solution gave a red precipitate, which was collected by filtration, washed with water and dried. Purification was effected by reprecipitation from acetone-diethyl ether to afford a red solid. Yield 19 mg (51%). δ_H (300 MHz, $(CD_3)_2CO$) 8.91 (2 H, d, J = 6.9 Hz, C_5H_4N), 8.34–8.27 (6 H, $C_6H_4(AsMe_2)_2$ + C_5H_4N), 8.21 (1 H, d, J = 16.4 Hz, CH), 7.85 (4 H, m, $C_6H_4(AsMe_2)_2$), 7.78 (2 H, d, J = 8.5 Hz, C_6H_4), 7.65 (2 H, d, J = 8.5 Hz, C_6H_4), 7.61–7.43 (4 H, 2CH + C_5H_4N), 7.23–7.14 (3 H, C_5H_4N + CH), 4.55 (3 H, s, Me), 1.91 (12 H, s, 4AsMe), 1.80 (12 H, s, 4AsMe). (Found: C, 36.92; H, 3.97; N, 2.09. Calc. for $C_{41}H_{51}As_4ClF_{12}N_2P_2Ru$•$2H_2O$: C, 36.91; H, 4.16; N, 2.10%). *m/z*: 504 ([M – $2PF_6$]$^{2+}$). Red slabs suitable for X-ray crystallography were grown via slow diffusion of diethyl ether vapour into an acetonitrile/DMF solution.

***trans*-[Ru^{II}Cl(pdma)$_2$(Phbpvb$^+$)][PF_6]$_2$ 97.** This compound was prepared in a fashion identical to **95** using [Phbpvb$^+$]PF_6HPF_6•$3H_2O$ (94 mg, 0. 133 mmol) in place of bpvb to afford a red solid. Yield 39 mg (24%). δ_H (300 MHz, $(CD_3)_2CO$) 9.20 (2 H, d, J = 7.2 Hz, C_5H_4N), 8.46 (2 H, d, J = 7.0 Hz, C_5H_4N), 8.32 (4 H, m, $C_6H_4(AsMe_2)_2$), 8.16 (1 H, d, J = 16.3 Hz, CH), 7.92 (2 H, m, C_6H_4), 7.89 (4 H, m, $C_6H_4(AsMe_2)_2$), 7.81–7.66 (8 H, C_6H_4 + CH + Ph), 7.56 (2 H, d, J = 6.7 Hz, C_5H_4N), 7.46 (1 H, d, J = 16.3 Hz, CH), 7.24–7.15 (3 H, C_5H_4N + CH), 1.90 (12 H, s, 4AsMe), 1.80 (12 H, s, 4AsMe). (Found: C, 40.53; H, 3.47; N, 2.02. Calc. for $C_{46}H_{53}As_4ClF_{12}N_2P_2Ru$: C, 40.62; H, 3.93; 2.06 %). *m/z*: 534 ([M – $2PF_6$]$^{2+}$). Red needles suitable for X-ray crystallography were grown via slow diffusion of diethyl ether vapour into an acetonitrile/DMF solution.

***trans*-[Ru^{II}Cl(pdma)$_2$(Pymbpvb$^+$)][PF$_6$]$_2$ 98.** This compound was prepared in a fashion identical to **95**, using [Pymbpvb$^+$]PF$_6$•2.5H$_2$O (95 mg, 0.172 mmol) in place of bpvb to afford a red/brown solid. Yield 37 mg (21%). δ_H (300 MHz, $(CD_3)_2CO$) 10.05 (2 H, d, J = 7.3, C_5H_4N), 9.22 (2 H, d, J = 4.8, $C_4H_3N_2$), 8.53 (2 H, d, J = 7.3 Hz, C_5H_4N), 8.33 (4 H, m, $C_6H_4(AsMe_2)_2$), 8.28 (1 H, d, J = 16.7 Hz, CH), 7.96 (1 H, t, J = 4.8 Hz, $C_4H_3N_2$), 7.89–7.84 (6 H, $C_6H_4(AsMe_2)_2$ + C_6H_4), 7.79 (1 H, J = 16.3 Hz, CH), 7.70 (2 H, d, J = 8.4 Hz, C_6H_4), 7.58 (2 H, d, J = 6.7 Hz, C_5H_4N), 7.48 (1 H, d, J = 16.4 Hz, CH), 7.25–7.18 (3 H, C_5H_4N + CH), 1.90 (12 H, s, 4AsMe), 1.81 (12 H, s, 4AsMe). (Found: C, 36.91; H, 3.53; N, 3.96. Calc. for $C_{44}H_{51}As_4ClF_{12}N_4P_2Ru$•3H$_2$O: C, 37.32; H, 4.06; N, 3.96%). *m/z*: 536 ([M – 2PF$_6$]$^{2+}$).

***trans*-[Ru^{II}Cl(pdma)$_2$(bpeb)]PF$_6$ 99.** This compound was prepared in a fashion identical to **95**, using bpeb (200 mg, 0.713 mmol) in place of bpvb to afford an orange/red solid. Yield 30 mg (22%). δ_H (300 MHz, $(CD_3)_2CO$) 8.62 (2 H, d, J = 6.2 Hz, C_5H_4N), 8.31 (4 H, m, $C_6H_4(AsMe_2)_2$), 7.84 (4 H, m, $C_6H_4(AsMe_2)_2$), 7.72 (2 H, d, J = 6.9 Hz, C_5H_4N), 7.63 (2 H, d, J = 8.6 Hz, C_6H_4), 7.60 (2 H, d, J = 8.6 Hz, C_6H_4), 7.47 (2 H, d, J = 6.0 Hz, C_5H_4N), 7.15 (2 H, d, J = 6.9 Hz, C_5H_4N), 1.91 (12 H, s, 4AsMe), 1.81 (12 H, s, 4AsMe). ν(C≡C) 2219w cm^{-1} (Found: C, 41.80; H, 4.07; N, 2.20. Calc. for $C_{40}H_{44}As_4ClF_6N_2PRu$•H$_2$O: C, 41.71; H, 4.02; N, 2.43%). *m/z*: 988 ([M – PF$_6$]$^+$).

***trans*-[Ru^{II}Cl(pdma)$_2$(Mebpeb$^+$)][PF$_6$]$_2$ 100.** This compound was prepared in a fashion identical to **96**, using salt **99** (30 mg, 0.026 mmol) in place of **95** in DMF (1.5 cm^3) and methyl iodide (0.4 cm^3). A red solid was isolated. Yield 25 mg (74%). δ_H (300 MHz, $(CD_3)_2CO$) 9.08 (2 H, d, J = 6.7 Hz, C_5H_4N), 8.32–8.26 (6 H,

$C_6H_4(AsMe_2)_2$ + C_5H_4N), 7.83 (4 H, m, $C_6H_4(AsMe_2)_2$), 7.73 (4 H, C_6H_4 + C_5H_4N), 7.61 (2 H, d, J = 8.5 Hz, C_6H_4), 7.05 (2 H, d, J = 6.7 Hz, C_5H_4N), 4.59 (3 H, s, Me), 1.90 (12 H, s, 4AsMe), 1.80 (12 H, s, 4AsMe). ν(C≡C) 2220m and 2179w cm^{-1} (Found: C, 38.82; H, 4.13; N, 2.76. Calc. for $C_{41}H_{47}As_4ClF_{12}N_2P_2Ru \cdot 0.5Me_2CO$: C, 38.58; H, 3.81; N, 2.12%). *m/z*: 502 ($[M - 2PF_6]^{2+}$).

5.3 Results and Discussion

5.3.1 Molecular Design and Synthesis

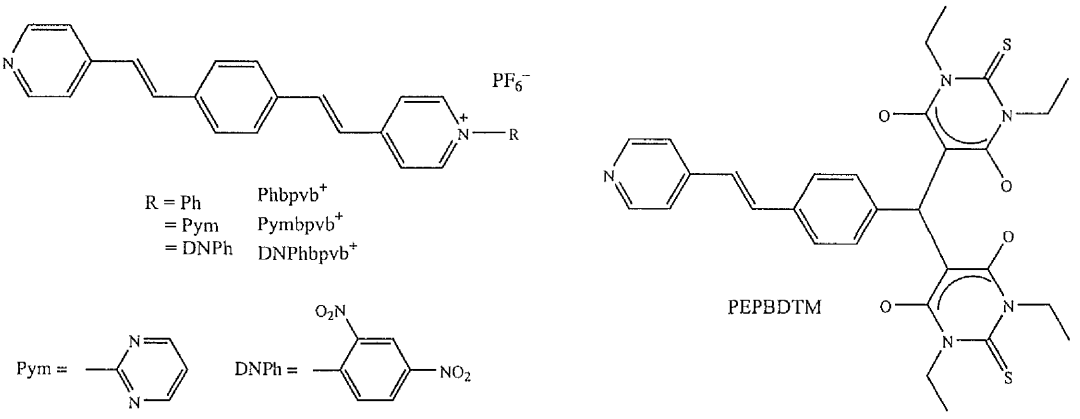

Figure 52: Structures of the extended ligands

Figure 52 shows the structures of the extended ligands and the structures of the novel complexes **94–100** are depicted in Figure 53.

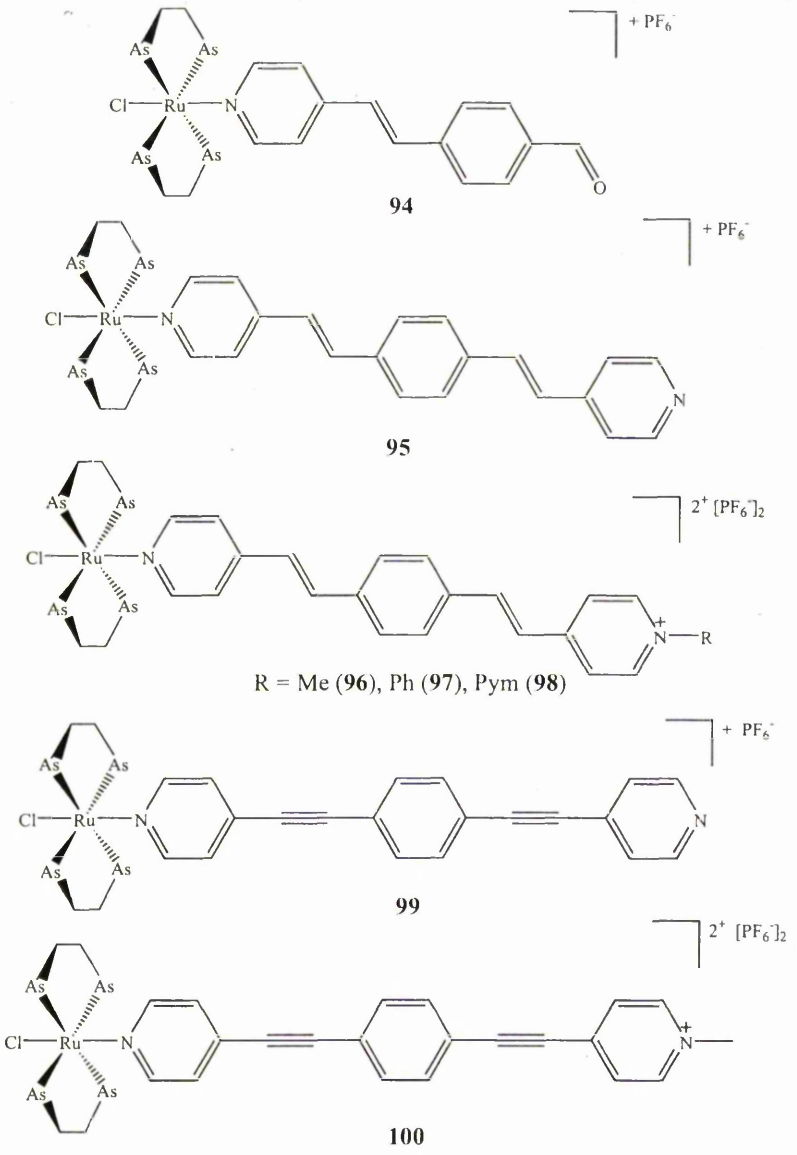

Figure 53: Structures of the complex salts **94–100**

The novel compounds **95–100** were designed to probe the effects of extending the length of the π-conjugated bridge by the incorporation of a 1,4-phenylene unit on the optical and NLO properties. Related Ru^{II} ammine compounds studied within the group have been found to have relatively large contributions of ILCT (as well as MLCT) transitions to the NLO responses, combined with increased optical transparencies when compared with related polyenyl chromophores.[9] Although the

^{1}H NMR spectra of **95**–**100** are quite complicated, they do show diagnostic patterns which can be fully assigned. CHN elemental analyses and mass spectrometry allow for further conformation of identity and purity.

The ligating unit Mebpvb$^+$ was not isolated, but prepared already coordinated by the methylation of the free pyridyl N atom in complex salt **95** to give **96**. Such a synthetic approach is not suitable for complexes of related *N*-aryl ligands. Therefore the species Phbpvb$^+$ and Pymbpvb$^+$ were synthesized by Knoevenagel-type condensation reactions between FEP and the corresponding picolinium salt using pyridine as the base. Such base-catalyzed condensation reactions provide a convenient route for the formation of α,β-unsaturated alkenes. The general reaction mechanism is outlined in Figure 54:[19]

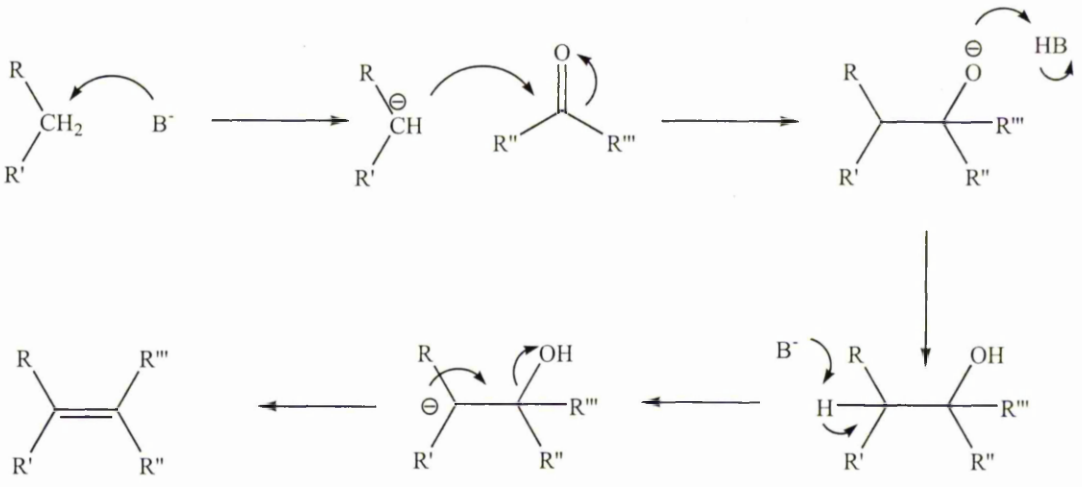

Figure 54: General reaction mechanism for Knoevenagel condensation reactions

Deprotonation by a base (B) such as pyridine yields a carbanion, which attacks the carbonyl group, subsequent dehydration affords the alkene product.

An attempted base-catalysed condensation between FEP and *N*-(2,4-dinitrophenyl)picolinium chloride was unsuccessful, affording none of the desired *N*-(2,4-dinitrophenyl)-1,4-bis(*E*-2-(4-pyridyl)ethenyl)benzene (DNPhbpvb$^+$) product. However, a nucleophilic substitution reaction of bpvb with 1-chloro-2,4-dinitrobenzene in refluxing ethanol, as shown in Figure 55, did appear to produce this compound, although the ^{1}H NMR spectra showed a mixture of products. The presence of a number of closely-spaced but identically-shaped signals, together with reasonable CHN analyses, perhaps indicates that a mixture of at least two of the four possible *E*/*Z* isomers was produced.

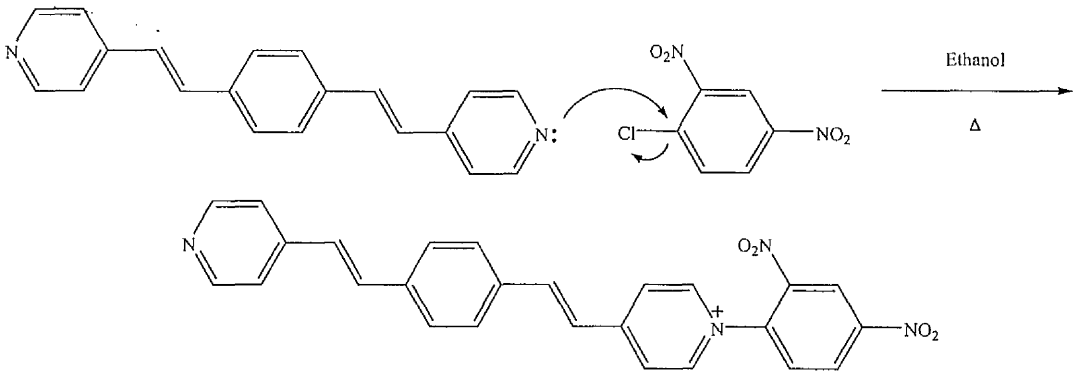

Figure 55: Reaction mechanism for the proposed formation of DNPhbpvb$^+$

The 1,3-diethyl-2-thiobarbituric acid unit is a powerful electron acceptor,[20-23] and polyene derivatives containing this group have been found to exhibit very large NLO responses.[20,24-27] It was hoped that the reaction of 1,3-diethyl-2-thiobarbituric acid with FEP would produce the Knoevenagel product 1,3-diethyl-5-[(*E*-2-(4-pyridyl)ethenyl)benzylidene]-2-thiobarbituric acid, but instead the disubstituted Michael adduct ((*E*-2-(4-pyridyl)ethenyl)phenyl)bis(1,3-diethyl-2-thiobarbitur-5-yl)methane (PEPBDTM) was produced (Figure 56).

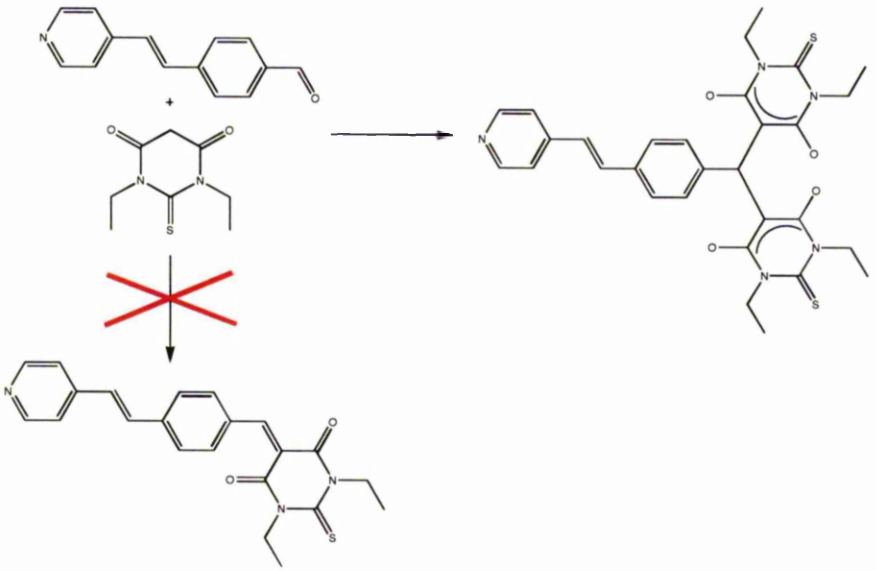

Figure 56: Reaction scheme for the formation of PEPBDTM

Carbon-carbon double bonds are generally unreactive towards nucleophiles due to the formation of an unstabilized anion. However, α,β-unsaturated carbonyl compounds can undergo nucleophilic addition due to the formation of an enolate anion, which provides resonance stabilization, as depicted in Figure 57.

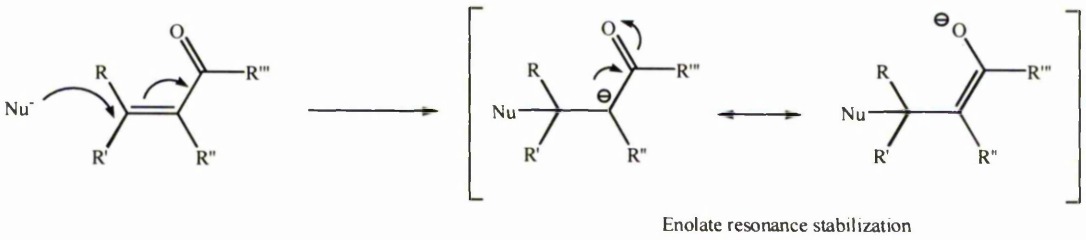

Figure 57: Stabilization of an enolate anion

This type of reaction is known as a Michael addition.[19] The formation of Michael adducts often follows Knoevenagel condensations,[28] and it has been shown that increased Lewis acidity of the Knoevenagel products by the incorporation of electron-withdrawing substituents favours Michael addition.[29] Similar reactivity

behaviour has been reported in related compounds.[30] It is worth noting that PEPBDTM contains two protons shared between the four carbonyl/hydroxy groups, as demonstrated by a crystallographic study on the analogous phenyl compound.[31]

The synthesis of the ligand bpvb (Figure 58) employed the Heck reaction, which involves the coupling of 4-vinylpyridine with 1,4-dibromobenzene in the presence of palladium(II) acetate and triphenylphosphine.

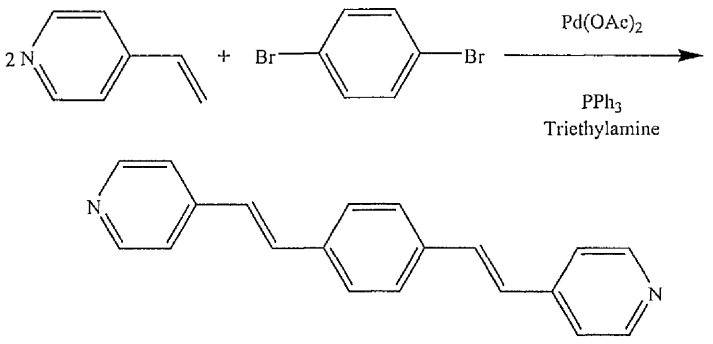

Figure 58: Reaction scheme for the formation of bpvb

The Heck reaction is quite general and involves the coupling of an aryl or vinyl halide with an activated alkene to form a new alkene, as represented in Figure 59.

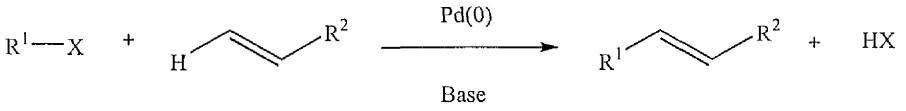

Figure 59: Generic scheme for the Heck reaction

The mechanism comprises a catalytic cycle (Figure 60),[31] involving the oxidative addition of the halide, insertion of the alkene and formation of the product by β-

hydride elimination. The presence of triphenylphosphine causes the *in situ* formation of the active Pd(0) complex from $Pd^{II}(OAc)_2$ and the base regenerates the Pd(0) catalyst.

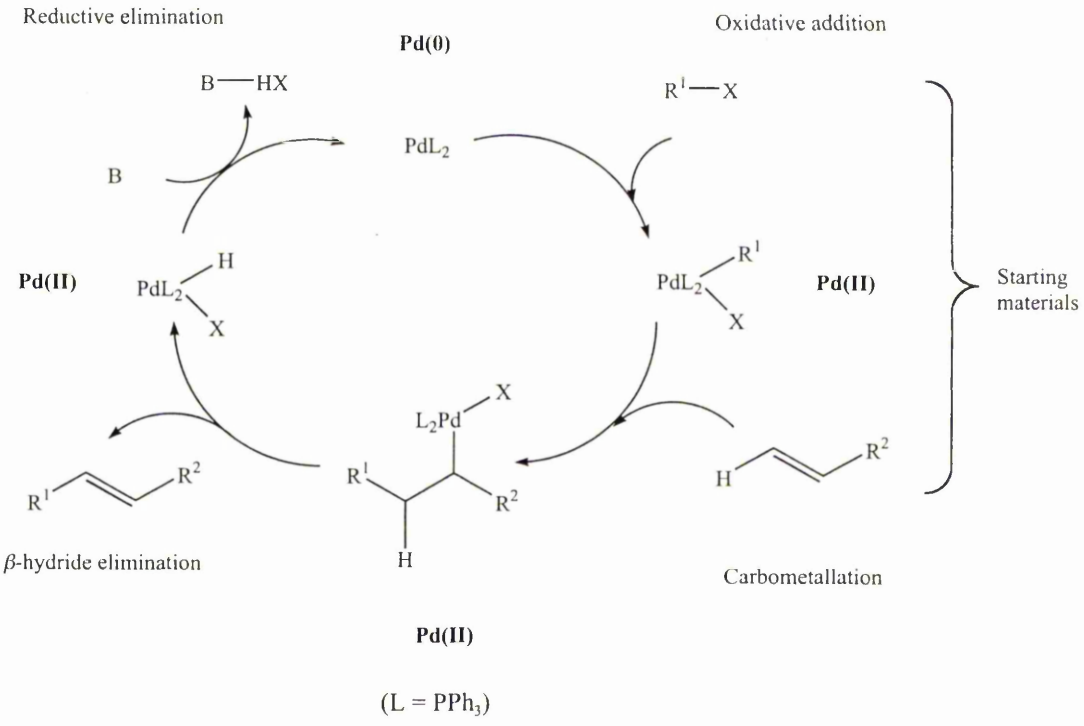

Figure 60: The catalytic cycle of the Heck reaction

The ligand bpeb was synthesized by an Eglington coupling reaction between 4-ethynylpyridine and 1,4-diiodobenzene catalyzed by bis(triphenylphosphine)palladium(II) dichloride and copper(I) bromide (Figure 61). The mechanism for this reaction has already been discussed in Chapter 4.

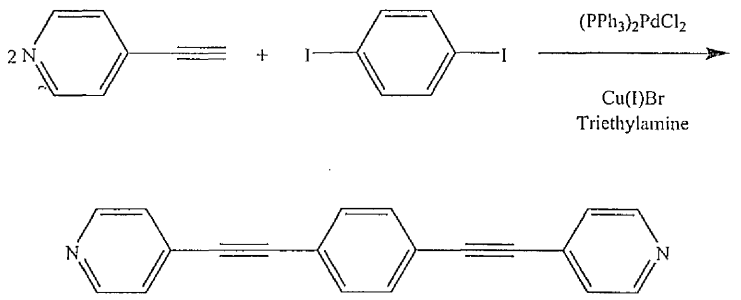

Figure 61: Reaction scheme for the formation of bpeb

The new pro-ligands [Phbpvb$^+$], [Pymbpvb$^+$] and PEPBDTM were designed with a view to form complexes with many different transition metal centres, *e.g.* $\{Ru^{II}(NH_3)_5\}^{2+}$, $\{Fe^{II}(CN)_5\}^{3-}$, *etc.* Unfortunately however, the solubility of these pro-ligands (with the bpvb derivatives as their PF_6^- salts) is quite limited, being good only in DMSO or DMF at room temperature or in acetone or acetonitrile when heated. Because the *trans*-$\{Ru^{II}Cl(pdma)_2\}^+$ centre is quite robust and can be heated to reflux in acetonitrile, it was chosen to focus on the preparation of complexes of this type.

Unfortunately, we have been unable to synthesize a complex of PEPBDTM. ^1H NMR spectroscopy showed no evidence for formation of the desired product, despite manipulation of the reaction conditions. PEPBDTM has several potentially competing sites for coordination; the pyridyl nitrogen and the two thiocarbonyl groups. Coordination of FEP afforded complex salt **94**, but an attempted Knoevenagel reaction between this and 1,3-diethyl-2-thiobarbituric acid proved unsuccessful (Figure 62). Nevertheless, it can be anticipated that other reactions with **94**, such as Schiff base condensations, may be feasible.

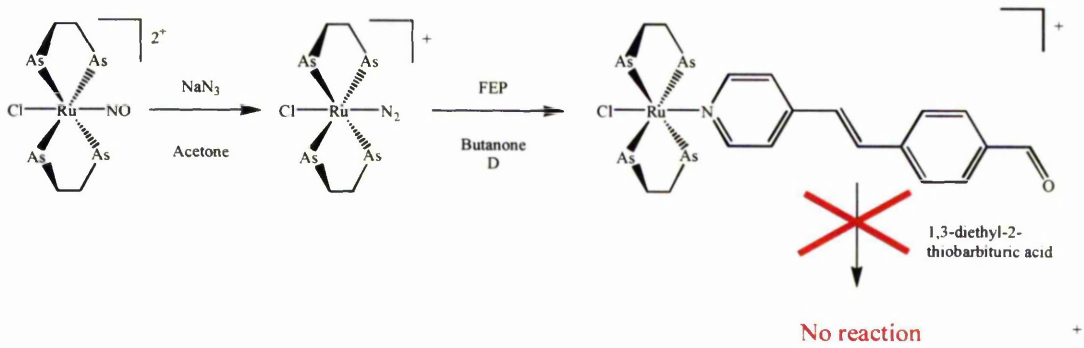

Figure 62: Attempted synthesis of *trans*-$[Ru^{II}Cl(pdma)_2PEPBDTM]^+$

The complex salts **94**, **95** and **99** were synthesized via complexation of the neutral ligands with the sodium azide-treated complex precursor *trans*-$[Ru^{II}Cl(pdma)_2(NO)][PF_6]_2$,[14] and **97** and **98** were prepared in a similar fashion, using the PF_6^- salts of the appropriate *N*-arylated cations. The complex salts **96** and **100** were prepared via methylation of **95** and **99**, respectively, using methyl iodide in DMF.

5.3.2 Electronic absorption spectroscopy studies

The electronic absorption spectra of complex salts **94–100** were recorded in acetonitrile at 293 K and the results are presented in Table 36, with a representative spectrum shown in Figure 63. The complexes show intense ILCT $\pi \rightarrow \pi^*$ transitions and intense, broad $d\pi[Ru] \rightarrow \pi^*[L_A]$ MLCT transitions with maxima in the region 430–480 nm, causing the observed orange or red colorations.

Table 36: UV/Vis absorption data for complex salts **94–100**[a]

Salt	λ_{max} [nm]	ε [$M^{-1} cm^{-1}$]	E_{max} [eV]	Assignment
94	442	8400	2.81	$d\pi \rightarrow \pi^*$
	322	31 900	3.85	$\pi \rightarrow \pi^*$
95	432	20 300	2.87	$d\pi \rightarrow \pi^*$
	350	51 700	3.54	$\pi \rightarrow \pi^*$
96	444	15 600	2.79	$d\pi \rightarrow \pi^*$
	372	34 400	3.33	$\pi \rightarrow \pi^*$
97	460	22 300	2.70	$d\pi \rightarrow \pi^*$
	398	36 700	3.12	$\pi \rightarrow \pi^*$
98	474 (sh)	25 600	2.62	$d\pi \rightarrow \pi^*$
	416	40 100	2.98	$\pi \rightarrow \pi^*$
99	438	15 000	2.83	$d\pi \rightarrow \pi^*$
	320	39 200	3.88	$\pi \rightarrow \pi^*$
100	446	15 500	2.78	$d\pi \rightarrow \pi^*$
	354	37 400	3.50	$\pi \rightarrow \pi^*$
	344 (sh)	35 900	3.60	$\pi \rightarrow \pi^*$
	276	24 100	4.49	$\pi \rightarrow \pi^*$

[a] Solutions *ca.* 3–8 × 10^{-5} M.

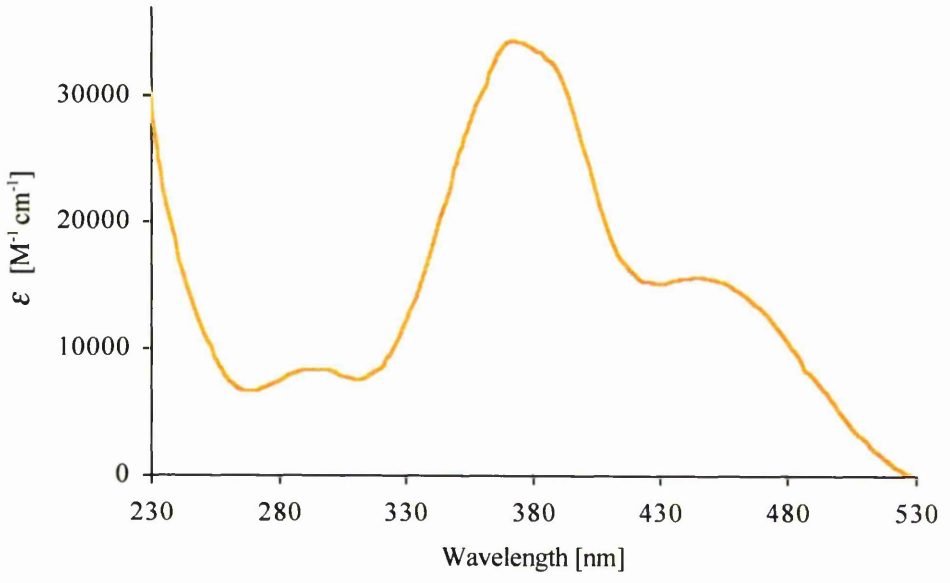

Figure 63: UV/Vis absorption spectrum for salt **97**.

As expected, red-shifts of the MLCT bands are observed upon methylation of the uncoordinated pyridyl nitrogen of salts **95** and **99** to give **96** and **100**, respectively. These effects are attributable to *N*-methylpyridinium being a better π-electron acceptor than pyridyl, but it is worth noting that the shifts are relatively small due to the extended nature of the chromophores. Complex salts **94** and **96** have similar MLCT E_{max} values, suggesting that the aldehyde group is of comparable acceptor strength to the *E*-2-(*N*-methyl-4-pyridinium)ethenyl group. However, the molar extinction coefficient for **94** is about 50% smaller than that of **96**, which is indicative of less efficient orbital overlap in the shorter conjugated system. Within the series **96**–**98**, increasing the π-acceptor strength of L_A causes the MLCT energy to decrease in the order $Mebpvb^+ > Phbpvb^+ > Pymbpvb^+$ (Figure 64). This trend is consistent with previous observations on related complexes[32] and can be ascribed to destabilization of the L_A-based LUMO as the π-acceptor ability of the ligand increases, as confirmed by the cyclic voltammetry measurements (see section 5.3.3).

The intensity of the MLCT absorption also increases with increasing L_A π-acceptor strength. The ILCT absorptions also red-shift in the same order, such that for **98** the ILCT and MLCT transitions are so close in energy that the MLCT band appears as a shoulder on the ILCT peak.

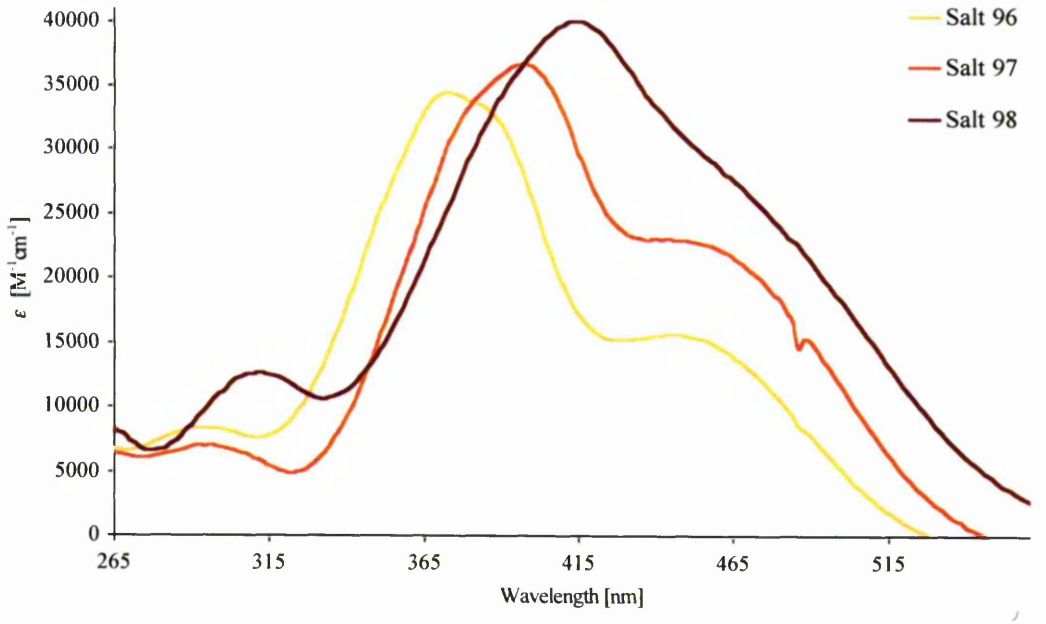

Figure 64: Effect of increasing the π-acceptor strength of L_A on the UV/Vis absorption spectra for **96–98**.

The MLCT spectra of **96** and **100** are very similar, showing that replacing the ethenyl units with ethynyl groups has no significant effect. However, the ILCT absorption spectra of these two compounds are quite different. In contrast, for the corresponding unmethylated complexes (**95** and **99**), changing the structure of the bridge affects both E_{max} and ε of the MLCT band to some extent.

5.3.3 Electrochemical studies

The new complex salts **94–100** were studied using cyclic voltammetry in acetonitrile and the results are presented in Table 37. A representative voltamogram for **94** is shown in Figure 65. All of the complexes show reversible $Ru^{III/II}$ oxidation waves, together with generally irreversible L_A-based reductions, although salts **94, 95** and **99** do show reversible L_A-based processes.

Table 37: Electrochemical data for complex salts **94–100**

Salt	E [V vs. Ag-AgCl] (ΔE_p [mV])[a]	
	$E_{1/2}[Ru^{III/II}]$	$E_{1/2}[L_A^{+/0}]$ or E_{pc}[b]
94	1.07 (55)	–1.26 (55)
		–1.42 (80)
95	1.05 (80)	–1.40 (100)
96	1.06 (65)	–0.95[b]
		–1.63[b]
97	1.06 (60)	–0.76[b]
		–1.60[b]
98	1.05 (70)	–0.55[b]
		–1.57[b]
99	1.10 (75)	–1.40 (95)
100	1.11 (75)	–0.89[b]
		–1.56[b]

[a] Solutions *ca.* 10^{-3} M in analyte and 0.1 M in $NBu^n_4PF_6$ at a platinum disc working electrode with a scan rate of 200 mVs^{-1}. Ferrocene internal reference $E_{1/2}$ = 0.43 V (ΔE_p = 70 mV). [b] For an irreversible process.

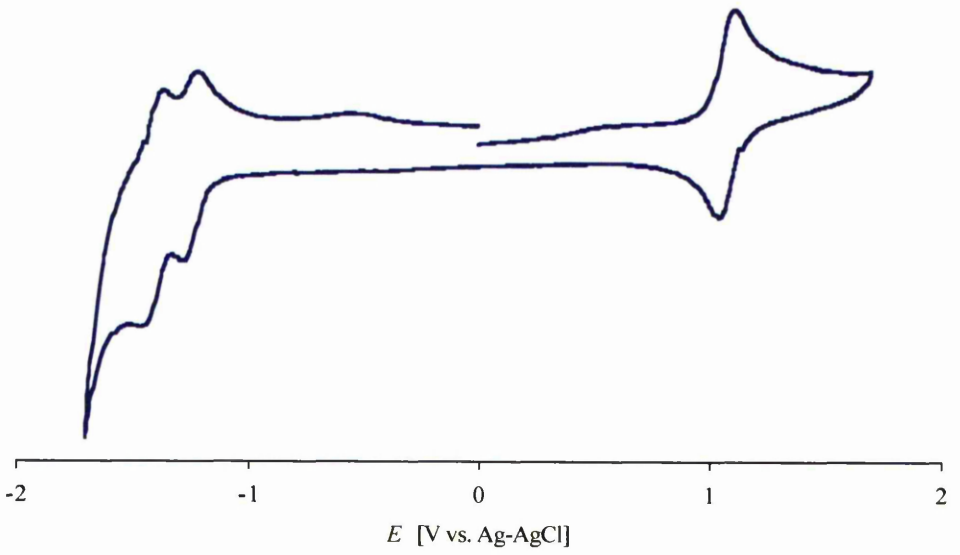

Figure 65: Cyclic voltammogram for complex salt **94**

Methylation of the uncoordinated pyridyl nitrogen of **95** and **99** (to form **96** and **100**, respectively) causes increased stabilization of the L_A-based LUMOs, as evidenced by the increased (although irreversible) reduction potentials with shifts to a more positive voltage. Since the $Ru^{III/II}$ $E_{1/2}$ values are unchanged upon methylation, the accompanying red-shifts of the MLCT absorption bands can be attributed solely to destabilization of the L_A-based LUMOs, with the energies of the Ru-based HOMOs being unaffected. The L_A-based reductions in salt **94** occur at more negative potentials when compared with those of the complexes of pyridinium-substituted ligands (**96**–**98** and **100**). Within the series **96–98** as the L_A π-acceptor strength increases, so too does the first L_A-based reduction potential, with shifts to a more positive voltage. Again, the $Ru^{III/II}$ $E_{1/2}$ value is constant for **96–98**, showing that the red-shifting of the MLCT band within this series is attributable only to stabilization of the L_A-based LUMO. Comparison of the ethenyl-containing complexes in **95** and **96** with their ethynyl counterparts in **99** and **100** reveals slightly higher $Ru^{III/II}$ $E_{1/2}$ values for the latter. This difference is due to the mild electron-donating properties

of the 4-ethenyl group making the Ru^{II} centre easier to oxidise. Comparison of the $L_A^{+/0}$ reduction potentials of salts **96** and **100** indicates that the ethynyl-containing complex is slightly more easily reduced, although no such effect is observed in **95** and **99**.

5.3.4 X-Ray crystallographic studies

Single crystal X-ray structures were obtained for the pro-ligand salt $[Phbpvb^+]PF_6 \cdot 0.5HPF_6 \cdot DMF$ (the disordered solvent was not refined) and complex salts **96**, **97** and **99**, and representations of the molecular structures are shown in Figures 66–69. Selected crystallographic and refinement details are shown in Table 38 and selected bond angles and lengths in Table 39 and 40. Unfortunately, none of these four structures are of high quality, attributable largely to included solvents, so all bond lengths and angles must be treated with care.

The twisting within the conjugated pyridinium-substituted systems (where py = pyridyl and pyr = pyridinium) can be represented by the following dihedral angles (°): for $[Phbpvb^+]PF_6 \cdot 0.5HPF_6 \cdot DMF$, py–Ph = 13.02(16), Ph–pyr = 13.28(14), pyr–Ph = 50.92; for **96**, py–Ph = 7.11(0.64), Ph–pyr = 2.28(0.68); for **97** (two independent cations), py–Ph = 1.50(2.18)/6.57(2.18), Ph–pyr = 13.20(1.90)/3.92(2.16), pyr–Ph = 42.51(1.60)/38.16(1.68); for **99**, py(coordinated)–Ph = 9.35(1.11); Ph–py = 8.59(1.14). Unfortunately, all of these materials adopt centrosymmetric space groups, therefore no significant bulk NLO behaviour can be expected.

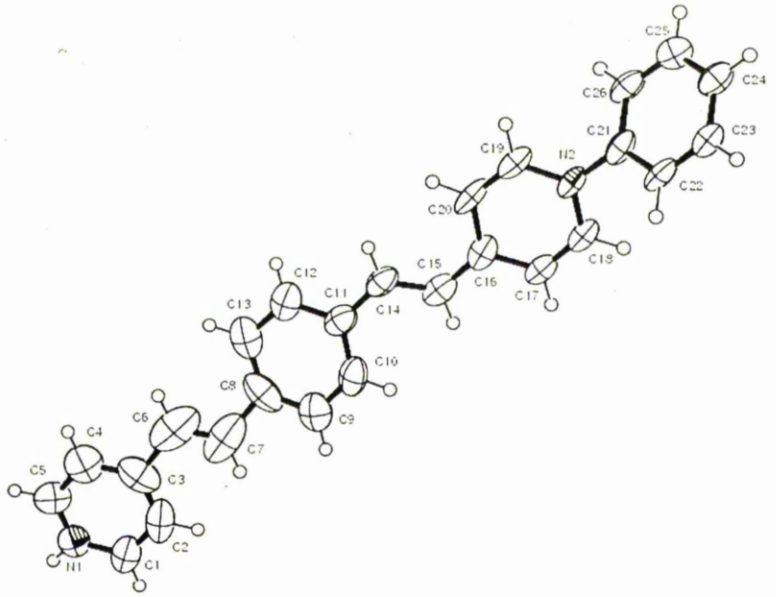

Figure 66: Structural representation of the protonated pro-ligand cation in salt $[Phbpvb^{+}]PF_6 \bullet 0.5HPF_6 \bullet DMF$ (50% probability ellipsoids)

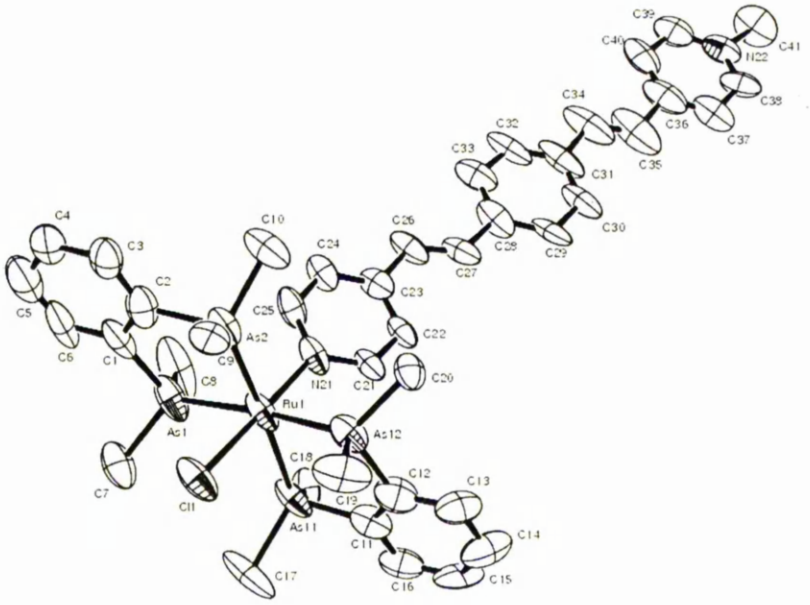

Figure 67: Structural representation of the complex cation in salt **96** (50% probability ellipsoids)

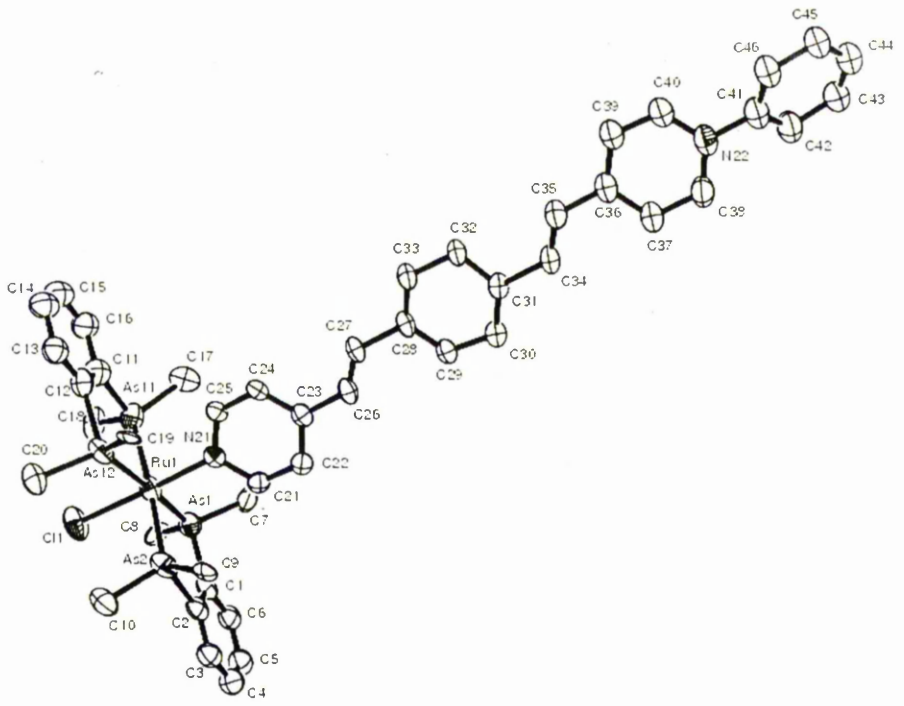

Figure 68: Structural representation of one of the two independent complex cations in salt **97** (50% probability ellipsoids)

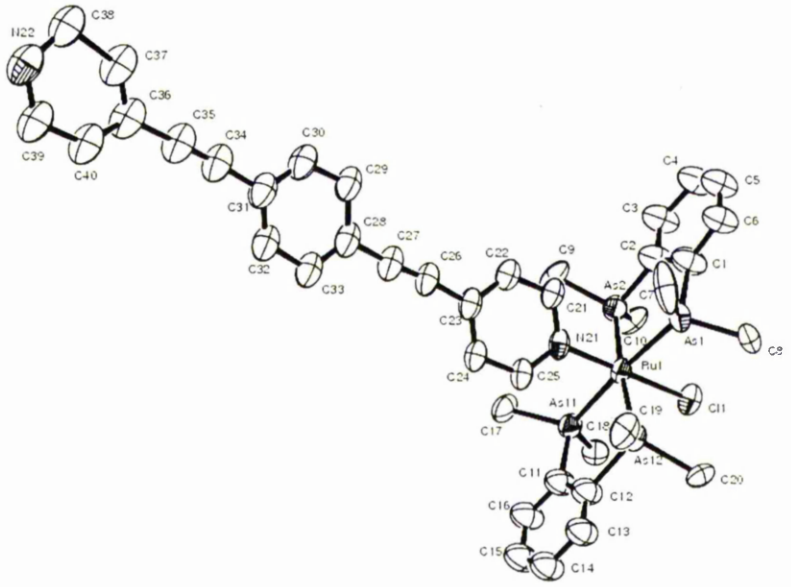

Figure 69: Structural representation of the complex cation in salt **99** (50% probability ellipsoids)

Table 38: Crystallographic and refinement details for salts [Phbpvb$^+$]PF_6•0.5HPF_6•DMF, **96**, **97**, and **99**

	[Phbpvb$^+$]PF_6•0.5HPF_6•DMF	**96**	**97**	**99**
Crystal system	Monoclinic	Monoclinic	Monoclinic	Monoclinic
Space group	*C2/c*	$P2_1/n$	$P2_1/n$	*C2/c*
Unit cell dimensions [Å,°]				
a	42.215(8)	9.5973(12)	9.345(2)	34.075(7)
b	10.309(2)	42.589(5)	53.743(9)	9.3403(19)
c	14.107(3)	15.082(2)	25.264(4)	32.136(6)
α	90	90	90	90
β	105.77(3)	105.201(10)	98.056(16)	102.73(3)
γ	90	90	90	90
Volume [Å^3]	5908	5949	12562	9977
Z	4	4	8	8
Absorption coefficient [mm^{-1}]	0.194	2.634	2.499	3.083
Reflections collected	33282	28132	46744	13131
Independent reflections	6697	8610	18289	5391
	(R_{int} = 0.1072)	(R_{int} = 0.0635)	(R_{int} = 0.0974)	(R_{int} = 0.0760)
Final *R* indices [$F^2>2\sigma(F^2)$]				
R1	0.1209	0.0955	0.1074	0.1333
wR2	0.2967	0.2765	0.2630	0.3419
R indices (all data)				
R1	0.2567	0.1663	0.2678	0.2359
wR2	0.3582	0.3289	0.3174	0.3956

Table 39: Selected interatomic distances (Å) and angles (°) for complex salts **96**, **97** (one cation only) and **99**

	96	**97**	**99**
Cl1–Ru1	2.443(3)	2.445(9)	2.418(6)
Ru1–N21	2.142(10)	2.108(12)	2.080(17)
Ru1–As1	2.4197(17)	2.405(7)	2.410(3)
Ru1–As11	2.4141(19)	22.412(7)	2.413(3)
Ru1–As12	2.4118(17)	2.413(7)	2.415(3)
Ru1–As2	2.4134(19)	2.407(7)	2.416(3)
N21–Ru1–As1	94.5(3)	95.1(6)	93.7(5)
N21– Ru1–As11	91.4(3)	84.4(3)	91.1(5)
As1–Ru1–As11	95.01(6)	93.5(3)	174.81(11)
N21–Ru1–As12	91.8(3)	90.1(6)	92.6(5)
As1–Ru1–As12	173.61(6)	174.4(5)	93.11(10)
N21–Ru1–As2	93.4(3)	93.5(6)	84.70(11)
As1–Ru1–As2	85.29(6)	84.9(3)	93.11(10)
As11–Ru1–As2	175.19(6)	175.4(5)	96.33(10)
As12–Ru1–As2	94.91(6)	96.8(3)	174.74(11)
N21–Ru–Cl1	179.1(3)	178.4(7)	179.1(4)
As1–Ru1–Cl1	84.60(10)	86.4(5)	86.84(17)
As11–Ru1–Cl1	88.64(10)	88.4(4)	88.39(17)
As12–Ru1–Cl1	89.04(10)	88.3(5)	88.16(17)
As2–Ru1–Cl1	86.61(10)	87.1(4)	86.71(17)

Table 40: Selected interatomic distances (Å) and angles (°) for

$[Phbpvb^{+}]PF_6 \cdot 0.5HPF_6 \cdot DMF$

C3–C6	1.627(12)
C6–C7	1.222(11)
C7–C8	1.583(12)
C11–C14	1.454(9)
C14–C15	1.357(8)
C15–C16	1.426(8)
C7–C6–C3	115.9(10)
C6–C7–C8	118.1(10)
C15–C14–C11	125.4(6)
C14–C15–C16	125.7(6)

5.3.5 Stark Spectroscopic studies

The complex salts **96–98** and **100** were studied using Stark spectroscopy in butyronitrile glasses at 77 K and the results are presented in Table 41. Representative absorption and Stark spectra for the MLCT bands of salts **96–98** are shown in Figure 70.

The MLCT bands of all these complex salts undergo red-shifting in the 77 K glass, as seen in related compounds,[33,34] except for that of salt **98** which shows a slight blue-shift. In acetonitrile at 293 K, the MLCT band red-shifts as the acceptor strength of L_A increases, but when in butyronitrile at 77 K the MLCT band red-shifts on moving from **96** to **97** and then shows a slight blue-shift on moving to **98**. However, it should be noted that the strong overlapping of the MLCT and ILCT

bands in **98** means that the quoted λ_{max} and E_{max} values should be viewed only as rough estimates.

Table 41: MLCT absorption and Stark spectroscopic data for salts **96–98** and **100**

Salt	λ_{max} [nm][a]	λ_{max} [nm][b]	E_{max} [eV][b]	f_{os}[b]	μ_{12} [D][c]	$\Delta\mu_{12}$ [D][d]	$\Delta\mu_{ab}$ [D][e]	c_b^2[f]	H_{ab} [cm^{-1}][g]	β_0 [10^{-30} esu][h]
96	444	471	2.63	0.4	6.4	18.8	22.8	0.09	6000	131
97	460	481	2.58	0.5	6.8	24.9	28.4	0.06	5000	203
98	474	464	2.67	0.4	6.3	31.0	33.4	0.04	4100	200
100	446	472	2.63	0.3	5.4	23.2	25.7	0.05	4450	114

[a] Measured in acetonitrile solutions at 293 K. [b] Measured in butyronitrile glasses at 77 K. [c] Calculated from eqn. 13. [d] Calculated from $f_{int}\Delta\mu_{12}$ using $f_{int} = 1.33$. [e] Calculated from eqn. 12. [f] Calculated from eqn. 14. [g] Calculated from eqn. 15. [h] Calculated from eqn. 7.

Within the series **96–98**, the nature of L_A has no significant effect on μ_{12} or f_{os}. $\Delta\mu_{12}$ and $\Delta\mu_{ab}$ both increase steadily within the series **96–98**, with $\Delta\mu_{ab}$ being larger in every instance. Steady decreases in both H_{ab} and c_b^2 are observed as the π-acceptor ability of L_A increases; as these quantities are related to the degree of orbital overlap, it is clear that the D–A electronic communication decreases on moving along the series **96–98**. The derived values for β_0 increase as the L_A acceptor strength increases on moving from **96** to **97**, but replacing the Ph group in **97** for 2-Pym in **98** causes no significant change in the NLO response. This unexpected result can be rationalized by considering that **98** has a lower than expected apparent value for E_{max}, as discussed above.

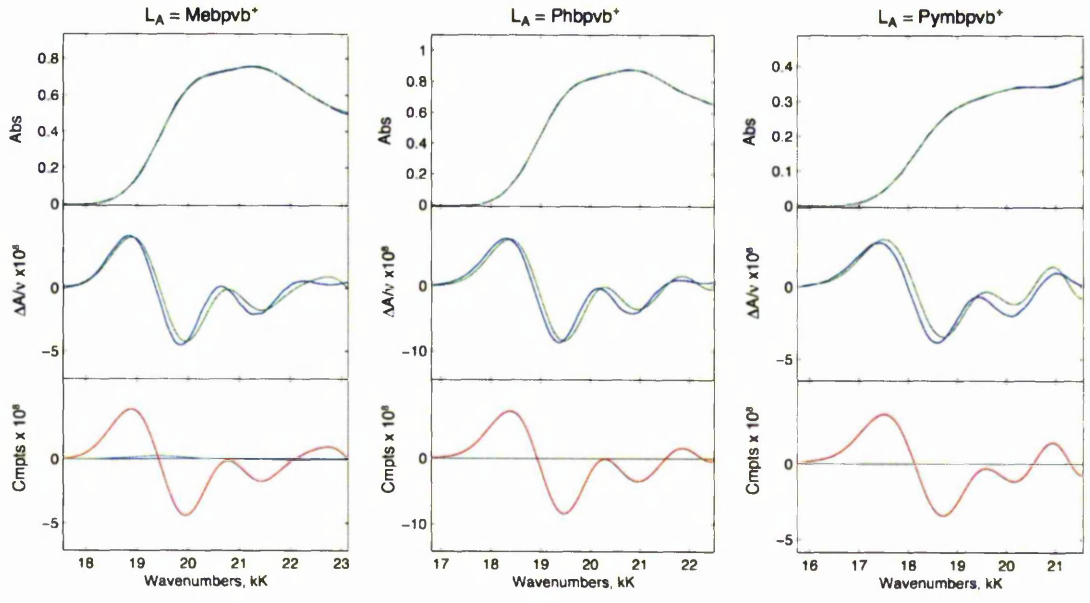

Figure 70: Absorption and electroabsorption spectra and calculated fits for the MLCT bands of salts **96**–**98** in external fields of 2.47, 2.47 and 2.48 × 10^7 V m^{-1}, respectively.

Top panel: absorption spectrum (blue line = experimental, green line = fit), middle panel: electroabsorption spectrum (blue line = experimental, green line = fit) according to the Liptay equation; bottom panel: contribution of the 0^{th} (blue line), 1^{st} (green line) and 2^{nd} (red line) derivatives of the absorption spectrum to the calculated fit.

Replacing the *trans*-CH=CH units in **96** for C≡C bonds in **100** causes slight decreases in both μ_{12} and f_{os}, though the two chromophores have similar MLCT absorption energies. $\Delta\mu_{12}$ and $\Delta\mu_{ab}$ are both larger for salt **100**. **96** has larger values for both H_{ab} and c_b^2, attributable to more effective D–A electronic communication in the ethenyl-containing complex. However, the NLO responses of salts **96** and **100** are of a similar magnitude and this observation can be ascribed to the effects of the smaller value of μ_{12} for **100** being offset by its larger $\Delta\mu_{12}$ value.

Because the ILCT bands of complex salts **96–98** are so intense and close in energy to the MLCT bands, it is likely that their corresponding transitions will contribute significantly to the overall NLO responses. The cutoff wavelength for our Stark setup is *ca.* 350 nm, which arises from several factors including the intensity of the light source, detector sensitivity and near-UV absorption by the ITO glass window used in the Stark cell. As the ILCT bands for salts **96–98** are in the region of 390–430 nm (in butyronitrile at 77 K) it is possible to analyse them using the Stark technique, and the resulting data is presented in Table 42. Representative absorption and Stark spectra for the ILCT bands of salts **96–98** are shown in Figure 71.

Table 42: ILCT absorption and Stark spectroscopic data for complex salts **96–98**

Salt	λ_{max} [nm][a]	λ_{max} [nm][b]	E_{max} [eV][b]	f_{os}[b]	μ_{12} [D][c]	$\Delta\mu_{12}$ [D][d]	$\Delta\mu_{ab}$ [D][e]	c_b^2[f]	H_{ab} [cm^{-1}][g]	β_0 [10^{-30} esu][h]
96	372	398	3.12	0.7	7.5	10.8	18.5	0.21	10 100	73
97	398	413	3.00	0.8	8.3	15.4	22.6	0.16	8900	137
98	416	430	2.88	0.9	9.0	21.0	27.7	0.12	7600	241

[a] Measured in acetonitrile solutions at 293 K. [b] Measured in butyronitrile glasses at 77 K. [c] Calculated from eqn. 13. [d] Calculated from $f_{int}\Delta\mu_{12}$ using f_{int} = 1.33. [e] Calculated from eqn. 12. [f] Calculated from eqn. 14. [g] Calculated from eqn. 15. [h] Calculated from eqn. 7.

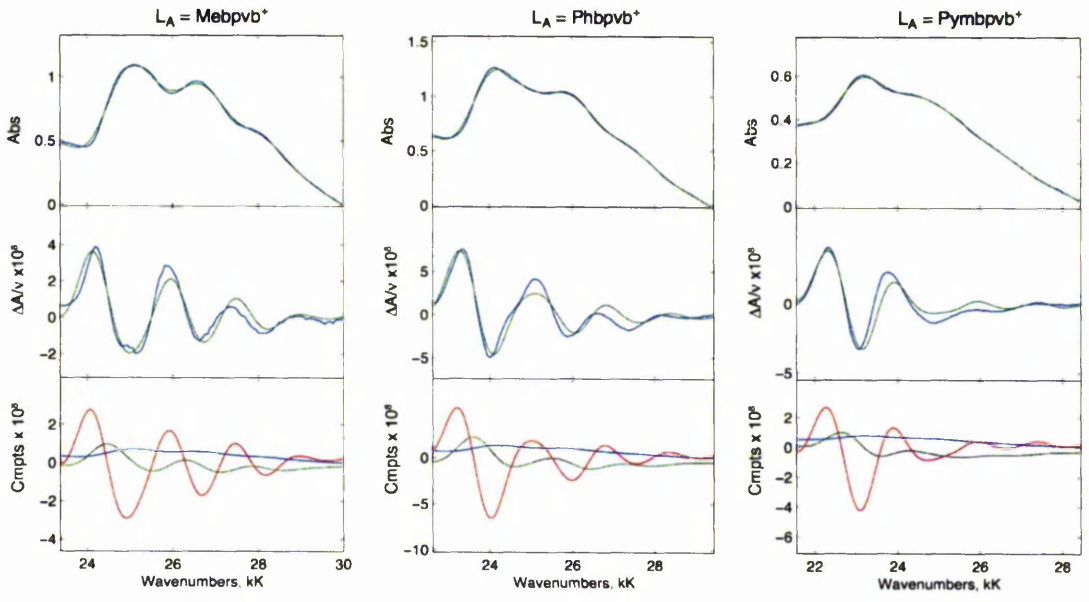

Figure 71: Absorption and electroabsorption spectra and calculated fits for the ILCT bands of salts **96–98** in a external fields of 2.47, 2.47 and 2.48 × 10^7 V m^{-1}, respectively.

Top panel: absorption spectra (blue line = experimental, green line = fit), middle panel: electroabsorption spectrum (blue line = experimental, green line = fit) according to the Liptay equation; bottom panel: contribution of the 0^{th} (blue line), 1^{st} (green line) and 2^{nd} (red line) derivatives of the absorption spectrum to the calculated fit.

Within the series **96–98**, μ_{12}, f_{os}, $\Delta\mu_{12}$ and $\Delta\mu_{ab}$ all increase and E_{max} decreases as the π-acceptor strength of L_A increases. The μ_{12} values of the ILCT absorptions are larger than those of the MLCT absorptions in every instance, correlating with the ILCT transitions being more strongly allowed. However, the $\Delta\mu_{12}$ values of the ILCT bands are smaller by *ca.* 40% when compared with those of the MLCT absorptions. The derived β_0 values associated with the ILCT transitions increase

steadily as the π-acceptor strength of L_A increases, attributable to μ_{12} and $\Delta\mu_{12}$ increasing while E_{max} decreases.

It is clear that both the MLCT and ILCT transitions in the simple dipolar chromophores under study lie along the same axis, so their contributions to the total NLO response are additive. The sums of β_0[MLCT] and β_0[ILCT] are shown in Table 43, and it is apparent that the contribution of the ILCT excitation to the overall static first hyperpolarizability increases steadily on moving along the series **96–98**, reaching as much as 45% for **98**. However, the lower than expected E_{max}[MLCT] and β_0[MLCT] for **98** may mean that the ILCT contribution in this case is actually less than that implied by the data presented below. Nevertheless, complex salts **96–98** evidently exhibit relatively large β_0[total] values, which make these and related chromophores promising candidates for further study.

Table 43: Estimated ILCT and MLCT contributions to the total NLO response for complex salts **96–98**

Salt	β_0[ILCT] [10^{-30} esu]	β_0[MLCT] [10^{-30} esu]	β_0[total] [10^{-30} esu]
96	73	131	204
97	137	203	340
98	200	241	441

5.4 Comparisons with polyenyl systems

One of the initial driving forces behind this work was the observation that Ru^{II} ammine complexes of the extended ligand $Mebpvb^{+}$ exhibit large NLO responses together with increased visible transparency, when compared with related polyenyl systems of similar length.[9] The effects of extending the conjugation in *trans*-$\{Ru^{II}Cl(pdma)_2\}^{+}$ pyridinium polyenyl complexes have been investigated as part of this thesis (see Chapter 3). For such complexes, β_0 increases with the number of *E*-ethylene units (up to $n = 2$), but this increase is accompanied by an unfavourable loss in visible transparency. The MLCT and Stark data for the *N*-methylpyridinium polyenyl complex salts (**73** $n = 0$, **75** $n = 1$, **76** $n = 2$ and **78** $n = 3$) are shown in Table 44, alongside that for **96–98**. Representative UV/Vis absorption spectra measured in butyronitrile glass at 77 K and acetonitrile at 293 K are shown in Figures 72 and 73.

Table 44: MLCT and Stark spectroscopic data for salts **73**, **75**, **76**, **78** and **96–98** measured in butyronitrile at 77 K

Salt	n	λ_{max} [nm]	E_{max} [eV]	μ_{12} [D]	$\Delta\mu_{12}$ [D]	β_0[MLCT] [10^{-30} esu]	β_0[total] [10^{-30} esu]
73	0	491	2.53	6.6	14.3	113	
75	1	515	2.41	6.0	16.9	123	
76	2	506	2.45	10.0	20.6	401	
78	3	501	2.48	10.5	22.2	468	
96		471	2.63	6.4	18.8	131	204
97		481	2.58	6.8	24.9	203	340
98		464	2.67	6.3	31.0	200	441

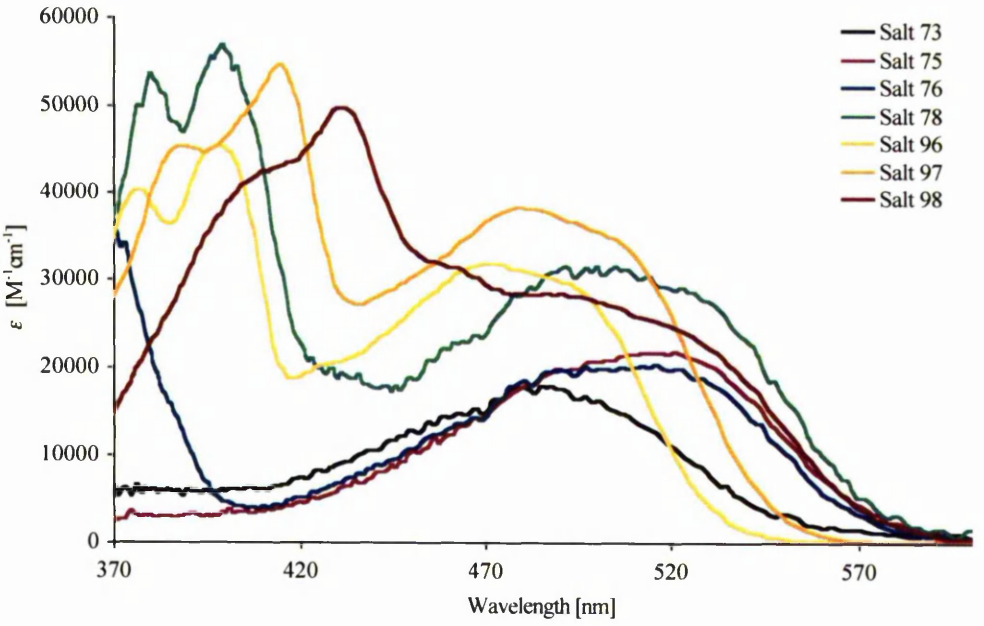

Figure 72: UV-visible absorption spectra for salts **73**, **75**, **76**, **78** and **96–98** in butyronitrile at 77 K

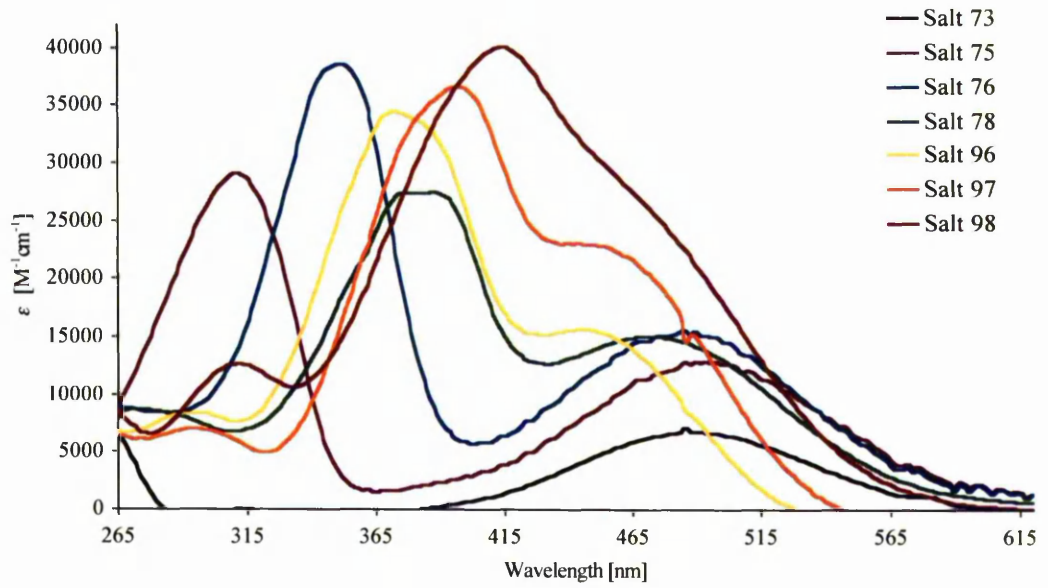

Figure 73: UV-visible absorption spectra for salts **73**, **75**, **76**, **78** and **96–98** in acetonitrile at 293 K

The μ_{12} values for **96–98** are comparable to those of the $n = 0$ or 1 complexes (**73** and **75**), but are lower by *ca.* 40% when compared with those of **76** and **78**. The $\Delta\mu_{12}$ values for **97** and **98** are larger than those of their polyenyl counterparts. The β_0[total] for **98** is similar to β_0[MLCT] for **78**, although it should be noted that the NLO response for salt **78** can be expected to also have a significant ILCT contribution which we have unfortunately been unable to measure (λ_{max}[ILCT] = 394 nm in acetonitrile at room temperature). Given the absorption profiles, **96** has a considerable gain in visible transparency compared with the $n = 3$ chromophore in **78** (which also has a *N*-methylpyridinium A group and a similar length). This potential benefit is however accompanied by at least a 2-fold decrease in the estimated NLO response. Although **98** may have a β_0 value approaching that of **78**, no accompanying increase in visible transparency is achieved. Therefore the insertion of a 1,4-phenylene ring is not an effective strategy for combating the transparency-efficiency trade-off in these pdma complexes.

5.5 Conclusion

The work presented in this chapter describes the synthesis of novel *N*-aryl analogues of Mebpvb$^+$ and their complexation to the *trans*-{Ru^{II}Cl(pdma)$_2$}$^+$ centre. The optical and electronic properties of the compounds have been investigated and the effects of the extending the π-conjugation by the addition of a 1,4-phenylene ring probed.

Increasing the π-acceptor strength of the bpvb ligand by either methylation or arylation causes red-shifting of both the MLCT and ILCT absorptions. The NLO responses associated with both the ILCT and MLCT excitations have been analyzed

using Stark spectroscopy. Generally β_0[ILCT] and β_0[MLCT] increase with the π-acceptor strength of L_A, although **98** has a lower than expected β_0[MLCT] value, which is probably caused by underestimation of E_{max} due to the strong overlapping of the ILCT and MLCT absorption bands. Comparisons with the related polyenyl-containing complexes show that the insertion of a 1,4-phenylene unit into the π-conjugated pathway maintains large NLO responses, but with no significant gains in the visible transparency.

5.6 Future work

Although several new complexes have been prepared, an inherent problem with the PF_6^- salts of the new extended pro-ligands $Phbpvb^+$ and $Pymbpvb^+$ is their poor solubility in most organic solvents at room temperature, being only appreciably soluble in DMF or DMSO. Therefore the coordination of these ligands to other metal centres is limited. Test reactions with the precursor $[Ru^{II}(NH_3)_5(H_2O)]^{2+}$ in DMF were unsuccessful. The solubility of these compounds could potentially be increased by counter-anion exchange, for example using species such as tetraphenylborate or tosylate.

The pyridyl aldehyde FEP could be condensed with a variety of other A groups to affording new potential ligands, the introduction of more polar groups may increase the solubility of these compounds. Although attempts to react complex salt **94** with 1,3-diethyl-2-thiobarbituric acid were unsuccessful, there is scope for further experiments using different reaction conditions. A range of other reagents such as barbituric acid or acceptor-substituted anilines may well react with **94** to form new

extended complex chromophores. There is also potential for complexing FEP with other metal centres and then carrying out related condensation reactions.

5.7 References

1. J. Zyss in *Conjugated Polymeric Materials: Opportunities in electronics, optoelectronics and molecular electronics,* Ch 4. Eds. J. L. Bredas and R. R. Chance, Kleuwer Academic, Dordrecht, 1989
2. W. Tam, L-T. Cheng, J. D. Bierlein, L. K. Cheng, Y. Wang, A. E. Feiring, G. R. Meredith, D. F. Eaton, J. C. Calabrese and G. L. J. A. Rikken in *Materials for nonlinear optics, chemical perspectives,* Ch. 9. Eds. S. R. Marder, J. E. Sohn and G. D. Stucky, ACS Symposium Series 455, ACS, Washington DC, 1991
3. F. Wang, A. W. Harper, M. S. Lee, L. R. Dalton, H. Zhang, A. Chen, W. H. Steier and S. R. Marder, *Chem. Mater.,* 1999, **11**, 2285 – 2288
4. C. Bosshard, *Adv. Mater.,* 1996, **8**, 385 – 397
5. J. L. Oudar and D. S. Chemla, *J. Chem. Phys.,* 1977,**66**, 2666 – 2668
6. J. L. Oudar, *J. Chem. Phys.,* 1997, **67**, 446 – 457
7. J. L. Oudar and H. Le Person, *Opt. Comm.,* 1975, **15**, 248 – 262
8. *Nonlinear Optics of Organic Molecules and Polymers,* Eds. H. S. Nalwa and S. Miyata, CRC Press, Boca Raton, FL. 1997
9. B. J. Coe, L.A. Jones, J. A. Harris, B. S. Brunschwig, I. Asselberghs, K. Clays, A. Persoons, J. Garin and J. Orduna, *J. Am. Chem. Soc.,* 2004, **126**, 3880 – 3891
10. V. Alain, S. Rédoglia, M. Blandchard-Desce, S. Lebus, K. Lukaszuk, R. Wortmann, U. Gubler, C. Bosshard and P. Günter, *Chem. Phys.,* 1999, **245**, 51 – 71
11. H. Meier, J. Gerold and D. Jacob, *Tet. Lett.,* 2003, **44**, 1915 – 1918

12. J. A. Mata, S. Uriel, R. Llusar and E. Peris, *Organometallics,* 2000, **19**, 3797 – 3802

13. H. Meier, J. Gerold, H. Kolshorn, W. Baumann and M. Bletz, *Angew. Chem. Int. Ed. Eng.,* 2002, **41**, 292 – 295

14. P. G. Douglas, R. D. Feltham and H. G. Metzger, *J. Am. Chem. Soc.,* 1971, **93**, 84 – 90

15. K. Ichimura and S. Watanabe, *J. Polym. Sci., Polymer Chem. Ed.,* 1982, **20**, 1419 – 1432

16. B. J. Coe, J. A. Harris, I. Asselberghs, K. Clays, G. Olbrechts, A. Persoons, J. T. Hupp, R. C. Johnson, S. J. Coles, M. Hursthouse and K. Nakatani, *Adv. Funct. Mater.,* 2002, **12**, 110 – 116

17. A. J. Amoroso, A. M. W. Cargill Thompson, J. P. Maher, J. A. McCleverty and M. D. Ward. *Inorg. Chem.,* 1995, **34,** 4828 – 4835

18. N. R. Champness, A. N. Khlobystov, A. G. Majuga, M. Schröder and N. V. Zyk, *Tet. Lett.,* 1999, **40**, 5413 – 5416

19. *Organic Chemistry*, M. Jones Jr., Norton, New York 1997

20. V. Vohra, S. Suresh, S. Ponrathnam, C. R. Rajan and F. Kajzar, *J. Polym. Chem.* 2000, **38**, 962 – 971

21. M. Blanchard-Desce, V. Alain, P. V. Bedworth, S. R. Marder, A. Fort, C. Runser, M. Barzoukas, S. Lebus and R. Wortmann, *Chem. Eur. J.,* 1997, **3**, 1091 – 1104

22. V. Alain, A. Fort, M. Barazoukas, C. –T. Chen, M. Blanchard-Desce, S. R. Marder and J. W. Perry, *Inorg. Chim. Acta,* 1996, **242**, 43 – 22

23. G. U. Bublitz, R. Ortiz, C. Runser, A. Fort, M. Barazoukas, S. R. Marder and S. G. Boxer, *J. Am. Chem. Soc.,* 1997, **119**, 2311 – 2312

24. S. R. Marder, B. Kippelen, A. K. –Y. Jen amd N. Peyghambarian, *Nature*, 1997, **388**, 845 – 851

25. S. R. Marder, L. –T. Chen, B. G. Tiemann, A. C. Friedli, M. Blanchard-Desce, J. W. Perry and J. Skindhoj, *Science*, 1994, **263**, 511 – 514

26. Y. –W. Cao, X. –D. Chai, S. –G. Chen, Y. –S. Jiang, W. –S. Yang, R. Lu, Y. –Z. Ren, M. Blanchard-Desce, T. –J. Li and J. –M. Lehn, *Synth. Met.,* 1995, **71**, 1733 – 1734

27. J. Garín, J. Orduna, J. I. Rupérez, R. Alcalá, B. Villacampa, C. Sánchez, N. Martín, J. L. Segura and M. González, *Tet. Lett.,* 1998, **39**, 3577 – 3580

28. L. F. Tietze and U. Beifuss in *Comprehensive Organic Synthesis: Vol. 2.* Ed. B. M. Trost, Pergamon, Oxford, 1991

29. F. J. Kunz, P. Margaretha and O. E. Polansky, *Chimia,* 1970, **24**, 165 – 181

30. J. Adamson, B. J. Coe, H. L. Grassam, J. C. Jeffery, S. J. Coles and M. B. Hursthouse, *J. Chem. Soc., Perkin Trans. 1,* 1999, 2483 – 2488

31. *Organic Chemistry*, J. Clayden, N. Greeves, S. Warren and P. Wothers, Oxford University Press, Oxford, 2001

32. B. J. Coe, T. Beyer, J. C. Jeffery, S. J. Coles, T. Gelbrich, M. B. Hursthouse and M. E. Light, *J. Chem. Soc. Dalton Trans.,* 2000, 797 – 803

33. B. J. Coe, J. A. Harris and B. S. Brunschwig, *J. Phys. Chem. A,* 2002, **106**, 897 – 905

34. Y. K. Sutin, B. S. Brunschwig, C. Creutz and N. Sutin, *J. Phys. Chem.,* 1996, 100, 8157 – 8169

Appendix:

Physical Measurements

A.1 General Physical Measurements

The ^{1}H NMR spectra of the complex salts described in chapters 2, 3 and 5 were recorded on a Varian XL-300 spectrometer or the Bruker 500 spectrometer, while the corresponding measurements on the compounds described in chapter 4 were recorded on a Gemini 200 spectrometer. All chemical shifts are referenced to TMS. The fine splittings of the pyridyl or phenyl ring AA'BB' patterns are ignored and the signals reported as simple doublets, with *J* values referring to the two most intense peaks. Elemental and thermogravimetric (TG) analyses were performed by the Microanalytical Laboratory, University of Manchester. UV/Vis spectra were generally recorded using a Hewlett-Packard 8452A diode array spectrophotometer, except for the results presented in Table 1 which were measured using an α-Helios double-beam spectrophotometer which has a range further into the NIR region. IR spectra were obtained as KBr discs with an ATI Mattson Genesis Series FTIR instrument. Mass spectra were recorded using +electrospray on a Micromass Platform Spectrometer. Cyclic voltammetric measurements were carried out with an EG&G PAR model 283 potentiostat/galvanostat. An EG&G PAR K0264 single compartment microcell was used with a Ag–AgCl reference electrode (3 M NaCl, saturated AgCl) and a platinium-wire auxiliary electrode. For the measurements described in chapter 2, a glassy carbon working electrode was used and water and methanol were distilled before use. The measurements described in chapters 3–5 involved a platinum working electrode and acetonitrile (HPLC grade) was distilled twice before use. KNO_3 and $[NBu^n_4]PF_6$, the latter twice recrystallized from ethanol and dried *in vacuo*, were used as the supporting electrolytes. Solutions containing

ca. 10^{-3} M analyte (0.1 M electrolyte) were deaerated by purging with N_2. All $E_{1/2}$ values were calculated from $(E_{pa} + E_{pc})/2$ at a scan rate of 200 mV s^{-1}.

A.2 X-Ray Crystallography Studies

Crystals of **70**, **74**, **75**, **92**, **96**, **97** and **99** were obtained by slow diffusion of diethyl vapour into acetonitrile solutions. Crystals of **58** were grown by the slow diffusion of ethanol vapour into an aqueous solution, while those of **84** and $[Phbpvb^+]PF_6 \cdot 0.5HPF_6 \cdot DMF$ were obtained by slow diffusion of diethyl ether vapour into nitromethane or DMF/acetonitrile solutions, respectively. The crystals chosen for diffraction studies had the following approximate dimensions and appearances: 0.60 × 0.60 × 0.10 mm, purple block (**84**•$9H_2O$); 0.20 × 0.10 × 0.08 mm, yellow block (**70**•2.5MeCN); 0.15 × 0.10 × 0.10 mm, orange rod (**74**•2MeCN); 0.60 × 0.40 × 0.20 mm, red block (**75**); 0.40 × 0.20 × 0.02 mm, dark red plate (**92**); 0.70 × 0.20 × 0.05 mm, purple block (**84**•$MeNO_2$); 0.18 × 0.16 × 0.04 mm, orange shard $[Phbpvb^+]PF_6 \cdot 0.5HPF_6 \cdot DMF$; 0.42 × 0.30 × 0.07 mm, red slab (**96**); 0.76 × 0.18 × 0.03 mm, red blade (**97**); 0.44 × 0.08 × 0.04 mm, orange blade (**99**). Crystals of the salts $Na_2[Fe^{II}(CN)_5(MeQ^+)] \cdot 9H_2O$ (**58** • $9\ H_2O$) and *trans*-$[Ru^{II}(NH_3)_4(py)(Mebpbd^+)](PF_6)_3 \cdot MeNO_2$ (**84**•$MeNO_2$) were attached to a Hamilton Cryoloop, using fomblin oil (perfluoropolymethylisopropyl ether) and mounted on a Bruker APEX CCD X-ray diffractometer. Cryocooling to 100 K was carried out by using an Oxford Cryosystems 700 Series Cryostream Cooler. Intensity measurements were collected using graphite-monochromated, MoKα radiation from a sealed X-ray tube with a monocapillary collimator. The intensities of reflections of a sphere were collected with an exposure time per frame of 5 s. Data processing was

carried out by using the Bruker SAINT[1] software package and a semi-empirical absorption correction was applied using SADABS.[1] The data for all of the other crystals were collected on a Nonius Kappa CCD area-detector X-ray diffractometer controlled by the Collect software package.[2] The data were processed by Denzo[3] and corrected for absorption by using the empirical method employed in Sortav[4,5] from within the MaXus suite of programs.[6] All structures were solved by direct methods and refined by full-matrix least-squares on all F_0^2 data using SHELXS-97[7] and SHELXL-97.[8] All non-hydrogen atoms were refined anisotropically with hydrogen atoms included in idealized positions with thermal parameters riding on those of the parent atom. The crystal of [Phbpvb$^+$]PF_6•0.5HPF_6•DMF contained a molecule of highly disordered solvent (presumably DMF) which was removed using the SQUEEZE program. One of the PF_6^- anions was disordered over two sites (and a symmetry operation). There was a hydrogen atom between two pyridine nitrogen atoms related by a symmetry operation forming a strong H–bond, but it was not possible to accurately locate this hydrogen atom and it was therefore fixed to the N with half occupancy to best model the situation. There was also an extra PF_6^- for every pair of cations. The crystal of **96** contained highly disordered acetonitrile molecules which were removed using the SQUEEZE program and the two PF_6^- anions were disordered over two sites. The crystal of **97** also contained some highly disordered solvent (acetonitrile) which was removed using the SQUEEZE program, and the entire cationic complex was disordered over two sites. The crystal of **99** contained unrefinable solvent (probably acetonitrile again) which was removed using the SQUEEZE program, and disorder in the PF_6^- anion was also observed.

The crystal structures of **58** and **84** were solved by M. Helliwell at the University of Manchester. All other crystal structures were solved by M. E. Light (**70**, **74** and **75**), S. J. Coles (**92**) and P. N. Horton ([Phbpvb]PF_6 **96**, **97** and **99**) at the EPSRC crystallographic service at the University of Southampton.

A.3 Hyper-Rayleigh Scattering Studies

The HRS measurements in Chapter 2 were performed by Dr Inge Asselberghs. In Chapter 4 salts **80**, **81**, **83**, **84**, **86** and **87** were measured by the Author and salts **91–93** by Shen Ting Hung. All measurements were performed at the University of Leuven.

Details of the HRS experiment have been reported elsewhere,[9–12] and the experimental procedure was as previously described.[13] β values were determined using the electric-field-induced second harmonic generation β_{1064} values for *p*-nitroaniline (29.2×10^{-30} esu in acetonitrile, 32.0×10^{-30} esu in methanol)[14] and β_{800} values for crystal violet (388×10^{-30} esu in methanol) as external references. All measurements, except those for the protic switching experiments in Chapter 2, were performed using the 1064 nm Nd:YAG laser (Quanta-Ray GCR-5, 8 ns pulses, 7 mJ, 10 Hz). All protic switch measurements were carried out using the 800 nm fundamental of a regenerative mode-locked Ti^{3+}:sapphire laser (Spectra Physics, model Tsunami®, 100 fs pulses, 1 W, 80 MHz).Dilute (10^{-5}–10^{-6} M) solutions (in methanol or water for chapter 2 and acetonitrile for chapter 4) were used to ensure linear dependencies of $I_{2\omega}/I_{\omega}^{2}$ on solute concentration, precluding the need for Lambert-Beer correction factors. Samples were filtered (Millipore, 0.45 μm), and

showed no fluorescence. One dimensional hyperpolarizability is assumed i.e. $\beta_{1064} = \beta_{zzz}$ and a relative error of ±15% is estimated.

A.4 Stark Spectroscopic Measurements

All Stark spectroscopic measurements were performed by Dr. James Harris at the California institute of technology.

The Stark apparatus, experimental methods and data analysis procedure were exactly as previously reported,[15,16] with the only modification being that a Xe arc lamp was used as the light source in the place of a W filament bulb. Butyronitrile or glycerol–water (50:50 vol %) were used as the glassing media, for which the local field correction f_{int} is estimated as 1.33.[15,16] The Stark spectrum for each compound was measured a minimum of three times using different field strengths, and the signals were always found to be quadratic in the applied field. A two-state analysis of the ICT transitions gives

$$\Delta\mu_{ab}^2 = \Delta\mu_{12}^2 + 4\mu_{12}^2 \tag{12}$$

where $\Delta\mu_{ab}$ is the dipole moment difference between the diabatic states, $\Delta\mu_{12}$ is the observed (adiabatic) dipole moment difference, and μ_{12} is the transition dipole moment. Analysis of the Stark spectra in terms of the Liptay treatment[17,18] affords $\Delta\mu_{12}$, and the transition dipole moment, μ_{12} can be determined from the oscillator strength f_{os} of the transition by

$$|\mu_{12}| = \left[f_{os} / \left(1.08 \times 10^{-5} E_{max}\right)\right]^{1/2} \tag{13}$$

where E_{max} is the energy of the ICT maximum (in wavenumbers). The degree of delocalization c_b^2 and electronic coupling matrix element H_{ab} for the diabatic states are given by

$$c_b^2 = \frac{1}{2}\left[1 - \left(\frac{\Delta\mu_{12}^2}{\Delta\mu_{12}^2 + 4\mu_{12}^2}\right)^{1/2}\right] \tag{14}$$

$$|H_{ab}| = \left|\frac{E_{max}(\mu_{12})}{\Delta\mu_{ab}}\right| \tag{15}$$

If the hyperpolarizability tensor β_0 has only nonzero elements along the ICT direction, then this quantity is given by equation 7. A relative error of ±20% is estimated for the β_0 values derived from the Stark data and using equation 7.

A.5. References

1. *SAINT* (Version 6.45) and *SADABS* (Version 2.10), Bruker AXS Inc.; Madison: Wisconsin, USA, 2003
2. R. Hooft, *Collect*, Data collection software; Nonius BV: Delft, The Netherlands, 1998
3. Z. Otwinowski and W. Minor, *Methods Enzymol.*, 1997, **276**, 307 – 326
4. R. H. Blessing, *Acta. Crystallogr., Sect. A,* 1995, **51**, 33 – 38
5. R. H. Blessing, *J. Appl. Crystallogr.*, 1997, **30**, 421 – 426
6. S. Mackay, C. J. Gilmore, C. Edwards, M. Tremayne, N. Stewart and K. Shankland, MAXUS, a computer program for the solution and refinement of crystal structures from diffraction data, University of Glasgow: Glasgow, U.K., Nonius BV, Delft, The Netherlands and MacScience Co. Ltd., Yokohama, Japan, 1998
7. G. M. Sheldrick, *Acta Crystallogr., Sect. A,* 1990, **46**, 467 – 473
8. G. M. Sheldrick, *SHELXL 97*, Program for crystal structure refinement; University of Göttingen: Göttingen, Germany, 1997.
9. K. Clays and A. Persoons, *Phys. Rev. Lett.*, 1991, **66**, 2980 – 2983
10. K. Clays and A. Persoons, *Rev. Sci. Instrum.*, 1992, **63**, 3285 – 3289
11. E. Hendrickx, K. Clays, A. Persoons, C. Dehu and J. L. Bredas, *J. Am. Chem. Soc.*, 1995, **117**, 3547 – 3555
12. E. Hendrickx, K. Clays and A. Persoons, *Acc. Chem. Res.,* 1998, **31**, 675 – 683
13. S. Houbrechts, K. Clays, A. Persoons, Z. Pikramenou and J. –M. Lehn, *Chem Phys, Lett.*, 1996, **258**, 485 – 489

14. M. Stähelin, D. M. Burland and J. E. Rice, *Chem. Phys. Lett.,* 1992, **191**, 245 – 250

15. B. J. Coe, J. A. Harris, B. S. Brunschwig, *J. Phys. Chem. A,* 2002, **106**, 897 – 905.

16. Y. K. Shin, B. S. Brunschwig, C. Creutz, N. Sutin, *J. Phys. Chem.,* 1996, **100**, 8157 – 8169

17. W. Liptay, in *Excited States*, Vol. 1, Ed. E. C. Lim, Academic Press, New York, 1974, pp. 129 – 229

18. G. U. Bublitz, S. G. Boxer, *Annu. Rev. Phys. Chem.,* 1997, **48**, 213 – 242